Precast Concrete Pier Systems for Rapid Construction of Bridges in Seismic Regions

by

David G. Hieber
Graduate Research Assistant

Jonathan M. Wacker
Graduate Research Assistant

Marc O. Eberhard
Professor

John F. Stanton
Professor

Department of Civil and Environmental Engineering
University of Washington
Seattle, Washington 98195

Washington State Transportation Center (TRAC)
University of Washington, Box 354802
1107 NE 45th Street, Suite 535
Seattle, Washington 98105-4631

Washington State Department of Transportation
Technical Monitor
Jugesh Kapur
Bridge Design Engineer, Bridge and Structures Office

Prepared for
Washington State Transportation Commission
Department of Transportation
and in cooperation with
U.S. Department of Transportation
Federal Highway Administration

December 2005

TECHNICAL REPORT STANDARD TITLE PAGE

1. REPORT NO. WA-RD 611.1	2. GOVERNMENT ACCESSION NO.	3. RECIPIENT'S CATALOG NO.
4. TITLE AND SUBTITLE PRECAST CONCRETE PIER SYSTEMS FOR RAPID CONSTRUCTION OF BRIDGES IN SEISMIC REGIONS		5. REPORT DATE December 2005
		6. PERFORMING ORGANIZATION CODE
7. AUTHOR(S) David G. Hieber, Jonathan M. Wacker, Marc O. Eberhard John F. Stanton		8. PERFORMING ORGANIZATION REPORT NO.
9. PERFORMING ORGANIZATION NAME AND ADDRESS Washington State Transportation Center (TRAC) University of Washington, Box 354802 University District Building; 1107 NE 45th Street, Suite 535 Seattle, Washington 98105-4631		10. WORK UNIT NO.
		11. CONTRACT OR GRANT NO. Agreement T2695, Task 53
12. SPONSORING AGENCY NAME AND ADDRESS Research Office Washington State Department of Transportation Transportation Building, MS 47372 Olympia, Washington 98504-7372 Kim Willoughby, Project Manager, 360-705-7978		13. TYPE OF REPORT AND PERIOD COVERED Final Research Report
		14. SPONSORING AGENCY CODE
15. SUPPLEMENTARY NOTES This study was conducted in cooperation with the U.S. Department of Transportation, Federal Highway Administration.		

16. ABSTRACT

Increasing traffic volumes and a deteriorating transportation infrastructure have stimulated the development of new systems and methods to accelerate the construction of highway bridges. Precast concrete bridge components offer a potential alternative to conventional reinforced, cast-in-place concrete components. The use of precast components has the potential to minimize traffic disruptions, improve work zone safety, reduce environmental impacts, improve constructability, increase quality, and lower life-cycle costs.

This study compared two precast concrete bridge pier systems for rapid construction of bridges in seismic regions. One was a reinforced concrete system, in which mild steel deformed bars connect the precast concrete components. The other was a hybrid system, which uses a combination of unbonded post-tensioning and mild steel deformed bars to make the connections.

A parametric study was conducted using nonlinear finite element models to investigate the global response and likelihood of damage for various configurations of the two systems subjected to a design level earthquake. A practical method was developed to estimate the maximum seismic displacement of a frame from the cracked section properties of the columns and the base-shear strength ratio.

The results of the parametric study suggest that the systems have the potential for good seismic performance. Further analytical and experimental research is needed to investigate the constructability and seismic performance of the connection details.

17. KEY WORDS Bridges, piers, substructures, rapid construction, seismic performance, connections, precast concrete, prestressed concrete	18. DISTRIBUTION STATEMENT No restrictions. This document is available to the public through the National Technical Information Service, Springfield, VA 22616

19. SECURITY CLASSIF. (of this report) None	20. SECURITY CLASSIF. (of this page) None	21. NO. OF PAGES	22. PRICE

DISCLAIMER

The contents of this report reflect the views of the authors, who are responsible for the facts and the accuracy of the data presented herein. The contents do not necessarily reflect the official views or policies of the Washington State Transportation Commission, Department of Transportation, or the Federal Highway Administration. This report does not constitute a standard, specification, or regulation.

TABLE OF CONTENTS

LIST OF FIGURES

LIST OF TABLES

EXECUTIVE SUMMARY

Increasing traffic volumes and a deteriorating transportation infrastructure have stimulated the development of new systems and methods to accelerate the construction of highway bridges in order to reduce traveler delays. Precast concrete bridge components offer a potential alternative to conventional reinforced, cast-in-place concrete components. The increased use of precast concrete components could facilitate rapid construction, minimize traffic disruption, improve work zone safety, reduce environmental impacts, improve constructability, and lower life-cycle costs. .

This study compared two precast concrete bridge pier systems for rapid construction of bridges in seismic regions. The systems made use of precast concrete cap-beams and columns supported on cast-in-place concrete foundations. One was a reinforced concrete system, in which mild steel deformed bars connected the precast concrete components and provided the flexural strength of the columns. The other was a hybrid system, which used a combination of unbonded post-tensioning and mild steel deformed bars to make the connections and provide the required flexural stiffness and strength.

A parametric study of the two systems, which included pushover and earthquake analyses of 36 reinforced concrete frames and 57 hybrid frames, was conducted using nonlinear finite element models to investigate the global response of various frame configurations. In the earthquake analyses, the frames were subjected to five ground motions having peak ground accelerations with a 10 percent probability of exceedance in 50 years (10 percent in 50) and five ground motions having peak ground accelerations

with a 2 percent probability of exceedance in 50 years (2 percent in 50), resulting in a total of 930 earthquake analyses.

A practical method was developed to estimate maximum seismic displacements on the basis of the cracked section properties of the columns and base-shear strength ratio. The ratio of the maximum displacement calculated with nonlinear analysis to the displacement calculated with the practical method had a mean of 0.98 and a standard deviation of 0.25 for the reinforced concrete frames. For the hybrid frames, this ratio had a mean of 1.05 and a standard deviation of 0.26.

The expected damage at the two seismic hazard levels was estimated. For the 10 percent in 50 ground motions, this study found moderate probabilities of cover concrete spalling, minimal probabilities of bar buckling, and maximum strains in the longitudinal reinforcement that suggest bar fracture would rarely occur. For example, at an axial-load ratio of 0.10 and longitudinal reinforcement ratio of 0.01, the mean probability of cover concrete spalling was 0.12 for the reinforced concrete frames and 0.10 for the hybrid frames, while the mean probability of bar buckling was 0.0005 for both the reinforced concrete and hybrid frames. For this same axial-load ratio and reinforcement ratio, the mean maximum strain in the longitudinal mild steel was 0.015 for the reinforced concrete frames and 0.012 for the hybrid frames.

Large probabilities of cover concrete spalling, minimal probabilities of bar buckling, and moderate maximum strains in the longitudinal reinforcement were found for the 2 percent in 50 ground motions. For example, at an axial-load ratio of 0.10 and longitudinal reinforcement ratio of 0.01, the mean probability of cover concrete spalling was 0.68 for the reinforced concrete frames and 0.73 for the hybrid frames, while the

mean probability of bar buckling was 0.04 for the reinforced concrete and hybrid frames. For this same axial-load ratio and reinforcement ratio, the mean maximum strain in the longitudinal mild steel was 0.042 for the reinforced concrete frames and 0.025 for the hybrid frames.

This study found that the hybrid system exhibited particularly low residual drifts. This study also found the displacement ductility demand of the two systems to be similar for similar levels of axial-load ratio and total longitudinal reinforcement.

On the basis of the global nonlinear finite element analyses conducted during this study, the characteristics and numerical response quantities suggest that the systems have the potential for good seismic performance. Further research is needed to develop the connection details.

CHAPTER 1
INTRODUCTION

A significant cause of increasing traffic congestion in the Puget Sound Region, as well as in many other parts of the United States, is that traffic volumes continue to increase at the same time as the interstate highway system is approaching its service life (Freeby et al. 2003). To improve the condition of the deteriorating transportation infrastructure, significant bridge repairs and new bridge construction are necessary. Unfortunately, even though these solutions help reduce traffic congestion after the construction or rehabilitation is complete, they typically further increase traffic congestion during the construction or rehabilitation. Therefore, accelerated construction methods incorporating new practices, technologies, and systems are needed to facilitate rapid construction of bridges. The American Association of State Highway and Transportation Officials (AASHTO), the Federal Highway Administration (FHWA), and various state departments of transportation have been working together to develop these systems and methods that would allow for more rapid construction of bridges and other transportation infrastructure (FHWA 2004).

A majority of the highway bridges currently constructed in Washington State consist of prestressed concrete girders with a composite, reinforced, cast-in-place concrete deck slab supported by reinforced, cast-in-place concrete bridge piers and abutments. Cast-in-place concrete bridge construction significantly contributes to traffic disruption because it requires numerous, sequential on-site construction procedures and can be time-intensive.

Precast concrete bridge components offer a promising alternative to their cast-in-place concrete counterparts. Enormous benefits could arise from their use because precast concrete bridge components are typically fabricated off-site and then brought to the project site and quickly erected. Precast components also provide an opportunity to complete tasks in parallel. For example, the foundations can be cast on-site while the precast components are fabricated off-site. The use of precast components has the potential to minimize traffic disruptions, improve work zone safety, reduce environmental impacts, improve constructability, increase quality, and lower life-cycle costs. The use of precast concrete bridge elements can provide dramatic benefits for bridge owners, designers, contractors, and the traveling public (Freeby et al. 2003).

Several precast concrete bridge pier systems have been proposed and developed recently. Some of these are reinforced concrete frames that use mild reinforcing steel alone to connect the precast concrete components. Others are hybrid frames that use unbonded, post-tensioning tendons in conjunction with grouted, mild reinforcing steel to achieve the necessary connection. Precast pier systems have been developed for non-seismic regions (Billington et al. 1998, Matsumoto et al. 2002). In comparison, the development of connections between precast concrete components for use in seismic regions has been limited. Hybrid frames have the additional benefit of minimizing residual displacement by re-centering the frame after an earthquake.

1.1 BENEFITS OF RAPID CONSTRUCTION

1.1.1 Reduced Traffic Disruption

Construction-related traffic delays are not only frustrating; they can impose unacceptable delays on the traveling public and for the nation's commerce. This situation

is spurring interest in rapid construction methods. To reduce motorist inconvenience, lost time, and wasted fuel, some states are beginning to offer contractors bonuses for using rapid construction methods to complete projects earlier and charging them penalties for late completion (Ralls and Tang 2004).

Typically, highway bridges are constructed of cast-in-place reinforced concrete abutments and piers, precast concrete or steel girders, and a cast-in-place reinforced concrete deck slab. Although these practices generally produce durable bridges, they also contribute significantly to traffic delays because of the sequential nature of the construction. Foundations must be formed, poured, and cured before columns and pier caps can be placed. Columns and pier caps must be formed, poured, and cured before the girders and deck are placed. A construction schedule needs to include additional time delays to allow the concrete to cure between each operation (Freeby et al. 2003).

Precast bridge elements and systems allow for many of the tasks traditionally performed on-site, such as element fabrication, to be performed away from the construction site and traffic. Precast bridge elements and systems also allow many of the time-consuming tasks, such as erecting formwork, placing reinforcing steel, pouring concrete, curing concrete, and removing formwork, to occur off-site (Freeby et al. 2003). Precast elements can be transported to the site and erected quickly, significantly reducing the disruption of traffic and the cost of traffic control.

1.1.2 Improved Work Zone Safety

Bridge construction sites often require workers to operate close to high-speed traffic, at high elevations, over water, near power lines, or in other dangerous situations (Freeby et al. 2003). Precast elements allow many of the construction activities to occur

in a safer, more controlled environment, significantly reducing the amount of time workers must operate in a potentially dangerous setting.

1.1.3 Reduced Environmental Impact

Precast elements are advantageous for bridges constructed over water, wetlands, and other sensitive areas, in which environmental concerns and regulations discourage the use of cast-in-place concrete. Traditional bridge construction requires significant access underneath the bridge for both workers and equipment to perform tasks such as erection of formwork and placement of reinforcing steel. In environmentally sensitive areas, measures are typically required to ensure containment of spilled concrete from burst pump lines or collapsed forms. Precast concrete elements provide the contractor more options, such as top-down construction, which can significantly reduce the impact on the area below the bridge and the adjacent landscape.

1.1.4 Improved Constructability

Project sites, surrounding conditions, and construction constraints can vary significantly among projects. Some projects are in rural areas where traffic is minimal but the shipping distance for wet concrete is expensive. Other projects are on interstate highways in very congested urban areas where construction space and staging areas are limited by adjacent developments. Other projects may be at high elevations over a large water way. Precast concrete elements can relieve many constructability pressures by allowing many of the necessary tasks to be performed off-site in a more easily controlled environment.

1.1.5 Increased Quality

Precast concrete members are often more durable and of more uniform construction than their cast-in-place concrete counterparts because of the controlled fabrication environment and strict quality control in precast concrete production (Shahawy 2003). Precast operations are well established, repetitive, and systematic, ensuring high quality products. Curing of precast concrete elements can be more closely monitored and easily inspected in the controlled plant setting rather than on the construction site. The use of steel forms in precast operations can also lead to high quality finishes.

1.1.6 Lower Life-Cycle Costs

Precast concrete bridge elements can reduce the life-cycle cost of the bridge. If the cost of construction delays is included in the cost comparison between precast concrete elements and cast-in-place option, precast concrete elements are typically much more competitive than conventional construction methods because of the reduced on-site construction time (Sprinkel 1985). In the past, these delay costs have been omitted from most cost estimates, which has made the use of precast concrete components appear relatively expensive. With new contracting approaches, such as those that take into account the time required on site to complete a project, it is expected that the use of precast concrete components will become competitive with current methods.

1.2 RESEARCH OBJECTIVES

The goal of this study was to develop a precast concrete pier system to be used for the rapid construction of bridges. The primary objectives of the research presented in this report were as follows:

1. Identify promising precast concrete pier systems for rapid construction of bridges in active seismic regions, specifically Western Washington State, that are economical, durable, easily fabricated, and easily constructed.

2. Investigate the global response (both quasi-static and dynamic) of the proposed bridge pier systems by performing parametric studies with nonlinear finite element models.

3. Estimate the expected level of seismic damage in these systems.

1.3 SCOPE OF RESEARCH

The first research objective was addressed as follows:

- On the basis of the information gathered from a literature review and meetings with bridge engineers, contractors, and precast concrete producers (Hieber et al. 2004), two types of precast concrete pier systems were developed. The first system was an emulation of a prototype, cast-in-place, reinforced concrete pier, and the second was a hybrid system utilizing both mild reinforcement and prestressed strand.

- Numerous connections between the precast concrete elements were developed and investigated for constructability and ease of fabrication.

- The proposed precast concrete pier systems and connection details were discussed with WSDOT design and construction engineers, precast concrete fabricators, and bridge contractors.

The second research objective was fulfilled by following these steps:

- Nonlinear finite element models were developed for both the proposed reinforced concrete pier frame and hybrid pier frame by using the computer program OpenSees (OpenSees 2000).

- Key parameters were selected and varied during the nonlinear finite element analyses. These parameters were varied during the parametric studies described in the following two steps.

- Quasi-static pushover analyses were performed to create force-displacement curves. Cracked properties, first yield properties, and nominal yield displacements were obtained from the pushover analyses.

- The models were subjected to ten scaled ground motions (five motions with a 10 percent probability of exceedance in 50 years and five motions with a 2 percent probability of exceedance in 50 years). During these time history analyses, maximum and residual horizontal displacements were recorded.

- Comparisons were made between the reinforced concrete frame and the hybrid frame on the basis of results from the parametric studies. They also provided insight into the effects of varying the key parameters on maximum drift, residual drift, and ductility.

The third research objective was completed as follows:

- The probability of exceeding various limit states (including the onset of cover concrete spalling and bar buckling) was found to facilitate additional comparisons between the systems.

1.4 REPORT ORGANIZATION

This document contains eleven chapters and four appendices. Chapter 2 provides a summary of relevant previous research. Previous applications of precast concrete systems for rapid construction of bridges, studies addressing the use of hybrid frames in building construction, and recent developments and research related to hybrid precast concrete bridge components are addressed.

The proposed systems and connections are discussed in Chapter 3. General fabrication and construction issues relating to the proposed systems and connections are also described.

Chapter 4 describes the prototype bridge that was chosen for this study. Chapter 4 also explains the finite element model attributes, including material properties, pier geometry, and the finite element modeling properties.

In order to subject the nonlinear finite element models to time history analyses, a ground motion suite was created. Chapter 5 gives details on how design spectra were developed, the ground motion database was selected, ground motions were scaled, and the final ground motions suite was chosen.

Chapters 6 through 9 address the parametric studies and their results. The parameters that were selected to vary throughout the analyses are described. The results from the quasi-static pushover analyses, the 10 percent probability of exceedance in 50 years time history analyses, and the 2 percent probability of exceedance in 50 years time history analyses are presented for both the reinforced concrete frame and the hybrid frame.

On the basis of the results summarized in chapters 6 through 9, Chapter 10 compares the two proposed systems by calculating and comparing displacement ductility demands, the onset of cover concrete spalling, the onset of bar buckling, longitudinal bar rupture, and an ultimate limit state.

In Chapter 11, a summary is presented, conclusions are discussed, and further research is recommended.

CHAPTER 2
PREVIOUS RESEARCH

In the past, precast bridge components have been used predominantly for superstructure elements. The application of precast concrete components to bridge superstructures began in the 1950s on large-scale bridge projects, such as the Illinois Tollway project, where partial-depth deck panels were utilized (Ross Bryan Associates 1988). During the decades since their first use, precast concrete superstructure components have been used extensively for bridges throughout the country. Hieber et al. (2004) summarized four common precast concrete elements used for the rapid construction of bridge superstructure applications: full-depth precast concrete deck panels, partial-depth precast concrete deck panels, multi-beam precast concrete girder bridges, and pre-constructed composite bridge superstructure systems. Shahawy (2003) and Sprinkel (1985) summarized numerous other bridge superstructure systems for rapid construction of bridges, including aluminum bridge decks, prefabricated channel concrete sections, prefabricated steel systems, and fiber-reinforced concrete deck panels.

In recent years, research relating to and applications utilizing precast concrete substructure elements have appeared. Hieber et al. (2004) and Shahawy (2003) presented summaries of precast concrete bridge substructure systems developed for use in non-seismic regions.

This chapter summarizes some of the available information relating to precast concrete bridge pier systems developed for use in non-seismic regions (Section 2.1), the development and analysis of seismic connections between precast concrete building

10

components (Section 2.2), and research related to precast concrete substructure elements for use in seismic regions (Section 2.3).

2.1 PRECAST CONCRETE PIER COMPONENTS FOR NON-SEISMIC REGIONS

LoBuono, Armstrong, & Associates (1996) studied the feasibility of using precast concrete substructure systems in the State of Florida. The first phase of the study included a survey of all state departments of transportation, as well as major Florida contractors and precast concrete producers. They found that most of the parties surveyed were concerned with the connections between the components. The report also summarized the responses from the survey related to the perceived advantages and disadvantages of various precast concrete components.

Billington et al. (1999) presented a precast segmental pier system developed for the Texas Department of Transportation (TxDOT) for use as an alternative to cast-in-place concrete in non-seismic regions. This system contains three principal components: column components, a template component, and an inverted-T cap-beam component. With this system, bridge columns are created by stacking multiple, partial-height column segments on top of one another. After the columns are in place, the template component is placed on top of the columns, and finally the cap-beam is placed on the template. The column segments, template, and cap-beam are match-cast with epoxy joints to minimize on-site construction time. Although match-casting of the joints speeds on-site construction it increases the fabrication time and labor. To reap the benefits of efficient mass production and high levels of quality control found in precast fabrication plants, a standardized system was developed.

The criteria considered when the above system was developed were summarized in Billington et al. (2001). The system should

- be economical in comparison to current practice

- conform to current weight and length constraints established for fabrication, transportation, and erection

- take advantage of the knowledge and experience possessed by precast concrete fabrication plants and contractors

- improve the durability of the bridge piers

- meet current design specifications

- be compatible with a larger range of project types.

Matsumoto et al. (2002) summarized research conducted for the TxDOT related to the design and construction of column-to-cap-beam connections. Four full-scale single column and cap assemblies were built and tested. These incorporated the following types of connections: a single-line grout pocket, double line grout pocket, grouted vertical duct, and a bolted connection. On the basis of these tests, the researchers found that the four connection types were adequate to develop the required connection in non-seismic regions. Their paper presents recommendations for material properties, development lengths, and construction tolerances for each of the connections.

Several reports have extensively reviewed precast concrete pier systems for non-seismic regions, including bridge projects that have incorporated precast concrete pier concrete components (Billington et al. 1998, FHWA 2004, Hieber et al. 2004, and Shahawy 2003).

2.2 PRECAST CONCRETE BUILDING COMPONENTS FOR SEISMIC REGIONS

In the 1960s researchers began to investigate the applicability of precast concrete components for building construction in seismic regions. Blakeley and Park (1971) investigated four full-sized precast concrete beam-to-column assemblies, connected using post-tensioning under high intensity cyclic motion. Blakeley and Park (1971) found that the energy dissipation of the post-tensioned assemblies was small prior to crushing of the concrete but increased significantly after the concrete had been crushed. They also found considerable stiffness degradation as a result of the high-intensity cyclic loading.

The basic concept of incorporating precast concrete components in building construction was expanded and investigated with numerous research projects. Many of these projects focused on the connection between the precast concrete components. The connections have been scrutinized over the years because the success of precast concrete systems in seismic areas rests on the performance of these connections. The connection's detailing and design can affect the speed of erection, stability of the structure, the performance of connection over time, strength, and ductility (Stanton et al. 1986). Numerous studies have been conducted to develop potential connections for use with precast components in seismic regions, including Stanton et al. (1986), French et al. (1989a), and French et al. (1989b). Early connections initially studied included welded steel plates, mild reinforcing steel grouted in ducts, bolted connections, post-tensioning, and threaded bars screwed into couplers precast into the column or beam.

In the early 1990s the Precast Seismic Structural Systems (PRESSS) Research Program developed recommendations for the seismic design of buildings composed of precast concrete components. An overview of the research program's objectives and

13

scope is presented in Priestley (1991). The PRESSS research program included numerous studies directly related to the connections between precast concrete columns and beams. Three such studies focusing on connections using post-tensioning were reported by El-Sheikh et al. (1999), Preistley and MacRae (1996), and Priestley and Tao (1993). Each of these studies found the concept of using post-tensioning to connect precast concrete components for seismic applications to be satisfactory. The three studies also found that the residual displacement after seismic analyses was negligible. Similar conclusions were reported by Cheok et al. (1998) and Stone et al. (1995).

In recent years, methods and guidelines have been developed for the seismic design of precast concrete structural systems. As part of the PRESSS research program, Stanton and Nakaki (2002) developed design guidelines for the five precast concrete structural systems that were part of the PRESSS Phase III building that was tested at the University of California, San Diego. Proposed design guidelines were developed for unbonded post-tensioned walls, unbonded pre-tensioned frames, unbonded post-tensioned frames, yielding frames, and yielding gap frames. Stanton and Nakaki (2002) proposed and Jonsson (2002) expanded on a displacement-based design procedure for seismic moment-resisting concrete frames composed of precast concrete components.

2.3 PRECAST CONCRETE PIER COMPONENTS FOR SEISMIC REGIONS

A few analytical and experimental research studies have investigated proposed bridge pier systems that would assimilate the post-tensioned connections developed for building construction.

Hewes and Priestley (2001) described experimental testing of four large-scale precast concrete segmental bridge column components. Unbonded vertical post-

tensioning was threaded through ducts in stacked segmental bridge column components and was anchored to the foundation and the cap-beam. The specimens were subjected to simulated seismic loading. No relative slip occurred between the segments and residual displacements were minimal.

Mandawe et al. (2002) investigated the cyclic response of six column-to-cap-beam connections that did not contain post-tensioning. Instead, the connections employed epoxy-coated mild reinforcing steel grouted into ducts. The research was concluded from the results of the experimental tests that #9 epoxy-coated straight bars could be developed to fracture in 16 bar diameters and to yield in 10 bar diameters. Mandawe et al. (2002) also concluded that grouted epoxy-coated straight bars could be used to connect precast concrete bridge pier components in seismic regions.

Sakai and Mahin (2004) and Kwan and Billington (2003a and 2003b) performed analytical studies of precast concrete bridge pier systems reinforced with various proportions of mild reinforcing steel and unbonded vertical prestressing steel. These studies found that as the proportion of prestressing steel increased, the energy dissipation and residual displacements decreased.

Billington and Yoon (2004) proposed the use of ductile fiber-reinforced cement-based composite (DRFCC) material in the precast column in regions where plastic hinging could potentially occur. From experimental tests, Billington and Yoon (2004) found that the use of the DRFCC material resulted in additional hysteretic energy dissipation. They also found that the DRFCC material maintained its integrity better than traditional precast concrete, but also increased residual displacements.

CHAPTER 3
PROPOSED PRECAST SYSTEMS

The majority of highway bridges in Washington State include large amounts of cast-in place concrete. Cast-in-place concrete bridge construction can be time-intensive and requires numerous, sequential on-site procedures. For example, first the formwork is installed, the reinforcing steel is placed, fresh concrete is poured and allowed to cure, and finally the formwork is removed.

Precast concrete bridge components offer a potential alternative to cast-in-place construction. Precast concrete bridge components may be fabricated off site in a more controlled environment, improving quality and durability. Precast components also provide an opportunity to complete tasks in parallel. For example, the foundations can be cast on site while precast components are cast off site. Other potential benefits of precast components include minimized traffic disruptions, improved work zone safety, reduced environmental impacts, improved constructability, increased quality, and lower life-cycle costs.

Although precast bridge pier components have been used in non-seismic regions, such as the state of Texas (Billington et al. 1998), research on adequate connections for seismic regions has only begun recently. The goals of this study were to investigate the seismic performance of two precast pier systems and to develop promising connections that would exhibit good seismic behavior, providing a viable alternative to the traditional cast-in-place bridge pier.

This study developed and evaluated two precast bridge pier systems for rapid construction in the seismically active region of Western Washington State. The study

focused on the application of these systems to the two-column piers that are commonly used for highway overpass structures.

The first system was a reinforced concrete system that would emulate conventional cast-in-place concrete designs. This system would employ mild reinforcing steel along with grouted ducts or openings to connect a precast concrete cap-beam and precast concrete columns.

The second system considered was a hybrid system. The connections between precast cap-beam and columns in this system would incorporate unbonded, post-tensioned tendons as well as grouted, mild reinforcing steel. The unbonded, post-tensioned tendons would be located at the center of the column's cross-section and extend from an anchor in the cast-in-place concrete foundation to another anchor located in the cast-in-place concrete diaphragm above of the cap-beam. The mild reinforcing steel bars would be unbonded over a certain length at the top and bottom of the precast columns to avoid fracture of reinforcing bars in these regions where large deformation demands are anticipated.

To garner the full potential of the systems, both the columns and cap-beam would be precast. On the basis of a specific project's construction needs, one or the other component could be precast while the other component was cast-in-place. The system could also be used with a variety of superstructure and foundation types.

The constructability and seismic performance of connections between the components are crucial. Therefore, during this study, numerous potential connections were developed for the connections in the reinforced concrete and hybrid systems. The connections were discussed with WSDOT bridge engineers, local contractors, and local

precast concrete producers to gain their insight and gather suggestions, modifications, additions, or deletions to the connections proposed for the precast pier systems. The comments and ideas gathered from these individuals are included in this chapter.

This chapter describes the reinforced concrete system in Section 3.1 and the hybrid system in Section 3.2.

3.1 REINFORCED CONCRETE SYSTEM

This section describes the reinforced concrete system, a proposed construction sequence for the reinforced concrete system, and details relating to proposed column-to-cap-beam connections.

3.1.1 System Description

The proposed reinforced concrete system consists of precast concrete columns and a cap-beam connected with mild reinforcing steel grouted into ducts or openings. The flexural strength of the frame is developed through tension yielding of the mild reinforcing steel and compression of the concrete and mild reinforcing steel. The system is applicable for a variety of cast-in-place concrete foundation types. Figure 3.1 shows a sketch of a reinforced concrete pier supported on a drilled shaft foundation.

The precast concrete columns of this system emulate traditional reinforced, cast-in-place concrete columns. The American Heritage Dictionary (2000) defines emulation as an "effort to equal another." Emulation of the cast-in-place column entails fabricating a precast column on the basis of the geometry, material properties, and details of its cast-in-place concrete counterpart. Longitudinal reinforcing steel extends from the top and bottom of the precast column, as shown in Figure 3.1. The reinforcing steel extensions are meant to facilitate the connection between the column and the other components. The

steel extending from the tops of the columns extends into ducts or openings in the precast

concrete cap-beam. A portion of the reinforcement extends through the ducts into the

cast-in-place diaphragm, while the remainder is anchored in the ducts. Bars are added

where necessary to provide the required embedment to resist the forces that develop

during a seismic event.

PRECAST
COLUMN

PRECAST
CAP-BEAM

CAST-IN-PLACE
FOUNDATION

LONGITUDINAL
REINFORCEMENT
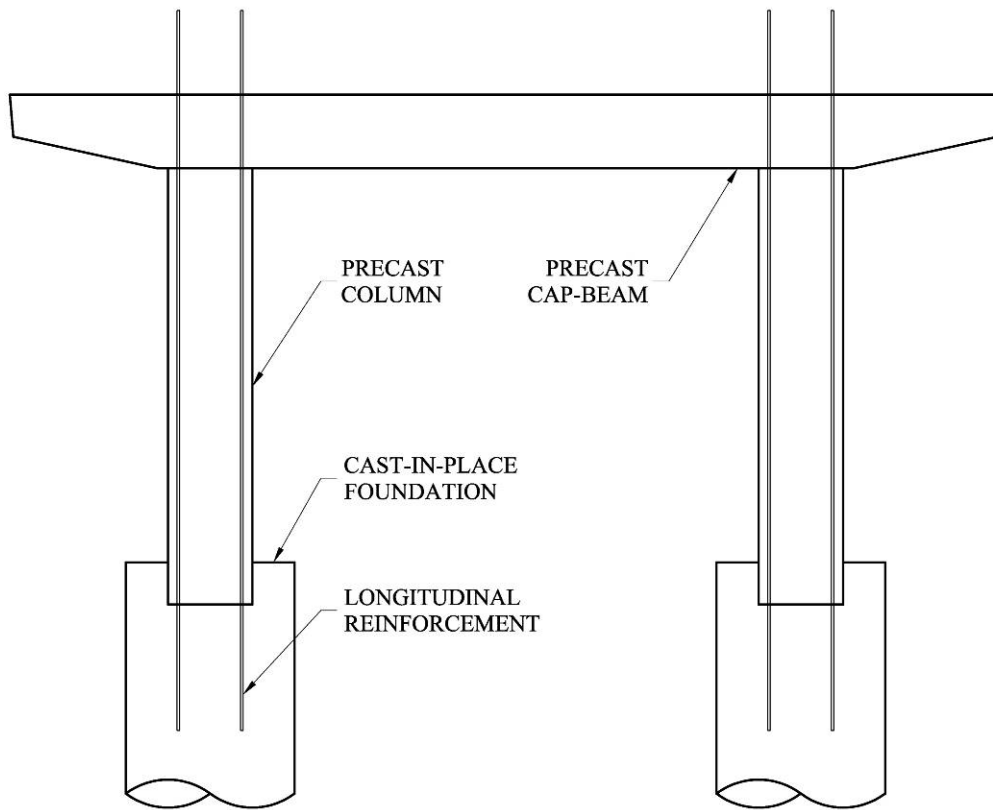
Figure 3.1: Elevation of Reinforced Concrete System Pier

With high-quality connections achieved between the components, this system is

expected to perform similarly to a conventional, cast-in-place concrete bridge pier during

a seismic event. As the pier swayed during a seismic event, the rotation caused from the

relative lateral movement between the cap-beam and the foundation would be

accommodated through the development of small cracks distributed throughout plastic-hinge regions located at the top and bottom of the columns. Figure 3.2 shows a sketch of cracks located near the base of a column. During cyclic loading, the frame would mainly dissipate energy through the hysteretic behavior of the mild reinforcing steel.
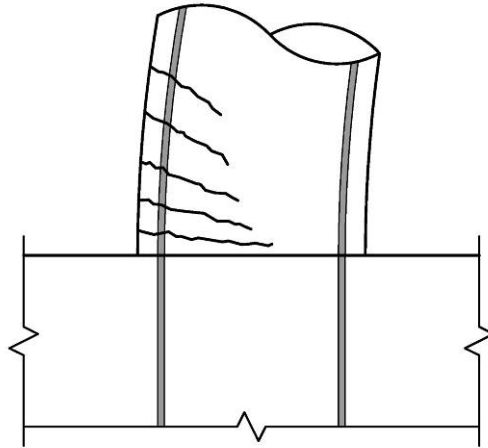
Figure 3.2: Expected Behavior of Connection in Reinforced Concrete Frames

3.1.2 Proposed Construction Sequence

The construction sequence for a bridge pier made with precast concrete components would be different than that for a cast-in-place bridge pier. A proposed construction sequence for the cast-in-place emulation system is illustrated in Figure 3.3 and is further described in this section.

1) CONSTRUCT CAST-IN-PLACE DRILLED SHAFT USING CONVENTIONAL METHODS

2) POSITION PRECAST COLUMN AND CONNECT TO FOOTING

3) POSITION PRECAST CROSSBEAM AND CONNECT TO PRECAST COLUMNS

4) PLACE GIRDERS ONTO CROSSBEAM

5) POUR BOTTOM OF CAST-IN-PLACE DIAPHRAGM

6) CONSTRUCT BRIDGE DECK EXCEPT PORTION OVER PIER(S)

7) POUR TOP PORTION OF DIAPHRAGM AND DECK OVER PIER(S)

8) CONSTRUCT TRAFFIC BARRIERS

Figure 3.3: Proposed Construction Sequence for Reinforced Concrete Frames

Step 1: Construct the Cast-in-Place Foundation

This precast concrete bridge pier system may be used with a variety of foundation types including spread footings and drilled shafts. The description provided here assumes a drilled shaft foundation. The construction of the drilled shaft and the fabrication of the precast components could occur simultaneously.

The drilled shaft foundation is constructed with conventional construction methods. Instead of pouring the concrete to the final desired elevation, the construction of the drilled shaft is stopped at a chosen distance below the final elevation. This distance is selected to provide adequate depth to allow the top of the column to be located at the correct elevation after the precast column, with longitudinal steel extensions, has been placed in the hole.

Figure 3.4 shows a sketch of the drilled shaft foundation. The dashed line labeled "construction joint with roughened surface" represents the elevation where the initial concrete pour is stopped to allow the placement of the precast column. Step 2 describes the placement of the precast column in the drilled foundation. The drilled shaft's reinforcing steel is shown extending past this elevation.

Step 2: Place the Precast Concrete Column and Connect It to the Foundation

The precast columns can be erected after the drilled shaft foundation has been constructed and the concrete is allowed to cure. When the precast column is placed, it is temporarily supported on a steel leg embedded in the bottom of the precast column, as shown in Figure 3.4. The temporary leg supports the column so that the top of the column is located at the correct elevation, whereas the bottom of the precast column is approximately 6 in. to 1 ft below the elevation for the top of the footing (Figure 3.4).

This embedment provides tolerance for the elevation of the top of the drilled shaft and increases the shear transfer between the column and the drilled shaft. Figure 3.5 shows a sketch of a precast column for the reinforced concrete frames.

SECTION A-A

ELEVATION VIEW
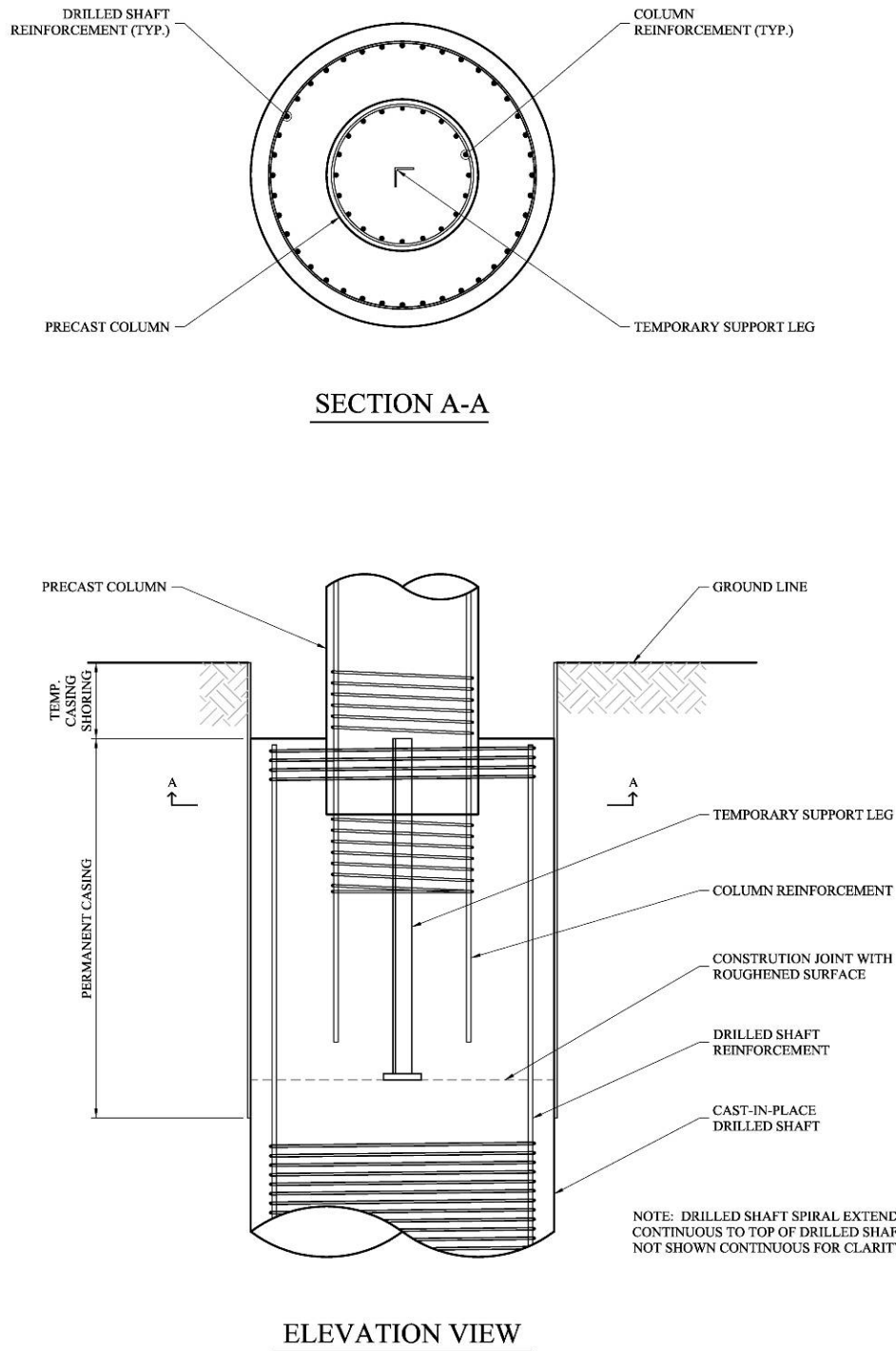
Figure 3.4: Proposed Footing-to-Column Connection for Reinforced Concrete Frames

23

EMBEDMENT LENGTH

LONGITUDINAL REINFORCEMENT

PRECAST COLUMN

A

A

EMBEDMENT LENGTH

TEMPORARY SUPPORT LEG

ELEVATION

4'-0"

SPIRAL REINFORCEMENT

LONGITUDINAL REINFORCEMENT

SECTION A-A

NOTE: COLUMN SPIRAL CONTINOUS BETWEEN EXTENTS SHOWN IN FIGURE. NOT SHOWN CONTINUOUS FOR CLARITY.
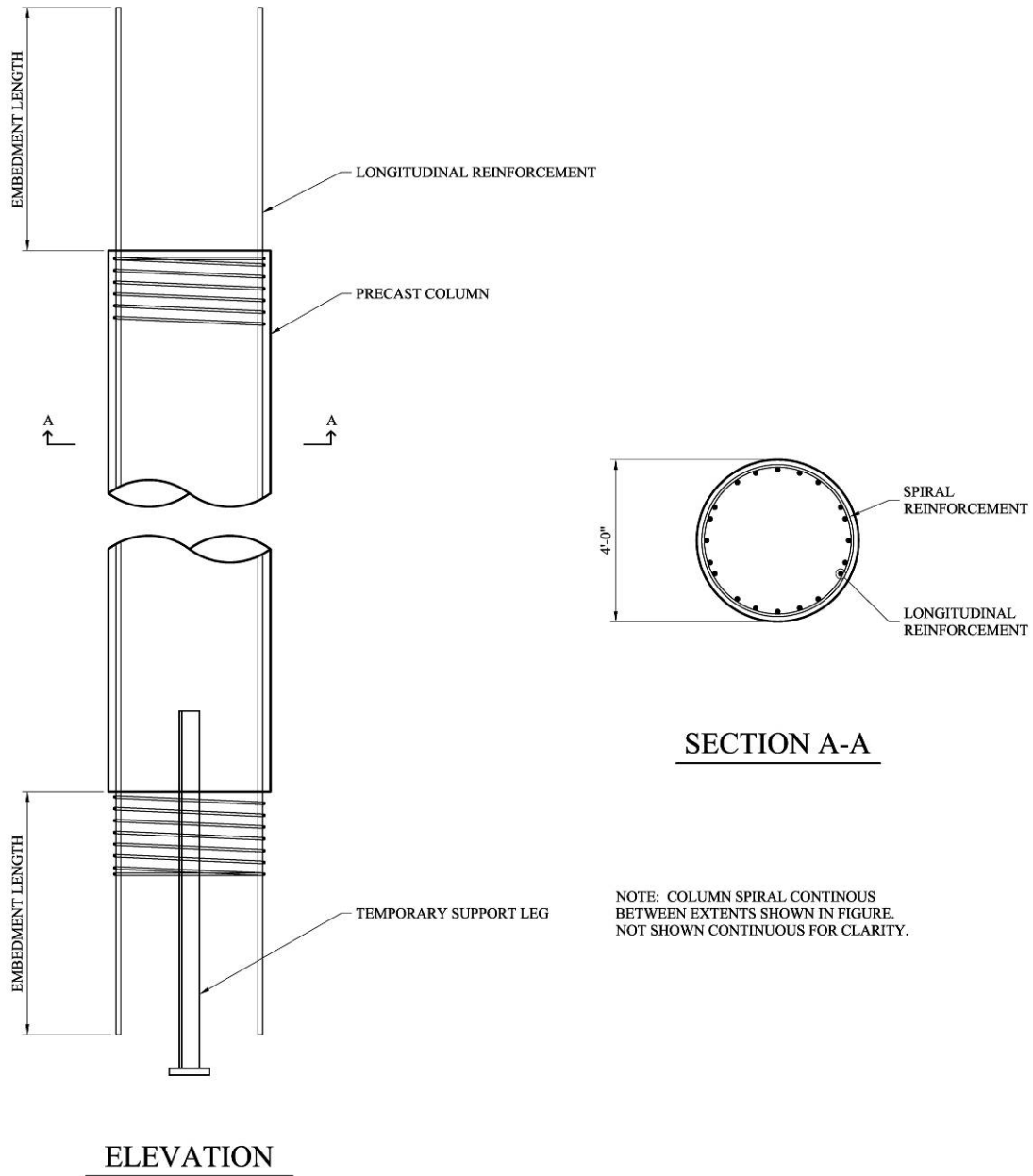
Figure 3.5: Precast Column for Reinforced Concrete Frames

The temporary support leg, shown in figures 3.4 and 3.5, supports the column before the remaining cast-in-place concrete is placed in the drilled shaft. Common structural steel shapes, such as angles or channels, may be utilized for the support leg and should be designed to support the weight of the column. The temporary support leg

protects the column's longitudinal reinforcing steel extensions against carrying any gravity load during construction.

The support leg can be outfitted with a leveling mechanism, such as a series of leveling bolts, to account for any variation in the top of the construction joint in the drilled shaft. Otherwise, shims may be placed in the drilled shaft to adjust the column to the required elevation. The temporary support leg supports the column in the vertical direction, but bracing is needed to make certain that the column's horizontal location is correct, as well as to ensure that the column is not tilted.

After the precast column has been placed and adequately supported, the remaining portion of the drilled shaft may be poured and allowed to cure. This completes the connection between the foundation and the precast column. Confinement in this region is provided by the drilled shaft's spiral reinforcement. Placement of the concrete in this region may become difficult because of the congestion caused by the column's and drilled shaft's reinforcing steel and the lack of accessibility for the vibration of the concrete. This is especially true for the area directly below the column. Self consolidating concrete may be used in this region to help alleviate the problem. To reduce the potential for air pockets developing below the column, the column base can be tapered.

Step 3: Place the Precast Concrete Cap-Beam and Connect It to the Columns

After the precast columns are securely in place, the precast concrete cap-beam can be placed onto the columns. The precast cap-beams described in this document are commonly referred to as partially raised cap beams. They make use of a precast portion, typically 3.5 ft deep, to support the girders and the deck slab during construction. A cast-

in-place diaphragm is then placed on top of the precast portion to create the full depth of the cap-beam.

The connections between the column and cap-beam are critical for constructability and good seismic performance. Two connections are proposed in Section 3.1.3. One makes use of slotted openings in the cap-beam, whereas the other makes use of a large opening in the cap-beam. A temporary collar is used during construction to position the cap-beam and provide support until the connection is grouted. The ease of placement of the cap-beam onto the columns can be directly affected by the tolerance provided in the ducts or openings in the cap-beam and the alignment of the columns. For multi-column piers, each column has to be positioned and aligned properly in relation to the other columns to ensure that the cap-beam will fit onto the columns. Templates can be used to ensure that the columns are positioned and oriented properly so the cap-beam will fit easily.

The precast portion of the cap-beam and the connections between the columns and the cap-beam should be designed to support the weight of the girders and the fresh deck slab concrete.

Step 4: Place the Girders on the Cap-Beam

After the precast concrete columns and cap-beam have been installed, the sequence follows the same steps that are commonly used with cast-in-place bridge piers and shown in WSDOT bridge standard drawings (WSDOT 2002c). The girders are placed on the cap-beam and secured in place. Care should be taken to ensure that the reinforcing bar extension from the column do not hinder the placement of the girders.

Step 5: Pour the Bottom Portion of the Cast-in-Place Diaphragm

The bottom 1-ft depth of the cast-in-place diaphragm is placed to provide lateral and longitudinal support for the bottom of the girders, so that they do not slide from their bearing location.

Step 6: Pour the Bridge Deck Slab Except for Portions over the Pier

The deck slab concrete is placed except for locations directly above the piers. This allows the girders to creep, shrink, and deflect as a result of the prestressing in the girders and the dead load from the girders and deck slab without cracking or damaging the diaphragm.

Step 7: Pour the Top Portion of the Cast-in-Place Diaphragm and the Remaining Deck Slab

The final diaphragm pour completes the connection of the girders to the pier, creating a deep cap-beam to resist live loads. This pour also makes the bridge continuous for live loads because it encapsulates the mild reinforcing bars and prestressing strand extending from the precast girder ends.

Step 8: Construct Traffic Barriers

The traffic barriers are the last components to be cast, completing the bridge construction sequence.

General Construction Issues

Depending on the geometry of the precast component, the weight may become excessive. Suggested weight limits for transportation and erection of the components range up to 180,000 lbs (WSDOT 2004). These suggested weight limits permit the use of a 48-in.-diameter column 90 ft long or a 3.5-ft by 5-ft cap-beam 65 ft long. Typical highway overpass piers constructed in Washington State fall within these limits.

3.1.3 Column-to-Cap-Beam Connections

This section describes two potential column-to-cap-beam connections for the reinforced concrete frames. Two significant difficulties that need to be overcome at the column-to-cap-beam connection are congestion of reinforcing steel and the short available embedment length. Embedment is needed to ensure adequate bond between the column longitudinal reinforcing steel extensions.   The first connection discussed is called the slotted opening connection, and the second connection is called the complete opening connection.

Slotted Opening Connection

The cap-beam is fabricated with three slots located above the column locations, as shown in Figure 3.6.   The longitudinal reinforcing bars extending from the top of the precast column are grouped, or bundled, to allow them to fit through the slots in the cap-beam when it is placed. Shims or a thin layer of grout may be used to level the cap-beam on top of the column and to ensure uniform bearing. The slots are then grouted and allowed to cure, completing the connection between the columns and the cap-beam. Use of the slotted opening connection can provide a horizontal tolerance of approximately 3 in. in all directions.

Figure 3.6 shows sketches of the cap-beam for the slotted opening connection. Figure 3.7 shows sketches of the cap-beam in place on top of the precast concrete column. In Figure 3.7 the grouping of the bars is apparent.

28

SECTION A-A

PRESTRESSING STRAND

TIE REINFORCEMENT (TYP.)

SPIRAL REINFORCEMENT

SECTION B-B

STIRRUP (TYP.)

5'-0"

PLAN VIEW

SECTION C-C
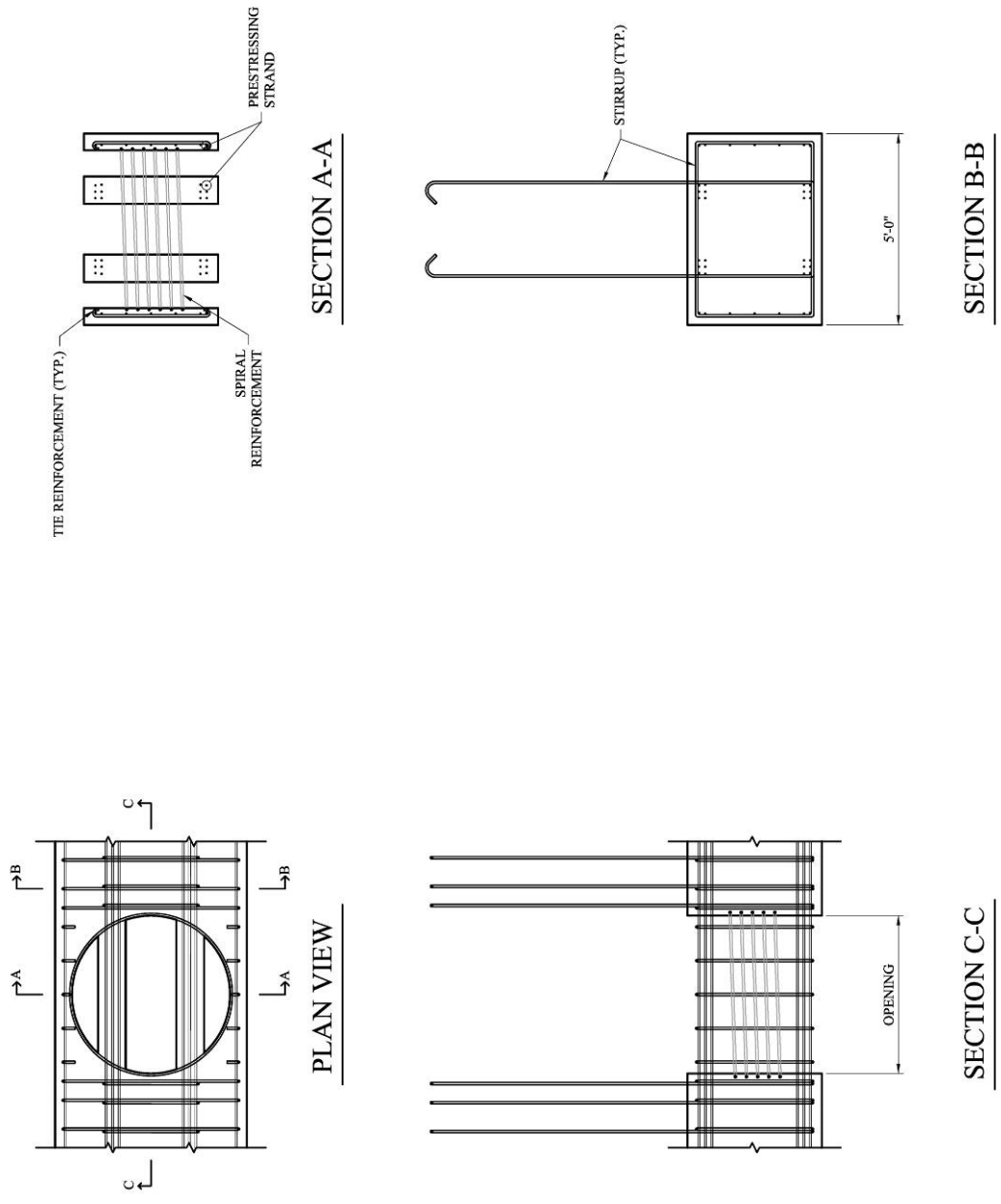
OPENING

Figure 3.6: Cap-Beam Details for Slotted Opening Connection for Reinforced Concrete Frames

29

PLAN VIEW

SECTION A-A   SECTION C-C
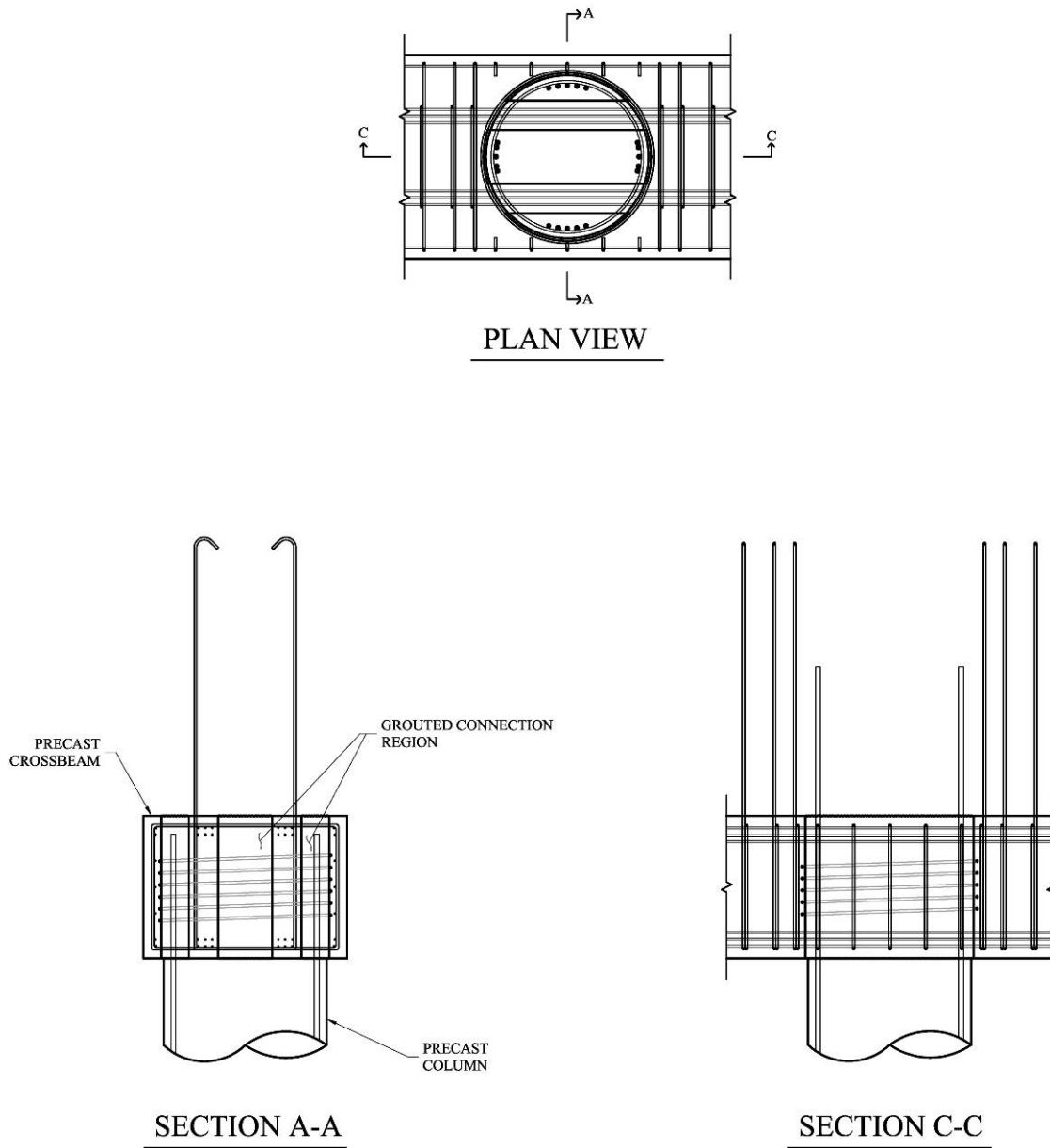
Figure 3.7: Column and Cap-Beam for Slotted Opening Connection for Reinforced Concrete Frames

The precast cap-beam contains four reinforced concrete strips between the three slots for the bundled reinforcing steel. From Section A-A in Figure 3.6 it is apparent that reinforcing and forming these strips may be difficult. The cap-beam shown in figures 3.6 and 3.7 utilizes prestressing strand to decrease the amount of steel required in the beam

30

for flexural resistance. Reducing the required area of steel in the cap-beam helps to reduce the congestion in the concrete strips. If prestressing is used, the compressive stress in the cap-beam over the column should be checked.

The concrete strips in the cap-beam above the columns must be designed for the high moments and shear forces encountered in these areas during transportation and erection. To increase the bearing strength of the cap-beam on the top of the columns, the slots may be tapered (thinner opening on the top) to reduce the potential for the grout in the slots to pop out.

Fabricating these stripped openings may present some difficulties. Although no reinforcing penetrates the opening, the openings are thin, deep, and irregularly shaped, as shown in Figure 3.7.

Grouping the column longitudinal bars, as shown in the plan view of Figure 3.7, may cause some potential problems. Grouping the bars in this fashion may significantly increase the required development lengths of the longitudinal bars in the cap-beam. This increased development length is problematic because the available development length in the cap-beam is limited by the depth of the cap-beam. Grouping of the bars may also require that additional longitudinal reinforcing steel be distributed in the column to comply with maximum spacing limits between longitudinal column bars. Grouping bars at the column-to-cap-beam connections may also decrease the efficiency of the columns at the critical location where plastic hinging occurs.

Complete Opening Connection

This connection is similar to the slotted opening connection except that instead of three slotted openings the cap-beam is fabricated with one large opening located above

the column locations.   The longitudinal reinforcing steel extending from the top of the column passes through the large opening. During construction the cap-beam is supported on a temporary collar located at the top of the column. The large opening is then grouted and allowed to cure, completing the connection. Figure 3.8 shows sketches of the cap-beam for the complete opening connection. Figure 3.9 shows sketches of the cap-beam in place on the precast concrete column.

This connection provides tolerances similar to those found in the slotted connection. The reinforcing bars are also distributed throughout the column's cross-section and the connection, which decreases the potential for pullout and provides better load distribution in the connection.

The very thin strips of concrete on both sides of the large opening in the cap-beam provide limited strength to resist bending and shear during transportation and erection. Therefore, these strips need to be designed to account for these loads, possibly incorporating prestressing steel. The large opening also introduces the potential, for the column to punch through the cap-beam. To help alleviate this potential the opening can be tapered.

It may be difficult to fabricate the large circular opening because the cap-beam's longitudinal reinforcing steel passes through the opening.

LONGITUDINAL REINFORCEMENT (TYP.)

TIE REINFORCEMENT (TYP.)

SECTION A-A

STIRRUP (TYP.)

SECTION B-B

OPENING IN CROSSBEAM

5'-4"

TIE REINFORCEMENT

STIRRUP (TYP.)

SPIRAL REINFORCEMENT

PLAN VIEW
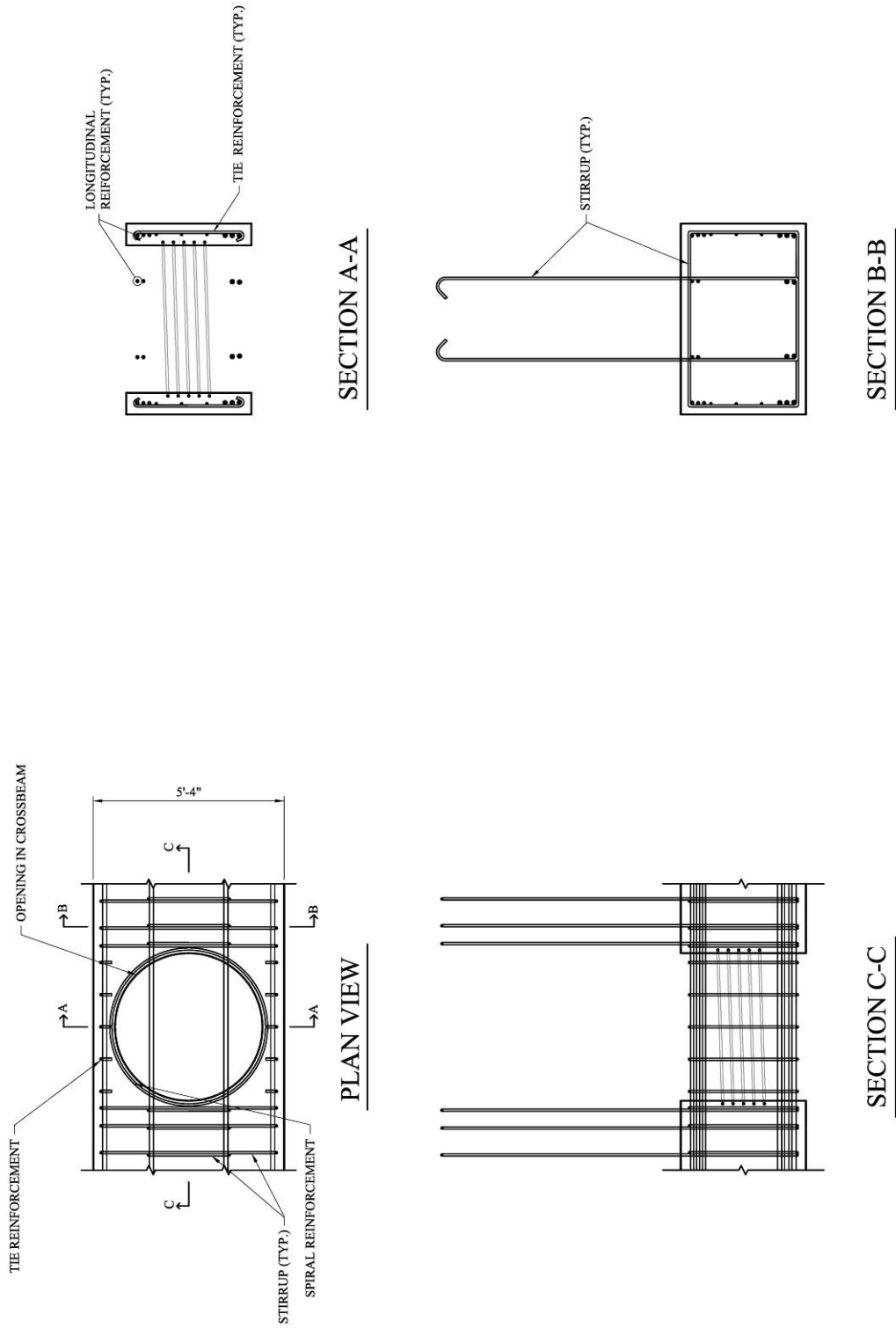
SECTION C-C

Figure 3.8: Cap-Beam Details for Complete Opening Connection for Reinforced Concrete Frames

PRECAST CROSSBEAM

GROUTED CONNECTION REGION

A

B

B

A

PRECAST COLUMN

PLAN VIEW

PRECAST CROSSBEAM

GROUTED CONNECTION REGION

TEMPORARY SHORING

PRECAST COLUMN

SECTION A-A
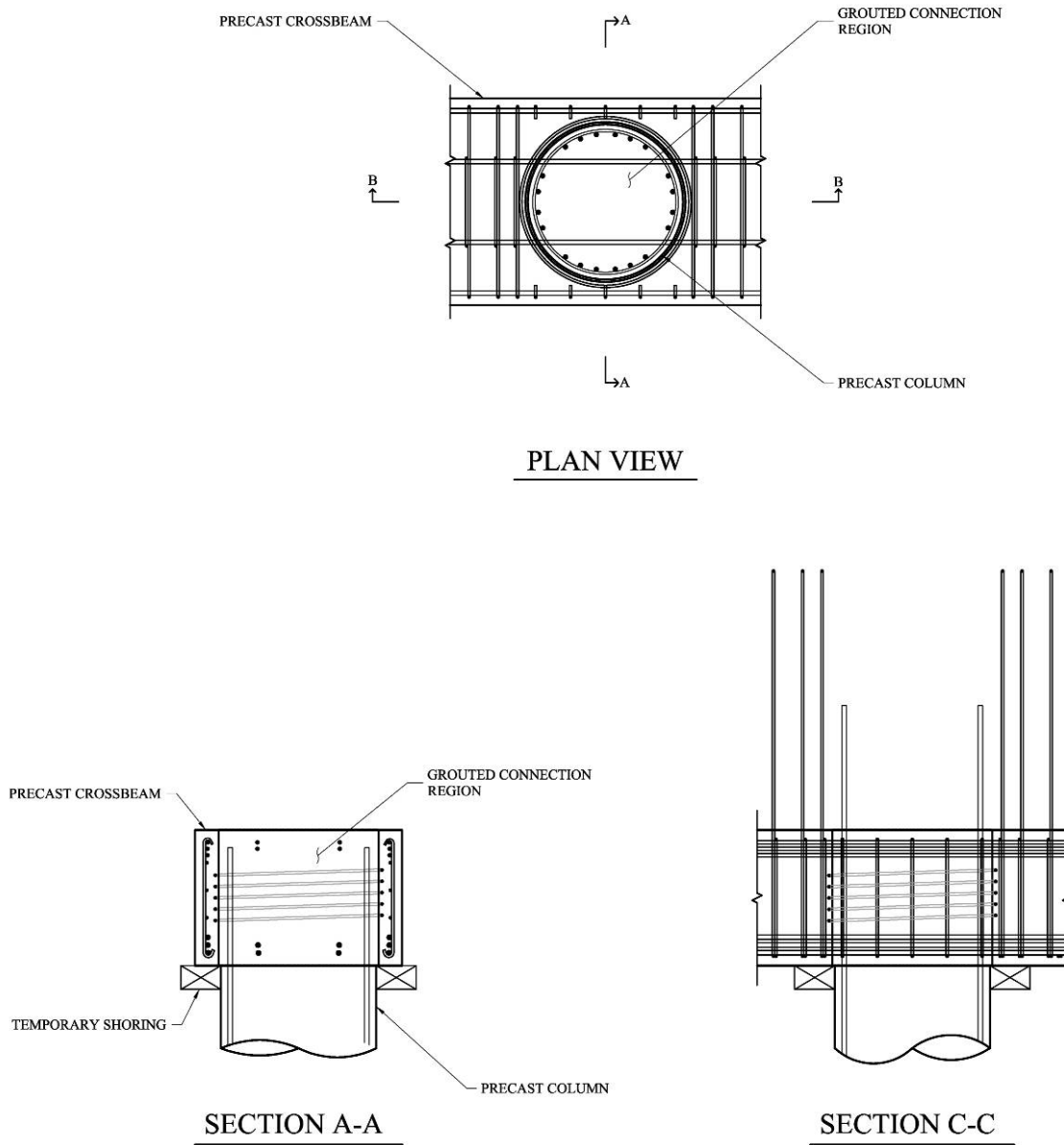
SECTION C-C

Figure 3.9: Column and Cap-Beam for Complete Opening Connection for Reinforced Concrete Frames

3.2 HYBRID SYSTEM

This section provides a brief description of the hybrid system, a proposed construction sequence, and details relating to the column-to-cap-beam connection.

3.2.1 System Description

The connections between the precast concrete columns and cap-beam in a hybrid system are achieved with mild steel deformed bars grouted or cast into ducts or openings, as well as unbonded prestressing strand. Because the connection uses both mild reinforcing steel and unbonded prestressing strand, less mild reinforcing steel is required to develop the connection than in a reinforced concrete frame. The prestressing strand is anchored into the foundation, threaded through a duct located in the center of the column, and anchored in the cast-in-place diaphragm. The system is applicable for a variety of cast-in-place concrete foundation types. Figure 3.10 shows a sketch of a hybrid pier supported on a drilled shaft foundation.
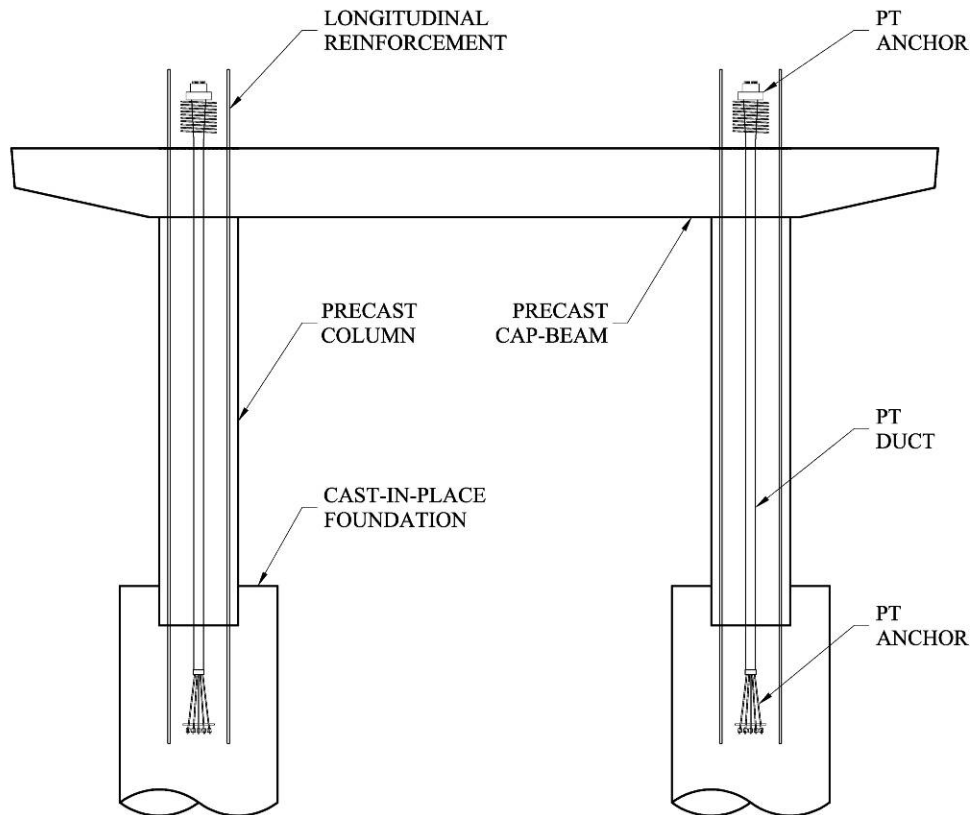
Figure 3.10: Elevation of Hybrid System Pier

The mild steel reinforcing bars in the columns are connected to the foundation and cap-beam, as shown in Figure 3.10, in a manner similar to that for the reinforced concrete frames. The prestressing tendons extend from the anchor in the foundation to an anchor located in the cast-in-place portion of the diaphragm, as shown in Figure 3.10.

The precast columns of this system are designed so that, as the pier sways during a seismic event, the rotation caused from the relative lateral movement between the cap-beam and the foundation is accommodated through one gap opening at the interfaces near the top and bottom of the column. Figure 3.11 shows a sketch of the single gap located at the base of the column. During cyclic loading, the frame dissipates energy th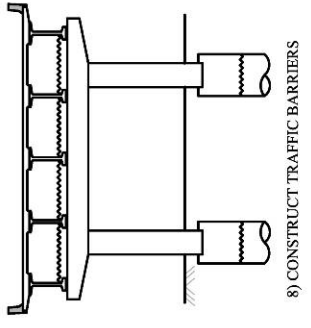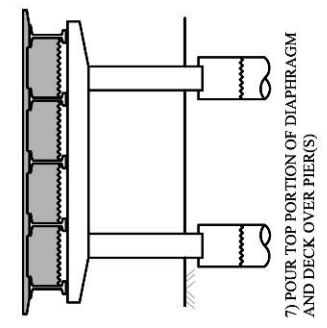rough the hysteretic behavior of the mild reinforcing steel. The unbonded post-tensioning tendons are designed so that they do not yield. By remaining elastic, the tendons do not provide any energy dissipation, but they do provide re-centering ability. The re-centering ability causes hybrid piers to have small residual displacements after an earthquake. The unbonded post-tensioning does not yield because the increase in strain as the frame sways is distributed over the length of the entire tendon. The deformed bars are anchored in the adjacent components with grouted sleeves, which provide much higher bond capacity than embedment in concrete. To prevent bar fracturing caused by large strain concentrations at the gap, it is necessary to debond the bars for a short distance on either side of the interface.

This system allows the proportion of mild reinforcing steel and unbonded prestressing tendon to be selected on the basis of the required response, either providing an increased re-centering ability or additional energy dissipation to limit maximum displacements.
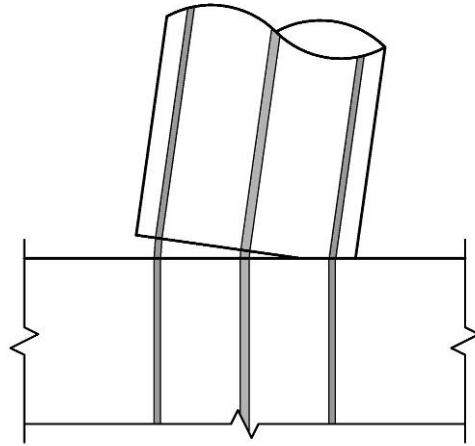
Figure 3.11: Expected Behavior of the Connection in Hybrid Frames

One important consideration is the protection of the prestressing steel from corrosion. To have confidence in the hybrid system it would be necessary to develop a corrosion protection system to reliably protect the prestressing steel from corrosion throughout the structure's design life.

3.2.2 Proposed Construction Sequence

The proposed construction sequence for the hybrid frame is very similar to that proposed for the reinforced concrete frame, except for a few significant modifications related to the stressing of the tendons. The proposed construction sequence for the hybrid frame is illustrated in Figure 3.12 and described in this section.

1) CONSTRUCT CAST-IN-PLACE DRILLED SHAFT USING CONVENTIONAL METHODS

2) POSITION PRECAST COLUMN AND CONNECT TO FOOTING

3) POSITION PRECAST CROSSBEAM AND CONNECT TO PRECAST COLUMN

4) PLACE GIRDERS ON CROSSBEAM

5) POUR BOTTOM OF CAST-IN-PLACE DIAPHRAGM AND STRESS POST-TENSIONING TENDONS

6) CONSTRUCT BRIDGE DECK EXCEPT PORTION OVER PIER(S)

7) POUR TOP PORTION OF DIAPHRAGM AND DECK OVER PIER(S)

8) CONSTRUCT TRAFFIC BARRIERS

Figure 3.12: Proposed Construction Sequence for Hybrid Frames

Step 1: Construct the Cast-in-Place Foundation

This step is the same as step 1 described in Section 3.1.2 for the reinforced

concrete system. Figure 3.13 shows a sketch of the drilled foundation for a hybrid frame.

38

DRILLED SHAFT
REINFORCEMENT (TYP.)

COLUMN
REINFORCEMENT (TYP.)

6" DIA. PT TENDON DUCT

PRECAST COLUMN

TEMPORARY SUPPORT LEG (TYP.)

SECTION A-A

PRECAST COLUMN

GROUND LINE

CRACK LOCATION

TEMP.
CASING
SHORING

PERMANENT CASING

DEAD END POST
TENSIONING ANCHOR

TEMPORARY SUPPORT LEG

COLUMN REINFORCEMENT

CONSTRUTION JOINT WITH
ROUGHENED SURFACE

DRILLED SHAFT
REINFORCEMENT

CAST-IN-PLACE
DRILLED SHAFT

NOTE: DRILLED SHAFT SPIRAL EXTENDS
CONTINUOUS TO TOP OF DRILLED SHAFT.
NOT SHOWN CONTINUOUS FOR CLARITY.

ELEVATION VIEW

Figure 3.13: Proposed Footing-to-Column Connection for Hybrid Frames

An important difference between this sketch and the equivalent sketch for the

reinforced concrete frame is that a single temporary support leg cannot be used because

39

the prestressing anchor is located directly below the center of the column. Instead, three small temporary support legs are used, allowing the post-tensioning tendons to extend out from the center of the column to the prestressing anchor in the foundation. Another important difference is the dashed line labeled "crack location" in Figure 3.13. The column is designed to crack, or develop a gap, as shown in Figure 3.11, at this location. This crack location will be described further in Section 3.2.3.

Step 2: Place the Precast Concrete Column and Connect It to the Foundation

This step is similar to step 2 for the reinforced concrete frame. Figure 3.14 shows a sketch of a column for a hybrid frame. The key differences are the inclusion of the post-tensioning strand and the designated cracking location.

The temporary support legs, shown in figures 3.13 and 3.14, allow the column to be supported at the correct elevation before the remaining cast-in-place concrete is placed in the drilled shaft. They also create a space to place the prestressing anchor. The length of the longitudinal extensions is based on the necessary bond length required to transfer the force between the drilled shaft and the column. The prestressing anchor should be located far enough below the bottom of the column to ensure that the prestressing force has transferred to the concrete by the time it reaches the base of the column.
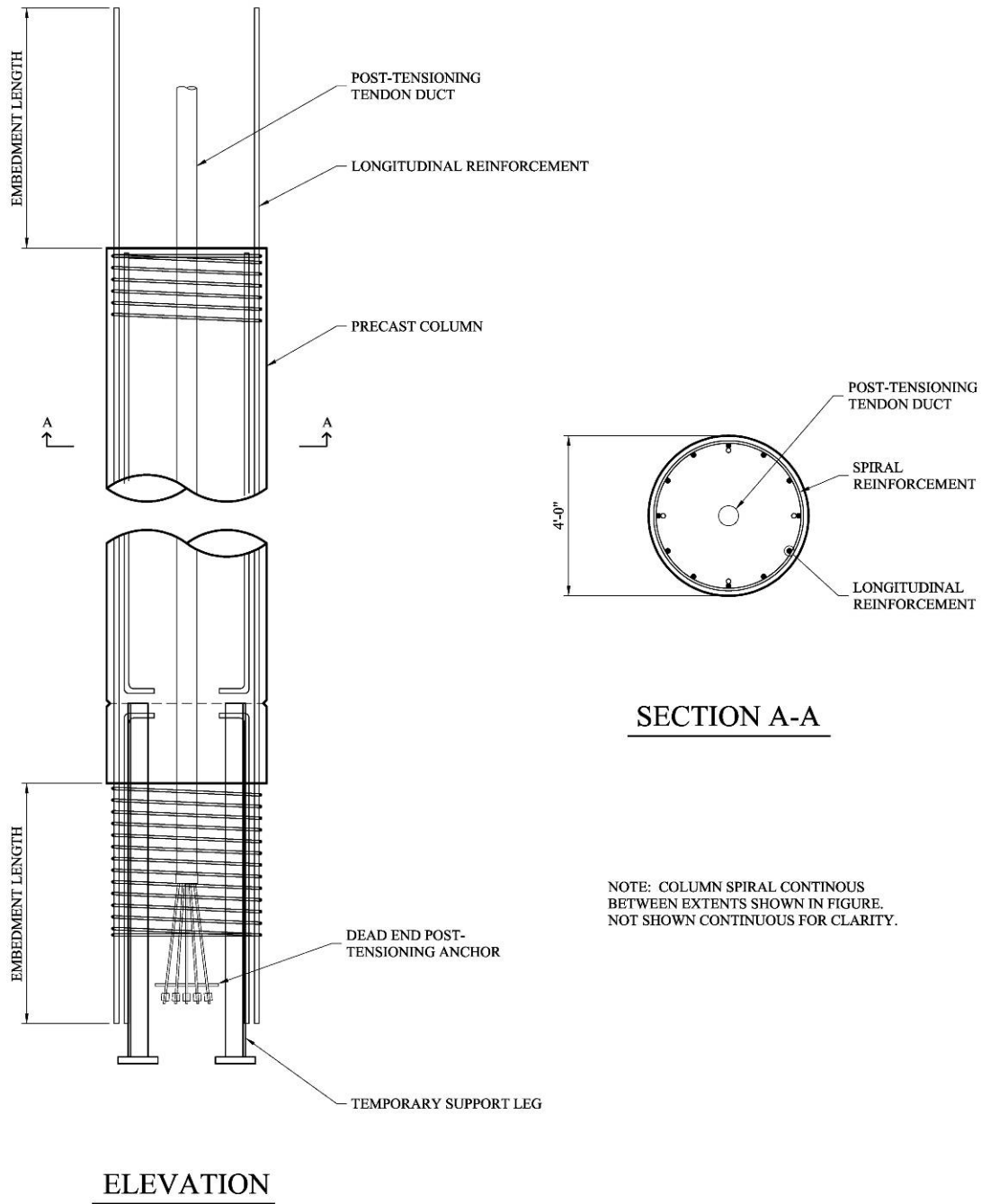
Figure 3.14: Precast Column for Hybrid Frames

After the precast column has been placed and adequately supported, the remaining portion of the drilled shaft may be poured and allowed to cure. This completes the connection between the foundation and the precast column. Confinement in this region is

provided by the drilled shaft's spiral reinforcement. Placement of the concrete in this region may become difficult because of the congestion caused by the column's and drilled shaft's reinforcement steel, the lack of accessibility for the vibration of the concrete, and the prestressing anchor. This is especially true for the area directly below the column. Self consolidating concrete may be used in this region to help alleviate the problem. To reduce the potential for air pockets developing below the column, the column base may be tapered.

Step 3: Place the Precast Concrete Cap-Beam and Connect It to the Columns

This step is similar to step 3 for the reinforced concrete frame. The important difference is the need to thread the post-tensioning strand through the ducts or opening in the cap beam and secure it until the anchor is placed in the cast-in-place diaphragm.

The connections between the column and cap-beam are critical for constructability and good seismic performance. The two connections described in Section 3.1.3 can be modified for use with the hybrid system. Essentially, the only changes required are to include the prestressing strand and to reduce the number of mild reinforcing steel bars. Reducing the number of required reinforcing bars can significantly help reduce the congestion in this connection. Section 3.2.3 describes one other connection, which employs individual splice sleeves, that may be used for the hybrid system.

Step 4: Place the Girders on the Cap-Beam

This step is the same as step 4 for the reinforced concrete system.

Step 5: Pour the Bottom Portion of the Cast-in-Place Diaphragm and the Stress Post-Tensioning Tendons

This step is the same as step 5 for the reinforced concrete system except that the depth of the pour may have to be increased to accommodate the placement of the prestressing anchors in the cast-in-place diaphragm.

After the prestressing anchors have been placed and the concrete in the diaphragm has been allowed to cure, the prestressing tendons are stressed, completing the connection between the cap-beam and the column.

Step 6: Pour the Bridge Deck Slab Except for Portions over the Pier

This step is the same as step 6 for the reinforced concrete system.

Step 7: Pour the Top Portion of the Cast-in-Place Diaphragm and the Remaining Deck Slab

This step is the same as step 7 for the reinforced concrete system.

Step 8: Construct Traffic Barriers

The traffic barriers are the last components to be cast.

General Construction Issues

Care must be taken to ensure that the prestressing steel and the anchorages are not exposed to agents that could cause corrosion. An acceptable corrosion prevention system must be developed to ensure complete protection of the strand and anchors throughout the life of the structure.

3.2.3 Details of Column-to-Cap-Beam Connections

The connections described in Section 3.1.3 could also be used for the hybrid system with slight modifications, such as the inclusion of post-tensioning strand and anchors. The number of mild reinforcing bars could also be reduced. This section describes a third connection that can be used for the hybrid system. Because the hybrid

frame requires less mild reinforcing steel, individual splice sleeves can be used to connect the cap-beam to the columns. As the cap-beam is lowered onto the columns, each individual splice sleeve receives a mild reinforcing bar. Use of individual splice sleeves makes fabrication easier because the sleeves do not need to be removed after fabrication.

Grouting of the individual splice sleeves may be difficult because of the limited clearance between the sides of the splice sleeves and the reinforcing bar. Also the limited tolerance provided by the splice sleeve may make the placement of the cap-beam on the column difficult. Figures 3.15 and 3.16 show the details for the individual splice sleeve connection.
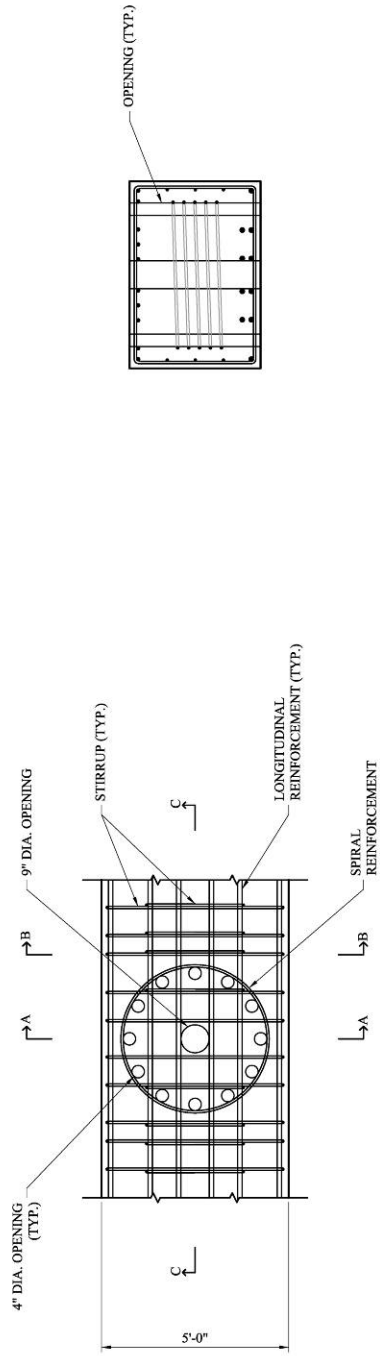
SECTION A-A
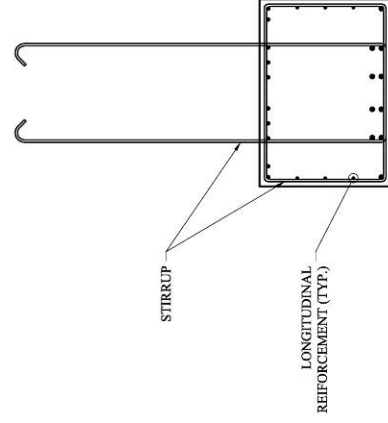
SECTION B-B
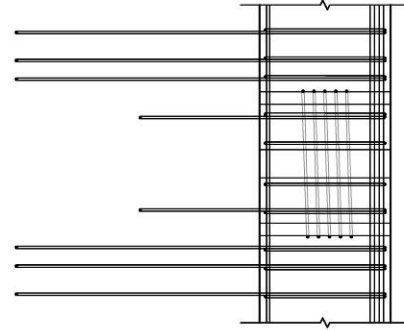
PLAN VIEW

SECTION C-C

Figure 3.15: Cap-Beam Details for Individual Splice Sleeve Connection for Hybrid Frames

PLAN VIEW

SECTION A-A   SECTION C-C
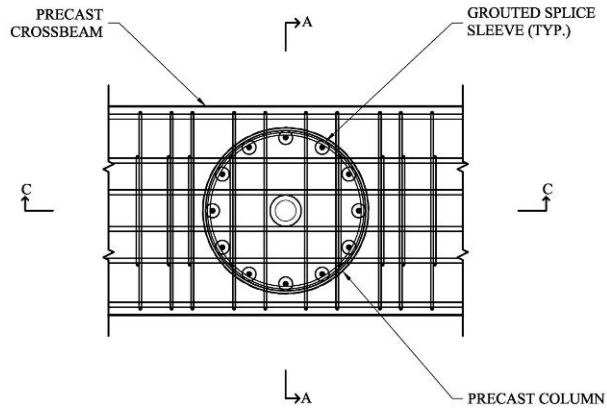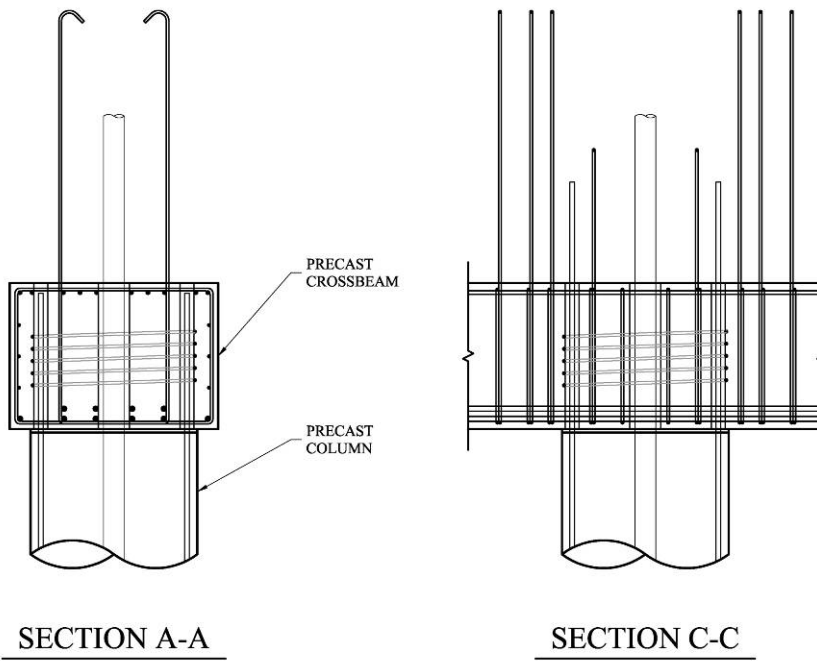
Figure 3.16: Column and Cap-Beam for Individual Splice Sleeve Connection for Hybrid Frames

CHAPTER 4
ANALYTICAL MODEL

Analytical models of the proposed bridge systems presented in Chapter 3 were developed to establish the systems' key characteristics, as well as to investigate their global responses to seismic loading.

A two-dimensional, nonlinear finite element model of a single frame was used to model the response of the proposed pier systems. The analyses included monotonic pushover analyses and dynamic earthquake analyses. An object-oriented framework used for nonlinear finite-element analyses, Open Systems for Earthquake Engineering Simulation (OpenSees), was used to create the models and perform the analyses (OpenSees 2000; Fenves et al. 2004). One of the important benefits of OpenSees is that it uses the scripting language *Tcl* to enter the commands for modeling frame geometry, applying static and dynamic loading, and defining solution formulations. The scripting language facilitates the execution of parametric studies by allowing analyses of various system configurations through repetitive looping of the analysis script. OpenSees was also selected for this study because, in recent years, OpenSees has seen increasing use, especially in the research community, and accommodates parametric studies. The *Tcl* script written during this research, which was generated to create the nonlinear finite-element models of the proposed bridge systems and perform the analyses, was described by Hieber (2005).

This chapter describes the prototype bridge that was selected for this study (Section 4.1), followed by the baseline characteristics for the proposed bridge systems described in Chapter 3 (Section 4.2), column characteristics (Section 4.3), cap-beam

characteristics (Section 4.4), and joint characteristics (Section 4.5). The methodologies used for the pushover analyses (Section 4.6) and the earthquake analyses (Section 4.7) are then described.

4.1 PROTOTYPE BRIDGE

A prototype bridge was selected to guide the development of the numerical models in OpenSees. The prototype bridge established the geometric conditions, design details, and material properties of the baseline frames for the proposed bridge systems. The following points were considered in selecting the prototype bridge from plans provided by WSDOT.

- Located in western Washington State

- Typical highway bridge configuration

- Designed with details similar to those currently used by WSDOT

The prototype bridge selected for this study was the three-span, prestressed concrete girder structure carrying State Route 18 over State Route 516 in King County, Washington (WSDOT 1996). The bridge was designed in 1995 on the basis of requirements found in the 1994 *AASHTO LRFD Bridge Design Specifications* and the *AASHTO Standard Specifications for Highway Bridges, Fifteenth Edition*.

The bridge is 297 ft long with spans of 80 ft, 137 ft, and 80 ft located on a tangent horizontal alignment. The superstructure is 38 ft wide and consists of five 74-in.-deep, Washington standard prestressed concrete girders (W74G) with a composite, reinforced concrete deck, 7.5-in. thick, supported on laminated elastomeric bearing pads. The bridge is continuous for live load.

The substructure consists of two-column, reinforced concrete piers supported on spread footings and reinforced concrete stub abutments founded on spread footings. The substructure units are aligned on a 40-degree skew. This skew was ignored during modeling. Figure 4.1 shows a typical elevation of the reinforced concrete piers for the bridge.
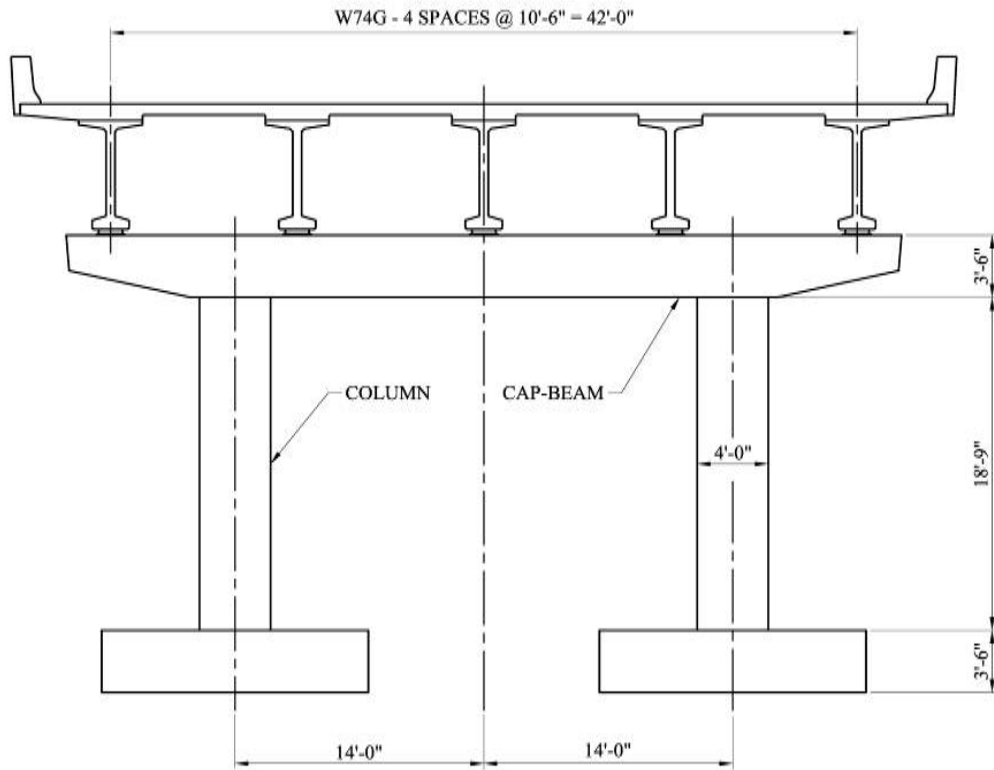
Figure 4.1: Typical Elevation of Reinforced Concrete Pier

Additional details related to the two-column, reinforced concrete piers that were of interest to this study are as follows:

- Column height, L_{col}: 225 in.
- Column diameter, D_{col}: 48 in.
- Column aspect ratio, L_{col}/D_{col}: 4.6875
- Column spacing, S_{col}: 336 in.

- Cap-beam depth (not including diaphragm), h: 42 in.
- Cap-beam width, b: 60 in.

- Column longitudinal reinforcement: 20 - #11 bars (31.2 sq in.)
- Column longitudinal reinforcement ratio, ρ: 0.017
- Column spiral reinforcement: # 6 bar, 3.5 in. pitch
- Reinforcing steel clear cover: 1.5 in.

- Design concrete density (WSDOT 2002a), γ_{con}:   0.160 kcf
- Design concrete compressive strength, $f_c^{'}$:   4000 psi (Class 4000)
- Design concrete modulus of elasticity, E_c: 4224 ksi
- Yield strength of reinforcing steel, f_y: 60 ksi
- Reinforcing steel modulus of elasticity, E_s: 29,000 ksi

- Column axial-load ratio, $P_{col}/(f_c^{'}A_g)$:   0.075 (est. dead load only)

4.2 BASELINE FRAMES

It was necessary to balance the desired accuracy of the response quantities with the time and effort required to develop the analytical models and perform the analyses. Performing a nonlinear finite-analysis on the entire bridge would have been time consuming and unnecessarily complex. Instead, simplifying assumptions, which are described in this section, were made to develop a two-dimensional, nonlinear finite element model of a single bridge pier. A single bridge pier model, or baseline frame, was created for each of the proposed bridge systems, one for the reinforced concrete frames and one for the hybrid frames. The baseline frames were created with the geometry, material, and loading characteristics of the prototype bridge described in Section 4.1.

50

Variations of these baseline frames were used in the parametric analyses, as described in chapters 6 through 9.

The baseline frame model used for the reinforced concrete frames is illustrated in Figure 4.2, whereas the baseline frame for the hybrid frames is shown in Figure 4.3. Essentially the only differences between the hybrid baseline frame and the reinforced concrete baseline frame are: the addition of prestressing and the modification of the joint characteristics. One of the two fundamental differences between the reinforced concrete baseline frame and the hybrid baseline frame was the inclusion of a prestressed tendon. To provide an anchorage point for the prestressing strand while accounting for its unbonded length into the foundation, nodes 14 and 24 and the "rigid link for pt" were included in the hybrid baseline frame. The 4-ft embedment length was selected, assuming a drilled shaft foundation.
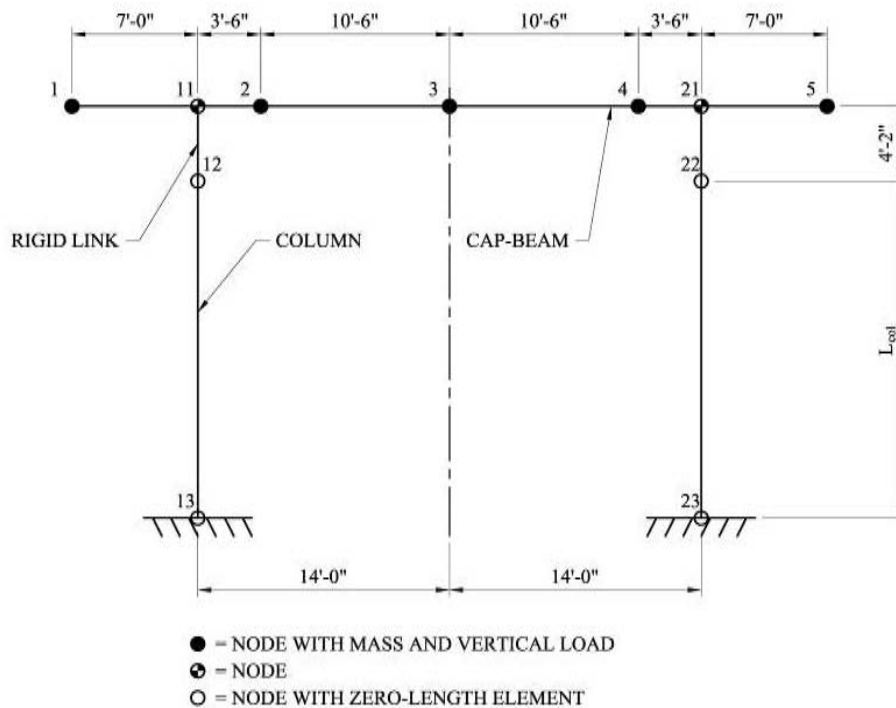
Figure 4.2: Elevation of Reinforced Concrete Baseline Frame

51
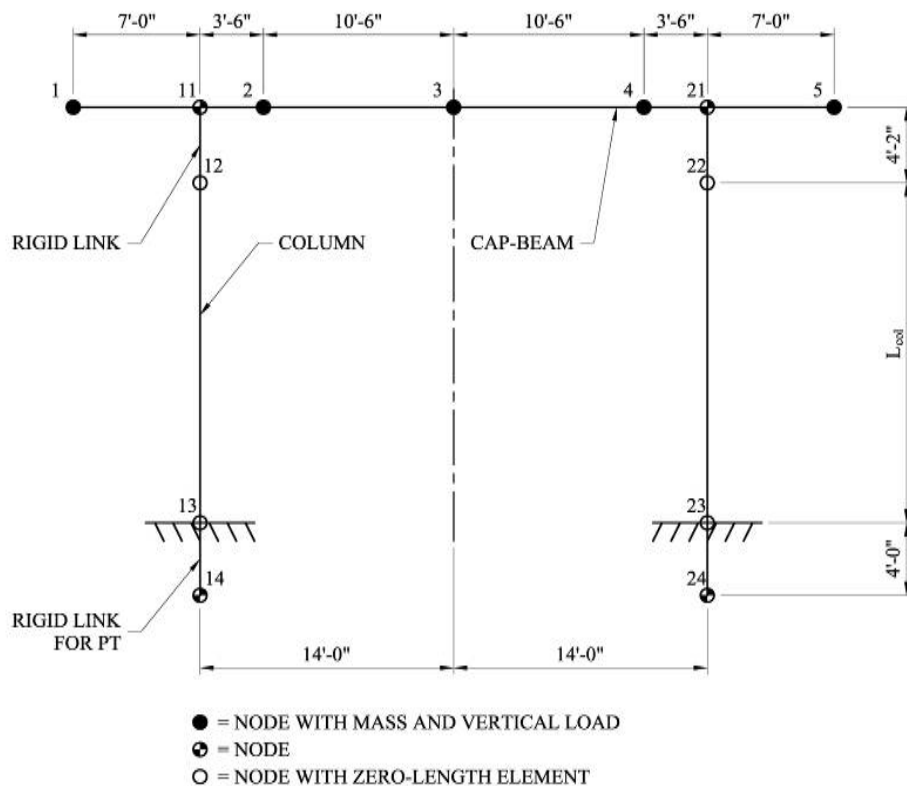
Figure 4.3: Elevation of Hybrid Baseline Frame

The three key components of the baseline frames (the columns, the cap-beam, and the joints) are discussed in sections 4.3 through 4.5.

The simplifications and assumptions used to develop the baseline frames shown in figures 4.2 and 4.3 are summarized below.

- To focus the investigation on the response of the individual frames and to reduce the number of sources of variability, the effects of the abutments and any other piers were neglected. The transverse stiffness of the deck slab was also neglected.

- The cap-beam was assumed to be infinitely rigid. This was accomplished by locking nodes 11 and 21 (shown in figures 4.2 and 4.3) against rotation, effectively reducing the system and improving convergence. Preliminary

52

analyses were performed to ensure that making the cap-beam rigid had a negligible effect on pier response.

- The foundations of the pier were assumed to be fully fixed. This assumption eliminated any soil-structure interaction, allowing the effect of pier characteristics on response to be isolated.

- The weight of the superstructure on the pier was represented with vertical load applied at the nodes corresponding to girder locations (nodes 1, 2, 3, 4, and 5). These nodes are indicated in figures 4.2 and 4.3 with a solid circle. The vertical loads were derived from the axial-load ratio (varied as described in chapters 6 through 9), the number of girders (5), and the number of columns (2) and were calculated as:

$$P_{girder} = \left(\frac{2}{5}\right)\left(\frac{P_{col}}{f_c' A_g}\right)\left(f_c' A_g\right) \tag{4.1}$$

- Horizontal mass was applied to nodes corresponding to girder locations and was obtained from dividing the vertical load by the acceleration due to gravity. The horizontal mass was included to account for the mass of the superstructure during earthquake analyses. Mass was not applied in the vertical direction because it excited very high frequency modes of vibration, possibly causing numerical errors in the finite element solution and resulting in erratic behavior.

- The columns were idealized as being mass-less; therefore, no mass was included in the model to represent the column mass.

- No viscous damping was considered in this study because of inconsistencies in pier response when damping was included. Priestley et al. (1996) indicated that Coulomb (friction) damping, radiation damping, and hysteretic damping are more common forms of damping for bridges than viscous damping. Coulomb damping typically occurs as movement takes place in bearings, connections, and joints. Radiation damping occurs as a consequence of soil-structure interaction and refers to the dissipation of energy as it spreads over an increasing volume of soil surrounding a bridge's foundation (Kramer 1996). Hysteretic damping refers to the energy dissipated during cyclic displacements and is found from the area within the hysteresis loop of the force-displacement response (Chopra 2001). Bridges have few nonstructural elements and, consequently, few obvious sources of damping that are not accounted for by hysteresis in the structural elements or radiation into the soil. Wacker (2005) found that the equivalent damping ratio for the hysteretic damping alone ranged between 10 and 25 percent. Because the damping modeled as viscous is likely much smaller than the hysteretic damping, the impact of ignoring it is likely to be small. Coulomb damping and radiation damping were also ignored during the analyses.

4.3 COLUMN CHARACTERISTICS

This section describes the characteristics of the columns created for the baseline frames, including geometric characteristics, modeling characteristics, and material characteristics.

- A constant column diameter of 48 in. was selected for the baseline frames. The basis for this assumption is presented in Chapter 6.

- The length of the column, L_{col}, was defined as the clear height between the top of the foundation and the bottom of the cap-beam. This quantity was varied as described in chapters 6 through 9.

- The circular columns were modeled as force-based, *nonlinearBeamColumn* elements with a *fiber* cross-section. The force-based elements considered the spread of plasticity along the length of the column. They were used during this study, instead of displacement-based elements, because they provided the ability to model nonlinearity with a single element for each structural member (Coleman and Spacone 2001). The *fiber* cross-section was defined by the column's cross-sectional geometry, the number of longitudinal reinforcement bars, and material properties.

- Five integration points were used along the length of the *nonlinearBeamColumn* element.

- The *fiber* cross-section contained three discretized sub-regions: the cover layer of unconfined concrete, the inner core region containing confined concrete, and the circular layer of longitudinal reinforcing steel. As part of his ongoing doctoral research study at the University of Washington, Michael Berry performed a study investigating the effect of the number of subdivisions chosen for the *fiber* cross-section and recommended the following for this study:
  o Number of subdivisions in the circumferential direction for the core: 20
  o Number of subdivisions in the radial direction for the core: 10
  o Number of subdivisions in the circumferential direction for the cover: 20
  o Number of subdivisions in the radial direction for the cover: 5

These values were used during the earthquake analyses to achieve accurate results in a reasonable time. Because the pushover analyses were less computationally intensive, the mesh size was halved to estimate the response more accurately.

- The cross-sectional area corresponding to a #11 deformed bar was used when the circular layer of longitudinal reinforcement steel was defined. By using the area corresponding to the #11 deformed bar, the actual longitudinal reinforcement ratio, ρ or ρ_{eq}, varied slightly in comparison to the target values described in chapters 6 through 9. To ensure symmetric placement of the bars about the column's axis of bending, an even number of bars was used for all of the columns.

- Material type *Concrete02* was used to model the unconfined, cover concrete. *Concrete02* uses the modified Kent-Park model to represent the concrete compressive stress-strain curve and straight lines for the rising and falling segments of the tension region. The modified Kent-Park stress-strain curve consists of a parabolic curve up to the concrete compressive strength followed by a downward sloping line to the concrete crushing strength (Kent and Park 1971). This representation is commonly used and is a modification of the one proposed by Hognestad (1951). The unloading stress-strain characteristics are based on Karsan and Jirsa (1969). *Concrete02* was selected because it provides tension strength and linear tension softening. The following material properties were used to model the unconfined, cover concrete:

  o Concrete compressive strength, $f_c^{'}$:   5.0 ksi

  o Strain at concrete compressive strength, ε_{c0}:   0.002

- o Ultimate concrete compressive strength, f_{cu}:   0.0 ksi

- o Strain at ultimate concrete compressive strength, ε_{cu}:   0.005

- o Initial slope on stress-strain curve (OpenSees 2000), E_c: $2f_c'/\varepsilon_{c0}$

- o Concrete tensile strength (MacGregor 1997), f_r: $7.5\sqrt{f_c'}$

- o Tension softening slope, E_t: $-E_c$

Although 0.003 is a common value assumed for ε_{cu} in design (MacGregor 1997),

the value of 0.005 was selected on the basis of the minimum crushing strain in

cover concrete presented by Park et al. (1982). The expression for E_c is derived

from the geometry of a parabola.

- The confined core concrete was modeled by using a new OpenSees material

  component, *Concrete04*, created by Nilanjan Mitra at the University of

  Washington. *Concrete04* is a modification of *Concrete02* that uses the pre- and

  post-peak curves proposed by Popovics (1973). Unlike the parabola used in the

  Kent-Park model that is defined by f_c' and ε_{c0} (the initial modulus of elasticity is

  found from the geometry of the parabola), the curves proposed by Popovics

  (1973) account for f_c', ε_{c0}, and E_c. As suggested by Priestley et al. (1996), the

  confined core concrete was modeled with no tension strength. On the basis of the

  properties presented above for the unconfined concrete, the following material

  properties were calculated for the confined concrete from the equations provided

  by Mander et al. (1988).

- o Concrete compressive strength, f_c':   7.0 ksi

- o Strain at concrete compressive strength, ε_{c0}:   0.006

- o Ultimate concrete compressive strength, f_{cu}:   5.9 ksi

- o Strain at ultimate concrete compressive strength, ε_{cu}: 0.020

- o Initial slope on stress-strain curve (WSDOT 2002(a)), E_c: 4722 ksi

- The deformed mild steel reinforcement was modeled by using *Steel02*, which uses the envelope from the commonly assumed bilinear stress-strain curve. To characterize the shape of the unloading branch, the Menegotto-Pinto (1973) equation is used to simulate the Bauschinger effect, in which nonlinear response develops at strains significantly lower than the yield strain (Paulay and Priestley 1992). The following material properties were used to define the reinforcing steel:

  - o Modulus of elasticity of mild steel, E_s: 29,000 ksi

  - o Yield strength of mild steel, f_y: 60 ksi

  - o Strain at yield strength of mild steel, ε_y: f_y/E_s

  - o Ultimate strength of mild steel, f_u: 90 ksi

  - o Strain at ultimate strength of mild steel, ε_u: 0.12

  - o Stain hardening ratio, *SHR*: $\left[\left(f_u - f_y\right)/\left(\varepsilon_u - \varepsilon_y\right)\right]/E_s$

- For the hybrid frames, the prestressing steel was modeled with an *elasticBeamColumn* element, with a modulus of elasticity of 28,500 ksi and negligible bending stiffness. An *elasticBeamColumn* element with negligible bending stiffness was used to represent the prestressing steel because truss elements cannot support thermal stresses in OpenSees. The prestressing was induced by applying a thermal stress to the element, as described in Wacker et al. (2005).

4.4 CAP-BEAM CHARACTERISTICS

Two components were used to represent the cap-beam. The first, shown as "Cap-Beam" in figures 4.2 and 4.3, represented the horizontal elements of the cap-beam that connect the nodes in the cap-beam. The elements were located at the elastic neutral axis of the cap-beam. The second component, shown as "Rigid Link" in the figures, was included to represent the finite size of the column-to-cap-beam joint, which was assumed to remain rigid.

It was assumed that the cap-beam would remain elastic during the analyses; therefore, it was modeled with an *elasticBeamColumn*. The cross-sectional area and the moment of inertia of the cap-beam elements were found for the prototype bridge's cap-beam, both with and without consideration for the contribution of the deck slab. The averages of these values were used for the baseline frames of this study. The resulting cross-section area and moment of inertia were 4920 in.^{2} and 6,230,000 in.^{4}, respectively. To ensure that flexural deformations in the rigid links would be negligible in comparison to the column deformations, they were given a cross-sectional area equal to the column's cross-sectional area and a moment of inertia 1000 times larger than the value used for the cap-beam.

4.5 JOINT CHARACTERISTICS

The reinforced concrete and hybrid baseline frames differed in the characteristics used to model the joints between the columns and the foundation and cap-beam (nodes 12, 13, 22, and 23 in figures 4.2 and 4.3). The joints were modeled using the *zeroLengthSection* element in OpenSees, which defines two nodes at the same location.

The zero length sections were given force-deformation relationships to represent the desired properties of the joints.

For the reinforced concrete baseline frame, the joints were given properties to represent the Lehman Bond-Slip Model (Lehman and Moehle 2000). This model was selected to represent the bond between the tension reinforcing steel and the concrete. The concrete in the joint was modeled by using *Concrete04* with the confined concrete properties defined in Section 4.4. The reinforcing steel was modeled by using a *Hysteretic uniaxialMaterial* in OpenSees with properties defined by the equations provided in Lehman and Moehle (2000).

For the hybrid baseline frame, the mild longitudinal reinforcing steel is unbonded for a given length, so the Lehman Bond Model was not used. The hybrid frames were developed to allow a crack to open at the joints at the top and bottom of the column. Therefore, it was necessary to develop properties for the joint that could simulate the opening of the joint. Wacker et al. (2005) developed a means of modeling this crack formation by modifying the reinforcing steel's stress-strain relationship by a factor to account for the unbonded length. The concrete's stress-strain relationship was also modified to account for an effective compressive depth of the foundation.

Additional information relating to the joints in the reinforced concrete and hybrid frames maybe be found in Wacker et al. (2005). Zero length elements were used to consider the stress-deformation relationship.

4.6 METHODOLOGY FOR PUSHOVER ANALYSES

In a displacement-controlled pushover analysis, the horizontal force applied to the frame is increased until the control node displaces by a specified distance. For this

study, the control node was located at the joint between the top of the rigid link and the cap-beam above the left column (node 11 in figures 4.2 and 4.3). Other characteristics of the pushover analyses included the following:

- The gravity loads described in this chapter were applied to the frame before the pushover analyses.

- For the hybrid frames, the post-tensioning force described in this chapter was applied to the frame before the pushover analyses.

- The OpenSees displacement controlled integrator, *DisplacementControl*, was used to apply the horizontal load (OpenSees 2000).

- A displacement step of 0.01 in. was used during the study.

- The frames were pushed to a maximum displacement of 24 in.

- Second-order $P - \Delta$ effects were considered by using the OpenSees geometric transformation *PDelta* (OpenSees 2000).

- A tolerance of 1.0e-6 and a maximum of 100 Newton-Raphson iterations per step were used with OpenSees's *NormDispIncr* to test force convergence (OpenSees 2000).

4.7 METHODOLOGY FOR EARTHQUAKE ANALYSES

Earthquake analyses were conducted for the 10 ground motions described in Chapter 5, five representing an event having a peak ground acceleration with a 10 percent probability of exceedance in 50 years and five representing an event having a peak ground acceleration with a 2 percent probability of exceedance in 50 years. Other characteristics of the earthquake analyses included the following:

- The gravity loads described in this chapter were applied to the model before the earthquake analysis began.

- For the hybrid frames, the post-tensioning force described in this chapter was applied to the frame before the earthquake analyses began.

- The OpenSees load pattern, *UniformExcitation*, was used with the implicit Newmark integration procedure.

- A time step, Δ_t, equal to $\Delta_{t,motion}/5$ was used for the earthquake analysis, where $\Delta_{t,motion}$ was the time step of the ground motion's time history. To ensure numerical stability, Chopra (2001) suggested employing a time step of $\Delta_t \leq T_n/\pi$ but also noted that in most earthquake analysis a smaller Δ_t, generally between 0.01 to 0.02 sec., is required to accurately define the response. To eliminate several convergence problems, it was necessary to use a time step equal to $\Delta_{t,motion}/5$ during this study. This resulted in time steps between 0.001 sec. and 0.005 sec., varying on the basis of the ground motion's original time step.

- Second-order $P - \Delta$ effects were considered by using the OpenSees geometric transformation object *PDelta* (OpenSees 2000).

- A tolerance of 1.0e-6 and a maximum of 100 Newton-Raphson iterations per step were used with OpenSees's *NormDispIncr* to test force convergence (OpenSees 2000).

CHAPTER 5
SELECTION OF GROUND MOTIONS

This chapter describes the development of the ground motions for the dynamic analyses described in chapters 7 and 9.

The principal goal of this study was to develop rapid bridge construction systems for use in Western Washington State. Therefore, the WSDOT Bridge Design Manual (WSDOT 2002a), hereafter referred to as the BDM, was consulted for guidance on typical practice relating to the seismic design of bridges. Article 4.1.5 of the BDM refers readers to the American Association of State Highway and Transportation Officials (AASHTO) Bridge Design Specifications (AASHTO 1998) and the U.S. Geological Survey's (USGS) ground acceleration maps for all seismic requirements.

To generate the suite of ground motions, two seismic hazard levels were selected, one representing events having a peak ground acceleration with a 10 percent probability of exceedance in 50 years (10 percent in 50) and one representing events having a peak ground acceleration with a 2 percent probability of exceedance in 50 years (2 percent in 50) (Section 5.1). For both levels of hazard, a database containing motions similar to those likely to occur in Western Washington State was selected (Section 5.2). Sixteen two-component time histories were chosen from the database, and an acceleration response spectrum was created for each of these ground motions (Section 5.3). The 10 percent in 50 and the 2 percent in 50 design acceleration response spectra were created as target spectra for the scaling procedure (Section 5.4). Each acceleration response spectrum was scaled to minimize the squared error between the acceleration response spectrum and the design acceleration response spectrum (Section 5.5). Finally, ten

ground motions were chosen from the scaled database for inclusion in the ground motion suite (Section 5.6).

5.1 SELECTION OF SEISMIC HAZARD LEVEL

To evaluate the seismic hazard at a given location, possible sources of seismic activity that could affect the location are identified and their potential for future seismic activity is determined. This process of evaluating the seismic hazard for a given location is referred to as a seismic hazard analysis. A seismic hazard analysis involves investigating the geologic evidence, applicable fault activity, magnitude indicators (such as potential fault rupture length or fault rupture area), tectonic evidence, historic seismicity, and instrumental seismicity to estimate the seismic hazard for the given location (Kramer 1996).

Because the proposed bridge systems were developed for use in Western Washington State rather than a particular location, a site-specific seismic hazard analysis was not performed. Instead, a suite of spectrum-compatible ground motions similar to those that could occur in Western Washington State was developed for two target levels of hazard.

The AASHTO specifications are based on a design-level earthquake with a uniform risk model of seismic hazard with a 10 percent probability of exceedance in a 50-year period (corresponding to a return period approximately equal to 475 years), as discussed in AASHTO Article C.3.10.2. To examine the global response of the proposed bridge systems to design-level earthquakes, ground motions were selected and developed that represented events with a 10 percent probability of exceedance in 50 years (10 percent in 50).

Although AASHTO requires that the 10 percent in 50 event be considered a minimum for non-critical bridges (critical bridges may require consideration of a larger event), this study did not want to limit the ground motion suite to the design-level event. The reasons for this decision were twofold. First, AASHTO may possibly increase the design level event to a 2 percent probability of exceedance in a 50-year period (2 percent in 50—corresponding to a return period approximately equal to 2475 years) (NCHRP 2001). It was important to gain confidence that the proposed bridge systems would perform satisfactorily should the design level event be increased. The second reason was that this study was interested in the response of proposed bridge systems to ground motions with a variety of probabilities of exceedance. Exposing the proposed systems to different ground motion levels provided additional insight into the global response of the proposed systems when subjected to seismic motions. To examine the global response of the proposed systems to large earthquakes, ground motions were selected and developed to represent the 2 percent in 50 event. AASHTO refers to this level event as the maximum probable earthquake.

5.2 GROUND MOTION DATABASE

The SAC Steel Project Suite, hereafter referred to as the SAC Suite, was chosen as the source of ground motion acceleration records in this study because it contains records developed for Seattle, Washington.

The SAC Suite contains scaled time histories for events of 10 percent in 50 and 2 percent in 50 for firm soil conditions in three United States locations (Boston, Seattle, and Los Angeles). The 20 two-component firm soil time histories for the Seattle area were chosen as potential time histories for this study. Of the 20 time histories, four were

identical, reducing the number of unique ground motions records to 16. The two components (fault-normal and fault parallel) were considered separately during the scaling and final selection procedure, resulting in a total of 32 time histories. Additional information regarding the ground motions contained in the SAC Suite may be found in a research report by Woodward-Clyde Federal Services (1997).

5.3 ACCELERATION RESPONSE SPECTRUM

M. A. Boit first introduced the concept of the response spectrum in 1932 (Chopra 2001). A response spectrum summarizes the maximum value of a response quantity for all possible single-degree-of-freedom systems subjected to a particular ground motion. The response spectrum is the plot of the maximum response quantity as a function of the system's natural period, T_n. Response spectra depend on the characteristics of the system, including the value of the damping ratio, ξ, and the nature of the ground motion.

An acceleration response spectrum, S_a vs. T_n (example shown in Figure 5.1), was created for each of the 32 time histories for a damping ratio, ξ, equal to 0.05. This value was chosen to correspond with the damping ratio used during the creation of the design acceleration response spectrum (Section 5.4). The linear acceleration method was used to create the acceleration response spectra (Chopra 2001).
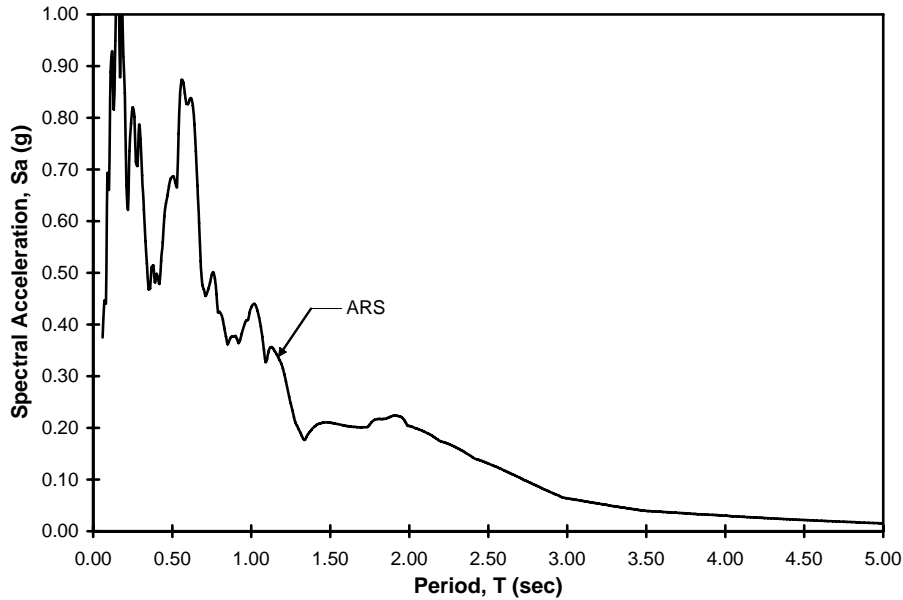
Figure 5.1: Acceleration Response Spectrum (Ground Motion 10-1)

5.4 DESIGN ACCELERATION RESPONSE SPECTRUM

The jagged shape of the acceleration response spectrum shown in Figure 5.1

represents the response of single-degree-of-freedom systems subjected to a particular

ground motion. For a different ground motion, the location of the peaks and valleys

would vary from those seen in Figure 5.1. Because of the inherent sensitivity to small

changes in period, it is not practical to use an acceleration response spectrum created

from an individual ground motion for design purposes.

For design, a design acceleration response spectrum is created by using smooth

curves or straight lines. Design response spectra are intended to represent the average

response to a variety of ground motions all having the same probability of exceedance. A

code-based design acceleration response spectrum is created with equations provided in

the applicable design code and is typically based on a damping ratio, ξ, of 0.05. For this

67

study, design acceleration response spectra were created by using Equation 5.1, taken

from AASHTO Article 3.10.6:

$$S_a = \frac{1.2ASg}{T^{2/3}} \le 2.5Ag \qquad (5.1)$$

where T_n = the period of vibration of the structure

A = the acceleration coefficient

S = the site coefficient

To utilize Equation 5.1, it was necessary to obtain values for S and A that were

consistent with Western Washington State's soil properties and seismicity. Because the

proposed bridge systems were not developed for a specific location, the default Soil

Profile (Type II) was used, as recommended by AASHTO Article 3.10.5, resulting in a

value of 1.2 for S.

The acceleration coefficient, A, which takes into account the maximum seismic

event expected to occur in a region for a given probability of exceedance, was directly

related to the seismic characteristics of Western Washington State and the seismic hazard

level chosen. To determine the value of A, Section 4.1.5 of the BDM directs designers to

the U.S. Geological Survey's (USGS) "Peak Ground Acceleration" maps (USGS 2005).

The *Pacific Northwest Seismic Hazard Map: Peak Acceleration (%g) with 10%*

Probability of Exceedance in 50 Years and the *Pacific Northwest Seismic Hazard Map:*

Peak Acceleration (%g) with 2% Probability of Exceedance in 50 Years were used for

this study. For Seattle, the USGS maps provided values for A of 0.3 for the 10 percent in

50 and 0.6 for the 2 percent in 50 events. On the basis of these S and A values, the

design acceleration response spectra were created with Equation 5.1 (see Figure 5.2).
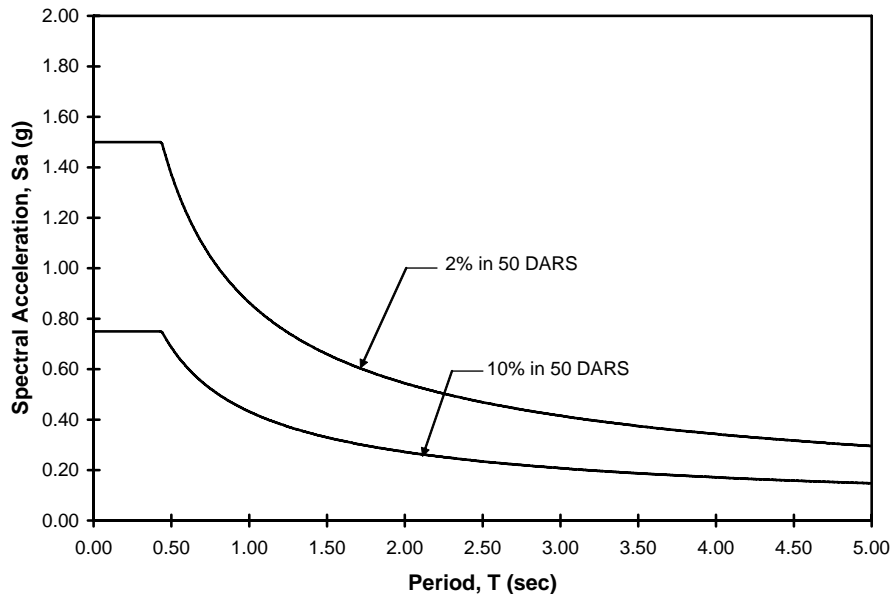
Figure 5.2: 10 Percent in 50 and 2 Percent in 50 Design Acceleration Response Spectrum

5.5 SCALING OF GROUND MOTIONS

To select a range of periods for scaling the acceleration response spectrum to the target design acceleration response spectrum, natural periods were estimated for the models, described in chapters 6 through 9, to determine the period range likely to be seen during this study. On the basis of preliminary calculations, a period range of 0.05 sec to 2.00 sec was chosen for the region.

For each of the 32 ground motions, factors were used to scale the amplitude of the acceleration response spectrum to minimize the sum of the squared error between the acceleration response spectrum and the 10 percent in 50 design acceleration response spectrum within the period range used for matching. To calculate the sum of the squared error, a uniform step of 0.005 sec was used within the period range of 0.05 sec and 2.00 sec. At each time step, the error was calculated as the difference between the

acceleration response spectrum and the design acceleration response spectrum. This value was then squared and added to the sum for the entire range used for matching. The scale factor corresponding to the minimum sum of the squared error was referred to as the motion's scale factor.

Instead of performing the same procedure for the 2 percent in 50 event, it was noted that the only difference between the 10 percent in 50 design acceleration response spectrum and the 2 percent in 50 design acceleration response spectrum was that the A value for the 2 percent in 50 design acceleration response spectrum was twice as large as the A value for the 10 percent in 50 design acceleration response spectrum. Therefore, if the same procedure was performed, the same ground motions would be chosen for the 2 percent in 50 event as were chosen for the 10 percent in 50 event, except with a scale factor twice as large. On the basis of this observation, the same five motions selected for the 10 percent in 50 event were also used for the 2 percent in 50 event, but with a scale factor that was twice as large.

5.6 SELECTION OF GROUND MOTIONS

AASHTO specifications (Article 4.7.4.3.4) suggest that five ground motions be considered for dynamic time history analysis when site-specific ground motions are not available. This resulted in a ground motion suite containing ten ground motions: five 10 percent in 50 motions and five 2 percent in 50 motions.

With the ground motions scaled, it was possible to choose which of the 32 should be included in the final ground motion suite. The five (of the 32) motions with the smallest sum of the squared error were chosen unless individual ground motions were eliminated on the basis of the following considerations. Smaller values of the sum of the

squared error were better than larger values because smaller values represented acceleration response spectrum data that were closer to the design acceleration response spectrum data. Individual ground motions were eliminated on the basis of the following considerations:

- The final scale factor was noted to verify that it did not exceed 5.0. Because the original scale factors for the ground motions (Woodward-Clyde Federal Services 1997) were scaled further during this study, the researchers felt that the ground motion amplitude could become excessively distorted if the final scale factor exceeded 5.0. The final scale factor was defined as the product of the original scale and the scale factor from this study.

- Ground motions from the same component pair were not used. The original SAC Suite ground motions contained 16 two-component histories; therefore, once one component from a pair was selected for inclusion in the ground motion suite, the other component was eliminated. This was done in an attempt to diversify the time histories selected for the final suite.

- Finally, the time histories and the acceleration response spectra were reviewed visually. Any ground motion or acceleration response spectrum that looked unusual or did not adequately match the design acceleration response spectrum was eliminated.

The ten ground motions selected for the suite are summarized in Table 5.1. The scale factor tabulated is the final scale factor, as described above. The *Peak Ground Acceleration* (PGA) shown is the PGA after all scaling was completed. Figure 5.3 shows an example of a scaled time history and scaled acceleration response spectrum

71

superimposed on the design acceleration response spectrum for an individual ground

motion. Figure 5.4 shows the average acceleration response spectrum superimposed on

the 10 percent in 50 design acceleration response spectrum. The average acceleration

response spectrum is superimposed on the 2 percent in 50 design acceleration response

spectrum and is shown in Figure 5.5. Figure 5.4 and Figure 5.5 also show the range used

for matching between the acceleration response spectrum and the design acceleration

response spectrum. Appendix A contains the final scaled, individual time histories and

acceleration response spectra for each of the ten motions.

Table 5.1: Final Ground Motion Suite

Ground Motion Name	SAC Suite Name	Scale Factor	Time Step (sec)	Duration (sec)	PGA (g)
10% in 50					
10 - 1	SE 03	2.286	0.020	60.000	0.311
10 - 2	SE 05	1.618	0.020	80.000	0.334
10 - 3	SE 23	0.635	0.005	20.000	0.303
10 - 4	SE 30	0.638	0.025	100.000	0.347
10 - 5	SE 39	0.782	0.020	80.000	0.304
2% in 50					
2 - 1	SE 03	4.572	0.020	60.000	0.622
2 - 2	SE 05	3.236	0.020	80.000	0.668
2 - 3	SE 23	1.270	0.005	20.000	0.606
2 - 4	SE 30	1.276	0.025	100.000	0.694
2 - 5	SE 39	1.564	0.020	80.000	0.608
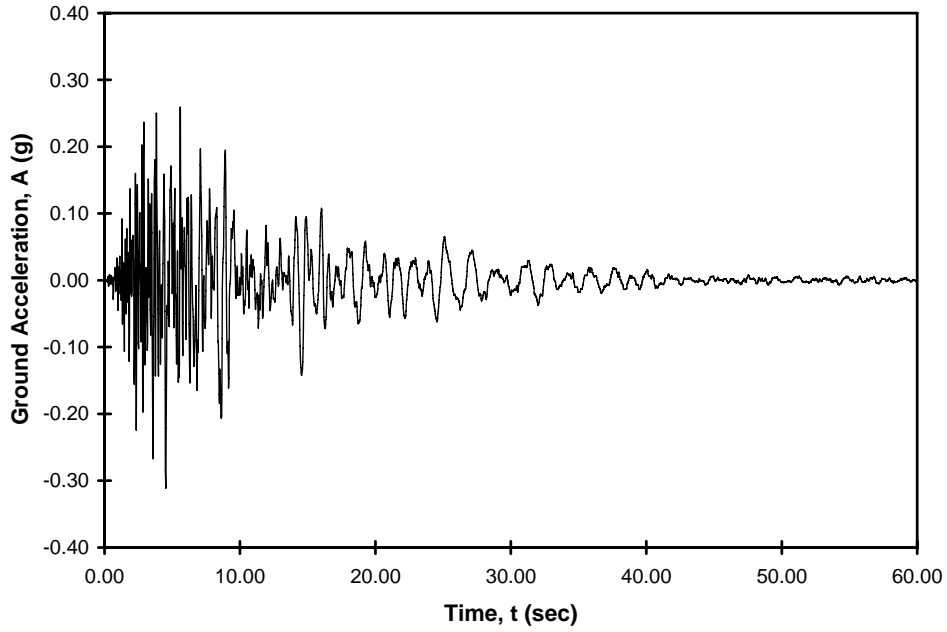
(a) Acceleration Time History
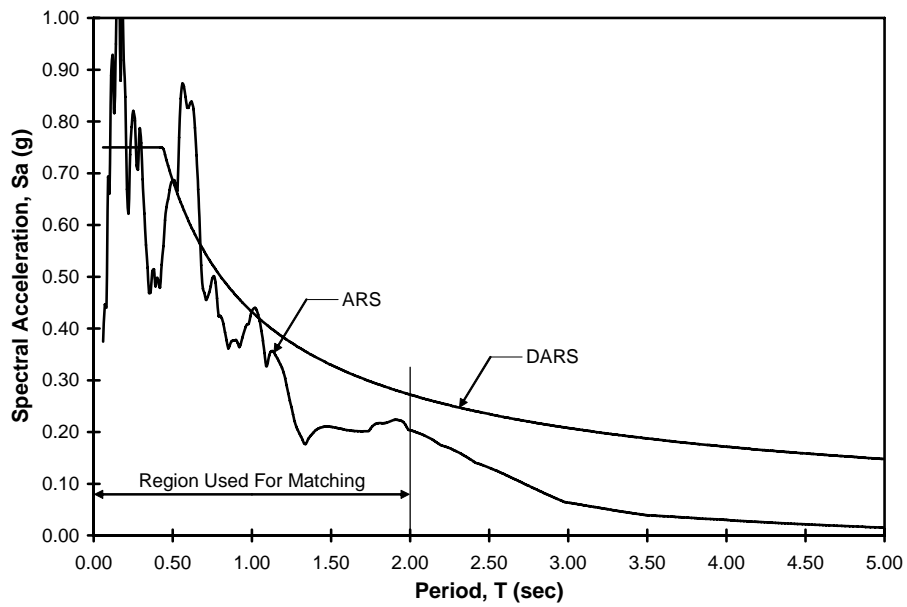
(b) Acceleration Response Spectrum and 10 Percent in 50 Design Acceleration Response Spectrum

Figure 5.3: Example of Ground Motion Characteristics (Ground Motion 10-1)
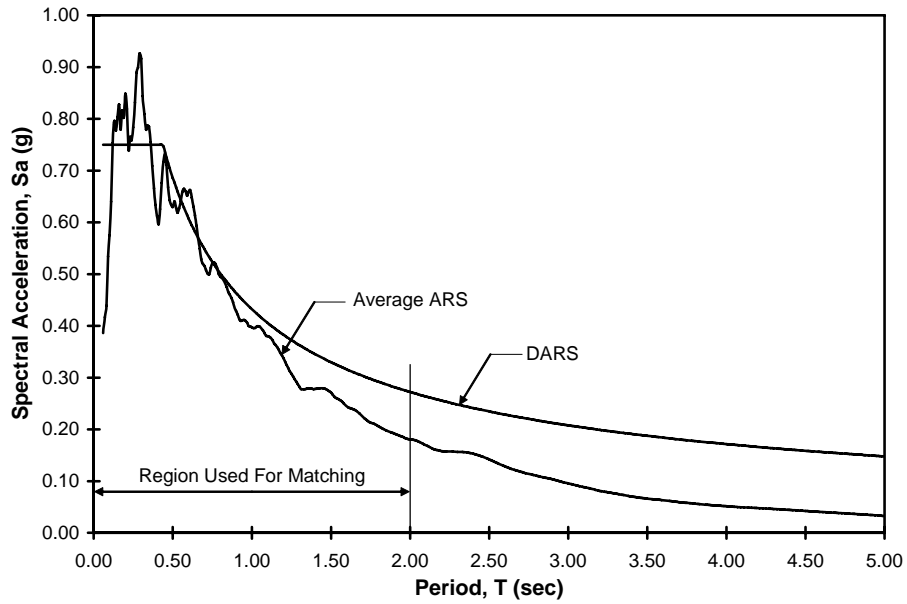
Figure 5.4: Average 10 Percent in 50 Acceleration Response Spectrum and 10 Percent in 50 Design Acceleration Response Spectrum
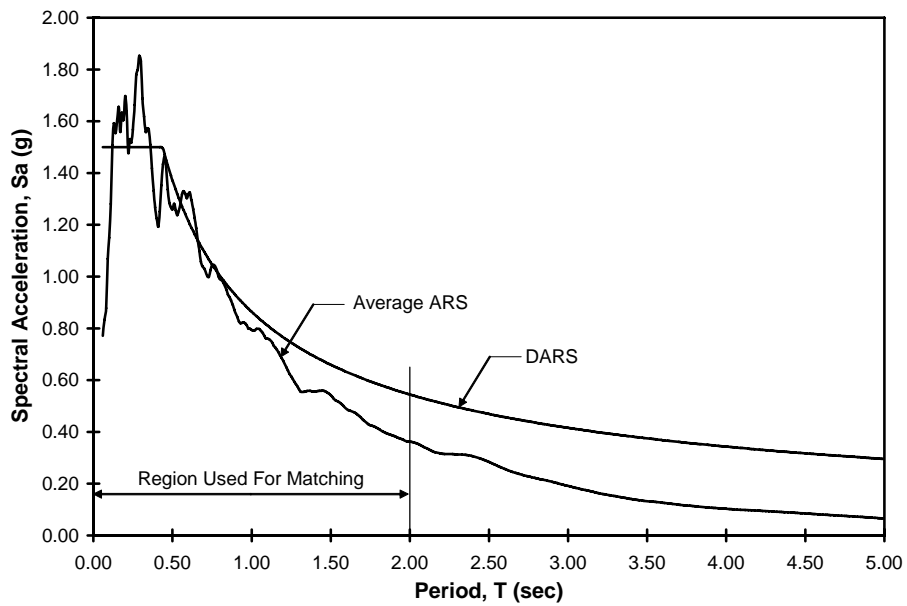
Figure 5.5: Average 2 Percent in 50 Acceleration Response Spectrum and 2 Percent in 50 Design Acceleration Response Spectrum

74

CHAPTER 6
PUSHOVER ANALYSES OF REINFORCED CONCRETE FRAMES

A parametric study was conducted to evaluate the proposed bridge systems for a variety of configurations and to provide a basis for comparing the expected performance of the reinforced concrete frames with that of the hybrid frames. The characteristics of the frames used during the parametric study were identical to those of the baseline frame described in Chapter 4, except for the parameters that were varied as described in this chapter. The parametric study included pushover analyses and earthquake analyses of the reinforced concrete frames and the hybrid frames. This chapter focuses on the pushover analyses of the reinforced concrete frames.

A pushover analysis is a common means of determining force-displacement characteristics by applying a unidirectional load or displacement of increasing magnitude to a frame (Kwan and Billington 2003a). Pushover analyses were conducted to quantify first yield, initial cracked properties, estimated nominal yield displacement, and maximum strength.

This chapter describes the parameters that were varied for the study (Section 6.1), key characteristics with which to compare pushover analyses (Section 6.2), and the results obtained from these analyses (sections 6.3 through 6.5).

6.1 RANGE OF REINFORCED CONCRETE PARAMETRIC STUDY

To evaluate the performance of the proposed reinforced concrete system for a variety of configurations, it was necessary to select parameters to vary during the parametric study.

The results of the pushover analyses were normalized to reduce the number of variables that required consideration. Suitable variables for use in the normalization process can be selected by considering an idealized circular column in which the concrete has no strength and in which the longitudinal reinforcement is elasto-plastic and is uniformly distributed over the column's cross-section. The horizontal resistance, H_o, of a two-column frame under fully plastic conditions is given as:

$$H_o = 2\left[\left(\frac{2}{L_{col}}\right)\left(\frac{\pi D_{col}^3}{32}\right)(\rho f_y)\right] \tag{6.1}$$

where L_{col} = column clear height between the top of the foundation and the bottom of the cap-beam

D_{col} = diameter of the column

ρ = longitudinal reinforcement ratio, A_s/A_g

f_y = longitudinal reinforcement yield strength, taken as 60 ksi

In this study, the normalized horizontal force, H_{normal}, was taken to be proportional to H/H_o, resulting in:

$$H_{normal} = \frac{HL_{col}}{D_{col}^3 \rho f_y} \tag{6.2}$$

where H is the effective horizontal force on the force-displacement curve resulting from a pushover analysis that considers second order $P - \Delta$ effects.

Preliminary analyses were performed to determine the variables with the most significant effect on pier performance. Figure 6.1 shows the normalized horizontal force, H_{normal}, plotted against the drift ratio, Δ/L_{col}, for column diameters equal to 36, 48, and 60 in. It is apparent from the figure that the column diameter only has a small influence

76

on the properties of the normalized force-displacement curve in the inelastic range.

Because of this small sensitivity, a column diameter of 48 in. was used for all frames in

this study. The information provided in this study can be scaled to provide estimates of

the desired forced-displacement response for frames with other column diameters.
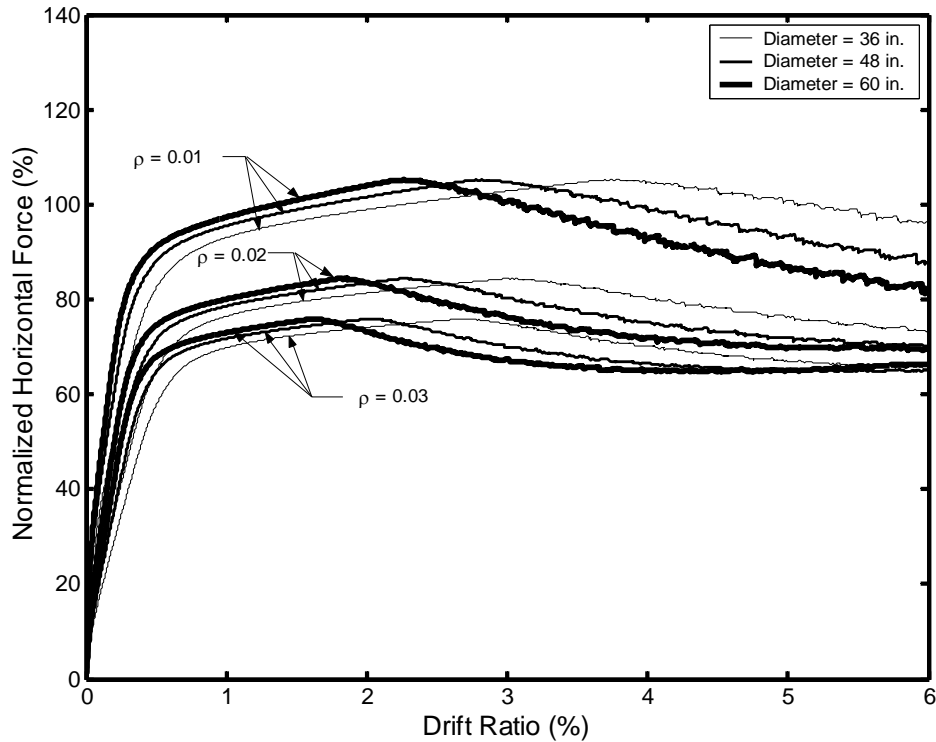
Figure 6.1: Effect of Column Diameter on Pushover Response

The following three parameters most significantly affected the results from the

preliminary pushover analyses and were chosen as the parameters to be varied during this

study:

- column aspect ratio, L_{col}/D_{col}
- longitudinal reinforcement ratio, $\rho = A_s/A_g$
- axial-load ratio, $P_{col}/(f'_c A_g)$

6.1.1 Column Aspect Ratio, L_{col}/D_{col}

The column aspect ratio was defined as the length of the column divided by the diameter of the column, L_{col}/D_{col} .

The importance of including L_{col}/D_{col} as one of the three parameters is evident by considering an idealized circular column in which the concrete has no strength and in which the longitudinal reinforcement is elastic and is uniformly distributed over the column's cross-section. Under elastic conditions the drift ratio, Δ/L_{col} , is proportional to $H_o L_{col}/D_{col}$. The impacts of varying the column aspect ratio are seen in the results for displacement and drift ratio corresponding to the states described in Chapter 10, the peak displacement encountered during earthquake analyses, and the maximum strength.

Article 1120.04 (5) of the WSDOT Design Manual (WSDOT 2002 b) requires a minimum vertical clearance of 16.5 ft for a bridge over a roadway. For a column diameter of 48 in., this resulted in a minimum L_{col}/D_{col} ratio of 4.125. This value was increased to 5, 6, and 7 for the L_{col}/D_{col} for this study.

6.1.2 Longitudinal Reinforcement Ratio, ρ

The longitudinal reinforcement ratio was defined as the area of the longitudinal mild steel divided by the gross area of the column's cross-section, A_s/A_g . Section 9.2.1d of the WSDOT Bridge Design Manual (WSDOT 2002a) provides an allowable range of 0.01 to 0.06 for a column's longitudinal reinforcement ratio, ρ . Priestley et al. (1996) also suggested a range of 0.005 to 0.04 for ρ with a practical design range of 0.01 to 0.03. The prototype frame described in Chapter 4 had a ρ value of 0.017.

On the basis of the allowable and suggested ranges, ρ values of 0.005, 0.01, 0.02, and 0.03 were chosen for this study, even though the ρ value of 0.005 does not fall within the permissible range provided by the WSDOT Bridge Design Manual. This low value was included to allow comparisons with the hybrid frames described in Chapter 8.

6.1.3 Axial-Load Ratio, $P_{col}/(f_c' A_g)$

The axial-load ratio was defined as the compressive axial-load on a column divided by the product of the concrete compressive strength and the gross area of the column's cross-section, $P_{col}/(f_c' A_g)$. P_{col} is the compressive axial-load for one column; therefore, the two-column frame's total load is two times P_{col}. Article 5.10.11.4.1 b of the AASHTO LRFD Bridge Design Specification (AASHTO 1998) permits axial-load ratios of up to 0.20. The prototype bridge described in Chapter 4 had a $P_{col}/(f_c' A_g)$ value of approximately 0.075. Therefore, on the basis of AASHTO's allowable range and the prototype bridge, axial-load ratios of 0.05, 0.10, and 0.15 were selected for this study.

6.1.4 Frame Designation

Thirty-six unique combinations occurred as a result of varying these three parameters. Frames were identified by the combination of their column aspect ratio, longitudinal reinforcement ratio, and axial-load ratio. For example, 5.005.05 was a frame with $L_{col}/D_{col} = 5$, $\rho = 0.005$, and $P_{col}/(f_c' A_g) = 0.05$; 7.020.10 was a frame with $L_{col}/D_{col} = 7$, $\rho = 0.020$, and $P_{col}/(f_c' A_g) = 0.10$.

6.2 KEY CHARACTERISTICS OF PUSHOVER RESPONSE

This section describes the key characteristics that were calculated from the results of the pushover analyses. These characteristics described the characteristics of the

individual frames as well as provided the basis for comparing the expected performance of the reinforced concrete frames with that of the hybrid frames. Sections 6.4 through 6.6 discuss the results obtained from the analyses.

6.2.1 Uncracked Properties

The uncracked stiffness, $k_{uncracked}$, represented the tangent stiffness of the force-displacement curve resulting from a pushover analysis. $k_{uncracked}$ was established from an eigenvalue analysis in OpenSees. The natural circular frequency of vibration, ω_n, was determined from the eigenvalue analysis of the frame before load was applied. From the known quantity ω_n and the mass, m, the uncracked stiffness was found from the following relationship:

$$k_{uncracked} = \omega_n{}^2 m \tag{6.3}$$

The uncracked natural period, $T_{n,uncracked}$, was calculated from ω_n with Equation 6.4.

$$T_{n,uncracked} = \frac{2\pi}{\omega_n} \tag{6.4}$$

6.2.2 First Yield

First yield was defined as the point at which the extreme tensile steel of the column first reached its yield strain or the column concrete compressive strain reached 0.002, whichever occurred first. $F_{firstyield}$ was defined as the effective force when first yield occurred, and $\Delta_{firstyield}$ was defined as the corresponding displacement at first yield.

$F_{firstyield}$ and $\Delta_{firstyield}$ are shown on the idealized force-displacement curve of Figure 6.2.

The drift ratio at first yield was given by $\Delta_{firstyield}/L_{col}$.
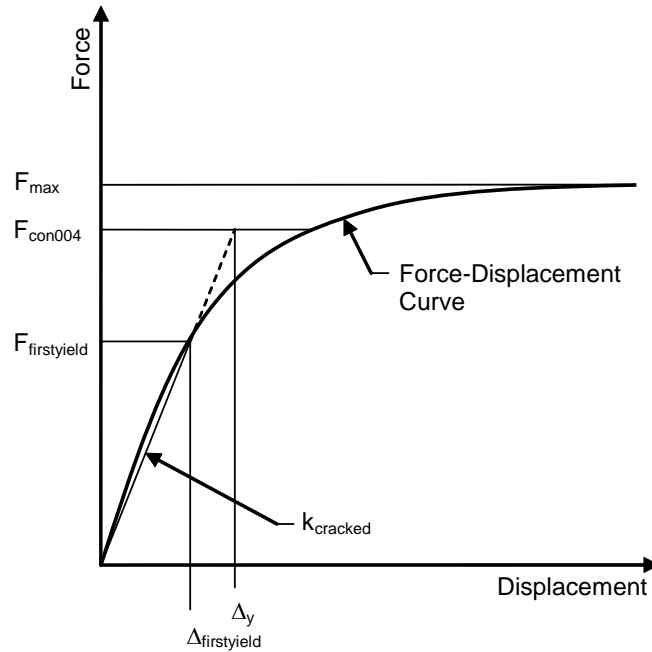
Figure 6.2: Idealized Force-Displacement Curve (Camarillo 2003)

6.2.3 Cracked Properties

The initial cracked stiffness, $k_{cracked}$, was found from the secant stiffness through

the first yield on the force-displacement curve and is shown in Figure 6.2. The following

relationship was used to calculate the initial cracked stiffness:

$$k_{cracked} = \frac{F_{firstyield}}{\Delta_{firstyield}}$$ (6.5)

The cracked natural period, $T_{n,cracked}$, was determined from the known values of

$k_{cracked}$ and mass, m , with Equation 6.6.

81

$$T_{n,cracked} = 2\pi \sqrt{\frac{m}{k_{cracked}}}$$

(6.6)

6.2.4 Stiffness Ratio, $k_{cracked}/k_{uncracked}$

The stiffness ratio was defined as the cracked stiffness divided by the uncracked stiffness. This ratio represented the loss of stiffness encountered as the force-displacement relationship became nonlinear as a result of cracking in the concrete columns.

6.2.5 Effective Force at Concrete Strain of 0.004, F_{con004}

F_{con004} corresponded to the effective force when the concrete compressive strain of 0.004 was first reached. It is illustrated in Figure 6.2.

6.2.6 Nominal Yield Displacement, Δ_y

To calculate displacement ductility (Chapter 10), it was necessary to define a yield displacement, Δ_y. The loading applied during the pushover analyses resulted in yielding of the frames and force-displacement curves that were nonlinear, as is seen in Figure 6.2. As suggested by Priestley et al. (1996), the force-displacement curve was idealized with an equivalent bilinear relationship by extrapolating $k_{cracked}$ up to F_{con004} to obtain Δ_y. The nominal yield displacement is shown in Figure 6.2 and was found with the following relationship:

$$\Delta_y = \frac{F_{con004}\Delta_{firstyield}}{F_{firstyield}}$$

(6.7)

6.2.7 Maximum Force, F_{max}

The maximum force, F_{max}, was defined as the largest lateral force achieved during the pushover analysis.

6.3 TRENDS IN STIFFNESS RATIO

The stiffness ratios calculated from the pushover analyses are discussed in this section. Table 6.1 summarizes the natural periods and stiffnesses of the 36 frames.

Table 6.1: Natural Periods and Stiffnesses, Reinforced Concrete Frames

Frame	Mass (kip-sec/in.^{2})	$T_{n,uncracked}$ (sec)	$T_{n,cracked}$ (sec)	$k_{uncracked}$ (kips/in.)	$k_{cracked}$ (kips/in.)	$\dfrac{k_{cracked}}{k_{uncracked}}$
5.005.05	2.342	0.262	0.544	1348.3	312.5	0.232
5.005.10	4.684	0.370	0.656	1348.3	430.3	0.319
5.005.15	7.026	0.454	0.740	1348.3	507.2	0.376
5.010.05	2.342	0.256	0.485	1410.6	393.2	0.279
5.010.10	4.684	0.362	0.616	1410.6	487.8	0.346
5.010.15	7.026	0.443	0.704	1410.6	559.4	0.397
5.020.05	2.342	0.245	0.407	1534.4	559.3	0.364
5.020.10	4.684	0.347	0.544	1534.4	625.1	0.407
5.020.15	7.026	0.425	0.639	1534.4	678.8	0.442
5.030.05	2.342	0.238	0.366	1636.6	689.7	0.421
5.030.10	4.684	0.336	0.499	1636.6	741.9	0.453
5.030.15	7.026	0.412	0.594	1636.6	785.2	0.480
6.005.05	2.342	0.331	0.690	842.8	194.3	0.231
6.005.10	4.684	0.468	0.829	842.8	269.1	0.319
6.005.15	7.026	0.574	0.935	842.8	317.6	0.377
6.010.05	2.342	0.324	0.616	882.1	243.3	0.276
6.010.10	4.684	0.458	0.781	882.1	302.9	0.343
6.010.15	7.026	0.561	0.893	882.1	348.1	0.395
6.020.05	2.342	0.310	0.517	960.1	345.8	0.360
6.020.10	4.684	0.439	0.691	960.1	387.0	0.403
6.020.15	7.026	0.538	0.812	960.1	420.7	0.438
6.030.05	2.342	0.300	0.465	1024.6	426.9	0.417
6.030.10	4.684	0.425	0.634	1024.6	459.4	0.448
6.030.15	7.026	0.520	0.755	1024.6	486.5	0.475
7.005.05	2.342	0.406	0.847	562.0	129.0	0.230
7.005.10	4.684	0.574	1.015	562.0	179.4	0.319
7.005.15	7.026	0.703	1.144	562.0	211.8	0.377
7.010.05	2.342	0.396	0.758	588.2	160.9	0.274
7.010.10	4.684	0.561	0.960	588.2	200.8	0.341
7.010.15	7.026	0.687	1.096	588.2	231.0	0.393
7.020.05	2.342	0.380	0.636	640.5	228.7	0.357
7.020.10	4.684	0.537	0.850	640.5	256.0	0.400
7.020.15	7.026	0.658	0.998	640.5	278.3	0.435
7.030.05	2.342	0.368	0.572	683.8	282.4	0.413
7.030.10	4.684	0.520	0.780	683.8	303.9	0.444
7.030.15	7.026	0.637	0.929	683.8	321.7	0.471

In Table 6.1, $k_{cracked}/k_{uncracked}$ ranges from 0.23 to 0.48. These values are similar to the values of 0.35 to 0.60 presented in Priestley et al. (1996) for typical circular reinforced concrete columns with longitudinal reinforcement ratios of between 0.01 and 0.03 and axial load ratios of between 0.10 and 0.30. The lower $k_{cracked}/k_{uncracked}$ range observed during this study could be explained by smaller cracked stiffnesses resulting from the bond model included in the frames and described in Lehman and Moehle (2000).

The following trends were observed in the plots of $k_{cracked}/k_{uncracked}$ shown in Figure 6.3.

- $k_{cracked}/k_{uncracked}$ increased as ρ increased. This trend is evident in Figure 6.3. For example, $k_{cracked}/k_{uncracked}$ increased by 81 percent between frames 5.005.05 and 5.030.05. Because $k_{uncracked}$ was calculated from the transformed section, $k_{uncracked}$ increased as ρ increased. This was expected because the additional theoretical transformed area of concrete (equal to nA_s where $n = E_s/E_c$) provided additional concrete area, resulting in an increased stiffness (Nawy 2000). $k_{cracked}$ also increased as ρ increased because the location of the neutral axis depended on ρ, and therefore, as dictated by the principles of mechanics, $k_{cracked}$ also depended on ρ (Nawy 2000). A change in ρ produced greater variation in $k_{cracked}$ than in $k_{uncracked}$, as indicated by the increased $k_{cracked}/k_{uncracked}$ as ρ increased. Priestley et al. (1996) also found that $k_{cracked}/k_{uncracked}$ increased as ρ increased.
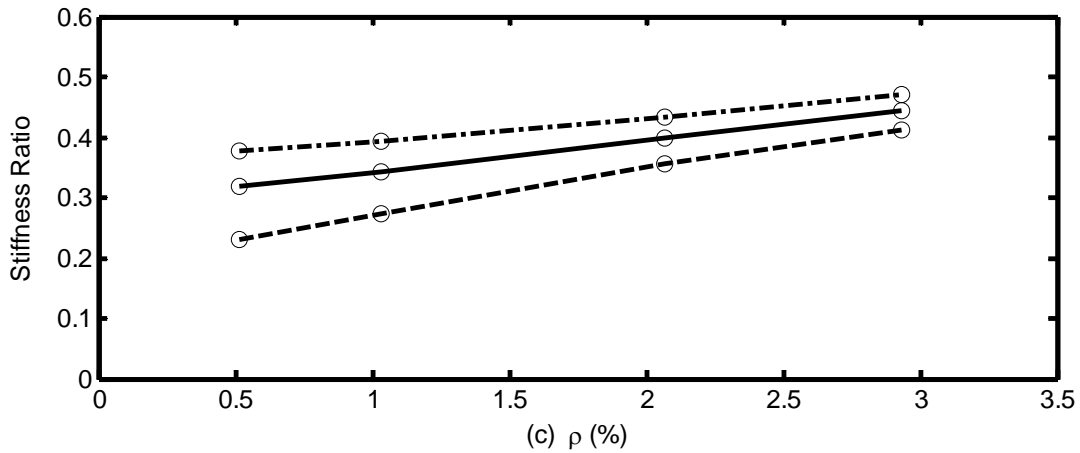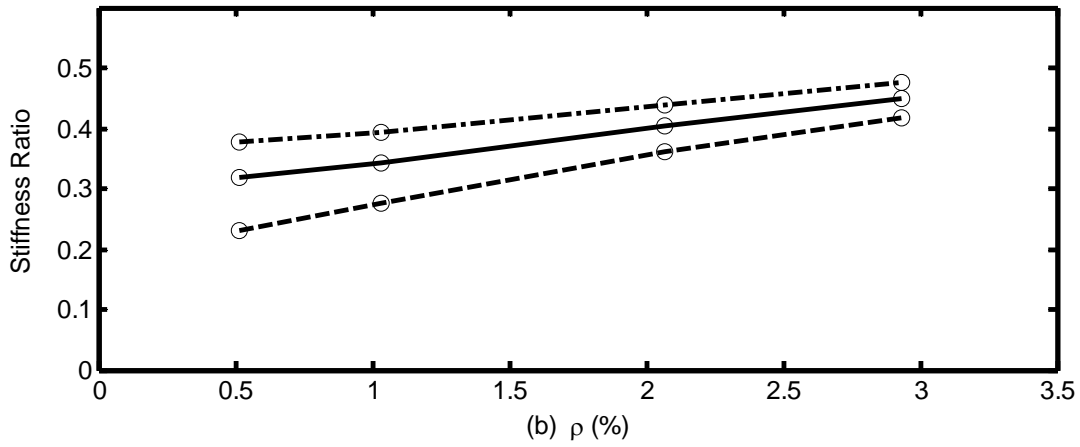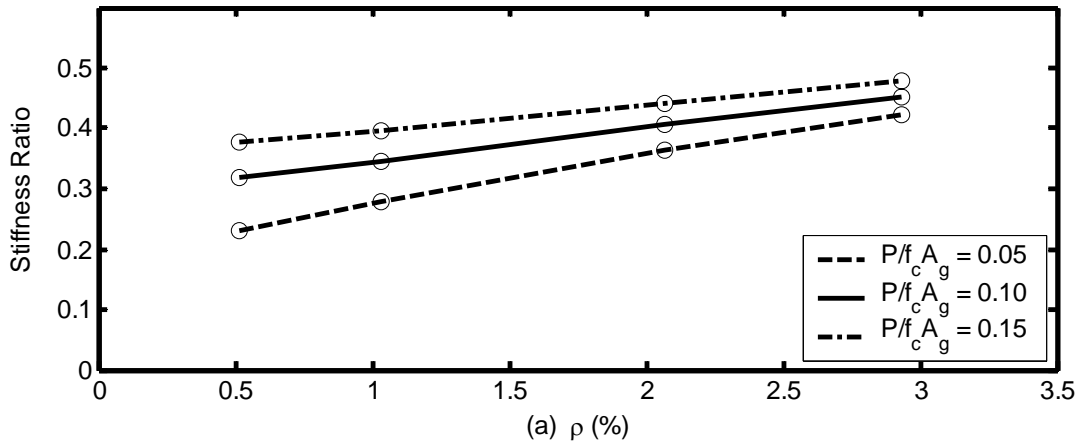
Figure 6.3: Stiffness Ratio, Reinforced Concrete Frames
(a) $L_{col}/D_{col} = 5$, (b) $L_{col}/D_{col} = 6$, and (c) $L_{col}/D_{col} = 7$

- $k_{cracked}/k_{uncracked}$ increased as $P_{col}/(f_c' A_g)$ increased (Figure 6.3). The increase was significantly larger for low values of ρ. An increase of 62 percent was observed between frames 5.005.05 and 5.005.15, while an increase of only 14 percent was observed between frames 5.030.05 and 5.030.15. $P_{col}/(f_c' A_g)$ had no influence on $k_{uncracked}$ but did affect $k_{cracked}$. Before the section cracked, the stiffness was based on the transformed gross section properties of the cross-section; therefore, the axial-load on the column had no impact on the uncracked stiffness. After the section cracked, as $P_{col}/(f_c' A_g)$ increased, the depth of the neutral axis also increased, resulting in the increased cracked stiffness. Paulay and Priestley (1992) provided recommended design values for cracked stiffness which indicate larger values for larger axial-loads. Priestley et al. (1996) also found that $k_{cracked}/k_{uncracked}$ increased as $P_{col}/(f_c' A_g)$ increased for typical circular reinforced concrete columns with longitudinal reinforcement ratios of between 0.01 and 0.03 and axial load ratios of between 0.10 and 0.30.

- As expected from the relationship for stiffness $\left(k = \alpha E I/L_{col}^3\right)$, both $k_{uncracked}$ and $k_{cracked}$ were affected by a variation in L_{col}/D_{col}. $k_{cracked}/k_{uncracked}$ remained effectively unchanged as L_{col}/D_{col} varied. This trend suggests that $k_{uncracked}$ and $k_{cracked}$ were similarly affected as L_{col}/D_{col} varied.

In summary, ρ had the greatest influence on $k_{cracked}/k_{uncracked}$; $P_{col}/(f_c' A_g)$ had a moderate impact on $k_{cracked}/k_{uncracked}$; and L_{col}/D_{col} had almost no impact on $k_{cracked}/k_{uncracked}$.

6.4 TRENDS IN NOMINAL YIELD DISPLACEMENTS

Nominal yield displacements, Δ_y, and their corresponding drift ratios, Δ_y/L_{col},

are summarized in Table 6.2. Δ_y varied between 1.0 in. and 2.6 in., while Δ_y/L_{col}

varied between 0.41percent and 0.78 percent.

Table 6.2: Yield and Strength Properties, Reinforced Concrete Frames

Frame	$F_{firstyield}$	$\Delta_{firstyield}$	$\dfrac{\Delta_{firstyield}}{L_{col}}$	F_{con004}	Δ_{yield}	$\dfrac{\Delta_{yield}}{L_{col}}$	F_{max}
	(kips)	(in.)	(%)	(kips)	(in.)	(%)	(kips)
5.005.05	254.9	0.816	0.34	327.5	1.048	0.44	331.3
5.005.10	362.4	0.842	0.35	428.1	0.995	0.41	429.0
5.005.15	458.3	0.904	0.38	521.4	1.028	0.43	523.7
5.010.05	365.5	0.929	0.39	490.2	1.247	0.52	530.0
5.010.10	466.5	0.956	0.40	586.1	1.202	0.50	590.7
5.010.15	558.3	0.998	0.42	673.7	1.205	0.50	674.4
5.020.05	577.3	1.032	0.43	800.9	1.432	0.60	881.1
5.020.10	670.0	1.072	0.45	880.3	1.408	0.59	926.3
5.020.15	755.8	1.113	0.46	953.5	1.405	0.59	974.6
5.030.05	748.8	1.086	0.45	1043.6	1.513	0.63	1155.1
5.030.10	836.8	1.128	0.47	1115.8	1.504	0.63	1191.8
5.030.15	919.4	1.171	0.49	1179.1	1.502	0.63	1231.4
6.005.05	211.5	1.089	0.38	269.8	1.388	0.48	269.9
6.005.10	300.2	1.116	0.39	351.8	1.307	0.45	353.2
6.005.15	379.2	1.194	0.41	428.1	1.348	0.47	431.0
6.010.05	303.6	1.248	0.43	405.6	1.667	0.58	428.8
6.010.10	386.8	1.277	0.44	483.3	1.596	0.55	483.4
6.010.15	462.2	1.328	0.46	554.5	1.593	0.55	555.5
6.020.05	480.0	1.388	0.48	664.7	1.922	0.67	723.9
6.020.10	556.0	1.437	0.50	728.6	1.883	0.65	753.6
6.020.15	626.3	1.489	0.52	787.5	1.872	0.65	793.9
6.030.05	622.8	1.459	0.51	867.1	2.031	0.71	953.1
6.030.10	694.9	1.513	0.53	925.0	2.013	0.70	976.0
6.030.15	762.5	1.567	0.54	975.6	2.005	0.70	1002.5
7.005.05	180.5	1.399	0.42	228.2	1.769	0.53	228.4
7.005.10	255.7	1.425	0.42	296.7	1.654	0.49	298.8
7.005.15	322.4	1.522	0.45	360.6	1.703	0.51	364.3
7.010.05	259.2	1.611	0.48	344.8	2.143	0.64	354.7
7.010.10	329.5	1.641	0.49	409.2	2.038	0.61	409.6
7.010.15	393.1	1.702	0.51	468.5	2.029	0.60	469.8
7.020.05	410.3	1.795	0.53	567.1	2.480	0.74	610.1
7.020.10	474.3	1.853	0.55	619.6	2.421	0.72	628.6
7.020.15	533.3	1.917	0.57	668.1	2.401	0.71	668.5
7.030.05	532.7	1.886	0.56	740.7	2.623	0.78	807.4
7.030.10	593.3	1.952	0.58	788.0	2.593	0.77	819.5
7.030.15	649.9	2.020	0.60	829.3	2.578	0.77	842.7

The following trends are evident from the plots of Δ_y and Δ_y/L_{col} shown in Figure 6.4. The trends are discussed for Δ_y/L_{col}, but similar trends were seen in Δ_y, although the variations observed in the Δ_y/L_{col} trends were significantly larger than those for Δ_y.

- Δ_y/L_{col} increased as ρ increased, as shown in Figure 6.4. For example, Δ_y/L_{col} increased by 43 percent between frames 5.005.05 and 5.030.05. This trend can be explained by investigating the change in stiffness and strength between frames 5.005.05 and 5.030.05. The ratio of $k_{cracked}$ between the two frames was equal to 0.45, whereas the ratio of F_{con004} between the two frames was 0.31. Because the increase in strength was greater than the increase in stiffness, it would be expected, given geometry, that Δ_y/L_{col} would also increase. From Table 6.2 it is also clear that the displacement at first yield also increased as ρ increased. This trend is explained by examining flexure of a square cross-section with a width equal to b. The neutral-axis, c, is directly related to the amount of steel in the section, as shown by the relationship $c = \left(\rho A_g f_y\right)/\left(0.85\beta f_c' b\right)$, where f_y is the yield strength of the longitudinal mild steel, f_c' is the concrete compressive strength, and β is the stress block depth factor. Mechanics dictate that as the neutral-axis increases the curvature increases, and accordingly, the displacement at first yield also increases.
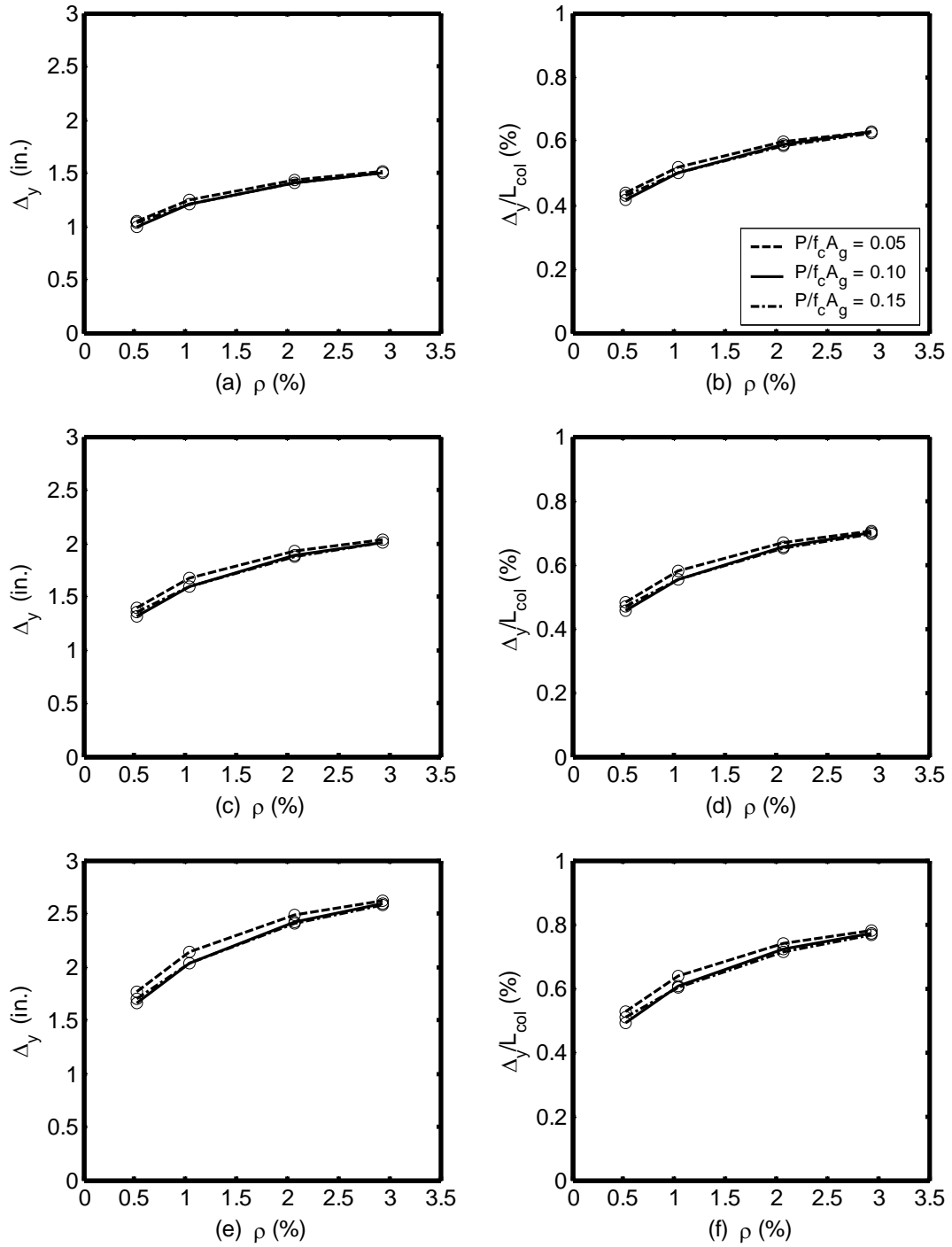
Figure 6.4: Yield Displacement, Reinforced Concrete Frames

(a) and (b) $L_{col}/D_{col} = 5$, (c) and (d) $L_{col}/D_{col} = 6$, and (e) and (f) $L_{col}/D_{col} = 7$

- Figure 6.4 indicates that Δ_y/L_{col} remained essential unchanged as $P_{col}/(f'_c A_g)$ increased. An increase was not observed in these results because $P_{col}/(f'_c A_g)$ similarly influenced cracked stiffness and strength. For example, the ratio of $k_{cracked}$ between frames 5.030.05 and 5.030.15 was 0.87 (Table 6.1) and the ratio of F_{con004} was also 0.87 (Table 6.2). Paulay and Priestley (1992) suggested that as the axial-load increases, the yield displacement should also increase.

- Δ_y/L_{col} increased as L_{col}/D_{col} increased (Figure 6.4). A 22 percent increase was seen between frames 5.030.15 and 7.030.15. This trend is explained by the decreased cracked stiffness as L_{col}/D_{col} increased.

These trends indicate that ρ had the greatest influence on Δ_y/L_{col}; L_{col}/D_{col} had a moderate impact on Δ_y/L_{col}; and $P_{col}/(f'_c A_g)$ effectively had no influence on Δ_y/L_{col}. For Δ_y, the largest impact was caused by L_{col}/D_{col}.

6.5 TRENDS IN MAXIMUM FORCE

As shown in Table 6.2, F_{max} ranged from 228 to 1231 kips. The large values corresponded to a short column, with a large ρ and $P_{col}/(f'_c A_g)$, while the small values corresponded to a tall column, with a small ρ and $P_{col}/(f'_c A_g)$. The following trends were observed in the results, shown in Figure 6.5.
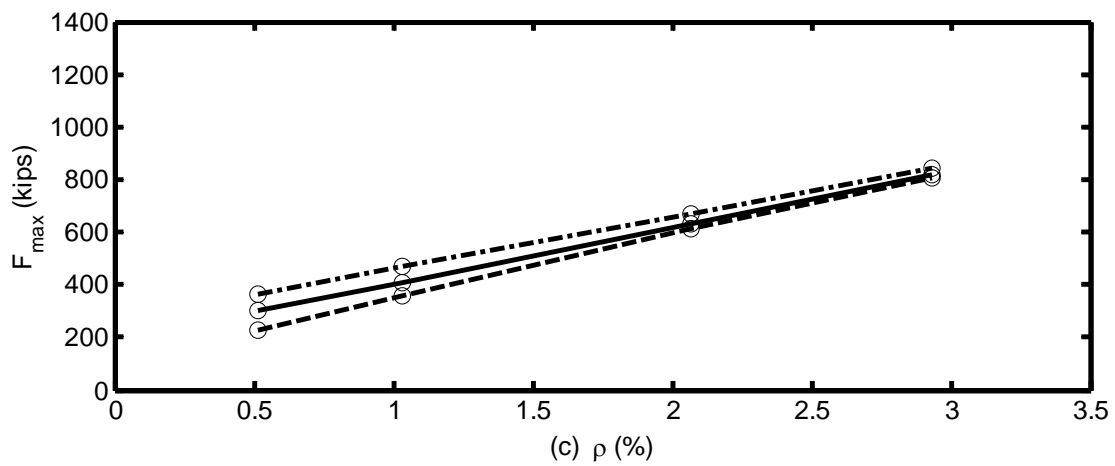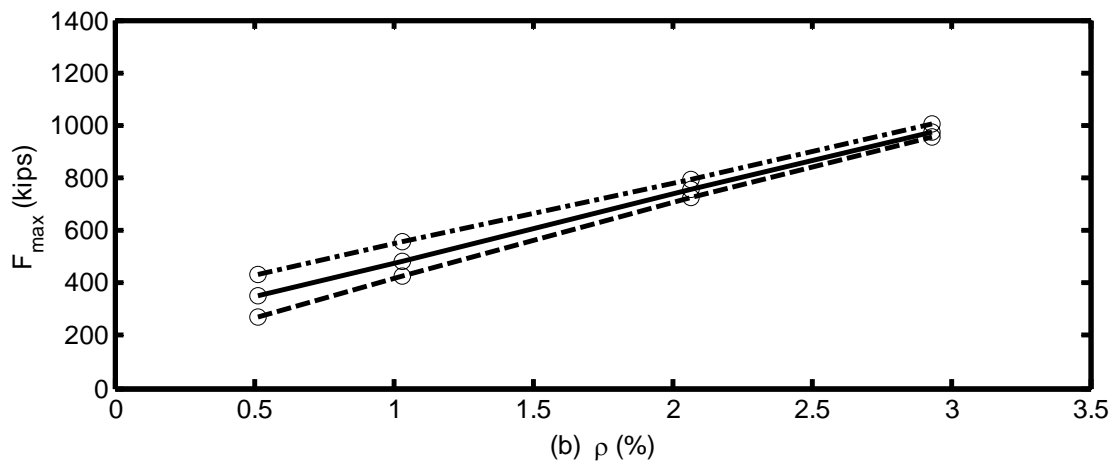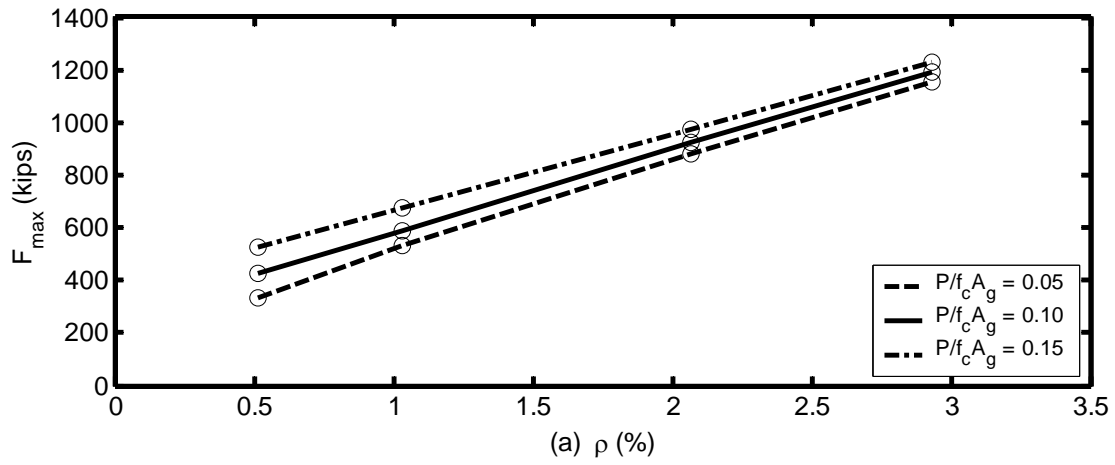
Figure 6.5: Maximum Force, Reinforced Concrete Frames
(a) $L_{col}/D_{col} = 5$, (b) $L_{col}/D_{col} = 6$, and (c) $L_{col}/D_{col} = 7$

- The maximum force, F_{max}, increased as ρ increased. An increase of 250 percent was observed between frames 5.005.05 and 5.030.05. The flexural strength of a column is directly related to the quantity of longitudinal reinforcing steel provided. Therefore, this trend can be attributed to an increased flexural strength provided by the increased steel.

- F_{max} increased as $P_{col}/(f_c'A_g)$ increased, as is evident in Figure 6.5. The increase was significantly larger for low values of ρ. An increase of 58 percent was observed between frames 5.005.05 and 5.005.15, whereas an increase of only 7 percent was observed between frames 5.030.05 and 5.030.15. The $P_{col}/(f_c'A_g)$ on bridge columns is normally around 0.10, which is relatively low. As a result, typical bridge columns fall below the balanced failure point on a column interaction diagram. Below the balanced failure point, an increase in compressive axial-load results in an increase in flexural strength, which corresponds with the trend observed.

- F_{max} decreased as L_{col}/D_{col} increased (Figure 6.5). For example, a decrease of 32 percent was observed between frames 5.030.15 and 7.030.15. As L_{col}/D_{col} increased, the cracked stiffness decreased, resulting in the decreased F_{max}.

These trends indicate that ρ had the greatest influence on F_{max}; $P_{col}/(f_c'A_g)$ had a varying impact on F_{max}; and L_{col}/D_{col} had the least influence on F_{max}.

CHAPTER 7
EARTHQUAKE ANALYSES
OF REINFORCED CONCRETE FRAMES

A parametric study was conducted to evaluate the proposed bridge systems described in Chapter 3 and provide a basis for comparison between the expected performance of the reinforced concrete frames and that of the hybrid frames. The parametric study included pushover analyses and earthquake analyses of the reinforced concrete frames and the hybrid frames.

This chapter addresses the earthquake analyses of the reinforced concrete frames that were conducted to quantify maximum displacements and residual displacements resulting from the 10 ground motions described in Chapter 5. The 10 ground motions included five ground motions with a 10 percent probability of exceedance in 50 years (10 percent in 50) and five ground motions with a 2 percent probability of exceedance in 50 years (2 percent in 50). This chapter describes the parameters that were varied for the study (Section 7.1), key characteristics used to compare earthquake analyses (Section 7.2), and the results obtained from these analyses (sections 7.3 through 7.7).

7.1 RANGE OF REINFORCED CONCRETE PARAMETRIC STUDY

The analyses were conducted on variations of the baseline frame described in Chapter 4. On the basis of preliminary pushover analyses, the following three parameters were varied, as described in Chapter 6:

- ○ column aspect ratio, L_{col}/D_{col}
- ○ longitudinal reinforcement ratio, $\rho = A_s/A_g$
- ○ axial-load ratio, $P_{col}/(f_c'A_g)$.

7.2 KEY CHARACTERISTICS OF EARTHQUAKE RESPONSE

This section describes the key characteristics that were calculated from the results of the earthquake analyses. These characteristics describe the response of the frames to the earthquake analyses and provide a basis for comparison between the reinforced frames and the hybrid frames. Sections 7.3 through 7.7 discuss the results obtained from the earthquake analyses of the reinforced concrete frames.

7.2.1 Maximum Displacement, Δ_{max}

The maximum displacement, Δ_{max}, was defined as the maximum absolute value displacement encountered during an earthquake analysis. The maximum displacement can provide insight into the likelihood that a particular frame/ground motion combination will result in spalling, bar buckling, or the occurrence of the ultimate limit state, as described in Chapter 10. The maximum displacement was also used to calculate the displacement ductility demand on the frame. The displacement ductility demand is a useful measure for comparing the earthquake response of different frames and will be explained in Chapter 10. The corresponding drift ratio at the maximum displacement was given as Δ_{max}/L_{col} .

7.2.2 Residual Displacement, $\Delta_{residual}$

The residual displacement, $\Delta_{residual}$, was defined as the displacement from the frame's initial equilibrium position after the ground motion excitation had ended. After an inelastic system has yielded, it may not vibrate around its original equilibrium position. With each subsequent occurrence of yielding, the system may shift to another location about which it will oscillate. Therefore, after the ground excitation has ended, a

frame that has yielded will typically not return to its original equilibrium point, resulting in a residual displacement (Chopra 2001).

For this study, the residual displacements were found by considering the free vibration of the frame after the ground motion had stopped. This was done because no viscous damping was included in the frame. The residual displacements were estimated by averaging the maximum and minimum displacements over a time range starting 4 sec. after the ground excitation had stopped, $\Delta_{t,stop+4\sec}$, and ending 9 sec. after the ground excitation had stopped, $\Delta_{t,stop+9\sec}$. The residual displacements were calculated from the following relationship:

$$\Delta_{residual} = \frac{\max(\Delta_{t,stop+4\sec} \rightarrow \Delta_{t,stop+9\sec}) + \min(\Delta_{t,stop+4\sec} \rightarrow \Delta_{t,stop+9\sec})}{2.0} \qquad (7.1)$$

7.3 TRENDS IN MAXIMUM DISPLACEMENT

This section discusses the maximum displacements encountered during the earthquake analyses. Tables B.1 and B.2, found in Appendix B, provide a complete summary of the maximum displacements for individual ground motions and mean values for both the 10 percent in 50 and 2 percent in 50 motions.

For the 2 percent in 50 ground motions, ten frame/ground motion combinations had a displacement of over 100 in., with OpenSees encountering convergence problems with each occurrence. It is difficult to say whether the convergence problems caused the extreme displacements, or the extreme displacements caused the convergence problems. For this study, these values were omitted when mean values were calculated. Eight of the 10 convergence problems occurred as a result of ground motion 2-3. The other two

convergence problems occurred with frame 5.005.15. The frames that had convergence problems had small longitudinal reinforcement ratios and large axial-load ratios.

For the 10 percent in 50 ground motions, the extreme values of the maximum displacement ranged from a minimum of 0.9 in. (frame 6.030.05, ground motion 10-3, $\Delta_{max}/L_{col} = 0.33$ percent) to a maximum of 10.7 in. (frame 7.005.15, ground motion 10-3, $\Delta_{max}/L_{col} = 3.19$ percent). For the 2 percent in 50 ground motions, the maximum displacement ranged from a minimum of 1.9 in. (frame 5.030.05, ground motion 2-1, $\Delta_{max}/L_{col} = 0.79$ percent) to a maximum of 28.4 in. (frame 7.005.10, ground motion 2-3, $\Delta_{max}/L_{col} = 8.47$ percent).

The same frame, frame 5.030.05, resulted in the minimum average displacement when subjected to the 10 percent in 50 ground motions (1.6 in.) and the 2 percent in 50 ground motions (2.3 in.). This was not the case with the maximum average displacement. Instead, frame 7.005.15 resulted in the largest average displacement for the 10 percent in 50 ground motions (7.7 in.), whereas frame 7.005.10 resulted in the largest average displacement for the 2 percent in 50 ground motions (14.9 in.). This inconsistency is a consequence of omitting the 10 frames that experienced convergence problems. With the 2 percent in 50 ground motions, motion 2-3 caused the largest displacement for each of the frames. Therefore, by omitting this motion's contribution to the average displacement for frame 7.005.15, frame 7.005.10 had a larger average displacement.

Figure 7.1 shows the mean and the mean plus one standard deviation maximum drift ratio for the 2 percent in 50 ground motions. Because the general trends observed in the maximum drift ratio were similar for the 2 percent in 50 ground motions and the 10 percent ground motions, only figures showing the results for the 2 percent in 50 ground

motions are included in this chapter. Figure B.1, found in Appendix B, presents the data for the 10 percent in 50 ground motions.
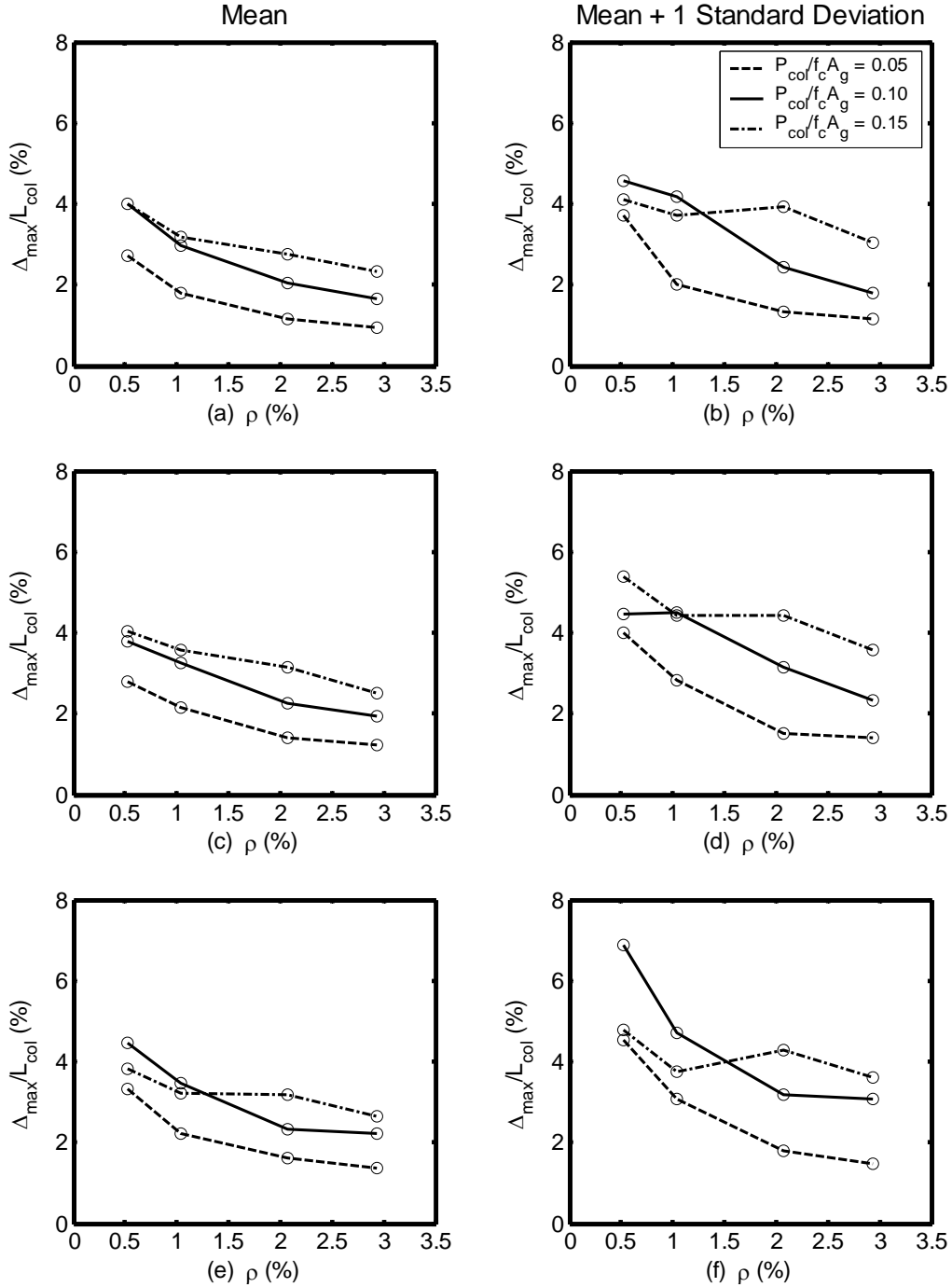
Figure 7.1: Trends in Drift Ratio, 2 Percent in 50, Reinforced Concrete Frames
(a) and (b) $L_{col}/D_{col} = 5$, (c) and (d) $L_{col}/D_{col} = 6$, and (e) and (f) $L_{col}/D_{col} = 7$

The results presented in Figure 7.1 display the following trends. The trends are discussed for the mean drift ratio, but the trends are also reflected in the responses from each individual ground motion. The inconsistencies described in the preceding paragraph are reflected in Figure 7.1 at the locations where the lines cross one another.

- Δ_{max}/L_{col} decreased as ρ increased, as is indicated in Figure 7.1. For example, the drift ratio decreased by 60 percent between frames as the reinforcement ratio increased from 0.005 to 0.030. From the results of the pushover analyses (Chapter 6), it was evident that a frame's strength and cracked stiffness increased as ρ increased. This increased strength, as well as cracked stiffness, resulted in a decreased Δ_{max}/L_{col} encountered during the earthquake analyses.

- Δ_{max}/L_{col} increased as $P_{col}/(f_c' A_g)$ increased. The drift ratio increased on average by 100 percent as the axial-load ratio increased from 0.05 to 0.15. This observation can be explained by considering the increased mass corresponding to an increased $P_{col}/(f_c' A_g)$. The mass applied to the frame was equal to compressive axial-load on the column divided by gravity. Given the relationship for the cracked natural period $\left(T_{n,cracked} = \sqrt{m/k_{cracked}}\right)$, it is evident that as mass increased, the cracked natural period also increased. The displacement response spectrum shown later in this chapter indicates that an increase in $T_{n,cracked}$ should result in an increase in the predicted displacement. The cracked natural period may also have increased further because the increased mass reduced the cracked stiffness as a result of the $P - \Delta$ effect.

- Δ_{max}/L_{col} was only slightly influenced by L_{col}/D_{col}. This observation is apparent from the data presented in Figure 7.1. An increase of 14 percent was observed between 5.030.15 and 7.030.15. The results of the pushover analyses of the reinforced concrete frames indicated that as L_{col}/D_{col} increased the frame stiffness decreased. The increased Δ_{max}/L_{col} resulted from the decreased stiffness. The impact of L_{col}/D_{col} is more significant when the results for the average Δ_{max} are examined instead of Δ_{max}/L_{col}. For example, Δ_{max} increased 60 percent between frames 5.030.15 and 7.030.15.

- Figure 7.1 indicates that the mean plus one stand deviation was approximately 50 percent larger than the mean values.

- The results for Δ_{max}/L_{col} from the 2 percent in 50 ground motions were about 50 percent larger than the results for the 10 percent in 50 ground motions. The graphs in Figure B.1 in Appendix B illustrate the data for the maximum drift ratio resulting from the 10 percent in 50 ground motions.

   These trends indicate that the $P_{col}/(f_c' A_g)$ had the greatest influence on Δ_{max}/L_{col};

ρ had a moderate impact; and L_{col}/D_{col} had the least impact on Δ_{max}/L_{col}. As explained above, L_{col}/D_{col} had a more significant impact on Δ_{max} than it did on Δ_{max}/L_{col}.

7.4 EFFECTS OF STRENGTH ON MAXIMUM DISPLACEMENT

This section examines other quantities that affected the resulting maximum displacement. To evaluate the impact of strength on maximum displacement, the maximum drift ratio, Δ_{max}/L_{col}, was plotted against the normalized force F_{con004}/P_{total},

where F_{con004} corresponded to the effective force when the compressive strain of the

extreme concrete fibers first reached 0.004 and $P_{total} = 2 * P_{col}$ for a two-column frame.

This ratio is commonly referred to as the base shear-strength ratio or strength ratio.

Figures 7.2 and 7.3 illustrate the mean and mean plus one standard deviation,

Δ_{max} / L_{col} , plotted against F_{con004} / P_{total} for the 2 percent in 50 ground motions. These

data are shown in figures B.2 and B.3 for the 10 percent in 50 ground motions (Appendix

B).
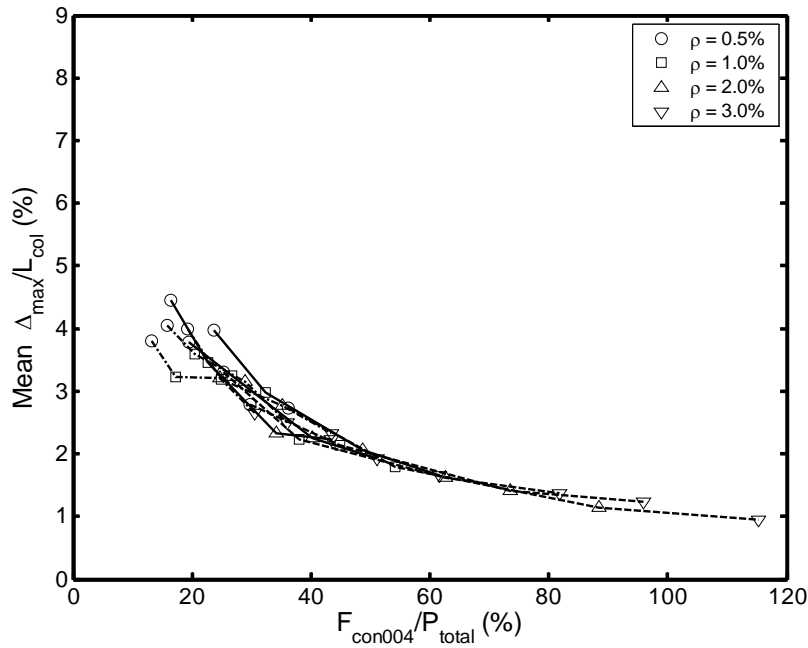
Figure 7.2: Effect of Strength on Mean Drift Ratio, 2 Percent in 50, Reinforced Concrete Frames
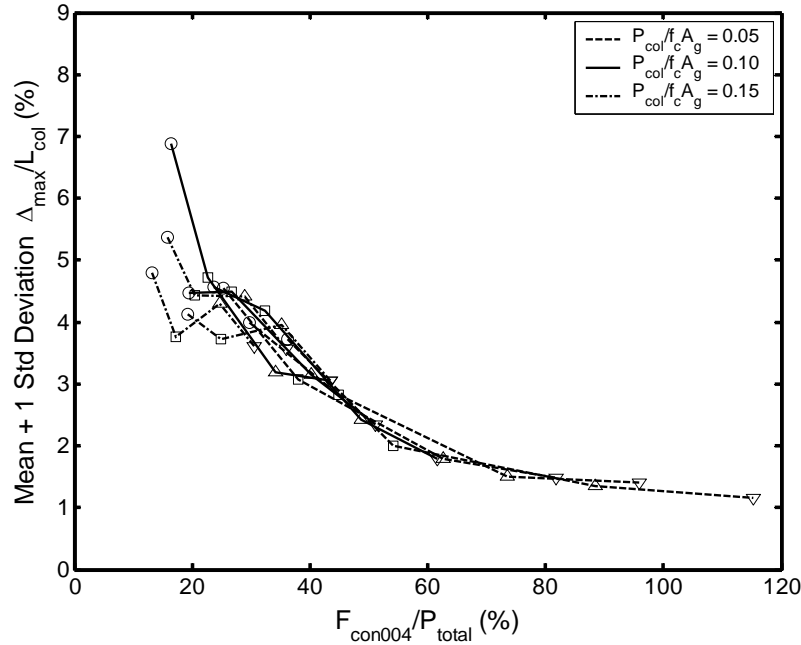
Figure 7.3: Effect of Strength on Mean Plus One Standard Deviation Drift Ratio, 2 Percent in 50, Reinforced Concrete Frames

The results shown in figures 7.2 and 7.3 fall onto relatively smooth curves. The following observations were noted from the plots:

- Δ_{max}/L_{col} decreased as F_{con004}/P_{total} increased. Frame 5.030.05 had the smallest Δ_{max}/L_{col} but the largest F_{con004}/P_{total}, whereas frame 7.005.15 had the largest Δ_{max}/L_{col} but the smallest F_{con004}/P_{total}.

- The relationship between F_{con004}/P_{total} and Δ_{max}/L_{col} was nonlinear.

- For typical bridge columns with axial-load ratios near 0.10, ρ had a significant impact on Δ_{max}/L_{col}, as discussed in Section 7.3.

- No definitive trends appear in the Δ_{max}/L_{col} versus F_{con004}/P_{total} relationships shown in figures 7.2 and 7.3, indicating no strong relation between maximum drift ratio and frame strength.

A design displacement response spectrum developed from the design acceleration response spectrum specified by AASHTO (Figure 7.4) is effectively linear in the range of periods considered in this study. It is expected that a plot of maximum drift ratio against a quantity related to the period of vibration will be basically linear. Therefore, Δ_{max}/L_{col} was plotted against a ratio that could account for strength as well as stiffness.
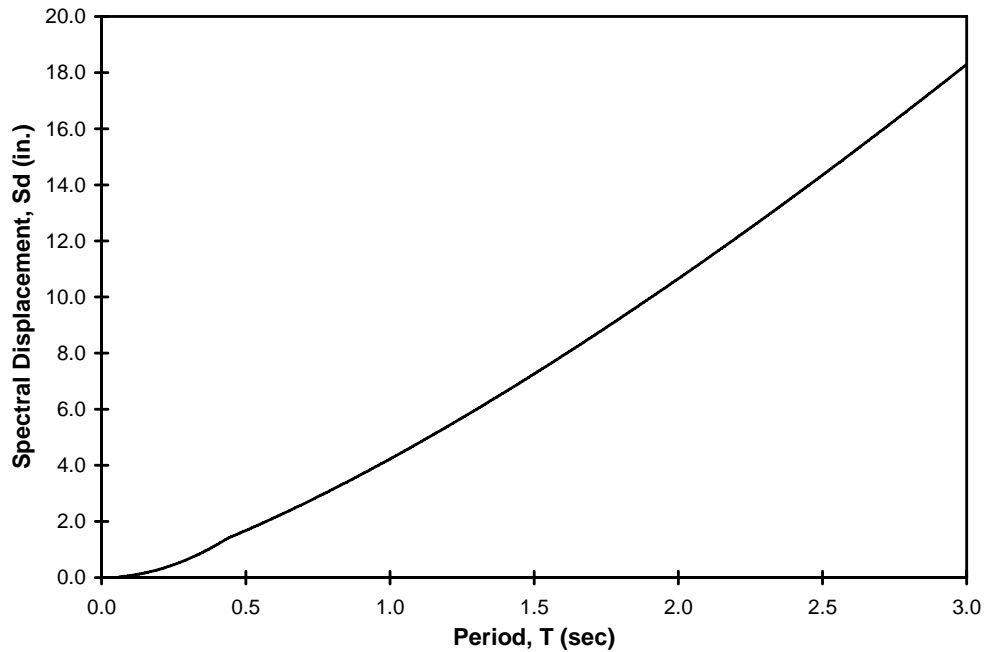
Figure 7.4: 10 Percent in 50 Design Displacement Response Spectrum

Priestley and Paulay (2002) suggested that strength and stiffness are basically proportional. Therefore, it can be assumed that stiffness, k, is equal to the product of a proportional constant, α, and the strength, F. For this study, the mass, m, was equal to the compressive axial-load on the frame, P_{total}, divided by gravity, g. These two relationships can be substituted into the equation for natural period

$$T_n = \sqrt{\frac{m}{k}} \qquad (7.2)$$

102

resulting in the following relationship:

$$T_n = \sqrt{\frac{P_{total}/g}{\alpha F}} \qquad (7.3)$$

For this study, the assumed strength of the frame was assumed to be F_{con004},

resulting in plots of the maximum drift ratio against $\sqrt{P_{total}/F_{con004}}$, shown in figures 7.5

and 7.6. The figures reflect a nearly linear relationship between the maximum drift ratio

and $\sqrt{P_{total}/F_{con004}}$. Because the design displacement response spectrum is linear in the

range of periods considered in this study, this observation suggests that the variation in

maximum drift ratio was at least partially a result of the increased $k_{cracked}$ as the

longitudinal steel ratio increased.
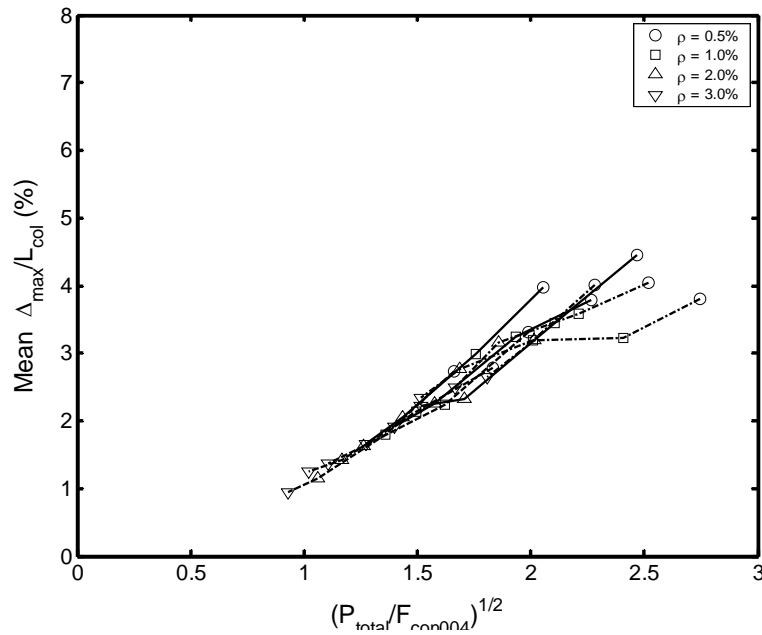
Figure 7.5: Effect of Stiffness on Mean Drift Ratio, 2 Percent in 50, Reinforced Concrete Frames
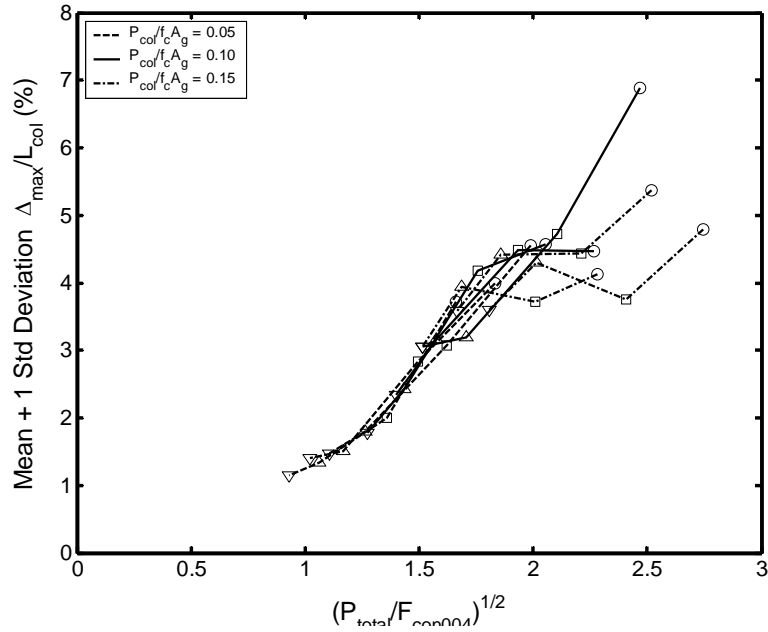
Figure 7.6: Effect of Stiffness on Mean Plus One Standard Deviation Drift Ratio, 2 Percent in 50, Reinforced Concrete Frames

7.5 COMPARISON OF MAXIMUM DISPLACEMENT WITH ELASTIC ANALYSIS

An elastic design response spectrum is used to estimate response quantities for a given ground motion. Therefore, to evaluate how closely the elastic design response spectra predicted the maximum displacements resulting from the earthquake analyses, the maximum displacements were compared with the expected displacements obtained from the elastic design response spectrum. When a frame undergoes nonlinear behavior, the maximum expected displacement can no longer be determined solely from its initial period and damping ratio. The design response spectra described in Chapter 5 were based on elastic response and a damping ratio of 0.05. No viscous damping was added for the frames in this study, and the behavior was inelastic and included hysteretic damping. These characteristics could have led to displacements that were larger or smaller than those predicted by the design displacement response spectrum.

104

To find the difference between the average response and that predicted by the design spectrum, the mean Δ_{max}/S_d was found. Modification factors were found to relate the actual maximum displacement with the predicted values. The predicted values for undamped, inelastic behavior could then be found from the following relationship:

$$\Delta_{predicted} = \psi S_d \qquad (7.4)$$

where ψ = modification factor

S_d = elastic design spectral displacement

The modification factor was calculated by averaging Δ_{max}/S_d for all the frames. This modification factor provided a means of determining how closely the actual maximum displacements compared with the predicted values from the design response spectra and was found from the following relationship:

$$\psi = \frac{\displaystyle\sum_{i=1}^{N_{frames}} \left[\left(\sum_{j=1}^{N_{motions}} \text{mean } \Delta_{max.ij}/S_{d.i} \right) \middle/ N_{motions} \right]}{N_{frames}} \qquad (7.5)$$

Modification factors were found for the mean and mean plus one standard deviation for the 10 percent in 50 and 2 percent in 50 ground motions and were as follows:

- $\psi = 1.35$ for the mean from the 10 percent in 50 ground motions
- $\psi = 1.61$ for the mean plus one standard deviation from the 10 percent in 50 ground motions
- $\psi = 1.37$ for the mean from the 2 percent in 50 ground motions
- $\psi = 1.76$ for the mean plus one standard deviation from the 2 percent in 50 ground motions

Combining the modification factors for the mean results led to an average value of 1.36, assuming each frame was given an equal weighting factor. The average value resulting from the combination of modification factors for the mean plus one standard deviation was 1.69

Using Equation 7.4 for each earthquake analysis with $\psi = 1.4$ led to a ratio of the maximum displacement to the predicted displacement, $\Delta_{max}/\Delta_{predicted}$, with a mean of 0.97 and standard deviation of 0.27. Given the results from each analysis, Equation 7.4 with $\psi = 1.7$ produced a mean $\Delta_{max}/\Delta_{predicted}$ equal to 0.80 and a standard deviation equal to 0.22.

Figures 7.7 and 7.8 show how well the predicted values corresponded to the mean Δ_{max} and the mean plus one standard deviation for the 2 percent in 50 ground motions. The predicted responses, as defined by Equation 7.4, are also illustrated on the figures. Figures B.6 and B.7, in Appendix B, show the same data for the 10 percent in 50 ground motions. It is apparent that $\Delta_{predicted}$ represented the average response well.
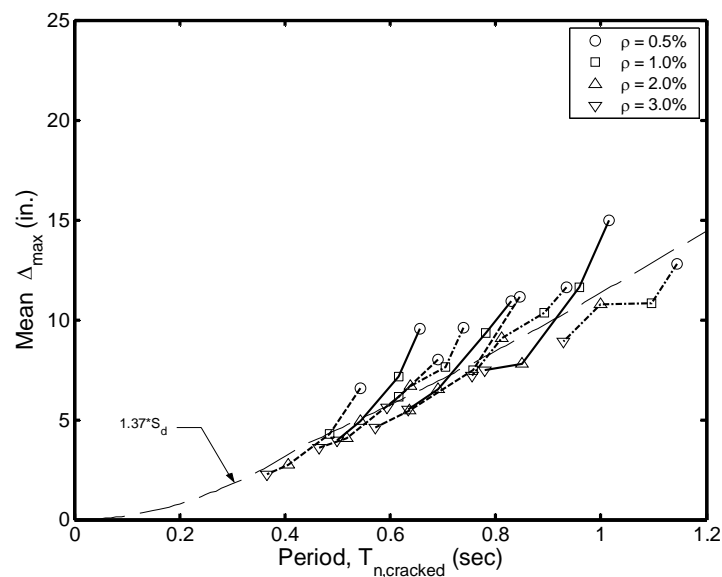
Figure 7.7: Predicted and Mean Response, 2 Percent in 50, Reinforced Concrete Frames
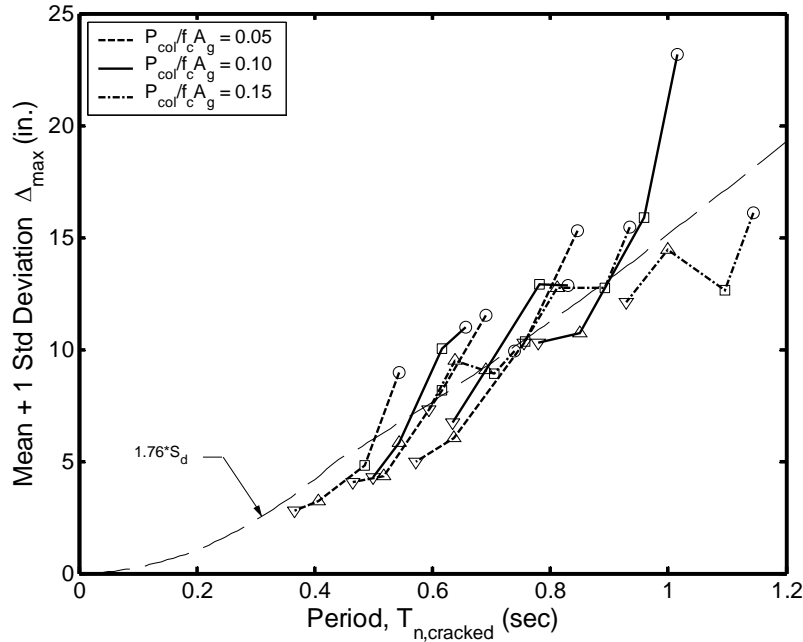
Figure 7.8: Predicted and Mean Plus One Standard Deviation Response, 2 Percent in 50, Reinforced Concrete Frames

Possible reasons for the discrepancies between the values predicted by the design displacement response spectrum and the values from the earthquake analyses, and therefore the need for the modification factors, include the following:

- The design response spectrum was based on a viscous damping ratio, ξ, of 0.05, whereas no viscous damping was included for the frames in this study. This could partially account for the under-prediction of the displacements from the design response spectrum.

- The design response spectrum was created for elastic systems, but the frames encountered inelastic behavior during the earthquake analyses. This inelastic behavior could account for actual displacements larger than those predicted by the design response spectrum.

107

- A difference existed between the target design spectrum and the scaled response spectrum for each individual ground motion. These differences are apparent in the figures of Appendix B.

7.6 INCORPORATION OF STRENGTH IN PREDICTION OF MAXIMUM DISPLACEMENT

To demonstrate the effect that strength had on the maximum displacement response, the mean Δ_{max}/S_d was plotted against a normalized strength, $F_{con004}/S_a m$, where S_d and S_a were the spectral displacement and spectral acceleration predicted from the smooth design spectra (Figure 7.9). The data shown in these plots suggested a bilinear relationship between Δ_{max}/S_d and $F_{con004}/S_a m$. Above a value of $F_{con004}/S_a m$ of about 0.04, Δ_{max}/S_d was approximately constant, whereas below this value, a linear relationship appeared appropriate. Therefore, the predicted values for undamped, inelastic behavior could be calculated with the following relationship:

$$\Delta_{predicted} = \begin{cases} \left[\alpha(\eta - X) + \beta\right]S_d & \text{for } F_{con004}/S_a m \leq \eta \\ \beta S_d & \text{for } F_{con004}/S_a m > \eta \end{cases} \tag{7.6}$$

where α = absolute value slope of the linear portion

η = value of $F_{con004}/S_a m$ corresponding to the transition from a linear relationship to a constant value. This value was taken as 0.04.

X = value of $F_{con004}/S_a m$

β = value for the constant portion

S_d = spectral displacement
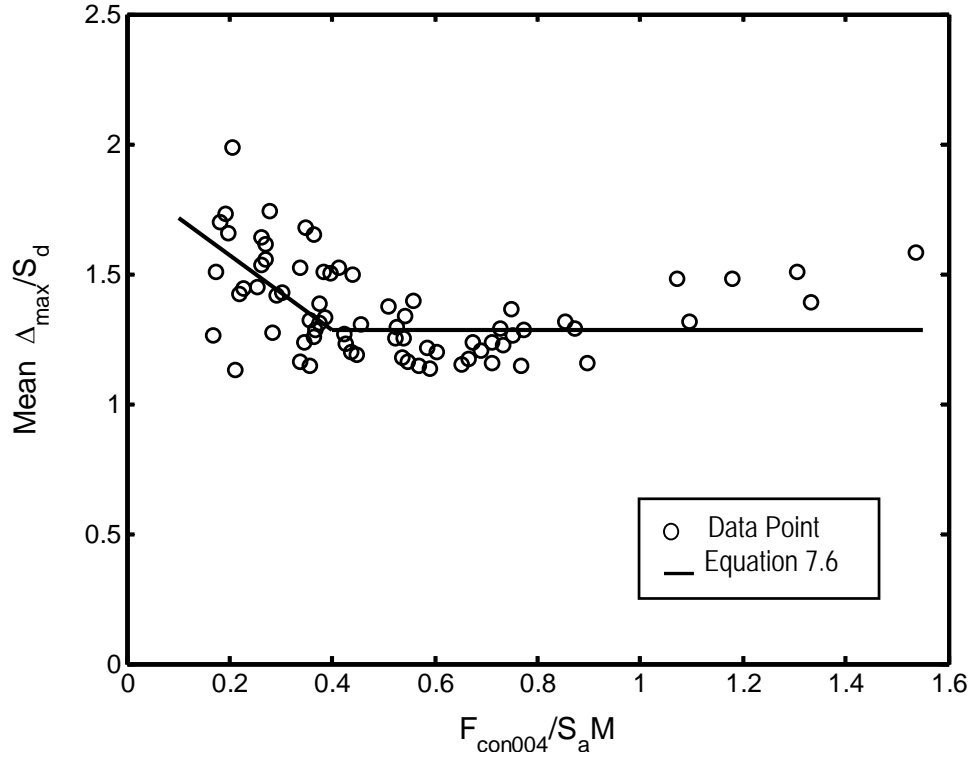
Figure 7.9: Bilinear Approximation for Maximum Displacement

Values for α and β were found by considering the maximum displacements for

the reinforced concrete frames subjected to both the 10 percent in 50 and 2 percent in 50

ground motions. A value of 1.43 was found for α by minimizing the sum of the squared

error between the predicted displacements and the actual displacements in the region

below 0.4. A value of 1.28 was found for β by averaging Δ_{max}/S_d for all the frames

with a $F_{con004}/S_a m$ above 0.4.

Using Equation 7.6 for each earthquake analysis with $\alpha = 2.0$, $\beta = 1.3$, and

$\eta = 0.4$ led to a ratio of the maximum displacement to the predicted displacement,

$\Delta_{max}/\Delta_{predicted}$, with a mean of 0.98 and standard deviation of 0.25. The overall statistics

were slightly better than the relationship provided in Section 7.5, but the accuracy

improved significantly for low values of the strength ratio. The predicted response

calculated from Equation 7.6 is shown in Figure 7.9.

7.7 TRENDS IN RESIDUAL DISPLACEMENT

A frame that has undergone significant yielding during a ground motion

excitation may not return to its original equilibrium position, resulting in a residual

displacement. The residual displacement can affect whether a structure needs to be

replaced after an earthquake or whether it can be repaired. If the residual displacements

do not require the structure to be replaced, they may still make repairing the structure

difficult. Therefore, residual displacements should be investigated independent of

maximum displacements (Kawashima et al. 1998).

For the 36 frames, residual displacements were calculated for each of the five 10

percent in 50 ground motions and the five 2 percent in 50 ground motions. The resulting

residual displacements from the 10 percent in 50 ground motions ranged from a

minimum of 0.0 in. (frame 5.005.10, ground motion 10-4, $\Delta_{residual}/L_{col} = 0.00$ percent) to

a maximum of 0.5 in. (frame 7.030.15, ground motion 10-3, $\Delta_{residual}/L_{col} = 0.16$ percent).

For the 2 percent in 50 ground motions, the residual displacements ranged from a

minimum of 0.0 in (frame 6.010.15, ground motion 2-4, $\Delta_{residual}/L_{col} = 0.00$ percent) to a

maximum of 2.9 in. (frame 7.030.10, ground motion 2-3, $\Delta_{residual}/L_{col} = 0.86$ percent).

Although the residual displacements resulting from ground motion 2-3 were

sizable, the resulting residual displacements on a whole were considerably smaller than

anticipated. The large weight used during this study may have contributed to the limited

residual displacements observed during this study. Field performance as well as

numerous research studies have suggested that reinforced concrete frames can experience

excessive residual displacements when subjected to a seismic event, whereas hybrid

frames experience significantly smaller residual displacements (Kawashima et al. 1998,

Zatar and Mutsuyoshi 2002, Sakai and Mahin 2004, and El-Sheikh et al. 1999). Because

the residual displacements were smaller than expected, especially when the results were

compared with the results of an elastic perfectly-plastic frame, a small-scale parametric

study was performed to determine the effects of the longitudinal mild steel's strain-

hardening ratio and the viscous damping ratio on the residual displacements. The strain-

hardening ratio was defined as the ratio between the steel's post-yielding tangent and its

initial elastic tangent. The strain-hardening ratio was varied during the parametric study

because Kawashima et al. (1998) suggested that the strain-hardening ratio has a

significant impact on residual drift.

Frame 7.020.05 was selected as the baseline frame for the parametric study

because it had one of the larger (but not the maximum) residual displacements ($\Delta_{residual} =$

0.8 in. and $\Delta_{residual}/L_{col} = 0.24$ percent) resulting from the 2 percent in 50 ground motions.

Strain-hardening ratios of 0.001, 0.005, 0.009, 0.015, and 0.020 were selected for this

study. The value of 0.009 was selected because it was the strain-hardening ratio used

throughout the original parametric study. Viscous damping ratios of 0.00, 0.01, 0.02,

0.03, and 0.04 were selected to provide a range of practical values. The results of the

parametric study are summarized in Table 7.1, while Figure 7.10 presents the effect of

the strain-hardening ratio and viscous damping ratio on residual drift graphically.

Table 7.1: Effect of Damping Ratio and SHR on Residual Displacement

Frame	Damping Ratio	SHR	Δ_{max} (in.)	$\dfrac{\Delta_{max}}{L_{col}}$ (%)	$\Delta_{residual}$ (in.)	$\dfrac{\Delta_{residual}}{L_{col}}$ (%)
7.020.05 -01	0.00	0.001	6.3	1.88	1.0	0.29
7.020.05 -02	0.00	0.005	6.3	1.86	0.9	0.27
7.020.05 -03	0.00	0.009	6.2	1.85	0.8	0.24
7.020.05 -04	0.00	0.015	6.1	1.82	0.7	0.20
7.020.05 -05	0.00	0.020	6.1	1.81	0.6	0.17
7.020.05 -06	0.01	0.001	6.2	1.84	0.9	0.27
7.020.05 -07	0.01	0.005	6.1	1.82	0.8	0.25
7.020.05 -08	0.01	0.009	6.1	1.80	0.8	0.23
7.020.05 -09	0.01	0.015	6.0	1.78	0.6	0.19
7.020.05 -10	0.01	0.020	5.9	1.77	0.6	0.17
7.020.05 -11	0.02	0.001	6.0	1.77	0.8	0.25
7.020.05 -12	0.02	0.005	5.9	1.76	0.8	0.23
7.020.05 -13	0.02	0.009	5.9	1.74	0.7	0.21
7.020.05 -14	0.02	0.015	5.8	1.72	0.6	0.18
7.020.05 -15	0.02	0.020	5.7	1.71	0.5	0.16
7.020.05 -16	0.03	0.001	5.7	1.70	0.7	0.22
7.020.05 -17	0.03	0.005	5.7	1.68	0.7	0.21
7.020.05 -18	0.03	0.009	5.6	1.67	0.6	0.19
7.020.05 -19	0.03	0.015	5.6	1.66	0.5	0.16
7.020.05 -20	0.03	0.020	5.5	1.65	0.5	0.15
7.020.05 -21	0.04	0.001	5.4	1.62	0.7	0.20
7.020.05 -22	0.04	0.005	5.4	1.61	0.6	0.18
7.020.05 -23	0.04	0.009	5.4	1.60	0.6	0.17
7.020.05 -24	0.04	0.015	5.3	1.59	0.5	0.15
7.020.05 -25	0.04	0.020	5.3	1.58	0.5	0.14
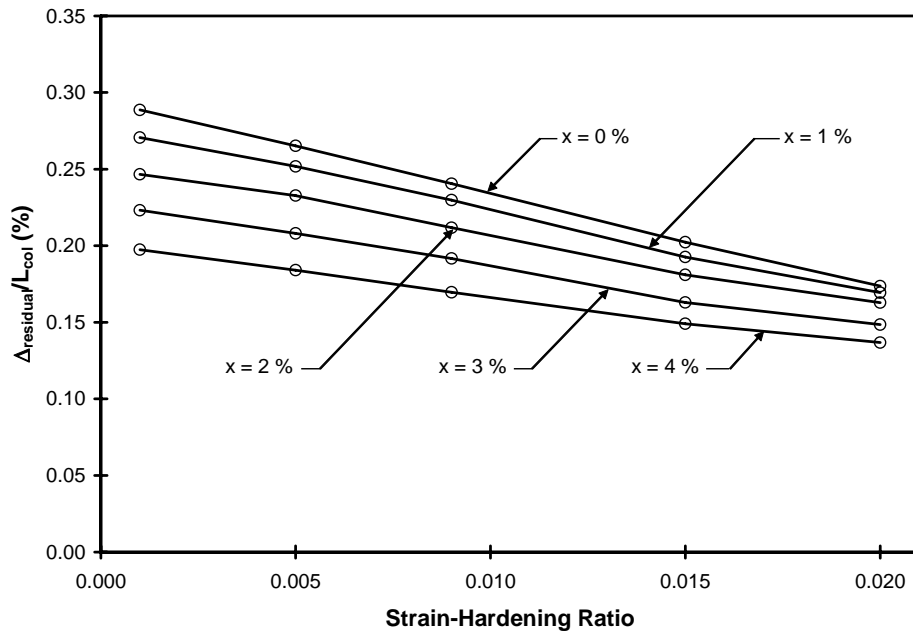
Figure 7.10: Effects of Damping Ratio and SHR on Residual Drift

The results summarized in Table 7.1 and pictured in Figure 7.10 show that varying the strain-hardening ratio from 0.001 to 0.020 resulted in a decrease in $\Delta_{residual}/L_{col}$ of 30 to 40 percent. As the damping ratio increased from 0 percent to 4 percent, a decrease in $\Delta_{residual}/L_{col}$ of 20 to 30 percent was observed. These observations indicate that the resulting residual displacements were significantly affected by the assumptions made during the modeling of the frames. This conclusion suggests that a detailed investigation is required to determine the effect of various parameters on residual displacements. Experimental test results are needed to calibrate the analytic models to accurately predict residual displacements. Therefore, complete residual displacement results are not presented here.

The results summarized in Table 7.1 also indicate that maximum displacements were not considerably affected by the strain-hardening ratio (3 percent variation between values of 0.001 and 0.020) or viscous damping ratio (14 percent variation between values of 0.00 and 0.04). This provides additional confidence in the maximum displacement results presented in this document.

CHAPTER 8
PUSHOVER ANALYSES OF HYBRID FRAMES

This chapter focuses on the pushover analysis of the hybrid frames that were part of the parametric study. The pushover analyses were conducted to determine first yield properties, initial cracked properties, estimated nominal yield displacement, and maximum strength of hybrid frames.

This chapter describes the parameters that were varied for the hybrid frames (Section 8.1), key characteristics that were useful for comparison among pushover analyses (Section 8.2), and key results obtained from these analyses (sections 8.3 through 8.5).

8.1 RANGE OF HYBRID PARAMETRIC STUDY

To evaluate the hybrid frame for a variety of configurations, the parameters to be varied had to be selected. The parameters varied for the reinforced concrete frame study alone were inadequate for the hybrid frame study because prestressing introduces additional parameters. Therefore, parameters had to be selected that would account for the factors introduced by the prestessing, such as combined moment capacity and re-centering ability, while also providing a sensible link between the parameters selected for the reinforced concrete frames and the hybrid frames. This section presents the rationale for the parameters that were varied for the hybrid frames. The following four parameters were selected to be varied during this study:

- ○ column aspect ratio, L_{col}/D_{col}
- ○ axial-load ratio, $P_{col}/(f_c' A_g)$
- ○ equivalent reinforcement ratio, $\rho_{eq} = \left(\rho_s f_y + \rho_p f_{py} \right) / f_y$

o re-centering ratio, $\lambda_{rc} = \left(P_{col} + A_p f_{p0} \right) / A_s f_y$.

On the basis of the reasoning provided in Section 6.1, a column diameter, D_{col}, of 48 in. was used for all hybrid frames. The results found during this study can be scaled to provide estimates for frames with other column diameters. To provide a basis for comparison between the reinforced concrete frames and the hybrid frames, parameters similar to those used for the reinforced concrete frames were selected.

The parameters selected for the reinforced concrete frames were all independent from one another; therefore, every combination of parameters was used (Chapter 6). On the other hand, the parameters selected for the hybrid frames were interdependent; therefore, every combination of the parameters would not result in quantities that were physically possible. For example, it is not possible to have a negative area of prestressing steel. The following paragraphs provide a description of the parameters.

8.1.1 Column Aspect Ratio, L_{col}/D_{col}

The column aspect ratio was defined as the clear height between the top of the foundation and the bottom of the cap-beam divided by the diameter of the column, L_{col}/D_{col} . The required minimum vertical clearance from Article 1120.04 (5) of the WSDOT Design Manual (WSDOT 2002b) is 16.5 ft. For the frames with 48-in.-diameter columns, this resulted in a minimum L_{col}/D_{col} of 4.125. This value was increased to 5, 6, and 7 for the L_{col}/D_{col} for this study.

8.1.2 Axial-Load Ratio, $P_{col}/(f_c' A_g)$

The axial-load ratio was defined as the compressive axial-load on a column divided by the product of the unconfined concrete compressive strength and the gross

area of the column's cross-section, $P_{col}/(f_c' A_g)$. Article 5.10.11.4.1 b of the AASHTO

LRFD Bridge Design Specification (AASHTO 1998) permits axial-load ratios of up to

0.20. The prototype bridge described in Chapter 4 had a $P_{col}/(f_c' A_g)$ value of

approximately 0.075. To include a variety of values in the allowable range, axial-load

ratios of 0.05, 0.10, and 0.15 were selected for this study.

8.1.3 Equivalent Reinforcement Ratio

The equivalent reinforcement ratio was selected to account for the contribution of

both mild reinforcing steel and prestressing steel to the lateral load resisting capacity of

the pier. The equivalent reinforcement ratio was defined by Equation 8.1.

$$\rho_{eq} = \frac{\rho_s f_y + \rho_p f_{py}}{f_y} \tag{8.1}$$

where $\rho_s =$ area of longitudinal mild steel divided by the gross cross-sectional area of

the column, A_s/A_g

$f_y =$ yield strength of the longitudinal mild steel, taken as 60 ksi

$\rho_p =$ area of prestressing steel divided by the gross cross-sectional area of the

column, A_p/A_g

$f_{py} =$ yield strength of the prestressing steel, taken as 243 ksi

Equivalent reinforcement ratios were chosen to represent hybrid frames with

strength similar to that of the reinforced concrete frames studied (chapters 6 and 7).

Accordingly, ρ_{eq} values of 0.005, 0.01, 0.02, and 0.03 were chosen for this study.

8.1.4 Re-centering Ratio, λ_{rc}

The re-centering ratio was defined by Equation 8.2.

$$\lambda_{rc} = \frac{P_{col} + A_p f_{p0}}{A_s f_y} \tag{8.2}$$

where P_{col} = compressive axial-load on a column

A_p = area of prestressing steel

f_{p0} = stress in prestressing steel at zero drift

A_s = area of longitudinal mild steel

f_y = yield strength of longitudinal mild steel, taken as 60 ksi

The re-centering ratio was selected to estimate the ability of the frames to re-center. It was assumed that the axial-load on the column, as well as the force from the prestressing steel, would cause the frame to re-center if they were larger than the resisting force from the longitudinal mild steel. For moderate to strong ground motions, re-centering was expected to occur when the re-centering ratio was near 1.0. As the re-centering ratio decreased below 1.0, the likelihood of re-centering was expected to decrease. Re-centering was expected to occur for small earthquakes, regardless of the re-centering ratio. Re-centering ratios of 0.0, 0.25, 0.50, 0.75, and 1.00 were chosen to evaluate the re-centering ability of the frames.

8.1.5 Frame Designation

Frames were identified by the combination of their column aspect ratio, equivalent reinforcement ratio, and re-centering ratio. For example, 5.020.050 was a frame with $L_{col}/D_{col} = 5$, $\rho_{eq} = 0.020$, and $\lambda_{rc} = 0.50$; 7.030.100 was a frame with $L_{col}/D_{col} = 7$, $\rho_{eq} = 0.030$, and $\lambda_{rc} = 1.00$. The axial-load ratio was not included in the frame designation because the results were tabulated and plotted for individual values of the axial-load ratio.

8.1.6 Practical Frame Combinations

The values presented in the previous paragraphs were target values. Instead of creating frames from every combination of the four parameters, it was necessary to solve for the variables in the parameters and use only the combinations that resulted in practical frames. Many of the combinations resulted in a negative required prestressing area. This is not physically possible, but the combinations represented frames that would most likely re-center without prestressing steel. Only combinations of the parameters that resulted in positive values of A_s and A_p were used for this study. The following method was used to determine which of the combinations resulted in practical values.

1. The yield strain of the prestressing steel was found from $\varepsilon_{py} = f_{py}/E_p$, where f_{py} was the yield strength of the prestressing steel and E_p was the modulus of elasticity of the prestressing steel. From AASHTO Article 5.4.4, f_{py} was taken as $0.9 f_{pu}$, where f_{pu} was the specified tensile strength of the prestressing steel and was assumed to be 270 kips based on Article 6.1.3 from the WSDOT Bridge Design Manual (WSDOT 2002a). E_p was taken as 28,500 ksi (AASHTO 1998).

2. The stress in the prestressing steel at zero drift, f_{p0}, was found from the following relationship:

$$f_{p0} = \left(\varepsilon_{py} - \frac{(\Delta/L_{col})D_{col}}{L_{col}} \right) E_p \leq 0.7 f_{pu} \tag{8.3}$$

A maximum drift ratio, Δ/L_{col}, of 0.02 was assumed on the basis of the results of the reinforced concrete frames subjected to 10 percent in 50 ground motions (Chapter 7). The upper limit of $0.7 f_{pu}$ for f_{p0} was taken from AASHTO Article

5.9.3. This estimate was conservative because the lever arm was most likely smaller than $D_{col}/2$, which would result in a larger f_{p0}. For most of the frames, the $0.7f_{pu}$ limit controlled.

3. The required area of longitudinal mild steel was found by rearranging Equation 8.1 as follows:

$$A_s = \left(\frac{\rho_{eq} f_y - \rho_p f_{py}}{f_y} \right) A_g \tag{8.4}$$

4. The required area of prestressing steel was then found from the re-center ratio as:

$$A_p = \frac{\lambda_{rc} f_y - P_{col}}{f_{p0}} \tag{8.5}$$

After the required area of longitudinal mild steel and prestressing steel was calculated, combinations that resulted in a negative value for A_p were omitted because these combinations of parameters represented frames that were expected to re-center without prestressing steel. The combinations that resulted in frames that were used for this study are summarized in tables 8.1 and 8.2 for axial-load ratios equal to 0.05 and 0.10, respectively.

Table 8.1: Reinforcing Properties, Hybrid Frames, $P_{col}/(f_c' A_g) = 0.05$

Frame	ρ_s (%)	A_s (in.^{2})	ρ_p (%)	A_p (in.^{2})	ρ_p/ρ_s (%)
5.020.025	1.897	34.3	0.017	0.3	0.892
5.030.025	2.759	49.9	0.076	1.4	2.758
5.010.050	0.862	15.6	0.017	0.3	1.962
5.020.050	1.552	28.1	0.110	2.0	7.083
5.030.050	2.069	37.4	0.211	3.8	10.217
5.010.075	0.862	15.6	0.051	0.9	5.885
5.020.075	1.207	21.8	0.178	3.2	14.712
5.030.075	1.724	31.2	0.296	5.4	17.163
5.005.100	0.517	9.4	0.008	0.2	1.635
5.010.100	0.690	12.5	0.085	1.5	12.260
5.020.100	1.035	18.7	0.220	4.0	21.250
5.030.100	1.552	28.1	0.355	6.4	22.884
6.020.025	1.897	34.3	0.017	0.3	0.892
6.030.025	2.759	49.9	0.076	1.4	2.758
6.010.050	0.862	15.6	0.017	0.3	1.962
6.020.050	1.552	28.1	0.110	2.0	7.083
6.030.050	2.069	37.4	0.211	3.8	10.217
6.010.075	0.862	15.6	0.051	0.9	5.885
6.020.075	1.207	21.8	0.178	3.2	14.712
6.030.075	1.724	31.2	0.296	5.4	17.163
6.005.100	0.517	9.4	0.008	0.2	1.635
6.010.100	0.690	12.5	0.085	1.5	12.260
6.020.100	1.035	18.7	0.220	4.0	21.250
6.030.100	1.552	28.1	0.355	6.4	22.884
7.020.025	1.897	34.3	0.017	0.3	0.892
7.030.025	2.759	49.9	0.076	1.4	2.758
7.010.050	0.862	15.6	0.017	0.3	1.962
7.020.050	1.552	28.1	0.110	2.0	7.083
7.030.050	2.069	37.4	0.211	3.8	10.217
7.010.075	0.862	15.6	0.051	0.9	5.885
7.020.075	1.207	21.8	0.178	3.2	14.712
7.030.075	1.724	31.2	0.296	5.4	17.163
7.005.100	0.517	9.4	0.008	0.2	1.635
7.010.100	0.690	12.5	0.085	1.5	12.260
7.020.100	1.035	18.7	0.220	4.0	21.250
7.030.100	1.552	28.1	0.355	6.4	22.884

Table 8.2: Reinforcing Properties, Hybrid Frames, $P_{col}/(f_c' A_g) = 0.10$

Frame	ρ_s (%)	A_s (in.^{2})	ρ_p (%)	A_p (in.^{2})	ρ_p/ρ_s (%)
5.020.050	1.897	34.3	0.034	0.6	1.783
5.030.050	2.414	43.7	0.127	2.3	5.254
5.020.075	1.552	28.1	0.110	2.0	7.083
5.030.075	2.069	37.4	0.228	4.1	11.034
5.010.100	0.862	15.6	0.025	0.5	2.942
5.020.100	1.379	25.0	0.161	2.9	11.647
5.030.100	1.724	31.2	0.304	5.5	17.653
6.020.050	1.897	34.3	0.034	0.6	1.783
6.030.050	2.414	43.7	0.127	2.3	5.254
6.020.075	1.552	28.1	0.110	2.0	7.083
6.030.075	2.069	37.4	0.228	4.1	11.034
6.010.100	0.862	15.6	0.025	0.5	2.942
6.020.100	1.379	25.0	0.161	2.9	11.647
6.030.100	1.724	31.2	0.304	5.5	17.653
7.020.050	1.897	34.3	0.034	0.6	1.783
7.030.050	2.414	43.7	0.127	2.3	5.254
7.020.075	1.552	28.1	0.110	2.0	7.083
7.030.075	2.069	37.4	0.228	4.1	11.034
7.010.100	0.862	15.6	0.025	0.5	2.942
7.020.100	1.379	25.0	0.161	2.9	11.647
7.030.100	1.724	31.2	0.304	5.5	17.653

8.2 KEY CHARACTERISTICS OF PUSHOVER RESPONSE

This section describes the key quantities, calculated from the results of the pushover analyses, that provided a basis for comparing the expected performance of the reinforced concrete frames and that of the hybrid frames.

8.2.1 Uncracked Properties

The uncracked stiffness, $k_{uncracked}$, represented the tangent stiffness at zero force on the force-displacement curve. The uncracked stiffness was computed indirectly from the natural circular frequency, ω_n, which was found with an eigenvalue analysis with OpenSees, and the mass, m.

$$k_{uncracked} = \omega_n^2 m \qquad (8.6)$$

The uncracked natural period, $T_{n,uncracked}$, was found as follows:

$$T_{n,uncracked} = \frac{2\pi}{\omega_n}$$
(8.7)

8.2.2 First Yield

First yield was defined as the point at which the column's extreme tensile steel first reached its yield strain or the column concrete compressive strain reached 0.002, whichever occurred first. The effective force at first yield was denoted as $F_{firstyield}$, while the corresponding displacement at first yield was denoted as $\Delta_{firstyield}$. An idealized force-displacement curve is shown in Figure 8.1 along with the $F_{firstyield}$ and the $\Delta_{firstyield}$. The drift ratio at first yield was defined as $\Delta_{firstyield}/L_{col}$.
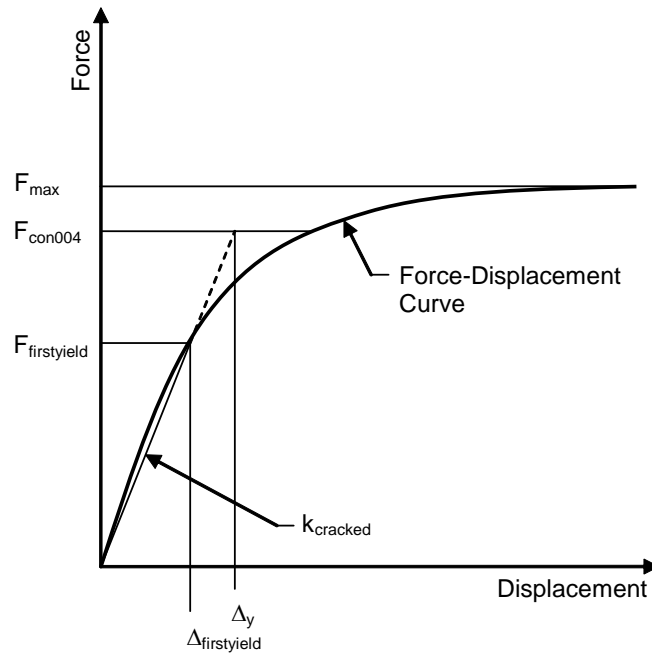
Figure 8.1: Idealized Force-Displacement Curve (Camarillo 2003)

8.2.3 Cracked Properties

The initial cracked stiffness, $k_{cracked}$, was found from the secant stiffness through

first yield (Figure 8.1).

$$k_{cracked} = \frac{F_{firstyield}}{\Delta_{firstyield}}$$

(8.8)

The cracked natural period, $T_{n,cracked}$, was found as:

$$T_{n,cracked} = 2\pi\sqrt{\frac{m}{k_{cracked}}}$$

(8.9)

8.2.4 Stiffness Ratio, $k_{cracked}/k_{uncracked}$

The stiffness ratio was defined as the cracked stiffness divided by the uncracked

stiffness. This ratio reflected the loss of stiffness due to cracking.

8.2.5 Effective Force at a Concrete Strain of 0.004, F_{con004}

The effective force on the force-displacement curve that corresponded to the

concrete compressive strain first reaching 0.004 was denoted as F_{con004} and is shown in

Figure 8.1. This value was used to calculate the nominal yield displacement.

8.2.6 Nominal Yield Displacement, Δ_y

A nominal yield displacement, Δ_y, had to be defined to calculate displacement

ductility (Chapter 10). The force-displacement curve would become nonlinear during the

pushover analysis, as is evident in the idealized force-displacement curve of Figure 8.1.

As suggested by Priestley et al. (1996), to estimate Δ_y, the force-displacement curve

was idealized with an equivalent bilinear relationship by extrapolating $k_{cracked}$ up to

F_{con004}. The nominal yield displacement was found from the following relationship:

$$\Delta_y = \frac{F_{con004}\Delta_{firstyield}}{F_{firstyield}} \tag{8.10}$$

8.2.7 Maximum Force, F_{max}

The largest lateral force achieved during the pushover analysis was denoted as F_{max}.

8.3 TRENDS IN STIFFNESS RATIO

The stiffness ratios that were calculated from the pushover analyses of the hybrid frames are discussed in this section. The results for frames with an axial-load ratio of 0.05 are summarized in Table 8.3, and the results for frames with an axial-load ratio of 0.10 are summarized in Table 8.4. The tables show that $k_{cracked}/k_{uncracked}$ ranged from 0.29 to 0.56. Similarly, Priestley et al. (1996) found that $k_{cracked}/k_{uncracked}$ ranged from 0.35 to 0.60 for typical circular reinforced concrete columns with longitudinal reinforcement ratios of between 0.01 and 0.03, and axial load ratios of between 0.10 and 0.30. The slightly lower values may reflect the cracked interface between the column and the foundation or cap-beam.

Table 8.3: Natural Periods and Stiffnesses, Hybrid Frames, $P_{col}/(f_c' A_g) = 0.05$

Frame	Mass (kip-sec/in.^{2})	$T_{n,uncracked}$ (sec)	$T_{n,cracked}$ (sec)	$k_{uncracked}$ (kips/in.)	$k_{cracked}$ (kips/in.)	$\dfrac{k_{cracked}}{k_{uncracked}}$
5.020.025	2.342	0.242	0.382	1575.6	633.8	0.402
5.030.025	2.342	0.234	0.337	1695.8	815.1	0.481
5.010.050	2.342	0.255	0.449	1418.9	458.6	0.323
5.020.050	2.342	0.247	0.377	1511.3	649.5	0.430
5.030.050	2.342	0.242	0.343	1572.7	787.2	0.501
5.010.075	2.342	0.256	0.431	1414.6	497.9	0.352
5.020.075	2.342	0.253	0.376	1447.3	655.7	0.453
5.030.075	2.342	0.248	0.343	1504.9	787.9	0.524
5.005.100	2.342	0.260	0.479	1366.4	402.6	0.295
5.010.100	2.342	0.259	0.423	1382.9	517.2	0.374
5.020.100	2.342	0.256	0.372	1412.8	668.2	0.473
5.030.100	2.342	0.251	0.341	1466.5	796.5	0.543
6.020.025	2.342	0.307	0.489	981.7	386.3	0.394
6.030.025	2.342	0.296	0.431	1055.7	497.6	0.471
6.010.050	2.342	0.323	0.574	885.2	280.4	0.317
6.020.050	2.342	0.313	0.482	941.6	397.5	0.422
6.030.050	2.342	0.307	0.438	979.0	482.3	0.493
6.010.075	2.342	0.324	0.550	882.4	305.2	0.346
6.020.075	2.342	0.320	0.479	901.9	403.1	0.447
6.030.075	2.342	0.314	0.437	936.7	484.2	0.517
6.005.100	2.342	0.329	0.611	852.9	247.5	0.290
6.010.100	2.342	0.327	0.539	862.7	318.8	0.369
6.020.100	2.342	0.324	0.474	880.4	412.1	0.468
6.030.100	2.342	0.318	0.434	912.8	490.6	0.537
7.020.025	2.342	0.376	0.605	652.5	252.5	0.387
7.030.025	2.342	0.363	0.533	701.2	325.5	0.464
7.010.050	2.342	0.396	0.709	589.1	183.7	0.312
7.020.050	2.342	0.384	0.596	626.0	260.6	0.416
7.030.050	2.342	0.377	0.541	650.3	316.4	0.487
7.010.075	2.342	0.397	0.679	587.2	200.4	0.341
7.020.075	2.342	0.393	0.590	599.7	265.2	0.442
7.030.075	2.342	0.385	0.539	622.2	318.5	0.512
7.005.100	2.342	0.403	0.754	568.0	162.8	0.287
7.010.100	2.342	0.401	0.663	574.2	210.1	0.366
7.020.100	2.342	0.397	0.583	585.5	271.8	0.464
7.030.100	2.342	0.391	0.535	606.3	323.2	0.533

Table 8.4: Natural Periods and Stiffnesses, Hybrid Frames, $P_{col}/(f_c' A_g) = 0.10$

Frame	Mass (kip-sec/in.²)	$T_{n,uncracked}$ (sec)	$T_{n,cracked}$ (sec)	$k_{uncracked}$ (kips/in.)	$k_{cracked}$ (kips/in.)	$\dfrac{k_{cracked}}{k_{uncracked}}$
5.020.050	4.684	0.343	0.502	1573.7	733.2	0.466
5.030.050	4.684	0.336	0.465	1637.9	854.0	0.521
5.020.075	4.684	0.350	0.502	1511.3	734.5	0.486
5.030.075	4.684	0.343	0.465	1569.8	854.2	0.544
5.010.100	4.684	0.361	0.555	1417.9	600.1	0.423
5.020.100	4.684	0.354	0.499	1476.8	743.9	0.504
5.030.100	4.684	0.351	0.468	1503.3	844.1	0.561
6.020.050	4.684	0.434	0.642	980.4	448.2	0.457
6.030.050	4.684	0.426	0.595	1019.6	522.6	0.513
6.020.075	4.684	0.443	0.641	941.6	450.6	0.479
6.030.075	4.684	0.435	0.594	977.1	524.0	0.536
6.010.100	4.684	0.457	0.708	884.5	369.4	0.418
6.020.100	4.684	0.448	0.636	920.1	457.5	0.497
6.030.100	4.684	0.445	0.597	935.7	519.3	0.555
7.020.050	4.684	0.533	0.794	651.7	293.4	0.450
7.030.050	4.684	0.523	0.735	677.3	342.3	0.505
7.020.075	4.684	0.544	0.791	626.0	295.8	0.473
7.030.075	4.684	0.534	0.733	649.0	344.0	0.530
7.010.100	4.684	0.560	0.872	588.7	243.1	0.413
7.020.100	4.684	0.550	0.784	611.7	300.9	0.492
7.030.100	4.684	0.545	0.736	621.5	341.7	0.550

The following trends were observed from the plots of $k_{cracked}/k_{uncracked}$ shown in figures 8.2 and 8.3.

- $k_{cracked}/k_{uncracked}$ increased as ρ_{eq} increased, as shown in figures 8.2 and 8.3. For example, $k_{cracked}/k_{uncracked}$ increased by 84 percent between frames 5.005.100 and 5.030.100 for an axial-load ratio of 0.05. The additional transformed area of concrete (equal to nA_s where $n = E_s/E_c$) increased $k_{uncracked}$ as ρ_{eq} increased. However, $k_{cracked}$ increased even more as ρ_{eq} increased because the neutral-axis of the cracked section was also influenced by ρ_{eq}. For typical circular reinforced concrete columns with longitudinal reinforcement ratios of between 0.01 and 0.03 (no prestressing included) and axial load ratios of between 0.10 and 0.30, Priestley et al. (1996) also found that $k_{cracked}/k_{uncracked}$ increased as ρ_{eq} increased.
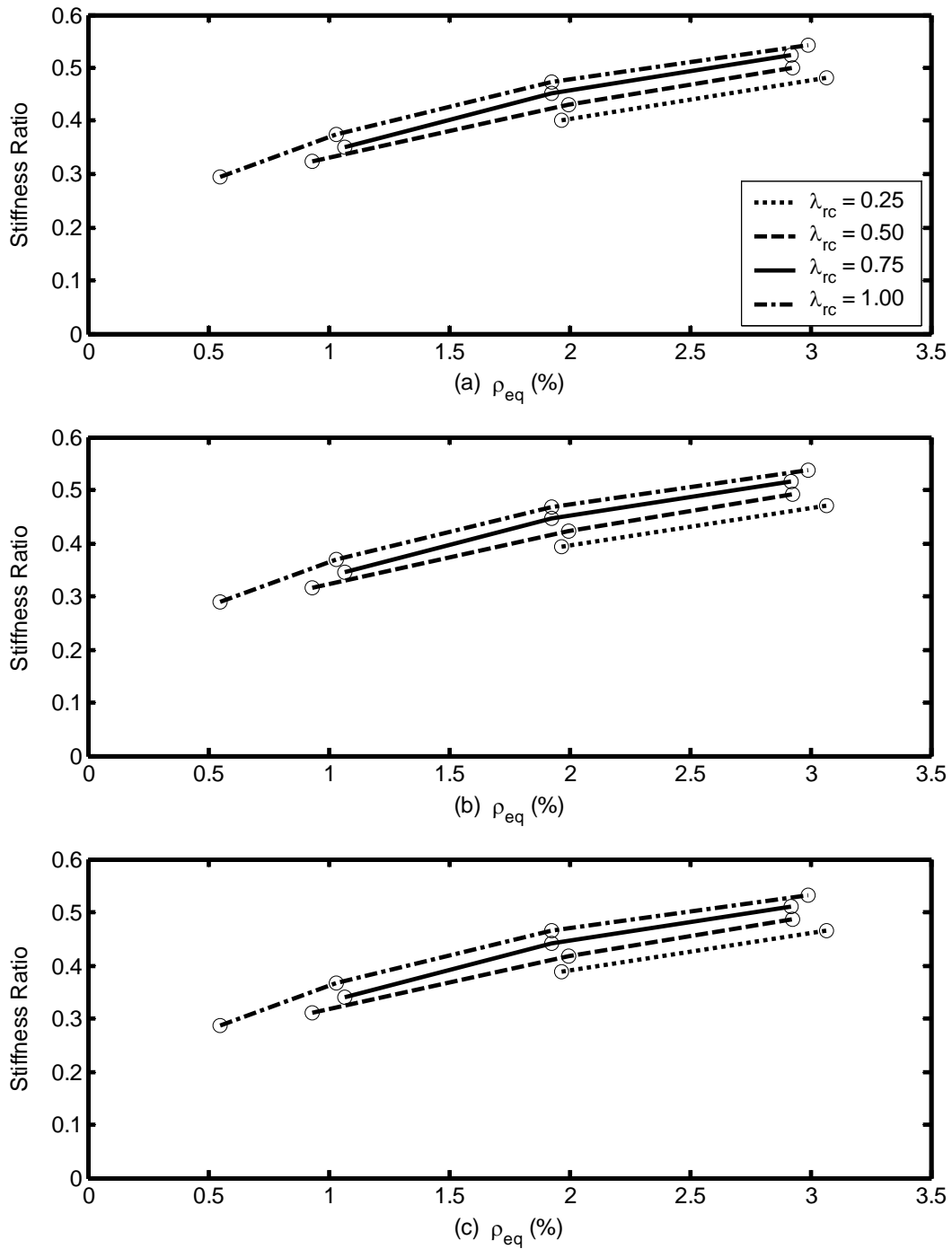
Figure 8.2: Stiffness Ratio, Hybrid Frames, $P_{col}/(f_c' A_g) = 0.05$

(a) $L_{col}/D_{col} = 5$, **(b)** $L_{col}/D_{col} = 6$, **and (c)** $L_{col}/D_{col} = 7$
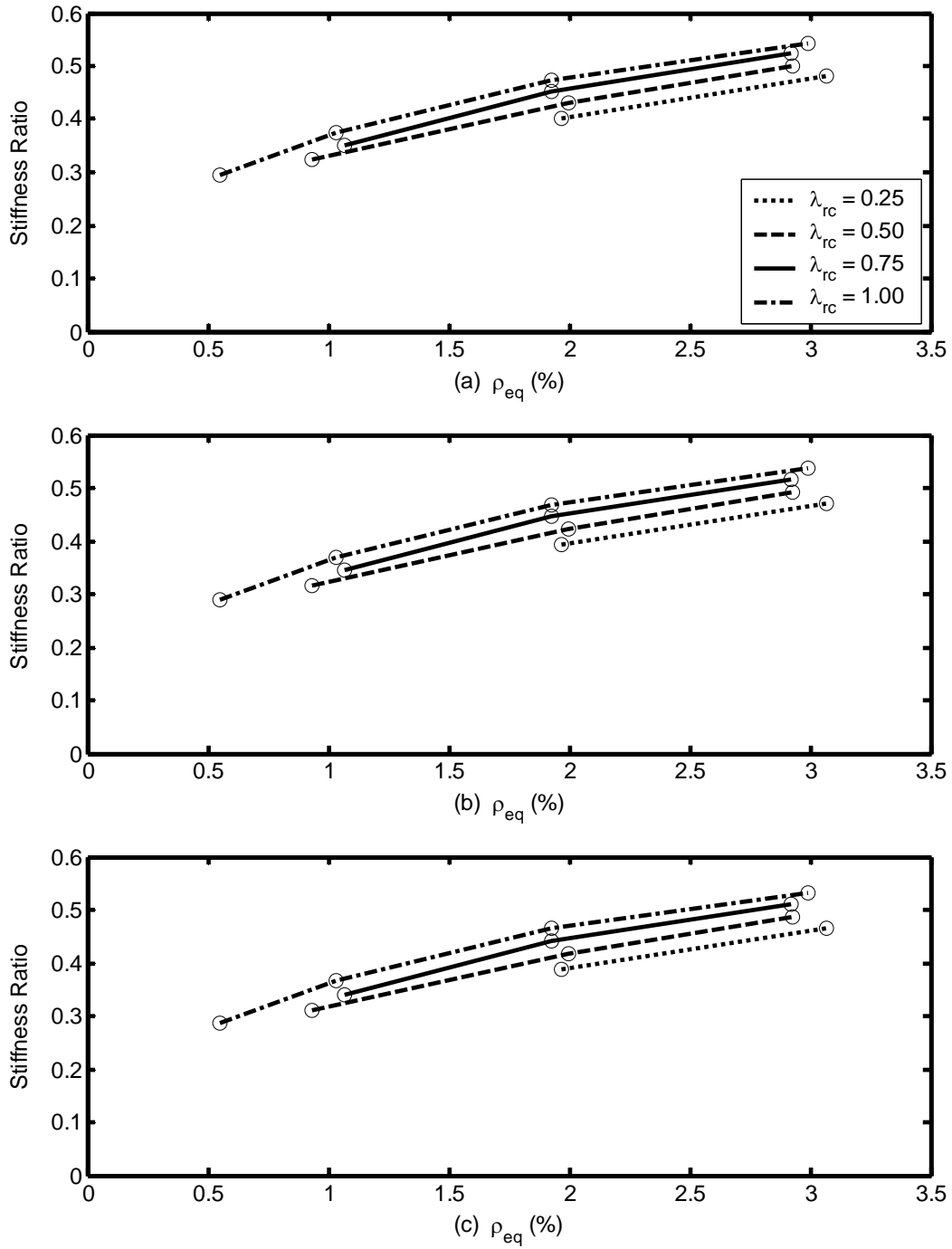
Figure 8.3: Stiffness Ratio, Hybrid Frames, $P_{col}/(f_c' A_g) = 0.10$
(a) $L_{col}/D_{col} = 5$, (b) $L_{col}/D_{col} = 6$, and (c) $L_{col}/D_{col} = 7$

128

- $k_{cracked}/k_{uncracked}$ increased slightly as $P_{col}/(f_c'A_g)$ increased (figures 8.2 and 8.3). The stiffness ratio increased by 13 percent for frame 5.010.100 as $P_{col}/(f_c'A_g)$ increased from 0.05 to 0.10. $k_{cracked}$ was influenced by $P_{col}/(f_c'A_g)$ because, as the axial-load ratio increased, the distance from the neutral-axis to the extreme compression face of the column cross-section also increased, resulting in an increased cracked stiffness. Paulay and Priestley (1992) presented values for the cracked stiffness with larger values for larger axial-loads. Priestley et al. (1996) also found that $k_{cracked}/k_{uncracked}$ increased as $P_{col}/(f_c'A_g)$ increased.

- $k_{cracked}/k_{uncracked}$ remained essentially unchanged as L_{col}/D_{col} varied. This trend indicated that $k_{cracked}$ and $k_{uncracked}$ were equally influenced by L_{col}/D_{col}. As expected from the relationship for stiffness $\left(k = \alpha EI/L_{col}^3\right)$, both $k_{uncracked}$ and $k_{cracked}$ decreased as L_{col}/D_{col} increased.

- From figures 8.2 and 8.3 it is evident that $k_{cracked}/k_{uncracked}$ slightly increased as λ_{rc} increased. For example, $k_{cracked}/k_{uncracked}$ increased by 18 percent for an axial-load ratio of 0.05 between frames 5.020.025 to 5.020.100. This trend was consistent with the trend observed for the axial-load ratio because as λ_{rc} increased, the additional prestressing increased the axial-load on the columns.

These trends indicate that ρ_{eq} had the greatest influence on $k_{cracked}/k_{uncracked}$; $P_{col}/(f_c'A_g)$ and λ_{rc} had a small impact on $k_{cracked}/k_{uncracked}$; and L_{col}/D_{col} had almost no effect on $k_{cracked}/k_{uncracked}$.

8.4 TRENDS IN NOMINAL YIELD DISPLACEMENTS

Table 8.5 summarizes the nominal yield displacements, Δ_y, and their corresponding drift ratios, Δ_y/L_{col}, for hybrid frames with an axial-load ratio equal to 0.05. Table 8.6 summarizes the same for frames with an axial-load ratio equal to 0.10. Values for Δ_y ranged from 0.8 in. to 2.3 in., while Δ_y/L_{col} varied from 0.35 percent to 0.68 percent.

Table 8.5: Yield and Strength Properties, Hybrid Frames, $P_{col}/(f_c^{'} A_g) = 0.05$

Frame	$F_{firstyield}$	$\Delta_{firstyield}$	$\dfrac{\Delta_{firstyield}}{L_{col}}$	F_{con004}	Δ_{yield}	$\dfrac{\Delta_{yield}}{L_{col}}$	F_{max}
	(kips)	(in.)	(%)	(kips)	(in.)	(%)	(kips)
5.020.025	523.8	0.826	0.34	760.7	1.200	0.50	783.9
5.030.025	729.7	0.895	0.37	1045.0	1.282	0.53	1103.0
5.010.050	321.2	0.700	0.29	451.2	0.984	0.41	452.0
5.020.050	522.0	0.804	0.33	733.7	1.130	0.47	776.2
5.030.050	686.5	0.872	0.36	941.8	1.196	0.50	1004.5
5.010.075	346.6	0.696	0.29	484.2	0.973	0.41	494.1
5.020.075	501.5	0.765	0.32	684.2	1.044	0.43	726.3
5.030.075	673.8	0.855	0.36	899.6	1.142	0.48	947.7
5.005.100	244.8	0.608	0.25	333.6	0.829	0.35	333.7
5.010.100	337.5	0.652	0.27	456.7	0.883	0.37	475.0
5.020.100	496.5	0.743	0.31	665.3	0.996	0.41	692.1
5.030.100	676.7	0.850	0.35	884.9	1.111	0.46	926.6
6.020.025	435.6	1.127	0.39	630.8	1.633	0.57	645.2
6.030.025	607.0	1.220	0.42	867.8	1.744	0.61	908.5
6.010.050	266.8	0.951	0.33	372.5	1.328	0.46	372.8
6.020.050	434.0	1.092	0.38	608.1	1.530	0.53	633.4
6.030.050	570.8	1.184	0.41	781.6	1.621	0.56	824.2
6.010.075	288.0	0.944	0.33	400.1	1.311	0.46	402.2
6.020.075	416.9	1.034	0.36	566.8	1.406	0.49	591.5
6.030.075	560.2	1.157	0.40	746.4	1.541	0.54	778.0
6.005.100	203.4	0.822	0.29	274.6	1.109	0.39	274.6
6.010.100	280.5	0.880	0.31	377.0	1.183	0.41	381.6
6.020.100	412.7	1.002	0.35	551.0	1.337	0.46	564.7
6.030.100	562.6	1.147	0.40	734.0	1.496	0.52	760.5
7.020.025	372.4	1.475	0.44	537.7	2.129	0.63	546.1
7.030.025	519.2	1.595	0.47	741.0	2.276	0.68	769.7
7.010.050	227.9	1.241	0.37	315.9	1.719	0.51	316.6
7.020.050	371.0	1.424	0.42	518.2	1.989	0.59	532.2
7.030.050	488.1	1.543	0.46	666.8	2.107	0.63	694.3
7.010.075	246.1	1.228	0.37	339.7	1.695	0.50	339.9
7.020.075	356.4	1.344	0.40	482.7	1.820	0.54	494.5
7.030.075	479.0	1.504	0.45	636.6	1.999	0.59	656.0
7.005.100	173.6	1.066	0.32	232.0	1.425	0.42	232.1
7.010.100	239.6	1.140	0.34	319.9	1.522	0.45	320.7
7.020.100	352.8	1.298	0.39	469.2	1.726	0.51	473.5
7.030.100	481.0	1.488	0.44	626.0	1.937	0.58	641.2

Table 8.6: Yield and Strength Properties, Hybrid Frames, $P_{col}/(f'_c A_g) = 0.10$

Frame	$F_{firstyield}$	$\Delta_{firstyield}$	$\dfrac{\Delta_{firstyield}}{L_{col}}$	F_{con004}	Δ_{yield}	$\dfrac{\Delta_{yield}}{L_{col}}$	F_{max}
	(kips)	(in.)	(%)	(kips)	(in.)	(%)	(kips)
5.020.050	621.3	0.847	0.35	854.9	1.166	0.49	876.5
5.030.050	777.2	0.910	0.38	1049.8	1.229	0.51	1092.4
5.020.075	604.8	0.823	0.34	808.6	1.101	0.46	826.6
5.030.075	772.8	0.905	0.38	1012.0	1.185	0.49	1049.7
5.010.100	419.5	0.699	0.29	556.1	0.927	0.39	557.3
5.020.100	603.8	0.812	0.34	795.0	1.069	0.45	810.2
5.030.100	750.8	0.890	0.37	959.8	1.137	0.47	985.6
6.020.050	515.8	1.151	0.40	707.0	1.578	0.55	716.2
6.030.050	645.4	1.235	0.43	869.5	1.664	0.58	892.5
6.020.075	502.1	1.114	0.39	668.5	1.484	0.52	673.9
6.030.075	641.8	1.225	0.43	838.0	1.599	0.56	858.5
6.010.100	348.1	0.942	0.33	458.0	1.240	0.43	458.6
6.020.100	501.2	1.096	0.38	657.2	1.437	0.50	661.5
6.030.100	623.4	1.200	0.42	794.6	1.530	0.53	808.7
7.020.050	440.2	1.500	0.45	600.8	2.048	0.61	602.1
7.030.050	551.1	1.610	0.48	740.2	2.162	0.64	751.9
7.020.075	428.4	1.449	0.43	567.8	1.920	0.57	569.1
7.030.075	547.9	1.593	0.47	713.2	2.073	0.62	723.7
7.010.100	296.8	1.221	0.36	387.2	1.593	0.47	387.4
7.020.100	427.7	1.422	0.42	558.3	1.856	0.55	558.3
7.030.100	532.1	1.557	0.46	676.1	1.979	0.59	682.7

In this section, the trends observed in figures 8.4 and 8.5 are discussed for Δ_y/L_{col}, but similar trends were evident in the results for Δ_y, though the variations were larger for Δ_y than for Δ_y/L_{col}.

- Δ_y/L_{col} increased as ρ_{eq} increased (figures 8.4 and 8.5). For example, for an axial-load ratio of 0.05, Δ_y/L_{col} increased by 31 percent between frames 5.005.100 and 5.030.100. This trend was a consequence of the effect of ρ_{eq} on strength and stiffness. The ratio of $k_{cracked}$ between frames 5.005.100 and 5.030.100 was 0.51, while the ratio of F_{max} between the two frames was 0.36, indicating that ρ_{eq} influenced $k_{cracked}$ more than F_{max}. Because the strength increased more between the two frames than the stiffness, the expectation, based on geometry, was that Δ_y/L_{col} would also increase.
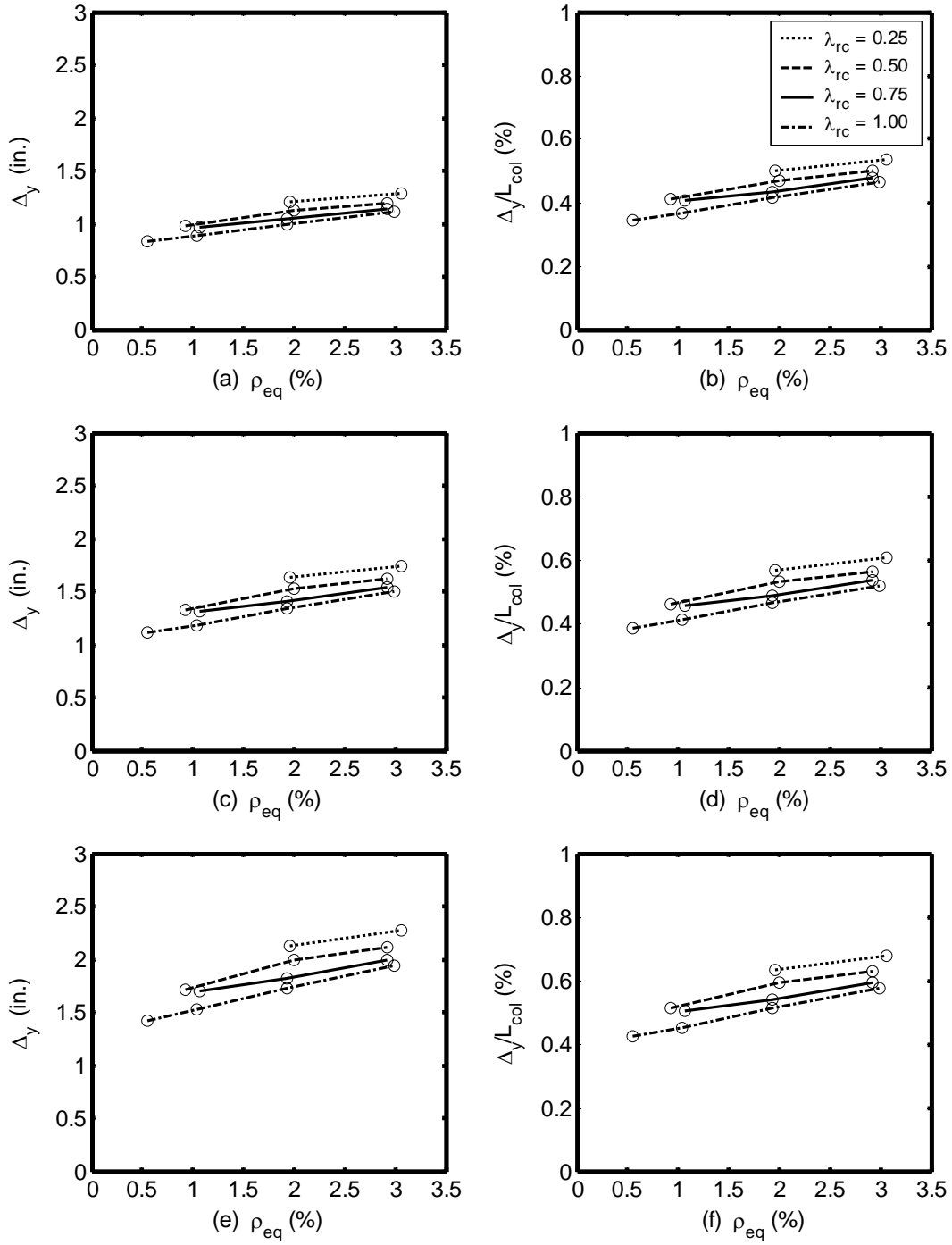
Figure 8.4: Yield Displacement, Hybrid Frames, $P_{col}/(f_c' A_g) = 0.05$

(a) $L_{col}/D_{col} = 5$, (b) $L_{col}/D_{col} = 6$, and (c) $L_{col}/D_{col} = 7$
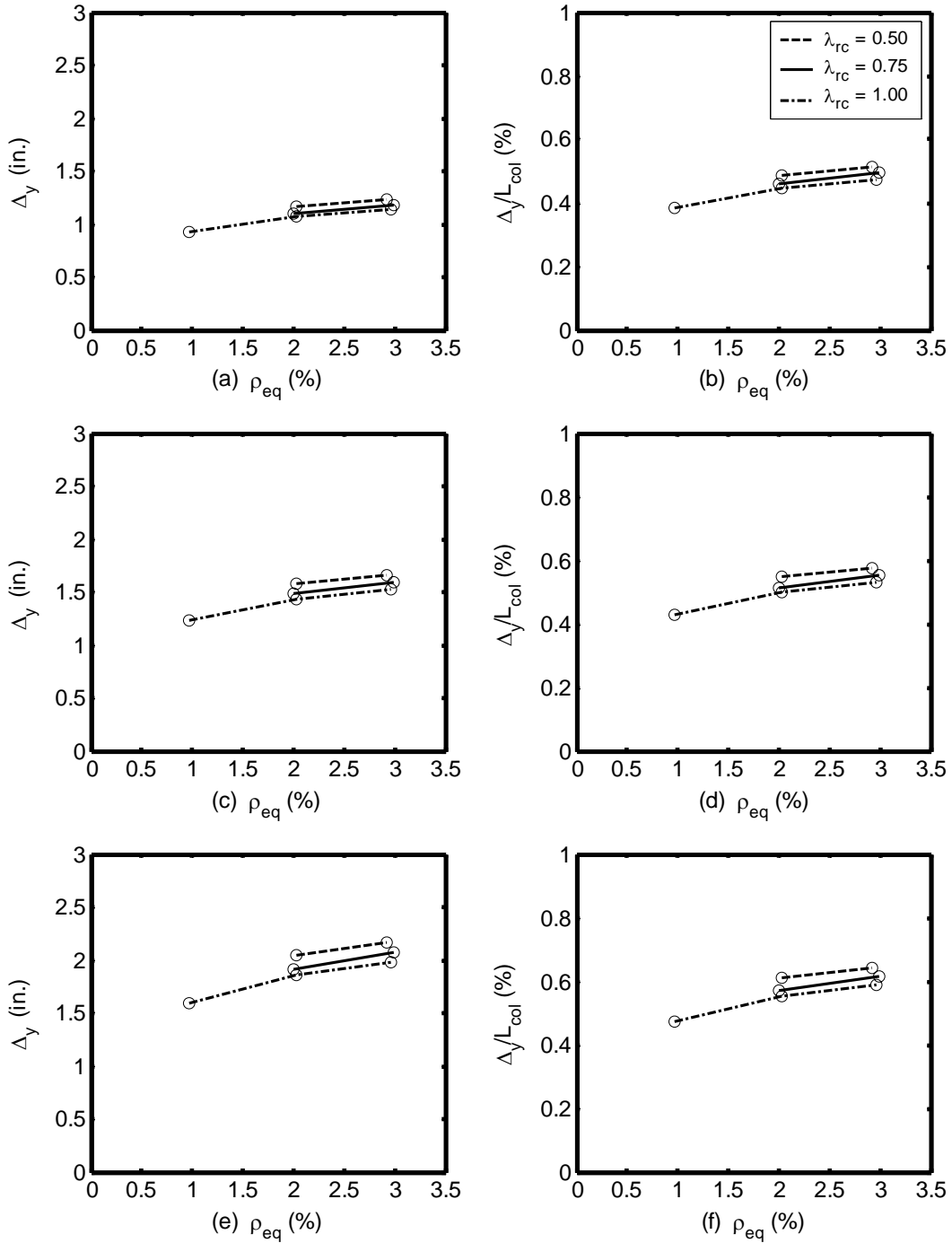
Figure 8.5: Yield Displacement, Hybrid Frames, $P_{col}\big/(f_c^{'}A_g) = 0.10$

(a) $L_{col}\big/D_{col} = 5$, **(b)** $L_{col}\big/D_{col} = 6$, **and (c)** $L_{col}\big/D_{col} = 7$

- The first yield displacement also increased as ρ_{eq} increased (tables 8.5 and 8.6). This trend can be demonstrated by evaluating the flexure of a reinforced concrete square cross-section with a width equal to b. The depth of the neutral axis, c, is directly related to the quantity of steel in the cross-section and is given by

  $c = \left(\rho A_g f_y\right) / \left(0.85 \beta f_c' b\right)$ where f_y is the yield strength of the longitudinal mild steel, f_c' is the concrete compressive strength, and β is the stress block depth factor. From this relationship it is apparent that as the longitudinal steel ratio increases, the depth of the neutral-axis also increases, resulting in an increase in the displacement at first yield.

- From figures 8.4 and 8.5 it is clear that Δ_y / L_{col} was essentially independent of $P_{col} / (f_c' A_g)$. No increase in Δ_y / L_{col} was observed in these results because $P_{col} / (f_c' A_g)$ affected the cracked stiffness as much as it affected the strength. For example, the ratio of $k_{cracked}$ between frame 5.030.100 as the axial-load varied from 0.05 to 0.10 was 0.94, and the ratio of F_{max} was the same. Geometry dictates that as the strength and the stiffness increase by the same amount, Δ_y / L_{col} should remain unchanged.

- Δ_y / L_{col} increased as L_{col} / D_{col} increased, as is evident in figures 8.4 and 8.5. For example, Δ_y / L_{col} increased by 26 percent between frames 5.030.100 and 7.030.100 for an axial-load ratio of 0.05. If the curvature at yield, ϕ_y, is assumed to be nearly constant and the yield displacement can be estimated as $\Delta_y = \phi_y L_{col}^2 / 6$, then an increase in L_{col} / D_{col} would result in an increased Δ_y / L_{col}.

- Δ_y/L_{col} decreased as λ_{rc} increased. The yield drift decreased by 13 percent

  between frames 5.030.025 and 5.030.100 for an axial-load ratio of 0.05. The

  results summarized in figures 8.4 and 8.5 suggest that as λ_{rc} increased, both the

  first yield displacement and yield displacement decreased. This can be explained

  by the increase in the depth of the neutral-axis due to increased axial load as the

  proportion of prestressing steel increased as λ_{rc} increased.

In summary, ρ_{eq} had the greatest impact on Δ_y/L_{col}; L_{col}/D_{col} and λ_{rc} had a

moderate effect on Δ_y/L_{col}; and $P_{col}/(f_c'A_g)$ had almost no impact on Δ_y/L_{col}.

8.5 TRENDS IN MAXIMUM FORCE

Tables 8.5 and 8.6 show that F_{max} ranged from 232 to 1103 kips. The following

trends were observed from the results shown in figures 8.6 and 8.7.

- F_{max} increased as ρ_{eq} increased (figures 8.6 and 8.7). For example, the maximum

  force increased 180 percent between frames 5.005.100 and 5.030.100 for an axial-

  load ratio of 0.05. The flexural strength of a column is directly related to the

  amount of longitudinal mild and prestressing steel provided in the cross-section.

  Therefore, this trend corresponded to the increased flexural strength resulting

  from the increased steel provided.

- F_{max} increased as $P_{col}/(f_c'A_g)$ increased (figures 8.6 and 8.7). An increase of 17

  percent was observed for frame 5.010.100 as $P_{col}/(f_c'A_g)$ increased from 0.05 to

  0.10. Because the axial-load ratios chosen for the hybrid frames were equal to or

  below 0.10, the frames typically fell below the balanced failure point on their

column interactive diagram. Below the balanced failure point, an increase in

compressive axial-load resulted in an increase in flexural strength.
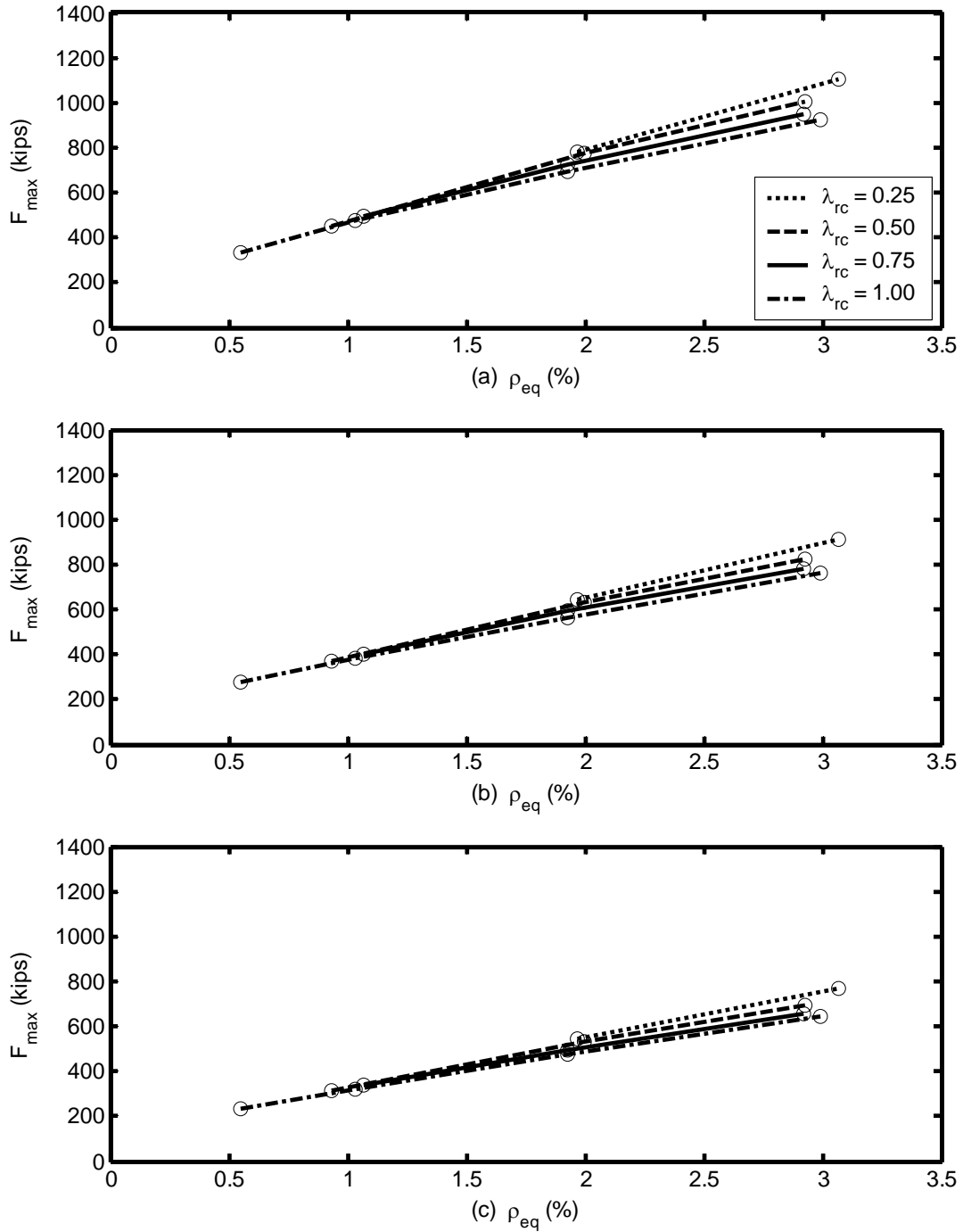
Figure 8.6: Maximum Force, Hybrid Frames, $P_{col}/(f_c^{'}A_g) = 0.05$

(a) $L_{col}/D_{col} = 5$, **(b)** $L_{col}/D_{col} = 6$, **and (c)** $L_{col}/D_{col} = 7$
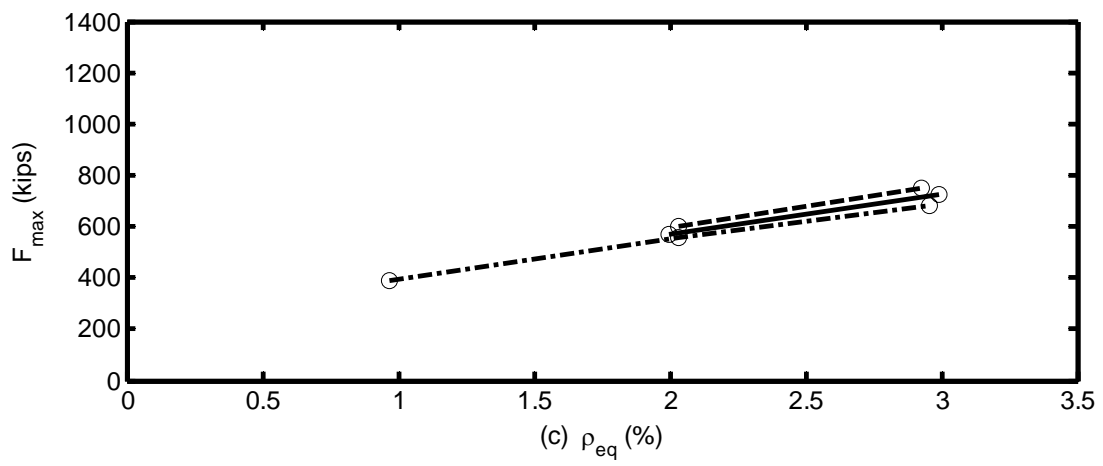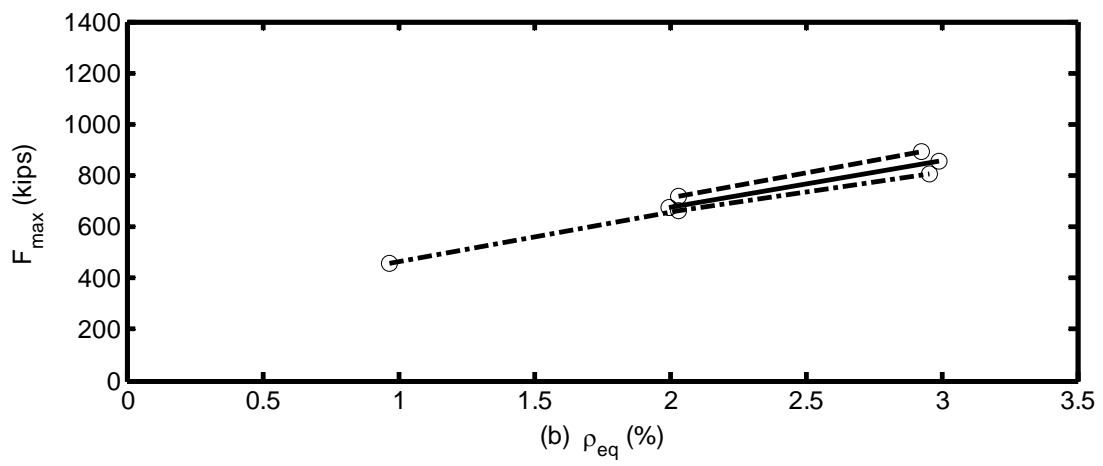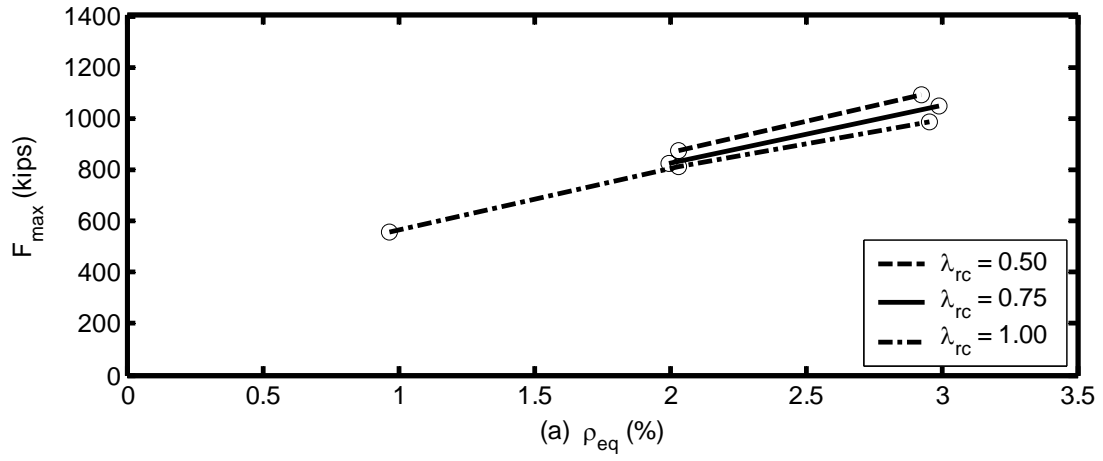
Figure 8.7: **Maximum Force, Hybrid Frames,** $P_{col}/(f_c' A_g) = 0.10$

(a) $L_{col}/D_{col} = 5$, **(b)** $L_{col}/D_{col} = 6$, **and (c)** $L_{col}/D_{col} = 7$

- F_{max} decreased as L_{col}/D_{col} increased. This trend may be observed in figures 8.6 and 8.7. For example, the maximum force decreased 31 percent between frames 5.030.100 and 7.030.100 for an axial-load ratio of 0.05. This decrease was caused by the increased lever arm for the lateral load as L_{col}/D_{col} increased.

- F_{max} decreased as λ_{rc} increased, as is shown in figures 8.6 and 8.7. A decrease of 16 percent was observed between frames 5.030.025 and 5.030.100 for an axial-load ratio of 0.05. This trend could be partially explained by the decreased longitudinal mild steel provided as λ_{rc} increased. Also, when the equivalent reinforcement ratio was calculated, it was assumed in Equation 8.1 that the prestressing steel had yielded. However, during the analyses the prestressing steel did not yield.

On the basis of the results, ρ_{eq} had the greatest influence on F_{max}; L_{col}/D_{col} had a moderate impact on F_{max}; and $P_{col}/(f_c' A_g)$ and λ_{rc} had the least impact on F_{max}.

CHAPTER 9
EARTHQUAKE ANALYSES OF HYBRID FRAMES

This chapter addresses the earthquake analyses of the hybrid frames performed in the parametric study. The hybrid frames were subjected to the 10 ground motions described in Chapter 5 to establish maximum displacements and residual displacements. The 10 ground motions contained five motions with a 10 percent probability of exceedance in 50 years (10 percent in 50) and five motions with a 2 percent probability of exceedance in 50 years (2 percent in 50). This chapter describes the parameters that were varied for the hybrid frames as part of the parametric study (Section 9.1), key quantities used to evaluate frame performance (Section 9.2), and the results found during these analyses (sections 9.3 through 9.7).

9.1 RANGE OF HYBRID PARAMETRIC STUDY

The parametric study considered variations of the baseline frame described in Chapter 4. As described in Chapter 8, the following four parameters were varied for the hybrid frames during the earthquake analyses:

- column aspect ratio, L_{col}/D_{col}
- axial-load ratio, $P_{col}/(f_c' A_g)$
- equivalent reinforcement ratio, $\rho_{eq} = \left(\rho_s f_y + \rho_p f_{py} \right)/f_y$
- re-centering ratio, $\lambda_{rc} = \left(P_{col} + A_p f_{p0} \right)/A_s f_y$.

9.2 KEY CHARACTERISTICS OF EARTHQUAKE RESPONSE

The same key quantities used to assess the performance of reinforced concrete frames were used to provide insight into the expected performance of the hybrid frames. These response quantities are presented in sections 9.3 through 9.7.

9.2.1 Maximum Displacement, Δ_{max}

The maximum displacement encountered in response to a given ground motion was denoted as the maximum displacement, Δ_{max}. The maximum displacement was used to calculate the displacement ductility demand as described in Chapter 10. Maximum displacement was also used to provide insight into the likelihood that a given limit state was exceeded (Chapter 10). The drift ratio corresponding to the maximum displacement was defined as Δ_{max}/L_{col}.

9.2.2 Residual Displacement, $\Delta_{residual}$

During the earthquake analysis of an inelastic frame, after yielding has occurred, the frame may not vibrate about its original equilibrium position. Each time the frame yields, the point about which the frame oscillates may shift. Therefore, after the ground motion excitation has ended, the frame's final position may not be the same as its initial position, with the remaining displacement referred to as the residual displacement. Residual displacement was defined as the difference between a frame's position before the ground motion excitation started (assumed to be 0.0 in.) and the frame's position after the ground motion excitation ended.

To estimate the residual displacement for this study, the free vibration of the frame after the ground motion had stopped was considered. This was done because viscous damping was not included in the frame analyses, and it would therefore take significant time for the vibration to damp out completely. To estimate the residual displacements, the maximum and minimum displacements over a time range starting 4 sec. after the ground excitation stopped, $\Delta_{t,stop+4\text{sec}}$, and ending 9 sec. after the ground

140

excitation stopped, $\Delta_{t,stop+9\sec}$, were averaged. The residual displacements were calculated from the following relationship:

$$\Delta_{residual} = \frac{\max(\Delta_{t,stop+4\sec} \to \Delta_{t,stop+9\sec}) + \min(\Delta_{t,stop+4\sec} \to \Delta_{t,stop+9\sec})}{2} \tag{9.1}$$

9.3 TRENDS IN MAXIMUM DISPLACEMENT

This section reviews the maximum displacements encountered during the earthquake analyses of the hybrid frames. Tables C.1 through C.4, found in Appendix C, provide a complete summary of the results for the 10 percent in 50 ground motions and the 2 percent in 50 ground motions for all the frames studied. The extreme values for the maximum displacement resulting from the 10 percent in 50 ground motions were as follows:

- Frames with axial-load ratio equal to 0.05
    - Minimum: 0.9 in. (frame 5.010.075, ground motion 10-3, $\Delta_{max}/L_{col} = 0.38$ percent)
    - Maximum: 4.6 in. (frame 7.005.100, ground motion 10-5, $\Delta_{max}/L_{col} = 1.37$ percent)
- Frames with axial-load ratio equal to 0.10
    - Minimum: 0.9 in. (frame 5.030.075, ground motion 10-3, $\Delta_{max}/L_{col} = 0.38$ percent)
    - Maximum: 6.6 in. (frame 7.010.100, ground motion 10-1, $\Delta_{max}/L_{col} = 1.96$ percent)

For the 2 percent in 50 ground motions, the maximum displacement ranged as follows:

- Frames with axial-load ratio equal to 0.05
    - Minimum: 1.7 in. (frame 5.030.025, ground motion 2-1, $\Delta_{max}/L_{col} = 0.72$ percent)

- Maximum: 17.3 in. (frame 7.005.100, ground motion 2-3, $\Delta_{max}/L_{col} = 5.14$ percent)

  o Frames with axial-load ratio equal to 0.10
  - Minimum: 3.6 in. (frame 5.030.050, ground motion 2-4, $\Delta_{max}/L_{col} = 1.50$ percent)
  - Maximum: 20.2 in. (frame 7.010.100, ground motion 2-3, $\Delta_{max}/L_{col} = 6.01$ percent)

Figures 9.1 and 9.2 show the mean and the mean plus one standard deviation maximum drift ratios plotted against the equivalent reinforcement ratios for the 2 percent in 50 ground motions. Figures 9.3 and 9.4 show these same values plotted against the ratio of prestressing steel to longitudinal mild steel, ρ_p/ρ_s, for the 2 percent in 50 ground motions. Because the general trends observed in the maximum drift ratio were also observed in the results from the 10 percent in 50 ground motions, only the results from the 2 percent in 50 ground motions are presented here. Figures C.1 through C.4, found in Appendix C, present similar data for the 10 percent in 50 ground motions.
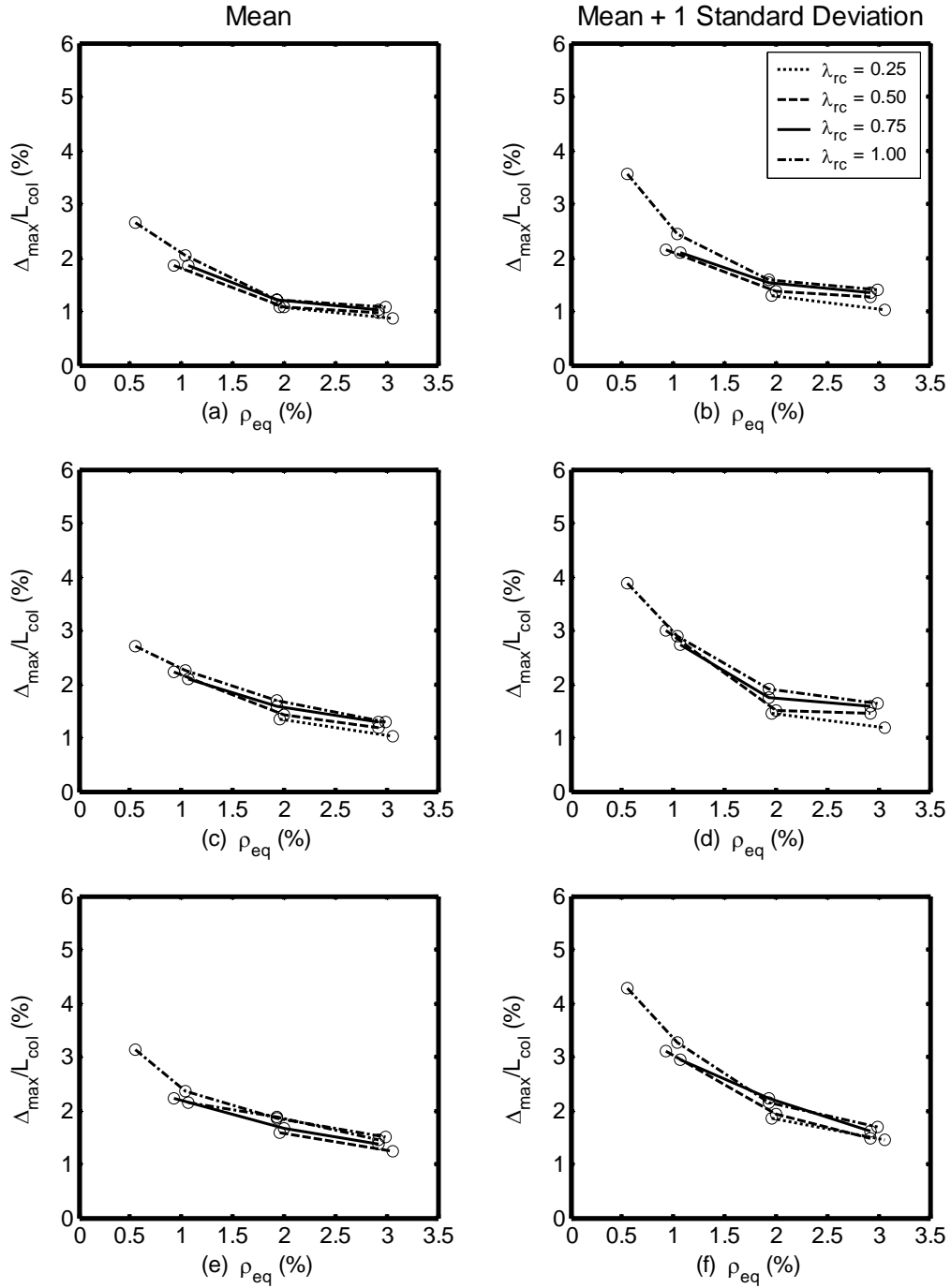
Figure 9.1: Trends in Drift Ratio, 2 Percent in 50, Hybrid Frames, $P_{col}/(f_c'A_g) = 0.05$
(a) and (b) $L_{col}/D_{col} = 5$, (c) and (d) $L_{col}/D_{col} = 6$, and (e) and (f) $L_{col}/D_{col} = 7$
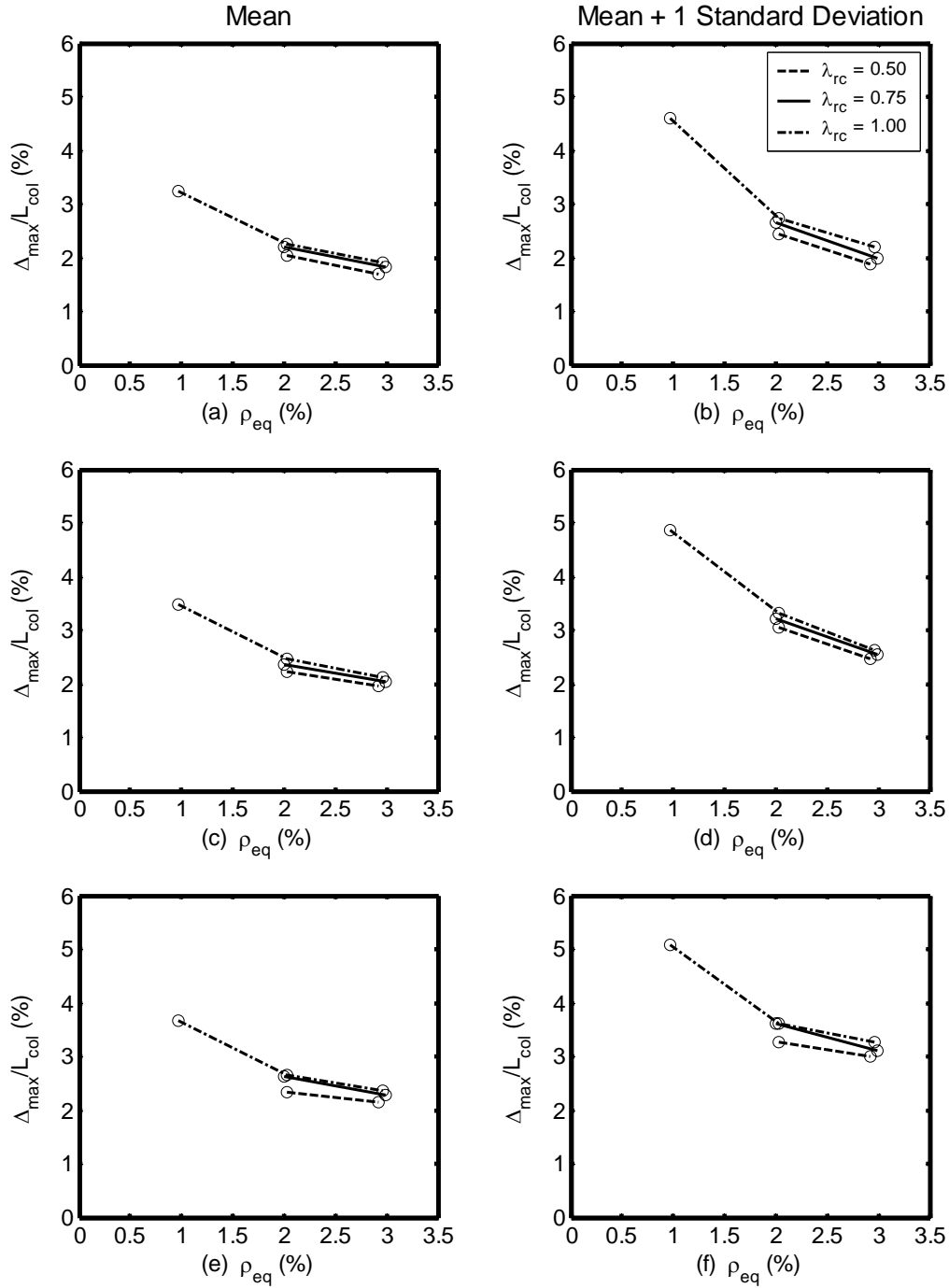
Figure 9.2: Trends in Drift Ratio, 2 Percent in 50, Hybrid Frames, $P_{col}/(f_c'A_g) = 0.10$

(a) and (b) $L_{col}/D_{col} = 5$, **(c) and (d)** $L_{col}/D_{col} = 6$, **and (e) and (f)** $L_{col}/D_{col} = 7$
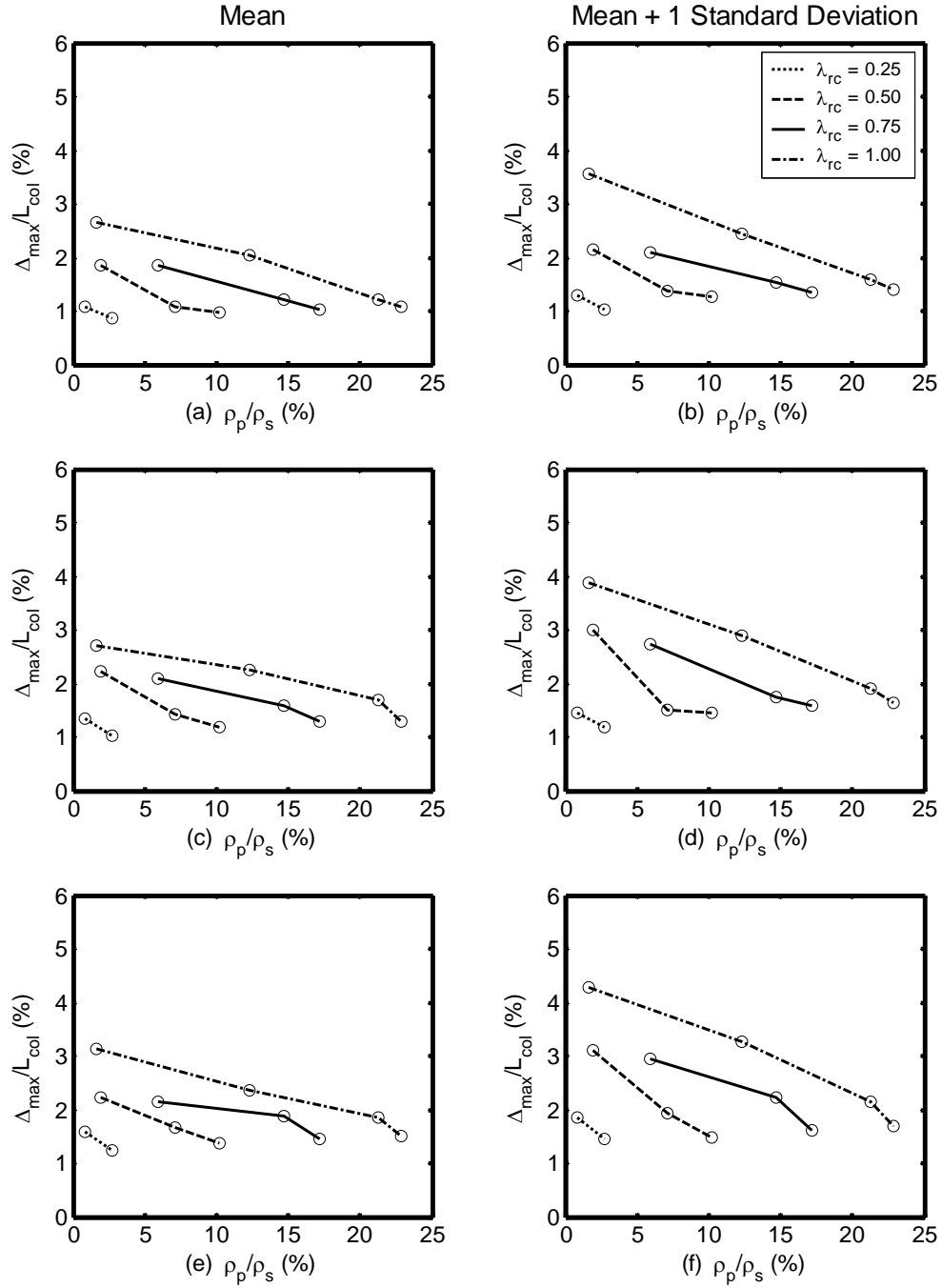
Figure 9.3: Effect of Steel Ratio, 2 Percent in 50, Hybrid Frames, $P_{col}/(f_c' A_g) = 0.05$

(a) and (b) $L_{col}/D_{col} = 5$ **, (c) and (d)** $L_{col}/D_{col} = 6$ **, and (e) and (f)** $L_{col}/D_{col} = 7$
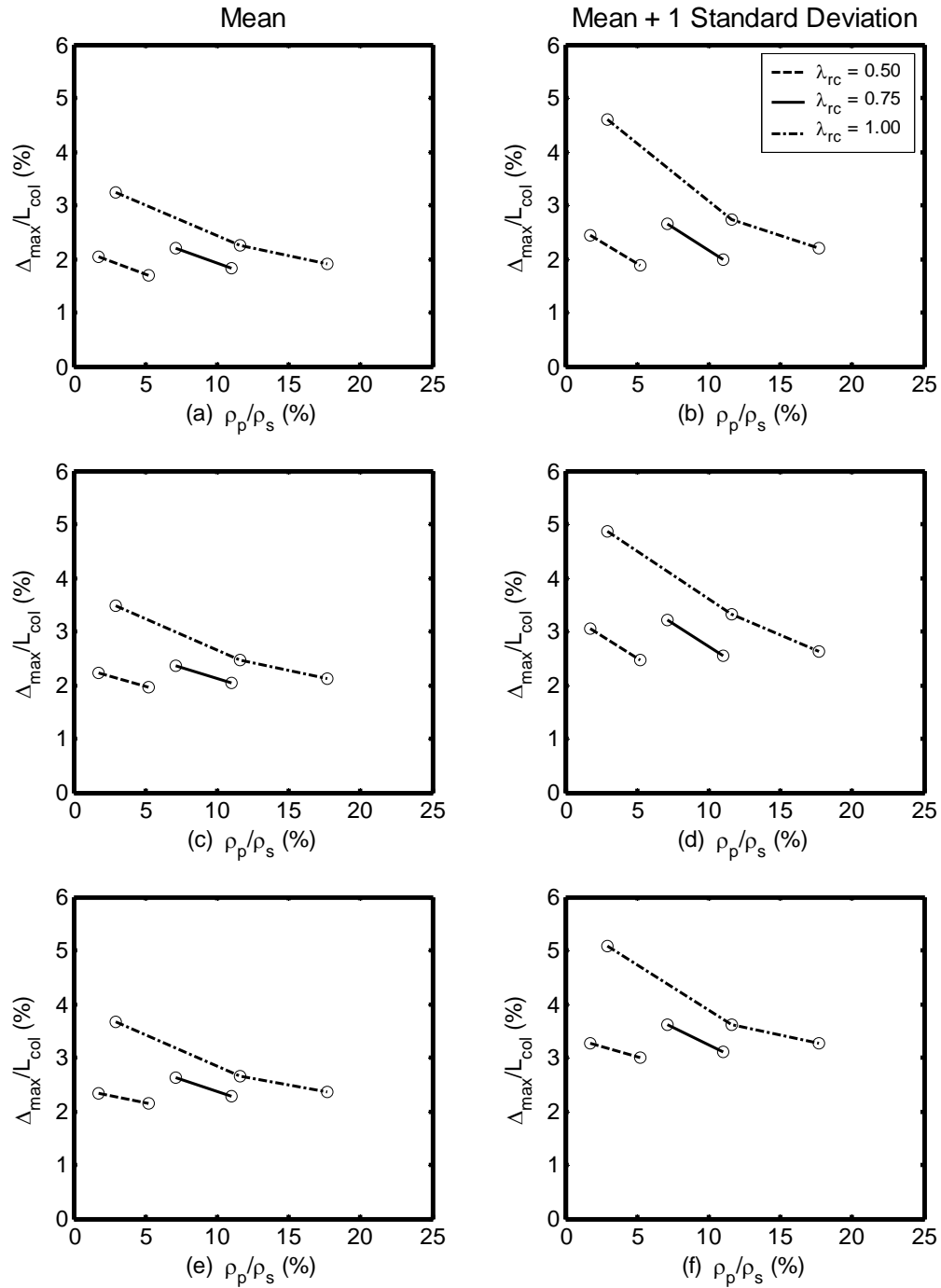
Figure 9.4: Effect of Steel Ratio, 2 Percent in 50, Hybrid Frames, $P_{col}/(f_c'A_g) = 0.10$
(a) and (b) $L_{col}/D_{col} = 5$**, (c) and (d)** $L_{col}/D_{col} = 6$**, and (e) and (f)** $L_{col}/D_{col} = 7$

The following trends were observed from the results presented in figures 9.1 through 9.4. The trends are described in relation to mean drift ratio, but the trends were also evident in the responses to individual ground motions.

- Δ_{max}/L_{col} decreased as ρ_{eq} increased, as is evident in figures 9.1 and 9.2. For example, Δ_{max}/L_{col} decreased by approximately 40 percent as the equivalent reinforcement ratio increased from 0.10 to 0.30. The results of the pushover analyses (Chapter 8) suggested that, as ρ_{eq} increased, the frame's strength and cracked stiffness also increased. It will become apparent in Section 9.4 that the increased stiffness most likely had a larger effect on decreasing Δ_{max}/L_{col} than did the increased strength.

- Δ_{max}/L_{col} increased as $P_{col}/(f_c'A_g)$ increased. This observation is seen by comparing Figure 9.1 with Figure 9.2. For example, for frame 5.030.100, Δ_{max}/L_{col} increased by 78 percent as the axial-load ratio increased from 0.05 to 0.10. This observation can be explained by considering the increased mass. Because the mass was assumed to be equal to the total axial-load divided by gravity, as the axial-load increased, the mass increased proportionally. From the relationship for the crack natural period $\left(T_{n,cracked} = \sqrt{m/k_{cracked}} \right)$ it is clear that the cracked natural period increased as the mass increased. The displacement response spectrum shown in Chapter 7 indicates that the expected displacement should increase as the crack natural period increase, as was seen in the results of the earthquake analyses. The natural period of the system may also have

increased further because the stiffness may have been reduced as a result of the $P - \Delta$ effects.

- Δ_{max}/L_{col} increased as L_{col}/D_{col} increased. This trend is reflected in Figure 9.2. An increase of approximately 30 percent was observed in Δ_{max}/L_{col} between frames 5.030.100 and 7.030.100 for an axial-load ratio of 0.10. The relationship between stiffness and column length $\left(k = \alpha EI_{col}/L_{col}^3 \right)$ indicates that as the column length increased, the frame's stiffness decreased. This corresponded to the results of the pushover analyses of the hybrid frames (Chapter 8). As explained in the previous paragraph, as the stiffness decreased, the cracked natural period increased, resulting in the larger Δ_{max}/L_{col} .

- Δ_{max}/L_{col} was almost independent of the λ_{rc} , as is clear from figures 9.1 and 9.2. For example, between frames 5.030.050 and 5.030.100, Δ_{max}/L_{col} increased by less that 10 percent. The pushover analyses of the hybrid frames showed that the cracked stiffness remained effectively unchanged as the re-centering ratio increased, and the maximum strength decreased slightly (approximately 15 percent) as the re-centering ratio increased. This trend suggests that the decreased maximum strength contributed to the increased Δ_{max}/L_{col} . Figures 9.3 and 9.4 reveal that for a given ρ_p/ρ_s , larger displacements will result from larger re-centering ratios. This can be explained by noting that for a given ρ_p/ρ_s , a frame with a larger re-centering ratio will have less mild longitudinal reinforcement steel than a frame with a smaller re-centering ratio. The results of the pushover analyses of the reinforced concrete frames (Chapter 6) showed that as the

148

longitudinal reinforcement ratio decreased, the cracked stiffness also decreased. As argued in the points above, a decreased stiffness results in a larger cracked natural period, which in turn results in larger displacements.

- Figures 9.1 and 9.2 indicate that the mean plus one standard deviation was approximately 30 percent larger than the mean values.

- The results for Δ_{max}/L_{col} from the 2 percent in 50 ground motions were about twice as large as the results for the 10 percent in 50 ground motions. Figures C.1 through C.4 in Appendix C illustrate the data for the maximum drift ratio resulting from the 10 percent in 50 ground motions.

In summary, $P_{col}/\left(f_c'A_g\right)$ had the largest impact on Δ_{max}/L_{col}; ρ_{eq} and L_{col}/D_{col} influenced Δ_{max}/L_{col} moderately; and λ_{rc} had the least effect on Δ_{max}/L_{col}. These trends were consistent with the results of the reinforced concrete frame earthquake analyses (Chapter 7).

9.4 EFFECTS OF STRENGTH ON MAXIMUM DISPLACEMENT

The trends observed in Section 9.3 suggest that both strength and stiffness affected the maximum displacements encountered during the earthquake analyses. This section further investigates the effect of strength and stiffness on the maximum displacement. To evaluate the impact of strength on the maximum displacement, the maximum drift ratio, Δ_{max}/L_{col}, was plotted against a normalized strength ratio, F_{con004}/P_{total}, where F_{con004} was the effective force corresponding to a concrete compressive strain equal to 0.004 (found from the pushover analyses described in

149

Chapter 8), and P_{total} was the total compressive axial-load on the frame ($P_{total} = 2*P_{col}$ for the two column frames). This ratio is often referred to as the base shear-strength ratio.

Figures 9.5 through 9.8 show the mean maximum drift ratio and the mean plus one standard deviation plotted against F_{con004}/P_{total} for the 2 percent in 50 ground motions for axial-load ratios equal to 0.05 and 0.10. The corresponding data for the 10 percent in 50 ground motions are presented in figures C.5 through C.8 in Appendix C.
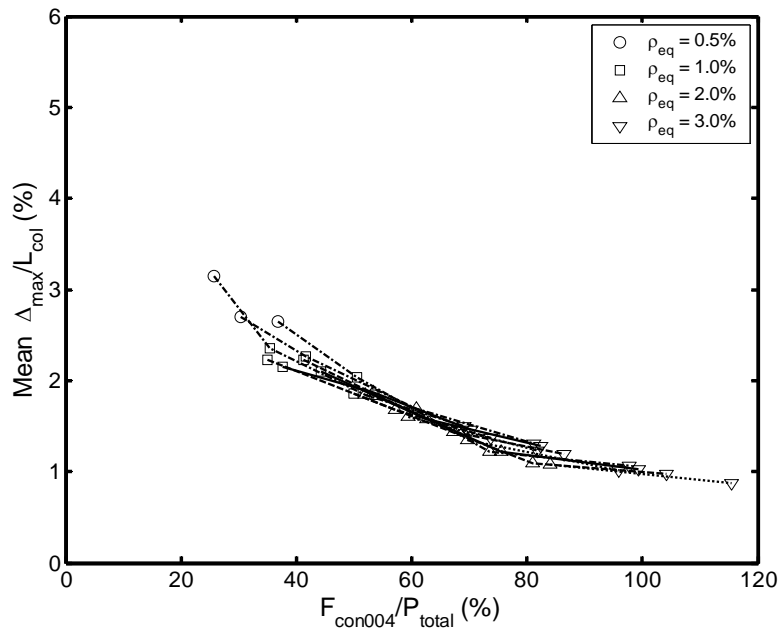
Figure 9.5: Effect of Strength on Mean Drift Ratio, 2 Percent in 50, Hybrid Frames,
$$P_{col}/(f_c'A_g) = 0.05$$
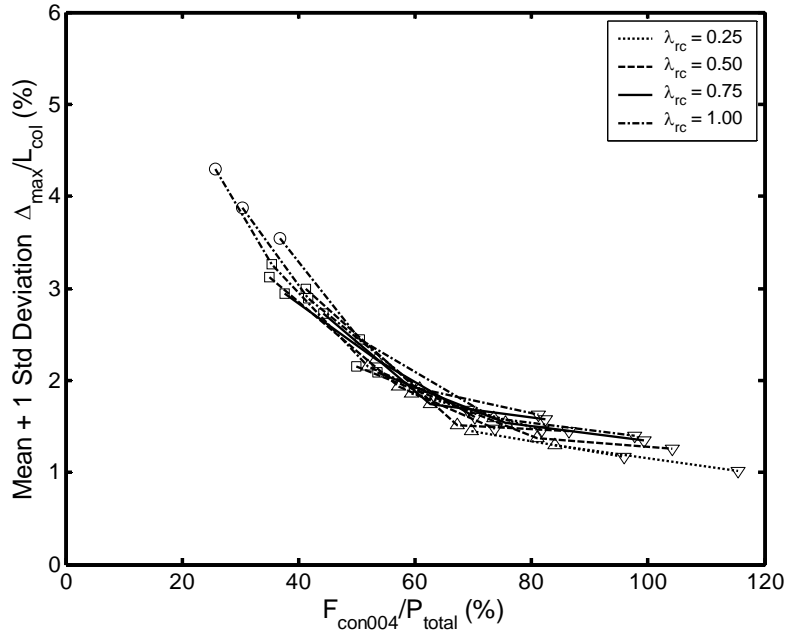
Figure 9.6: Effect of Strength on Mean Plus One Standard Deviation Drift Ratio, 2 Percent in 50, Hybrid Frames, $P_{col}/(f_c^{'}A_g) = 0.05$
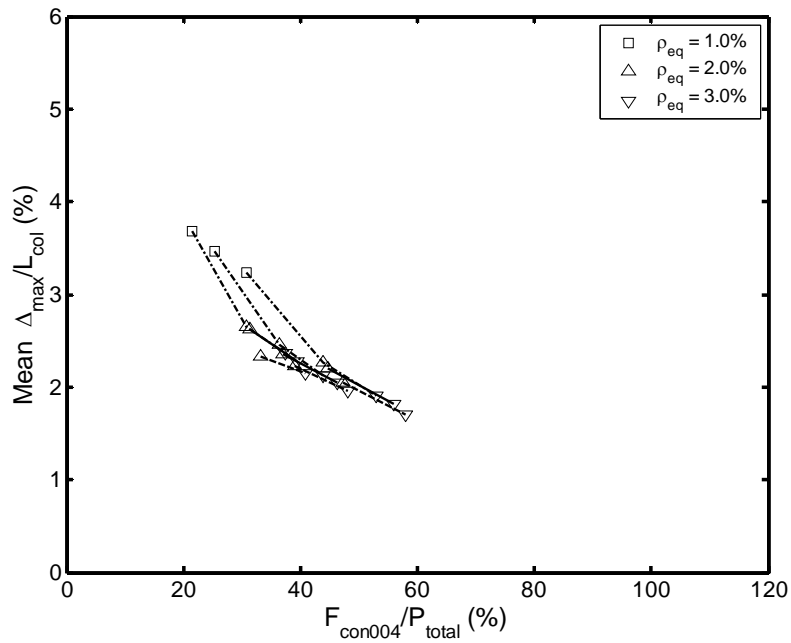
Figure 9.7: Effect of Strength on Mean Drift Ratio, 2 Percent in 50, Hybrid Frames, $P_{col}/(f_c^{'}A_g) = 0.10$
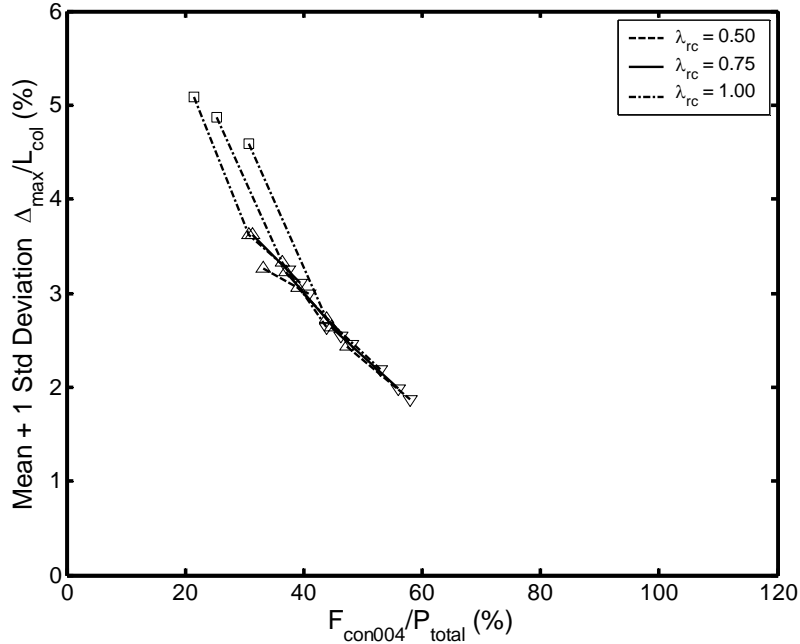
Figure 9.8: Effect of Strength on Mean Plus One Standard Deviation Drift Ratio, 2 Percent in 50, Hybrid Frames, $P_{col}/(f_c' A_g) = 0.10$

The results shown in figures 9.5 through 9.8 fell onto relatively smooth curves. The following observations were noted from the plots:

- Δ_{max}/L_{col} decreased as F_{con004}/P_{total} increased, suggesting that the maximum drift ratio was at least partially affected by strength.

- The relationship between F_{con004}/P_{total} and Δ_{max}/L_{col} was nonlinear.

The strength ratio can also be an indirect indicator of stiffness. Priestley and Paulay (2002) suggested that strength and stiffness are essentially proportional $(k = \alpha F)$. For this study, the mass on each frame was equal to the total axial-load divided by gravity, g. From these two relationships, the natural period can be expressed as:

$$T_n = \sqrt{\frac{P_{total}/g}{\alpha F}} \tag{9.2}$$

152

Because the assumed strength of a frame was taken as F_{con004}, the maximum drift ratio was plotted against $\sqrt{P_{total}/F_{con004}}$, as shown in figures 9.9 through 9.12. From these plots it is apparent that a linear relationship existed between Δ_{max}/L_{col} and $\sqrt{P_{total}/F_{con004}}$, which is an indirect measure of the structure's period.
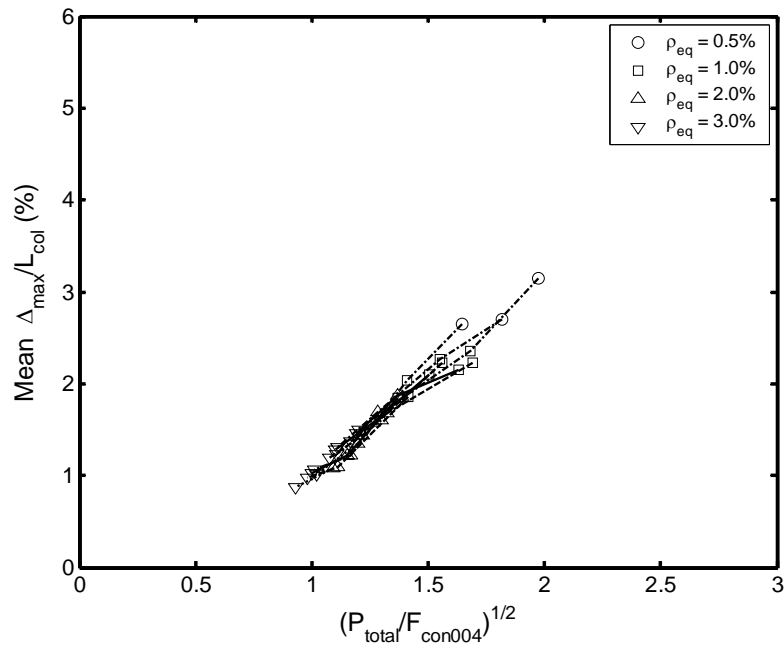
Figure 9.9: Effect of Stiffness on Mean Drift Ratio, 2 Percent in 50, Hybrid Frames,
$$P_{col}/(f_c' A_g) = 0.05$$
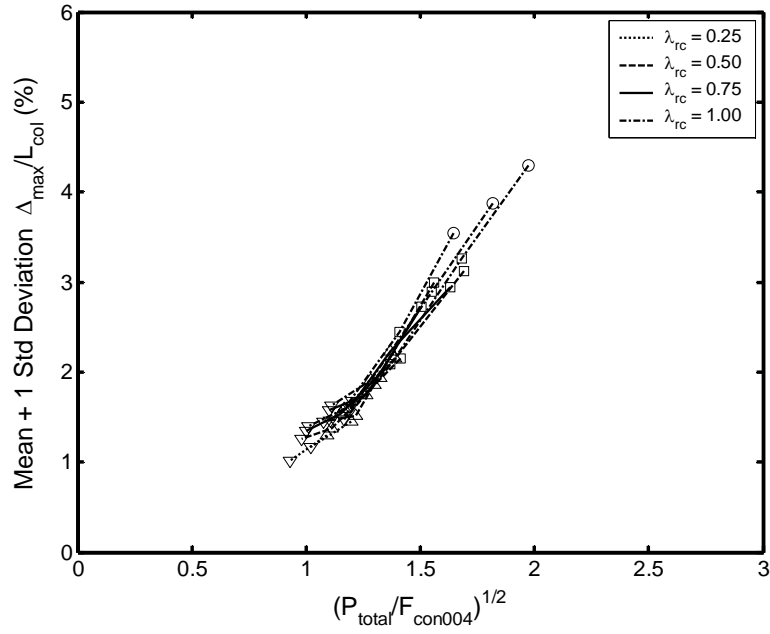
Figure 9.10: Effect of Stiffness on Mean Plus One Standard Deviation Drift Ratio, 2 Percent in 50, Hybrid Frames, $P_{col}/(f_c'A_g) = 0.05$
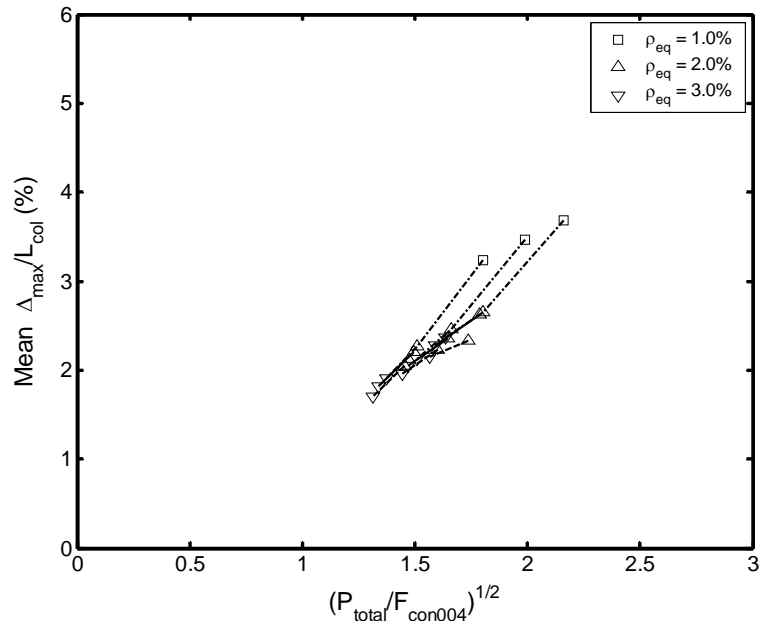
Figure 9.11: Effect of Stiffness on Mean Drift Ratio, 2 Percent in 50, Hybrid Frames, $P_{col}/(f_c'A_g) = 0.10$
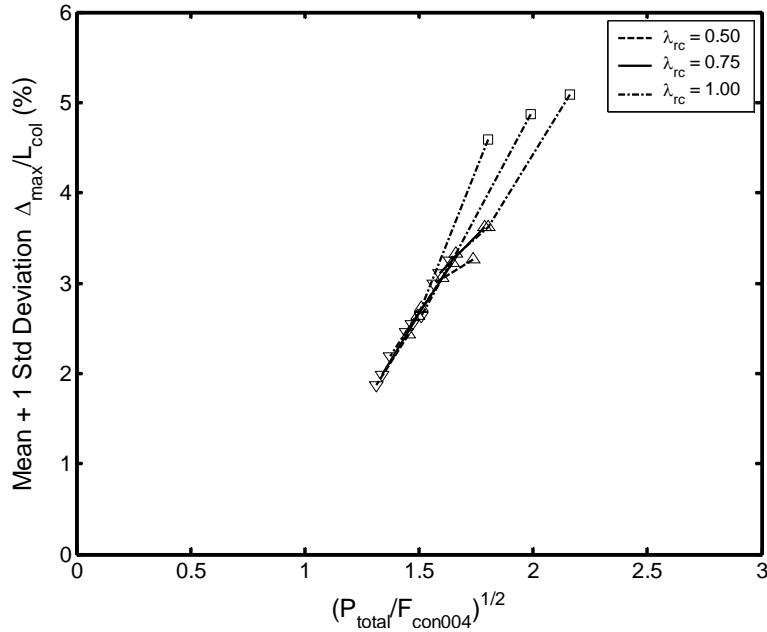
Figure 9.12: Effect of Stiffness on Mean Plus One Standard Deviation Drift Ratio, 2 Percent in 50, Hybrid Frames, $P_{col}/(f_c'A_g) = 0.10$

9.5 COMPARISON OF MAXIMUM DISPLACEMENT WITH ELASTIC ANALYSIS

The maximum displacements encountered during the earthquake analyses of the hybrid frames were compared with the displacements expected from the elastic design response spectra. After a frame experiences nonlinear behavior, the maximum expected displacement is no longer governed solely by its initial period and damping ratio. The design response spectra discussed in Chapter 5 were created with the assumption of a viscous damping ratio equal to 0.05. Because the frames in this study included no viscous damping and because they experienced nonlinear behavior, it was anticipated that the maximum displacements encountered during the earthquake analyses would be larger than those predicted by the elastic design response spectra.

Modification factors were found to relate the actual maximum displacements with the predicted values. The following relationship could then be used to estimate response

quantities for inelastic behavior without viscous damping:

$$\Delta_{predicted} = \psi S_d \qquad (9.3)$$

where ψ = modification factor

S_d = spectral displacement

The modification factor was calculated by averaging Δ_{max}/S_d for all the frames as

shown in the following relationship:

$$\psi = \frac{\sum\limits_{i=1}^{N_{frames}} \left[\left(\sum\limits_{j=1}^{N_{motions}} \text{mean } \Delta_{max.ij}/S_{d.i} \right) \middle/ N_{motions} \right]}{N_{frames}} \qquad (9.4)$$

The modification factors for the 10 percent in 50 ground motions were found

from Equation 9.4 to be as follows:

- o Frames with axial-load ratio equal to 0.05
  - $\psi = 1.43$ for the mean
  - $\psi = 1.73$ for the mean plus one standard deviation
- o Frames with axial-load ratio equal to 0.10
  - $\psi = 1.30$ for the mean
  - $\psi = 1.53$ for the mean plus one standard deviation

For the 2 percent in 50 ground motions, the modification factors were found to be

as follows:

- o Frames with axial-load ratio equal to 0.05
  - $\psi = 1.44$ for the mean
  - $\psi = 1.78$ for the mean plus one standard deviation
- o Frame with axial-load ratio equal to 0.10
  - $\psi = 1.49$ for the mean
  - $\psi = 1.94$ for the mean plus one standard deviation

Combining the modification factors for the mean results led to an average value of 1.42, assuming that each frame was given an equal weighting factor. The average value resulting from the combination of modification factors for the mean plus one standard deviation was 1.75.

Using Equation 9.3 for each earthquake analysis with $\psi = 1.4$ led to a ratio of the maximum displacement to the predicted displacement, $\Delta_{max}/\Delta_{predicted}$, with a mean of 1.02 and standard deviation of 0.27. Given the results from each analysis, Equation 9.3 with $\psi = 1.7$ produced a mean $\Delta_{max}/\Delta_{predicted}$ value equal to 0.84 and a standard deviation equal to 0.22.

Figures 9.13 through 9.16 show the maximum displacement plotted against the natural period for the 2 percent in 50 ground motions. The figures also show the predicted displacements from Equation 9.5. Figures C.13 through C.16, in Appendix C, show the same data for the 10 percent in 50 ground motions. From these figures it is apparent that $\Delta_{predicted}$ represented the average maximum response well.
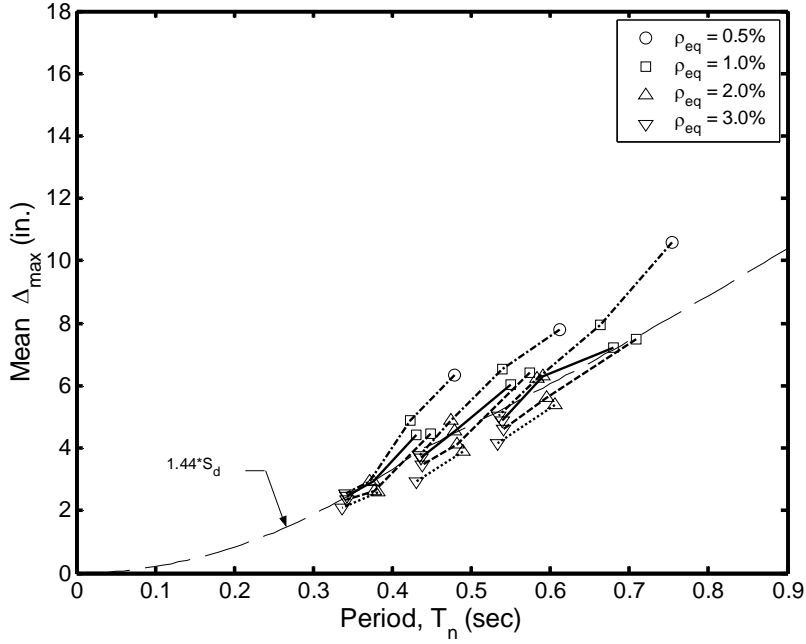
Figure 9.13: Predicted and Mean Response, 2 Percent in 50, Hybrid Frames, $P_{col}/(f_c^{'} A_g) = 0.05$
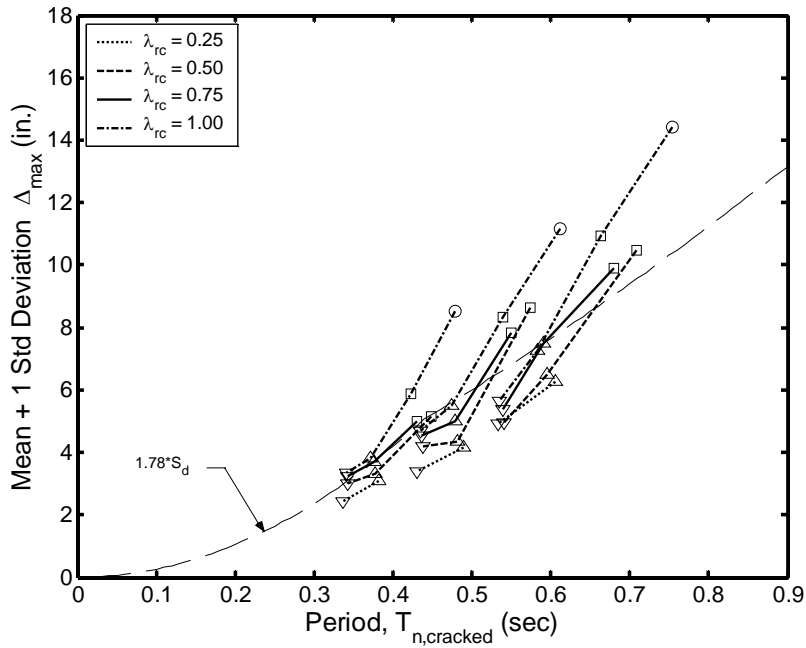
Figure 9.14: Predicted and Mean Plus One Standard Deviation Response, 2 Percent in 50, Hybrid Frames, $P_{col}/(f_c^{'} A_g) = 0.05$
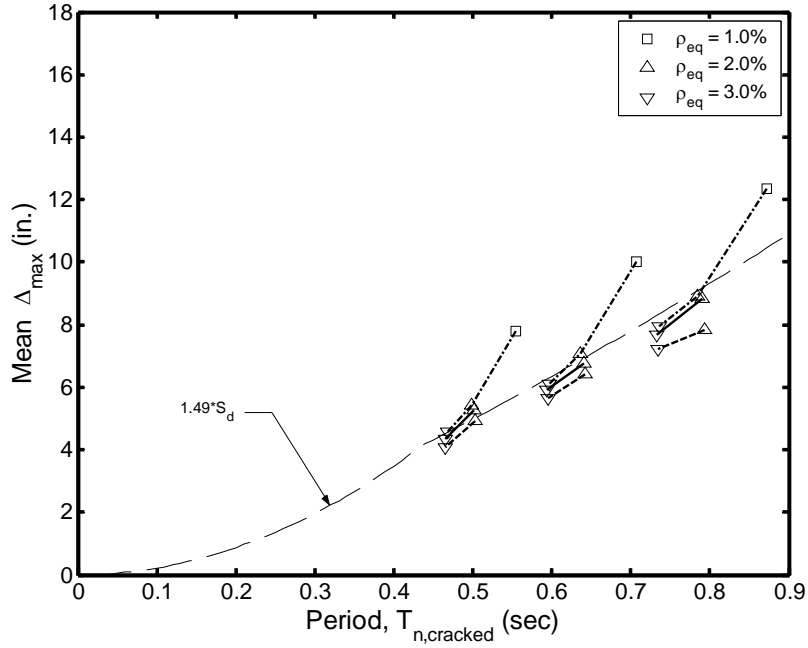
Figure 9.15: Predicted and Mean Response, 2 Percent in 50, Hybrid Frames, $P_{col}/(f_c^{'}A_g) = 0.10$
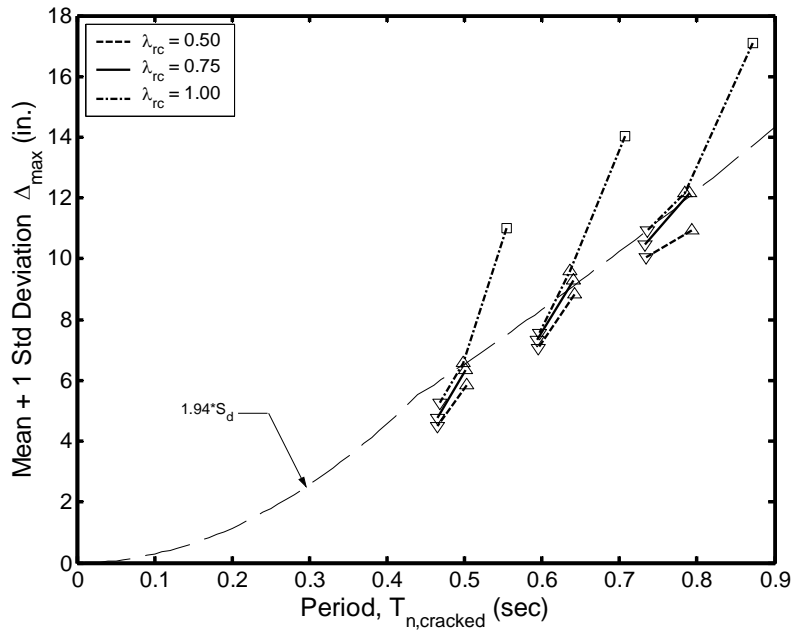
Figure 9.16: Predicted and Mean Plus One Standard Deviation Response, 2 Percent in 50, Hybrid Frames, $P_{col}/(f_c^{'}A_g) = 0.10$

9.6 INCORPORATION OF STRENGTH IN PREDICTION OF MAXIMUM DISPLACEMENT

To demonstrate the effect that strength has on the maximum displacement response, the mean Δ_{max}/S_d was plotted against a normalized strength, $F_{con004}/S_a\,m$, where S_d and S_a were the spectral displacement and spectral acceleration predicted from the smooth design spectra (Figure 9.17). The data shown in these plots suggested a bilinear relationship between Δ_{max}/S_d and $F_{con004}/S_a\,m$. Above a value of $F_{con004}/S_a\,m$ of about 0.04, Δ_{max}/S_d was approximately constant, whereas below this value, a linear relationship appeared appropriate. Therefore, the predicted values for undamped, inelastic behavior could be calculated with the following relationship:

$$\Delta_{predicted} = \begin{cases} \left[\alpha\left(\eta - X\right) + \beta\right]S_d & \text{for } F_{con004}/S_a m \leq \eta \\ \beta S_d & \text{for } F_{con004}/S_a m > \eta \end{cases} \tag{9.5}$$

where α = absolute value slope of the linear portion

η = value of $F_{con004}/S_a\,m$ corresponding to the transition from a linear relationship to a constant value. This value was taken as 0.04.

X = value of $F_{con004}/S_a\,m$

β = value for the constant portion

S_d = spectral displacement

160
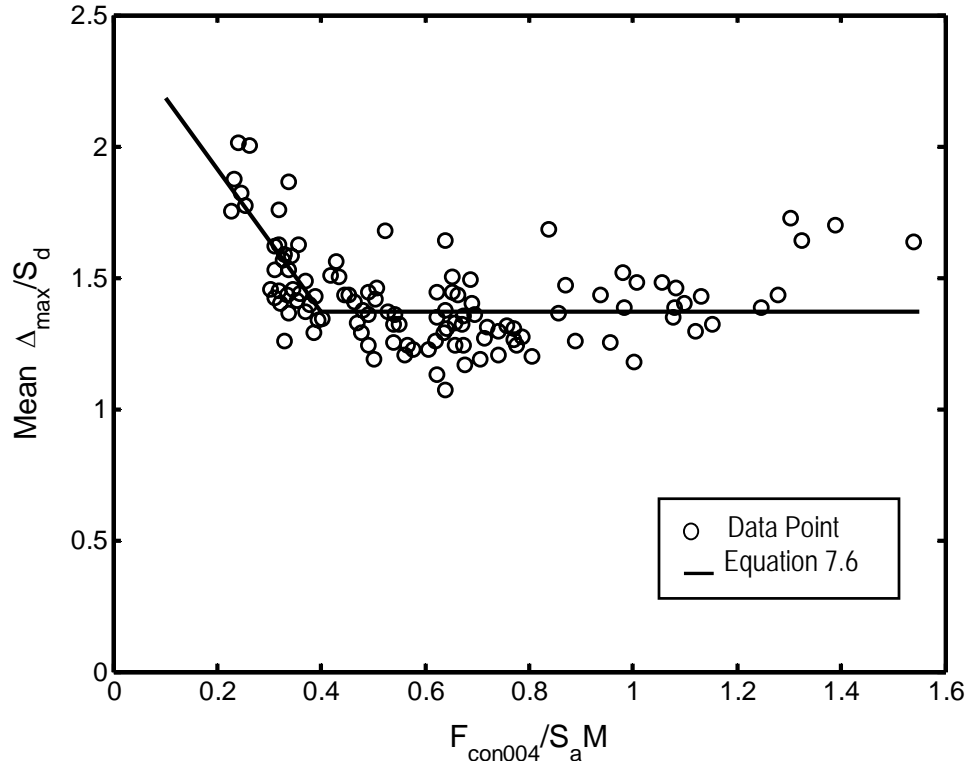
Figure 9.17: Bilinear Approximation for Maximum Displacement

Values for α and β were found by considering the maximum displacements for the reinforced concrete frames subjected to both the 10 percent in 50 and 2 percent in 50 ground motions. A value of 2.72 was found for α by minimizing the sum of the squared error between the predicted displacements and the actual displacements in the region below 0.4. A value of 1.37 was found for β by averaging Δ_{max}/S_d for all the frames with a $F_{con004}/S_a m$ of above 0.4.

Using Equation 9.5 for each earthquake analysis with $\alpha = 2.0$, $\beta = 1.3$, and $\eta = 0.4$ led to a ratio of the maximum displacement to the predicted displacement, $\Delta_{max}/\Delta_{predicted}$, with a mean of 1.05 and standard deviation of 0.26. The overall statistics improved slightly in comparison to the relationship discussed in Section 9.5, but the

161

accuracy improved significantly for low values of the strength ratio. The predicted

response calculated from Equation 9.5 is shown in Figure 9.17.

9.7 TRENDS IN RESIDUAL DISPLACEMENT

After a frame has undergone yielding during ground motion excitation it may not

return to its initial equilibrium position. This difference in position before and after the

ground excitation has stopped is referred to as the residual displacement. Residual

displacements can affect whether a structure needs to be replaced or simply repaired.

Residual displacements were found for the 10 percent in 50 ground motions and the 2

percent in 50 ground motions.

The range of the maximum residual displacement resulting from the 10 percent in

50 ground motions was as follows:

- o Frames with axial-load ratio equal to 0.05
    - Minimum: 0.0 in. (numerous frames and ground motions, $\Delta_{max}/L_{col} = 0.00$ percent)
    - Maximum: 0.2 in. (frame 7.005.100, ground motion 10-3, $\Delta_{max}/L_{col} = 0.05$ percent)
- o Frames with axial-load ratio equal to 0.10
    - Minimum: 0.0 in. (numerous frames and ground motions, $\Delta_{max}/L_{col} = 0.00$ percent)
    - Maximum: 0.3 in. (frame 7.020.0.50, ground motion 10-3, $\Delta_{max}/L_{col} = 0.09$ percent)

For the 2 percent in 50 ground motions, the extreme value of the maximum

residual displacement was as follows:

- o Frames with axial-load ratio equal to 0.05
    - Minimum: 0.0 in. (numerous frames and ground motions,

$\Delta_{max}/L_{col} = 0.00$ percent)

- Maximum: 1.1 in. (frame 7.020.025, ground motion 2-3, $\Delta_{max}/L_{col} = 0.32$ percent)

  o Frame with axial-load ratio equal to 0.10

    - Minimum: 0.0 in. (numerous frames and ground motions, $\Delta_{max}/L_{col} = 0.00$ percent)

    - Maximum: 1.5 in. (frame 7.030.050, ground motion 2-3, $\Delta_{max}/L_{col} = 0.45$ percent)

As described in Chapter 7, the strain-hardening ratio and viscous damping ratio selected to model the frame were found to significantly affect the resulting residual displacements. Therefore, complete residual displacement results are not presented. Nonetheless, the residual displacements for the hybrid frames tended to be smaller than those for the reinforced concrete frames. Also, as expected, the residual displacements generally decreased as the re-centering ratio increased. This suggests that prestressing does help reduce residual displacement.

An additional conclusion discussed in Chapter 7 is that the maximum displacements were not drastically affected by the strain-hardening ratio or viscous damping ratio, providing additional confidence in the maximum displacements presented in this document.

CHAPTER 10
SEISMIC PERFORMANCE EVALUATION

This chapter evaluates and compares the two proposed bridge systems by investigating various deformation measures (such as displacement ductility) and limit states (such as the onset of cover concrete spalling). Variations of the baseline reinforced concrete frame and hybrid frame described in Chapter 4 were subjected to pushover analyses and earthquake analyses. From the pushover analyses, key quantities such as first yield properties, initial cracked properties, nominal yield displacement, and maximum strength were calculated (chapters 6 and 8). The maximum displacements resulting from 10 ground motions were computed during the earthquake analyses (chapters 7 and 9). Some of these key quantities were utilized to provide further insight into the response of the proposed systems, as well as to provide a basis for comparing and contrasting the two proposed bridge systems.

Numerous states may occur when an axially loaded column is subjected to flexure. These states are briefly described below.

1. *Initial Cracking*. Initial cracking corresponds to the first flexural cracking in the column. After the column starts to crack, the stiffness decreases considerably. This change between the cracked and uncracked stiffness was evident in the results from the pushover analyses presented in chapters 6 and 8. Although reaching the cracking limit state can significantly decrease stiffness, and in turn affect the response of the frame during an earthquake, reaching the cracking limit state generally does not result in the need for repairs because the crack widths are small, and the cracks close at the end of the earthquake.

2. *First Yield.* First yield is reached when the column's extreme tensile steel first

reaches its yield strain. When the column reaches first yield, the stiffness

continues to decrease. The ratio of first yield to full yield, or the yielding of all

tensile reinforcing steel, depends on the column geometry and the number of bars

in the column. For a rectangular section with only two layers of reinforcement,

this ratio is near 1.0 because all the tensile reinforcing steel typically yields at the

same time. This ratio is significantly smaller for a circular column because first

yield may occur when only one bar yields. The values for first yield are

summarized in chapters 6 and 8.

3. *Onset of Cover Concrete Spalling.* Significant deterioration of the cover concrete

can result in cover concrete spalling. For well-confined columns, cover concrete

spalling will generally not significantly affect the seismic resistance of the frame

(Priestley et al. 1996). The need for repair is commonly associated with the onset

of cover concrete spalling. Depending on the extent of the damage, the cost to

repair the bridge may be significant, and the bridge may be temporarily out of

service.

4. *Onset of Bar Buckling.* As the axial strain in the column's core increases, the

concrete behaves nonlinearly, and more of the compression force, caused by the

column axial force and column moment, must be resisted by the longitudinal

reinforcing steel. Also, as the core expands under the axial load, lateral forces are

exerted on the longitudinal reinforcing steel. If the compression force and/or

lateral force become excessive, the longitudinal reinforcing bars may buckle

(Berry 2003). The onset of bar buckling generally requires expensive repairs and

possibly partial replacements, especially because bar buckling frequently causes fracture of the spiral reinforcement. Safety also becomes a concern after the onset of bar buckling, and the structure may be out of service for some time.

5. *Fracture of Longitudinal Bars.* Bar fracture can occur if the tensile strains in the longitudinal reinforcing bars become excessive. Fracture at lower strain levels can be precipitated by several cycles of alternating buckling and straightening. As with bar buckling, rupture of a longitudinal bar can result in significant damage that requires extensive repairs or replacement.

6. *Ultimate Limit State.* No unique definition exists for the ultimate limit state. In some cases the term is used to correspond to a physical event, such as bar rupture, whereas others have defined it as a significant loss of lateral resistance, such as a 20 percent decrease in lateral resistance from the maximum strength (Priestley et al. 1996). The definition of the ultimate state assumed for this study is described in Section 10.5. When the ultimate limit state is reached, the main concern is for safety. The structure most likely will be severely damaged and will require costly replacement. But it is important that enough reserve strength remains so that the bridge will not collapse.

States 3 through 6 were investigated during this study and are discussed further in later sections of this chapter. Section 10.1 presents results for displacement ductility, which is a measure of the inelastic deformation demand on the frame. Then the onset of cover concrete spalling (Section 10.2), the onset of bar buckling (Section 10.3), bar fracture (Section 10.4), and the proximity to ultimate limit state (Section 10.5) are

addressed further. Section 10.6 discusses the sensitivity of the response quantities to the
varied frame parameters.

10.1 DISPLACEMENT DUCTILITY DEMAND

In this research ductility was defined as the deformation at a given state divided
by the deformation at nominal yield. For a frame with yield displacement, Δ_y, and a
maximum expected displacement, Δ_{max}, the displacement ductility demand, μ_Δ, is
defined as:

$$\mu_\Delta = \frac{\Delta_{max}}{\Delta_y} \qquad (10.1)$$

A detailed discussion of ductility demands on reinforced concrete structures was
provided by Paulay and Priestley (1992).

The yield displacements were calculated and summarized in chapters 6 and 8, and
the maximum displacements were calculated and summarized in chapters 7 and 9.
Displacement ductility demands were calculated for each combination of ground motion
with reinforced concrete frame and ground motion with hybrid frame, with axial-load
ratios equal to 0.05 and 0.10. The results for the displacement ductility are presented in
detail in Appendix D (tables D.1 through D.3). Extreme values of displacement ductility
demand corresponding to the 10 percent in 50 ground motions were as follows:

- o Reinforced concrete frames
  - Minimum: 0.5 (frame 6.030.05, ground motion 10-3)
  - Maximum: 7.2 (frame 5.005.15, ground motion 10-5)
- o Hybrid frames with axial-load ratio equal to 0.05
  - Minimum: 0.5 (frame 7.030.100, ground motion 10-3)
  - Maximum: 3.9 (frame 6.005.100, ground motion 10-5)
- o Hybrid frames with axial-load ratio equal to 0.10

- Minimum: 0.8 (frame 5.030.075, ground motion 10-3)
- Maximum: 4.1 (frame 7.010.100, ground motion 10-3)

For the 2 percent in 50 ground motions, displacement ductility demand ranged as

follows:

- Reinforced concrete frames
  - Minimum: 1.3 (frame 5.030.05, ground motion 2-1)
  - Maximum: 17.2 (frame 7.005.10, ground motion 2-3)
- Hybrid frames with axial-load ratio equal to 0.05
  - Minimum: 1.2 (frame 6.030.025, ground motion 2-3)
  - Maximum: 12.1 (frame 7.005.100, ground motion 2-3)
- Hybrid frames with axial-load ratio equal to 0.10
  - Minimum: 2.1 (frame 7.030.050, ground motion 2-4)
  - Maximum: 13.8 (frame 6.010.100, ground motion 2-3)

Figure 10.1 presents the mean and the mean plus one standard deviation of the

displacement ductility for the reinforced concrete frames subjected to the 2 percent in 50

ground motions. Figures 10.2 and 10.3 present similar data for the hybrid frames with

axial-load ratios of 0.05 and 0.10, respectively. Appendix D contains the figures showing

the displacement ductility for the 10 percent in 50 ground motions (figures D.1 through

D.3). The general trends observed in displacement ductility for the 10 percent in 50

ground motions were similar to those apparent in the results for the 2 percent in 50

ground motions.
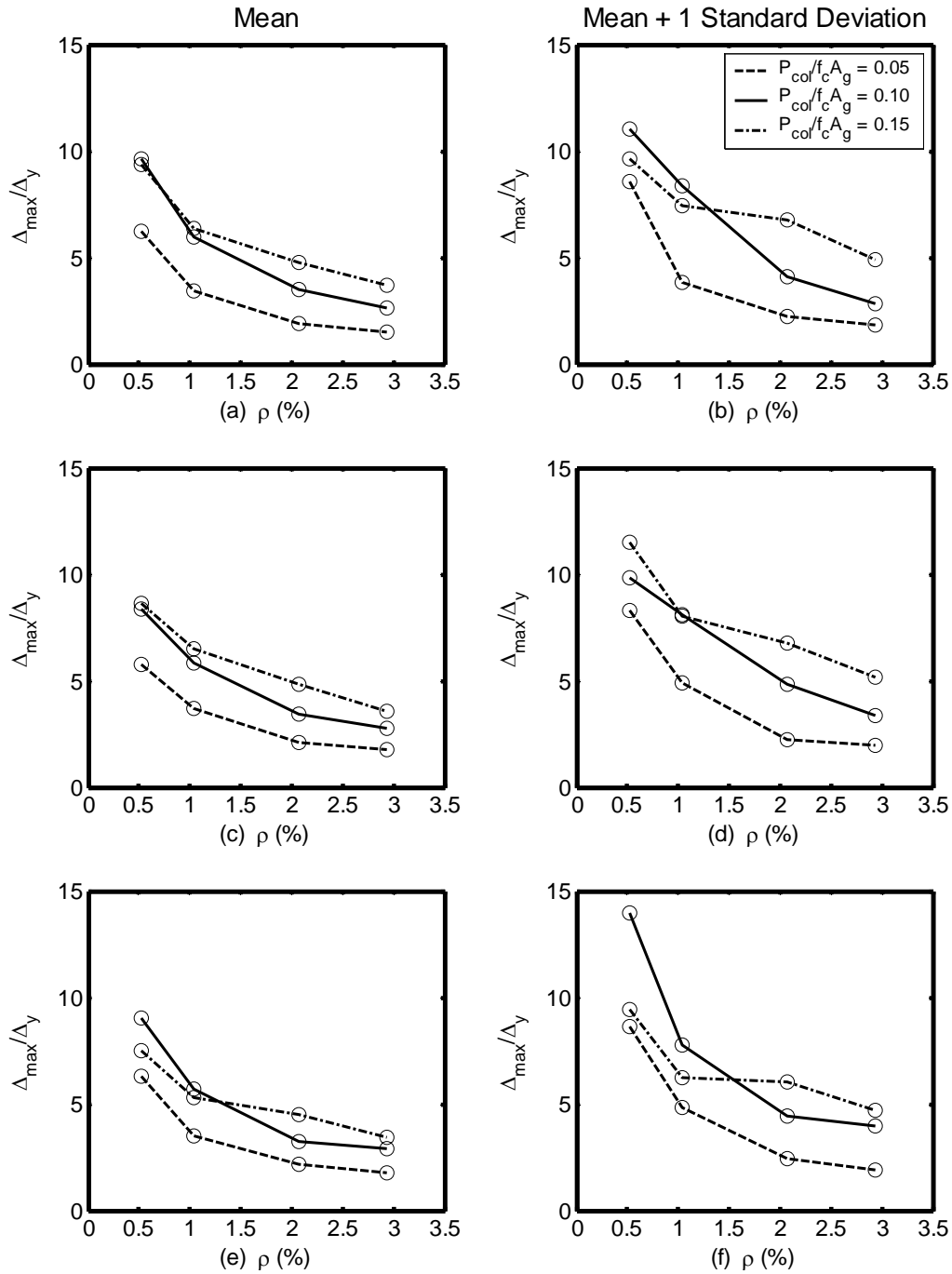
Figure 10.1: Displacement Ductility, 2 Percent in 50, Reinforced Concrete Frames
(a) and (b) $L_{col}/D_{col} = 5$, (c) and (d) $L_{col}/D_{col} = 6$, and (e) and (f) $L_{col}/D_{col} = 7$
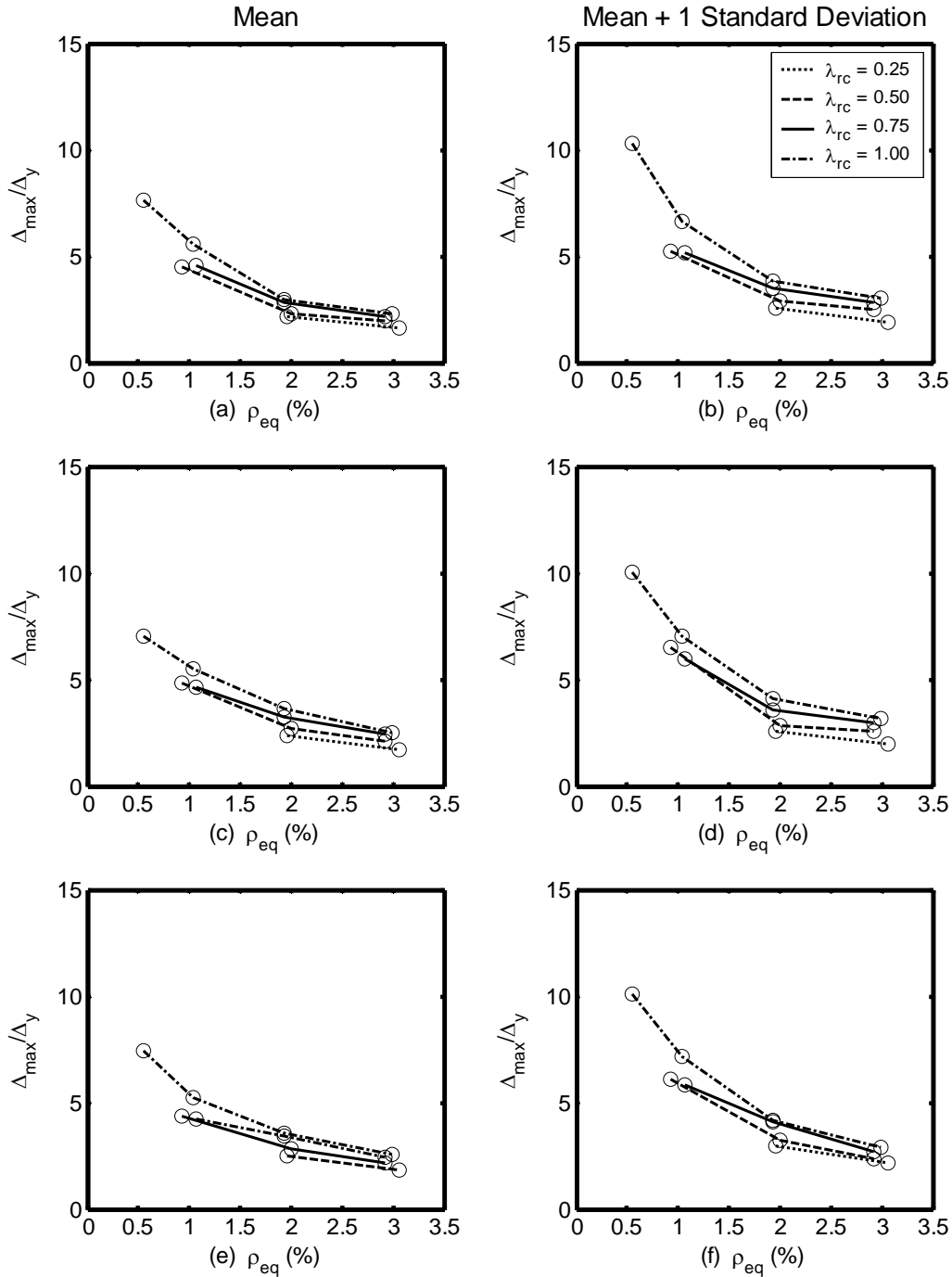
Figure 10.2: Displacement Ductility, 2 Percent in 50, Hybrid Frames, $P_{col}/(f_c^{'}A_g) = 0.05$
(a) and (b) $L_{col}/D_{col} = 5$, **(c) and (d)** $L_{col}/D_{col} = 6$, **and (e) and (f)** $L_{col}/D_{col} = 7$
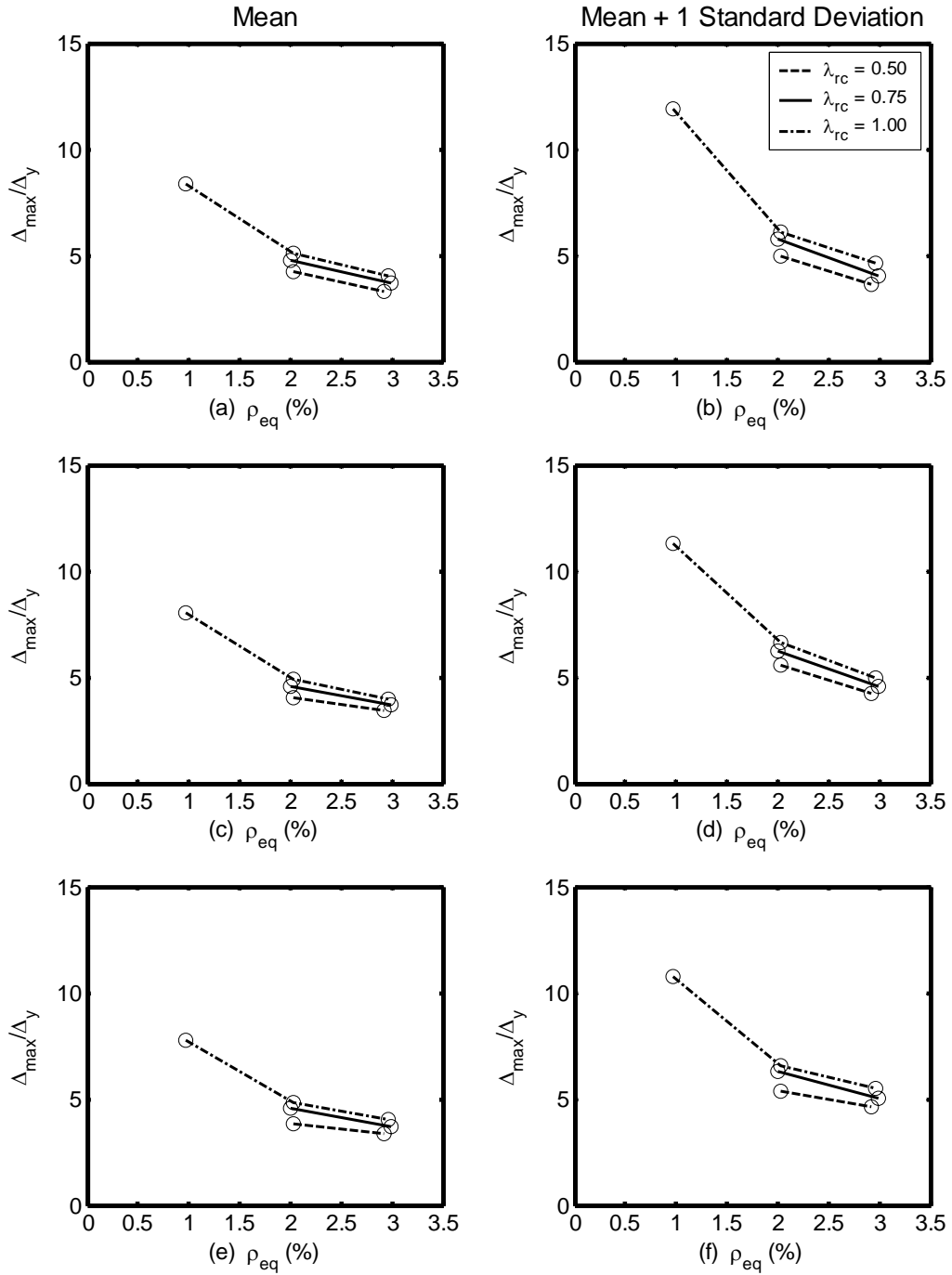
Figure 10.3: Displacement Ductility, 2 Percent in 50, Hybrid Frames, $P_{col}/(f_c'A_g) = 0.10$

(a) and (b) $L_{col}/D_{col} = $ **5,** (c) and (d) $L_{col}/D_{col} = $ **6, and** (e) and (f) $L_{col}/D_{col} = $ **7**

The data presented in figures 10.1 through 10.3 show the following trends:

- As the steel ratio, ρ or ρ_{eq}, increased, the displacement ductility demand decreased. A greater rate of decrease occurred at smaller steel ratios, as is evident in Figure 10.1 (a). This trend was expected because the earthquake analyses indicated that the maximum displacement decreased as the steel ratio increased. This trend is evident in each of the three figures.

- As the axial-load ratio, $P_{col}/(f_c'A_g)$, increased, the displacement ductility demand also increased. Figure 10.1 (c) illustrates this observation. Although some of the lines cross one another, especially at low steel ratios, this is solely a result of the frames that had numerical convergence problems. For most of the frames, the maximum displacement was a consequence of ground motion 2-3. For those frames, when the average values were calculated, they resulted in smaller average values because they lacked the large contribution from ground motion 2-3 (Section 7.4). This observation was also expected because the earthquake analyses revealed that as the axial-load ratio increased, and in turn the mass on the frame increased, the maximum displacement and the cracked stiffness increased. This observation indicates that the effect of the increased mass was larger than the effect of the increased stiffness.

- The displacement ductility demand was not significantly influenced by L_{col}/D_{col}. This is evident by comparing figures 10.3 (a) and (e). The pushover analyses showed that the yield displacement increased considerably with L_{col}/D_{col}, but the earthquake analyses showed that the maximum displacement also increased significantly with L_{col}/D_{col}. The insensitivity to L_{col}/D_{col} suggests that the yield

172

displacement and the maximum displacement were influenced about equally by the change in L_{col}/D_{col} .

- For the hybrid frames, the displacement ductility was almost independent of the re-centering ratio, λ_{rc} . Figure 10.3 shows that the displacement ductility demand increased slightly as the re-centering ratio increased. The small influence of the re-centering ratio on displacement ductility was anticipated because the pushover and earthquake analyses found that the re-centering ratio did not significantly affect any of the results.

- A comparison of the mean displacement ductility of the hybrid frame with the axial-load ratio, $P_{col}/(f_c'A_g)$, equal to 0.10 (Figure 10.3) and that of the reinforced concrete frame with the same axial-load ratio (Figure 10.1) showed that the reinforced concrete frames had only slightly larger displacement ductility demands than the hybrid frames.

- The mean plus one standard deviation was approximately 25 percent larger than the mean values as is evident in each of the figures.

- The displacement ductility values for the 10 percent in 50 ground motions were approximately half those for the 2 percent in 50 ground motions. The figures illustrating the displacement ductility values for the 10 percent in 50 ground motions can be found in Appendix D (figures D.1 through D.3).

10.2 ONSET OF COVER CONCRETE SPALLING

For well-confined reinforced concrete columns, the onset of cover concrete spalling is typically the first flexural state that requires repairs that may put the bridge temporarily out of service (Priestley et al. 1996).

Berry and Eberhard (2004) used 102 tests of rectangular columns and 40 spiral-reinforced columns to develop a relationship for estimating a column's displacement at the onset of cover concrete spalling from known quantities such as column geometry, reinforcing steel, and axial-load. Their relationship can also be used to estimate the probability of cover concrete spalling for a given displacement. They defined the mean displacement at the onset of cover concrete spalling using Equation 10.2.

$$\Delta_{spall} = \frac{1.6L_{col}}{100}\left(1 - \frac{P_{col}}{f_c' A_g}\right)\left(1 + \frac{L_{col}}{10D_{col}}\right) \qquad (10.2)$$

where L_{col} = column clear height between the top of the foundation and the bottom of the cap-beam

P_{col} = compressive axial-load on a column

f_c' = concrete compressive strength, taken as 5 ksi

A_g = gross cross-sectional area of a column

D_{col} = diameter of the column

Berry and Eberhard (2004) found that the probability of cover concrete spalling occurring could be described as a function of the maximum displacement divided by the estimated displacement at the onset of cover spalling given by Equation 10.2, $\Delta_{max}/\Delta_{spall}$. They found that for circular, reinforced concrete columns, the probability of the onset of cover concrete spalling could be estimated from a normal cumulative density function with a mean value of 1.07 and coefficient of variation, COV, equal to 0.352.

Equation 10.2 was developed from columns containing mild reinforcing steel only, therefore it does not explicitly account for the prestressing steel included in the hybrid frames of this study. To estimate the displacement at the onset of cover concrete spalling for the hybrid frames, Equation 10.2 was modified so that P_{col} was replaced by the sum of the axial-load and the axial compression force caused by the prestressing steel, P_{col_total}. Although no experimental results were used to verify this assumption, this modification was chosen because the only variable in Equation 10.2 that is directly influenced by the addition of prestressing is the axial load. The sum of the axial-load and the axial compression force caused by the prestressing steel was defined as follows:

$$P_{col\_total} = P_{col} + \rho_p A_g f_{p0} \tag{10.3}$$

where P_{col} = compressive axial-load on a column

ρ_p = area of prestressing steel divided by the gross cross-sectional area of a column, A_p/A_g

A_g = gross cross-sectional area of a column

f_{p0} = stress in prestressing steel at zero drift, calculated as described in Chapter 8

For this study, the quantity $\Delta_{max}/\Delta_{spall}$ was found for each combination of frame and ground motion, and from this value, the probability of the cover concrete spalling was estimated from statistical information that Berry and Eberhard (2004) provided. These estimated probabilities were conditional probabilities, meaning that they were the estimated probability of cover concrete spalling initiating given the occurrence of a 10 percent in 50 or 2 percent in 50 earthquake event (Halder and Mahadevan 2000). Complete results for the estimated probability of the onset of cover concrete spalling are

175

presented in tables E.4 through E.6 for the reinforced concrete frames and the hybrid

frames with axial-load ratios equal to 0.05 and 0.10. For the 10 percent in 50 ground

motions, the probability of onset of cover spalling ranged as follows:

- o Reinforced concrete frames
    - • Minimum: 0.01 (frame 7.030.05, ground motion 10-3)
    - • Maximum: 0.88 (frame 5.005.15, ground motion 10-5)
- o Hybrid frames with axial-load ratio equal to 0.05
    - • Minimum: 0.01 (numerous frames and ground motions)
    - • Maximum: 0.11 (frame 6.005.100, ground motion 10-5)
- o Hybrid frames with axial-load ratio equal to 0.10
    - • Minimum: 0.01 (numerous frames and ground motions)
    - • Maximum: 0.24 (frame 7.010.100, ground motion 10-3)

The maximum values of the probability of cover spalling occurring listed above

may be a bit misleading. Note that these values are the maximum probability of cover

spalling occurring for individual ground motions, not mean values. Also note that the

relatively large value for the reinforced concrete frames is a result of an axial-load ratio

of 0.15, a value that was not considered for the hybrid frames. When individual frames

are compared with similar axial-load ratios and longitudinal reinforcement ratios, the

probabilities of cover concrete spalling occurring are more similar. For example, with an

axial-load ratio equal to 0.10, a column aspect ratio of 7, a reinforcement ratio of 0.10,

and ground motion 10-3, the probability of the onset of cover concrete spalling is equal to

0.25 for the reinforced concrete frame and 0.24 for the hybrid frame.

The probability of the occurrence of cover spalling ranged as follows for the 2

percent in 50 ground motions:

- o Reinforced concrete frames
    - • Minimum: 0.03 (numerous frames and ground motions)

- Maximum: 1.00 (numerous frames and ground motions)
  - Hybrid frames with axial-load ratio equal to 0.05
    - Minimum: 0.02 (numerous frames and ground motions)
    - Maximum: 0.99 (frame 7.005.100, ground motion 2-3)
  - Hybrid frames with axial-load ratio equal to 0.10
    - Minimum: 0.10 (numerous frames and ground motions)
    - Maximum: 1.00 (numerous frames and ground motions)

For the reinforced concrete frames, the mean $\Delta_{max}/\Delta_{spall}$ and the mean probability

of the onset of cover concrete spalling are presented in Figure 10.4 for the 2 percent in 50

ground motions. Figures 10.5 and 10.6 show the same information for the hybrid frames

with axial-load ratios, $P_{col}/(f_c'A_g)$, equal to 0.05 and 0.10, respectively. The results for

the 10 percent in 50 ground motions are plotted in Appendix D (figures D.4 through D.6).

The mean probability values were found by assuming that each ground motion had an

equal probability of occurrence.
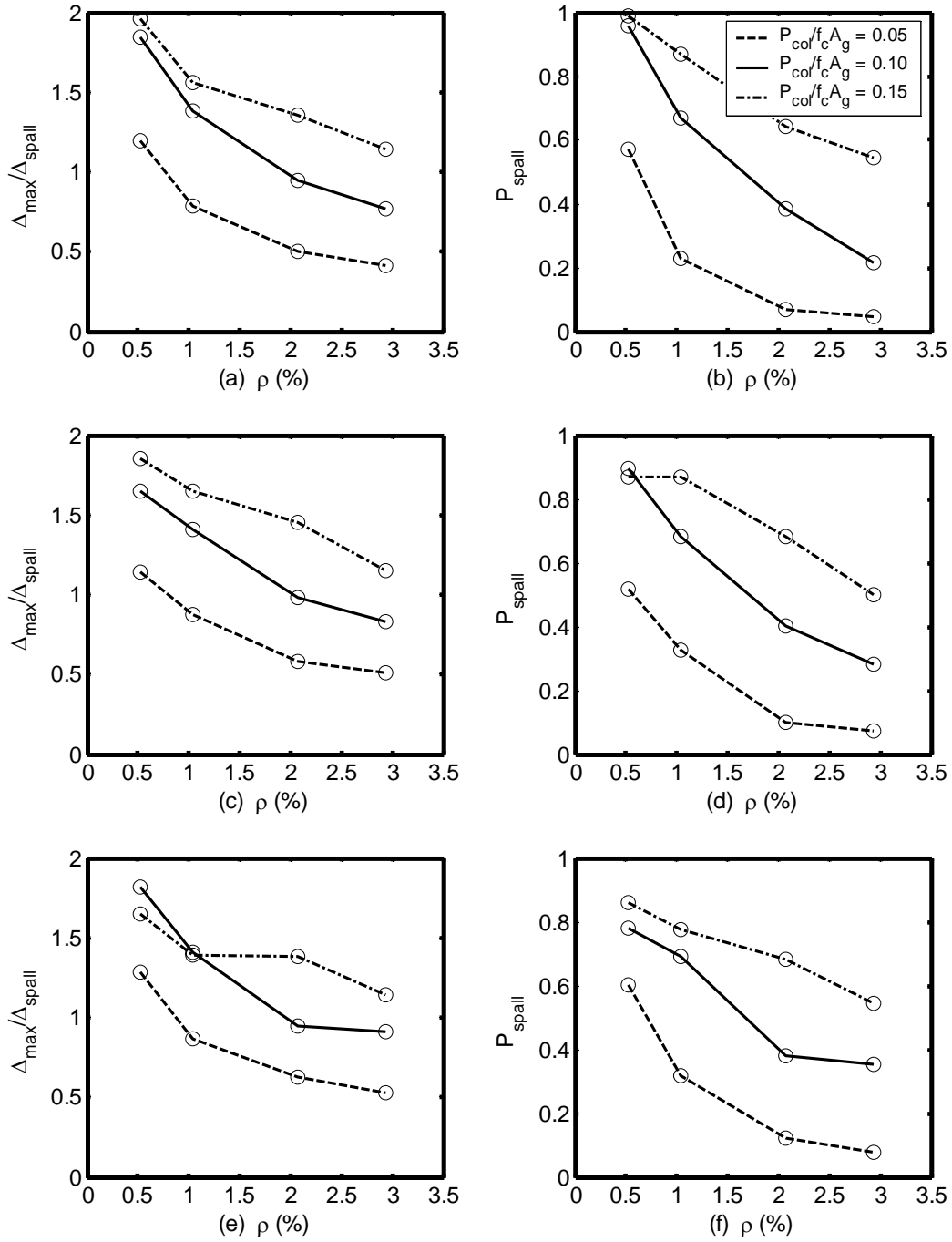
Figure 10.4: Cover Spalling, 2 Percent in 50, Reinforced Concrete Frames
(a) and (b) $L_{col}/D_{col} = 5$, (c) and (d) $L_{col}/D_{col} = 6$, and (e) and (f) $L_{col}/D_{col} = 7$
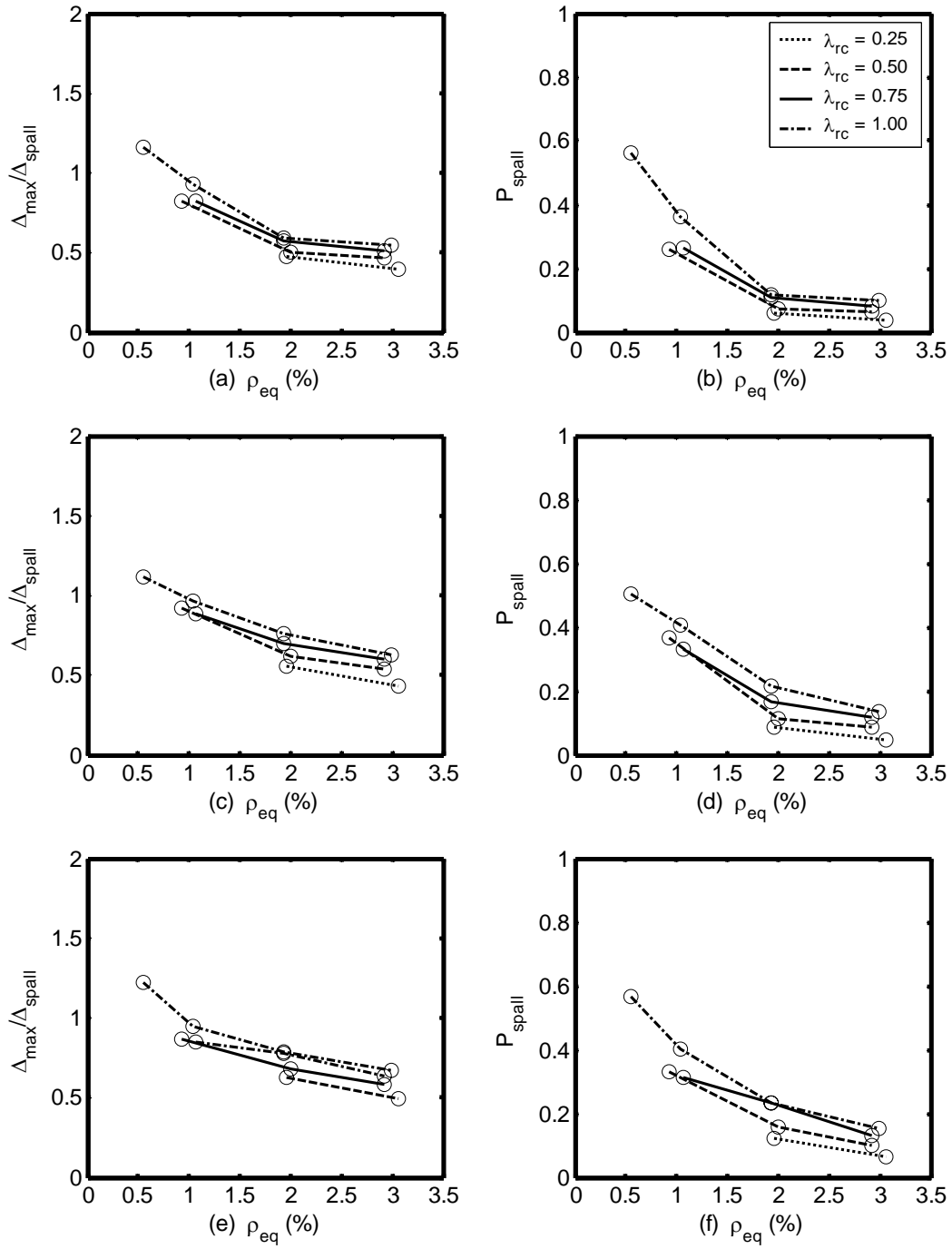
Figure 10.5: Cover Spalling, 2 Percent in 50, Hybrid Frames, $P_{col}/(f_c' A_g) = 0.05$
(a) and (b) $L_{col}/D_{col} = 5$, **(c) and (d)** $L_{col}/D_{col} = 6$, **and (e) and (f)** $L_{col}/D_{col} = 7$
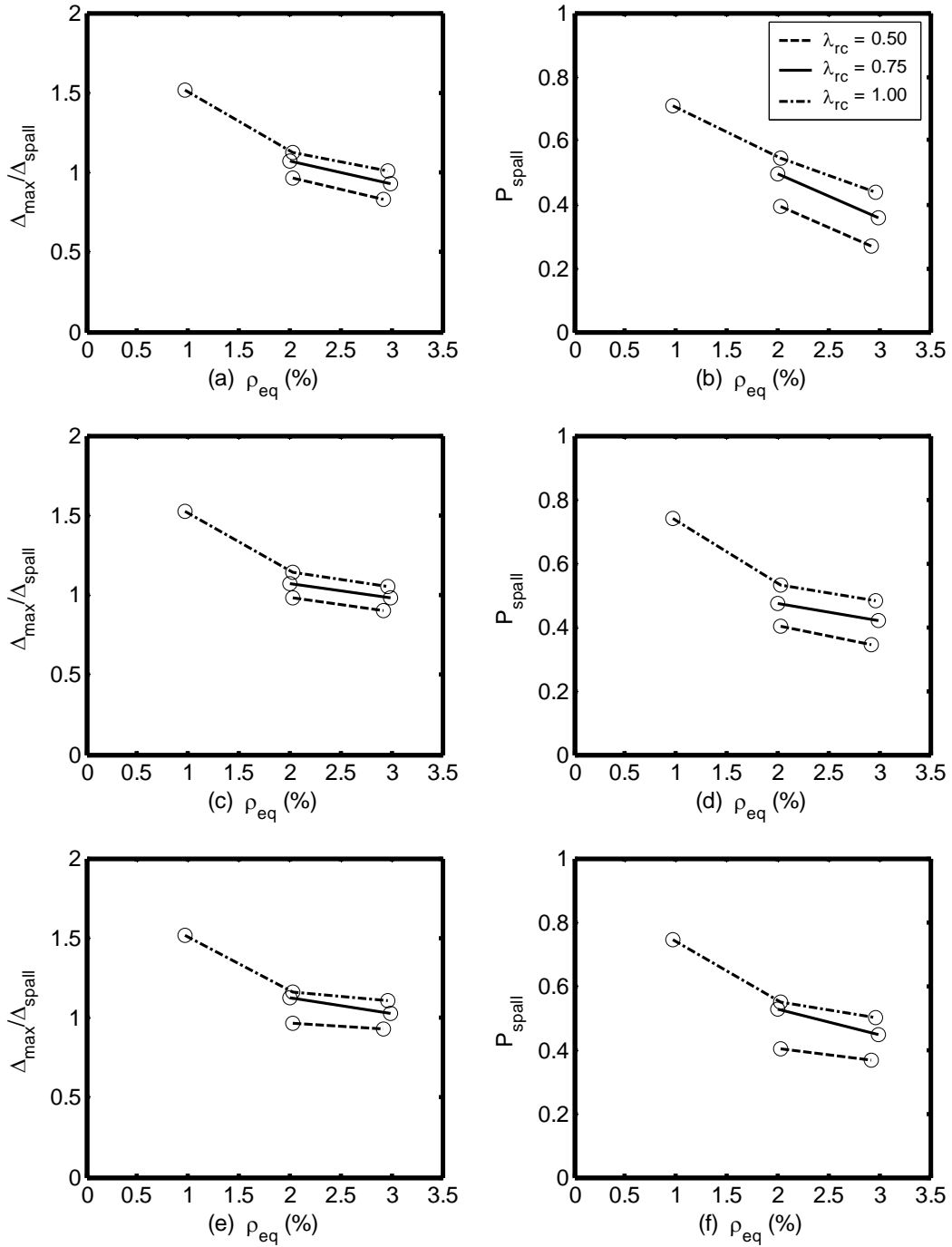
Figure 10.6: Cover Spalling, 2 Percent in 50, Hybrid Frames, $P_{col}/(f_c' A_g) = 0.10$
(a) and (b) $L_{col}/D_{col} = 5$**, (c) and (d)** $L_{col}/D_{col} = 6$**, and (e) and (f)** $L_{col}/D_{col} = 7$

The results shown in Figures 10.4 through 10.6 indicate the following:

- As the steel ratio, ρ or ρ_{eq}, increased, the probability of cover concrete spalling occurring decreased. A greater decrease occurred between smaller steel ratios, as is evident in Figure 10.6 (b). This trend was anticipated because the earthquake analyses revealed that the maximum displacement decreased as the steel ratio increased. A smaller maximum displacement resulted in a smaller $\Delta_{max}/\Delta_{spall}$, which in turn resulted in a smaller probability of the onset of cover concrete spalling.

- As the axial-load ratio, $P_{col}/(f_c'A_g)$, increased, the probability of cover concrete spalling occurring also increased. Figure 10.4 (b) illustrates the observation. Although some of the lines cross one another, such as in Figure 10.4 (d), this is solely a result of the frames that had convergence problems. For most of the frames, the maximum displacement was a consequence of ground motion 2-3. For those frames, when the average values were calculated, they resulted in smaller average values because they lacked the large contribution from ground motion 2-3. This observation can be partially explained because the earthquake analyses found that as the axial-load ratio increased, and in turn the mass on the frame increased, the maximum displacement increased. In addition, it can be seen from Equation 10.2 that as the axial-load ratio increased, Δ_{spall} decreased. Therefore, the increase in Δ_{max} and the decrease in Δ_{spall} contributed to the increase in the probability of cover concrete spalling occurring.

- The probability of the onset of cover spalling was not significantly influenced by L_{col}/D_{col}. This is evident by comparing between figures 10.6 (b) and (f). The earthquake analyses showed that the maximum displacement increased significantly as L_{col}/D_{col} increased. Equation 10.2 indicates that Δ_{spall} is also influenced by L_{col}/D_{col}, but not significantly.

- For the hybrid frames, the probability of cover concrete spalling occurring was almost independent of the re-centering ratio, λ_{rc}. A slight increase in the probability of the onset of cover concrete spalling is shown in Figure 10.6 as the re-centering ratio increased. The small influence of the re-centering ratio on displacement ductility was anticipated because the pushover analyses and earthquake analyses showed that the re-centering ratio did not significantly affect any of the results. The variation in the probability of the occurrence of cover concrete spalling could be partially explained by the modeling approximation of using P_{col_total} in Equation 10.2.

- A comparison of the probability of cover concrete spalling occurring for the hybrid frame with an axial-load ratio equal to 0.05 (Figure 10.5) and that of the reinforced concrete frame with the same axial-load ratio (Figure 10.4) shows that the two types of frames had similar probabilities. Closer inspection shows that the reinforced concrete frame had slightly larger values than the hybrid frame.

- The results shown in figures 10.4 through 10.6 indicate that there was a significant probability that the frames would experience spalling when subjected to 2 percent in 50 seismic events. The values for the probability of the onset of

182

cover concrete spalling were approximately 1/5 as large for the 10 percent in 50 ground motions. Figures D.4 through D.6 in Appendix D illustrate the values for the probability of cover concrete spalling occurring for the 10 percent in 50 ground motions.

10.3 ONSET OF BAR BUCKLING

The onset of bar buckling in a reinforced concrete column is especially undesirable. Once it has occurred, extensive repairs are typically required to return the bridge to service. If the damage is severe, repairing the columns may not be economically or technically feasible, and all or part of the bridge will need to be replaced.

Berry and Eberhard (2004) developed a relationship for estimating the mean displacement corresponding to the onset of bar buckling from known quantities such as column geometry, amount of reinforcing steel, and axial-load. The probability of the onset of bar buckling in the columns of the frames considered here was estimated from the values provided in their work.

Berry and Eberhard (2004) developed Equation 10.4 for estimating the displacement corresponding to the onset of bar buckling for circular, spiral-reinforced columns as:

$$\Delta_{bb} = \frac{3.25L_{col}}{100}\left(1 + k_{bb}\rho_{eff}\frac{d_b}{D_{col}}\right)\left(1 - \frac{P_{col}}{f_c'A_g}\right)\left(1 + \frac{L_{col}}{10D_{col}}\right) \qquad (10.4)$$

where L_{col} = column clear height between the top of the foundation and the bottom of the cap-beam

k_{bb} = taken as 150 for the circular, spiral-reinforced columns

ρ_{eff} = $\rho_t f_y / f_c'$ where ρ_t is the ratio of volume of spiral reinforcement to total

volume of the core

d_b = diameter of the longitudinal reinforcing bar

D_{col} = diameter of the column

P_{col} = compressive axial-load on a column

f_c' = concrete compressive strength, taken as 5 ksi

A_g = gross cross-sectional area of a column

Berry and Eberhard (2004) also found that the probability of the onset of bar buckling could be calculated from the maximum displacement divided by the estimated displacement at the onset of bar buckling given by Equation 10.4, Δ_{max}/Δ_{bb}. They found that for circular, reinforced concrete columns, the probability of the onset of bar buckling could be estimated from a normal cumulative density function with a mean value of 0.97 and coefficient of variation, COV, equal to 0.246.

The equations presented in Berry and Eberhard (2004) were developed from columns that contained mild reinforcing steel only; therefore, Equation 10.4 does not explicitly account for the prestressing steel included in the hybrid frames of this study. For the hybrid frames, Equation 10.4 was modified so that P_{col} was replaced by the sum of the axial-load and the axial compression force caused by the prestressing steel. The relationship for this sum, P_{col_total}, was given by Equation 10.3.

For each combination of frame and ground motion, the quantity Δ_{max}/Δ_{bb} was found. From these results the probability of bar buckling occurring was estimated from the normal cumulative density function. As with the probabilities discussed in Section 10.2, the estimated probabilities for the onset of bar buckling were conditional probabilities, indicating that they were the probability of bar buckling initiating given the

184

occurrence of a 10 percent in 50 or 2 percent in 50 earthquake event (Halder and Mahadevan 2000).

The results for the probability of the onset of bar buckling are summarized in tables D.7 through D.9 in Appendix D. For the 10 percent in 50 ground motions the probability of bar buckling initiating was essentially zero for all the frames studied. For the 2 percent in 50 ground motions, the probability of bar buckling ranged as follows:

- o Reinforced concrete frames
    - Minimum: 0.00 (numerous frames and ground motions)
    - Maximum: 0.67 (frame 7.005.15, ground motion 2-3)
- o Hybrid frames with axial-load ratio equal to 0.05
    - Minimum: 0.00 (most frames and ground motions)
    - Maximum: 0.07 (frame 7.005.100, ground motion 2-3)
- o Hybrid frames with axial-load ratio equal to 0.10
    - Minimum: 0.00 (most frames and ground motions)
    - Maximum: 0.25 (frame 6.010.100, ground motion 2-3)

For the reinforced concrete frames, the mean Δ_{max}/Δ_{bb} and the mean probability of bar buckling occurring are presented in Figure 10.7 for the 2 percent in 50 ground motions. Figures 10.8 and 10.9 show the same information for the hybrid frames with axial-load ratio equal to 0.05 and 0.10, respectively. These same results for the 10 percent in 50 ground motions may be found in figures D.7 through D.9 of Appendix D. The mean probability values were found by assuming that each ground motion had an equal probability of occurrence.
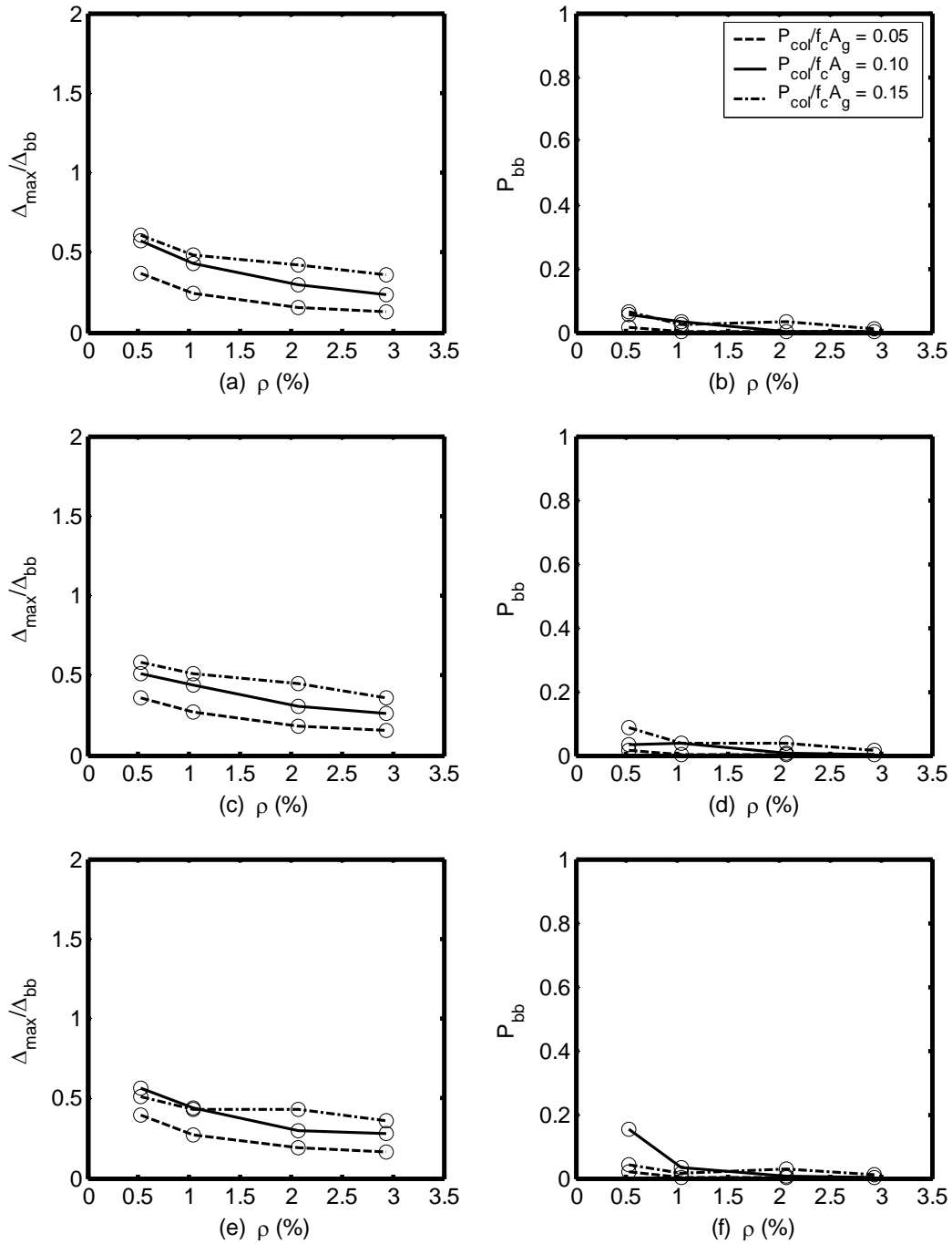
Figure 10.7: Bar Buckling, 2 Percent in 50, Reinforced Concrete Frames
(a) and (b) L_{col}/D_{col} = 5, (c) and (d) L_{col}/D_{col} = 6, and (e) and (f) L_{col}/D_{col} =7

186
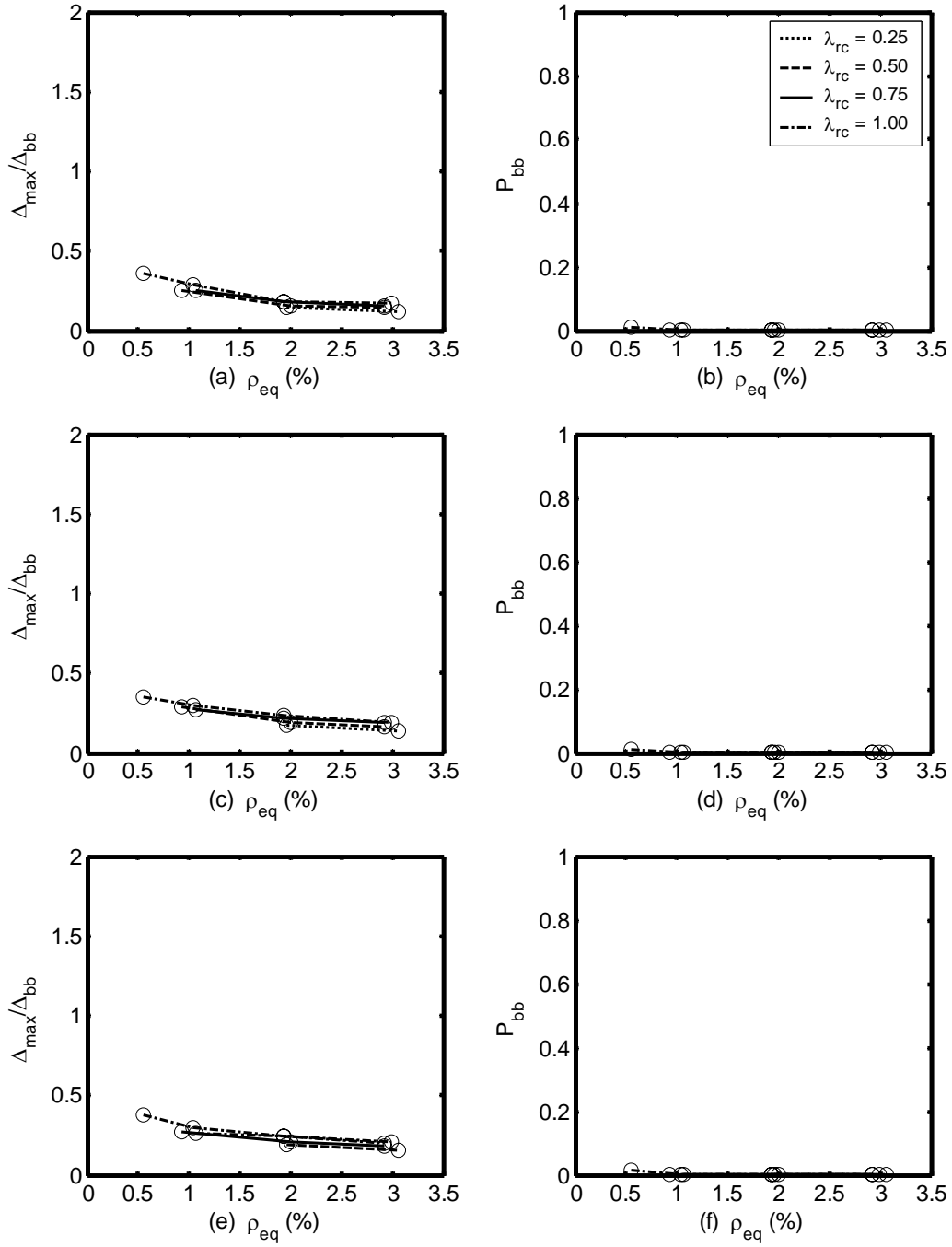
Figure 10.8: Bar Buckling, 2 Percent in 50, Hybrid Frames, $P_{col}/(f_c' A_g) = 0.05$

(a) and (b) $L_{col}/D_{col} = 5$**, (c) and (d)** $L_{col}/D_{col} = 6$**, and (e) and (f)** $L_{col}/D_{col} = 7$
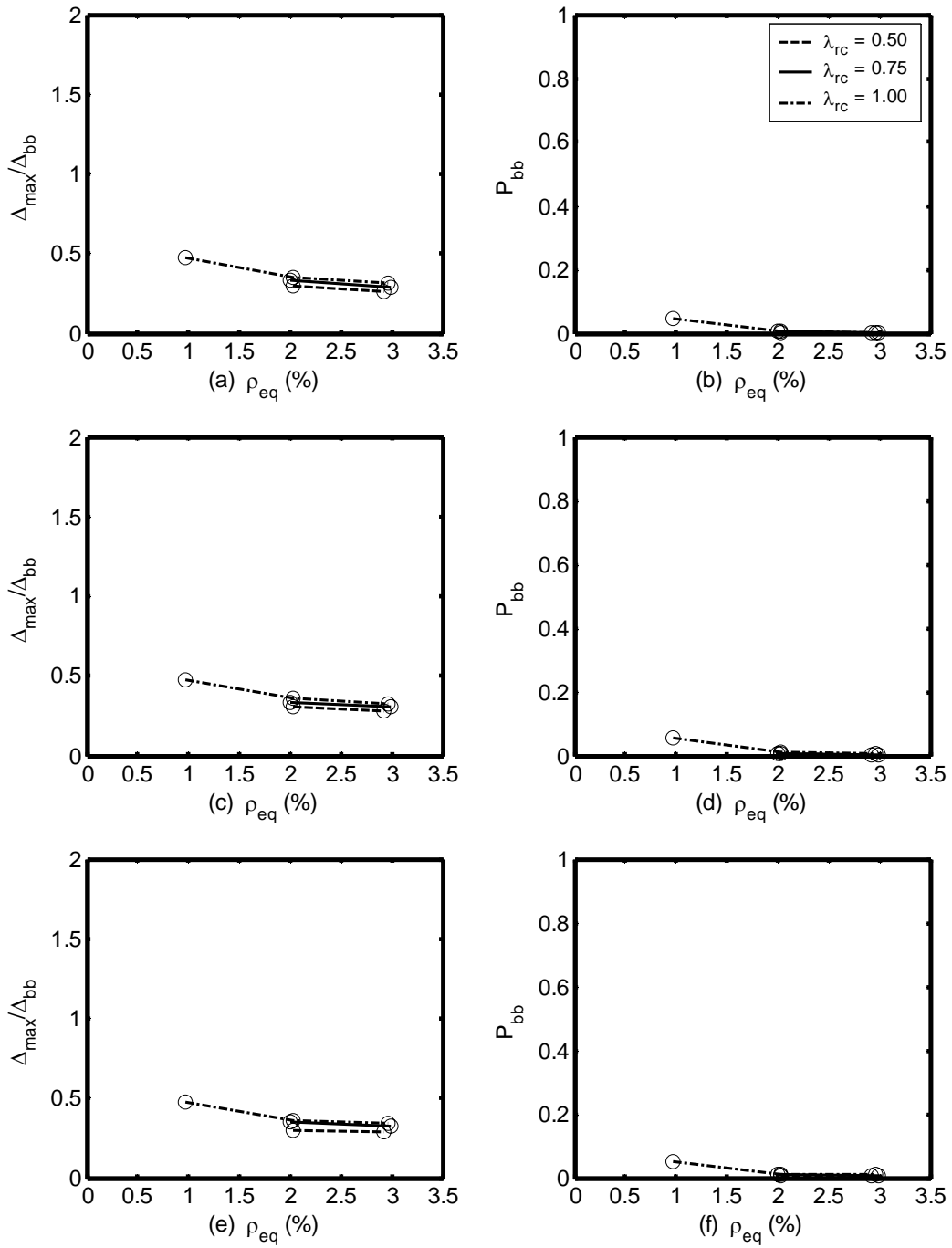
Figure 10.9: Bar Buckling, 2 Percent in 50, Hybrid Frames, $P_{col}/(f_c' A_g) = 0.10$
(a) and (b) $L_{col}/D_{col} = 5$**, (c) and (d)** $L_{col}/D_{col} = 6$**, and (e) and (f)** $L_{col}/D_{col} = 7$

The mean probability of bar buckling occurring remained below 0.15 for the reinforced concrete frames and remained below 0.05 for the hybrid frames. The following comments were noted from the results shown in figures 10.7 through 10.9.

- For small values of the steel ratio, the probability of the onset of bar buckling decreased as the steel ratio, ρ or ρ_{eq}, increased, as observed in Figure 10.9. This trend is consistent with the smaller maximum displacements encountered during the earthquake analyses as the steel ratio increased. A smaller maximum displacement resulted in a smaller Δ_{max}/Δ_{bb}, which in turn resulted in a smaller probability of bar buckling occurring.

- Because the probability of bar buckling occurring remained small, the axial-load ratio, $P_{col}/(f_c' A_g)$, was concluded to have an insignificant effect on the probability of the onset of bar buckling. This observation is evident in each of the figures.

- The probability of bar buckling occurring was not significantly influenced by L_{col}/D_{col}. This is evident by comparing between figures 10.9 (b) and (f). This observation is also evident from the plots of Δ_{max}/Δ_{bb} shown in figures 10.7 through 10.9. The earthquake analyses found that the maximum displacement increased significantly as L_{col}/D_{col} increased. Equation 10.4 also indicates that Δ_{bb} is influenced by L_{col}/D_{col}.

- For the hybrid frames, the probability of bar buckling occurring was not significantly affected by the re-centering ratio, λ_{rc}. This is evident from the plots of Δ_{max}/Δ_{bb} shown in the figures. For different values of λ_{rc}, the results for Δ_{max}/Δ_{bb} fall on top of each other.

- A comparison of the Δ_{max}/Δ_{bb} between the hybrid frame with an axial-load ratio equal to 0.05 (Figure 10.8) and the reinforced concrete frame with the same axial-load ratio (Figure 10.7) shows that the two types of frames had similar values.

- For the reinforced concrete frames, the results shown in Figure 10.7 indicate that the probability of bar buckling occurring remained below 0.15 for frames with low longitudinal reinforcement ratios and remained below 0.05 for frames with high reinforcement ratios when they were subjected to 2 percent in 50 seismic events. The results shown in figures 10.8 and 10.9 indicate that the probability of bar buckling occurring remained below 0.05 for all the hybrid frames. The values for the probability of the onset of bar buckling were nearly zero for all frames subjected to the 10 percent in 50 ground motions. Figures D.7 through D.9 in Appendix D illustrate the values for the probability of bar buckling for the 10 percent in 50 ground motions.

- Note that for hybrid frames, the strain in the mild steel is highly dependent on the chosen unbonded length. When a hybrid frame is designed, the necessary unbonded length can be chosen so that the mild steel does not exceed a chosen level of strain.

10.4 MAXIMUM STRAIN IN LONGITUDINAL MILD STEEL

Although strain hardening was included in the mild reinforcing steel used in the frames studied, as described in Chapter 4, bar fracture was not modeled. As the tensile strain in the longitudinal reinforcing steel increases, the potential for bar rupture also increases significantly. Although strain at bar rupture varies depending on the grade of

190

the bar, the bar diameter, hysteretic loading, and the manufacturer, Nawy (2000)

suggested a range of 0.05 and 0.12 for the fracture strain for an 8-in. gage length.

For this study, a steel strain threshold of 0.05 was selected. In frames that

contained longitudinal reinforcing steel that suffered strains higher than this value, bar

rupture was deemed possible. The strains encountered during the earthquake analyses are

summarized in the tables of Appendix D (tables D.10 through D.12). During the

earthquake analyses with the 10 percent in 50 ground motions, the maximum strain in the

longitudinal mild steel ranged as follows:

- o Reinforced concrete frames
    - Minimum: 0.001 (frame 6.030.05, ground motion 10-3)
    - Maximum: 0.057 (frame 5.005.15, ground motion 10-5)
- o Hybrid frames with axial-load ratio equal to 0.05
    - Minimum: 0.001 (numerous frames and ground motions)
    - Maximum: 0.022 (frame 6.005.100, ground motion 10-5)
- o Hybrid frames with axial-load ratio equal to 0.10
    - Minimum: 0.002 (numerous frames and ground motions)
    - Maximum: 0.016 (frame 6.010.100, ground motion 10-5)

The maximum strain in the longitudinal mild steel ranged as follows for the 2

percent in 50 ground motions:

- o Reinforced concrete frames
    - Minimum: 0.002 (frame 5.020.15, ground motion 2-3)
    - Maximum: 0.106 (frame 5.005.10, ground motion 2-5)
- o Hybrid frames with axial-load ratio equal to 0.05
    - Minimum: 0.003 (numerous frames and ground motions)
   - Maximum: 0.037 (frame 5.005.100, ground motion 2-5)
- o Hybrid frames with axial-load ratio equal to 0.10
    - Minimum: 0.006 (frame 6.030.100, ground motion 2-3)
    - Maximum: 0.033 (frame 5.010.100, ground motion 2-5)

For the reinforced concrete frames, the mean maximum strain in the extreme tensile steel, ε_{stl}, and the mean plus one standard deviation are presented in Figure 10.10 for the 2 percent in 50 ground motions. The same information is shown in figures 10.11 and 10.12 for the hybrid frames with axial-load ratios equal to 0.05 and 0.10, respectively. Figures D.10 through D.12, found in Appendix D, illustrate the same information for the 10 percent in 50 ground motions.
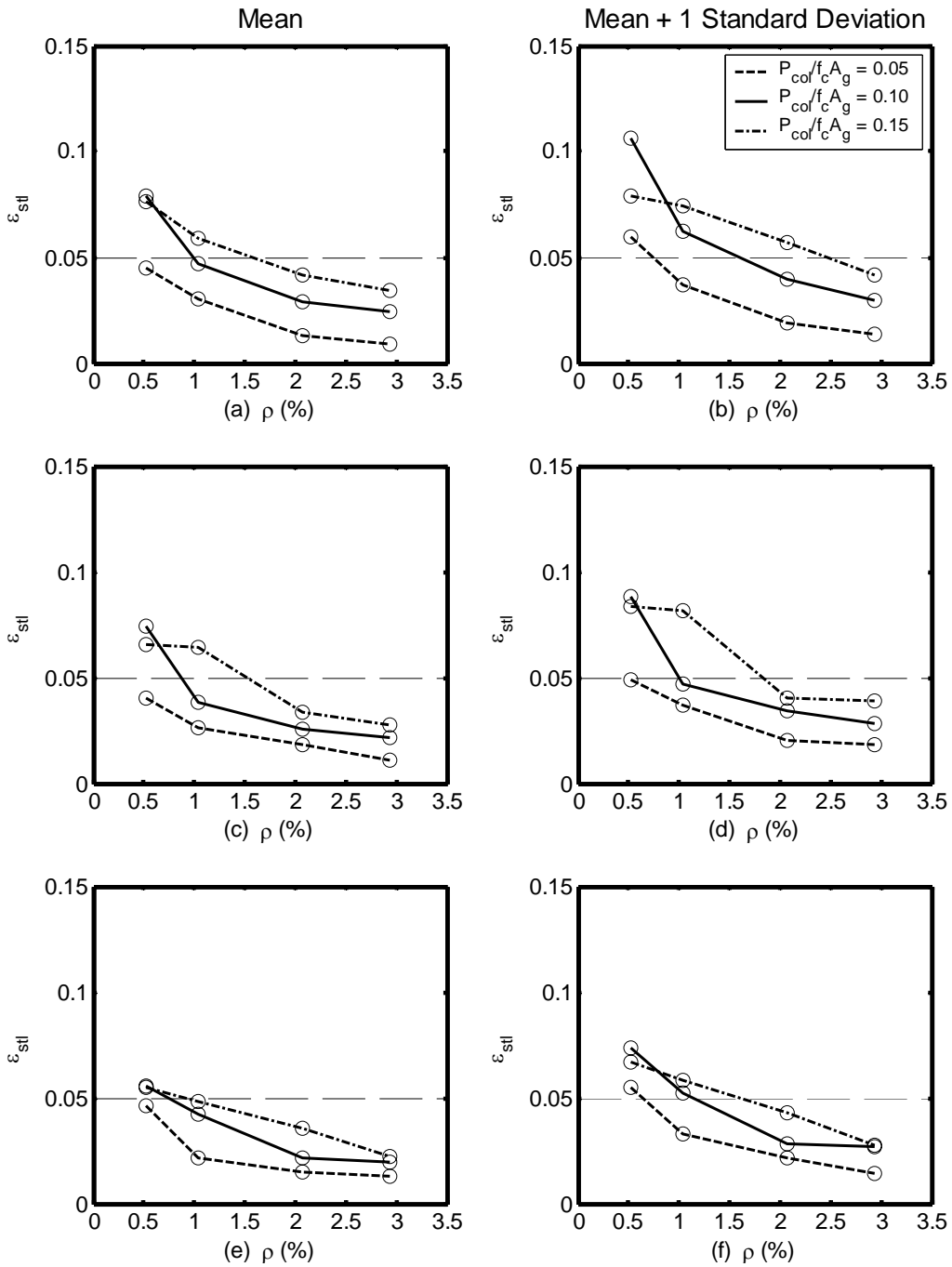
Figure 10.10: Maximum Steel Strain, 2 Percent in 50, Reinforced Concrete Frames

(a) and (b) $L_{col}/D_{col} = $ **5, (c) and (d)** $L_{col}/D_{col} = $ **6, and (e) and (f)** $L_{col}/D_{col} = $**7**
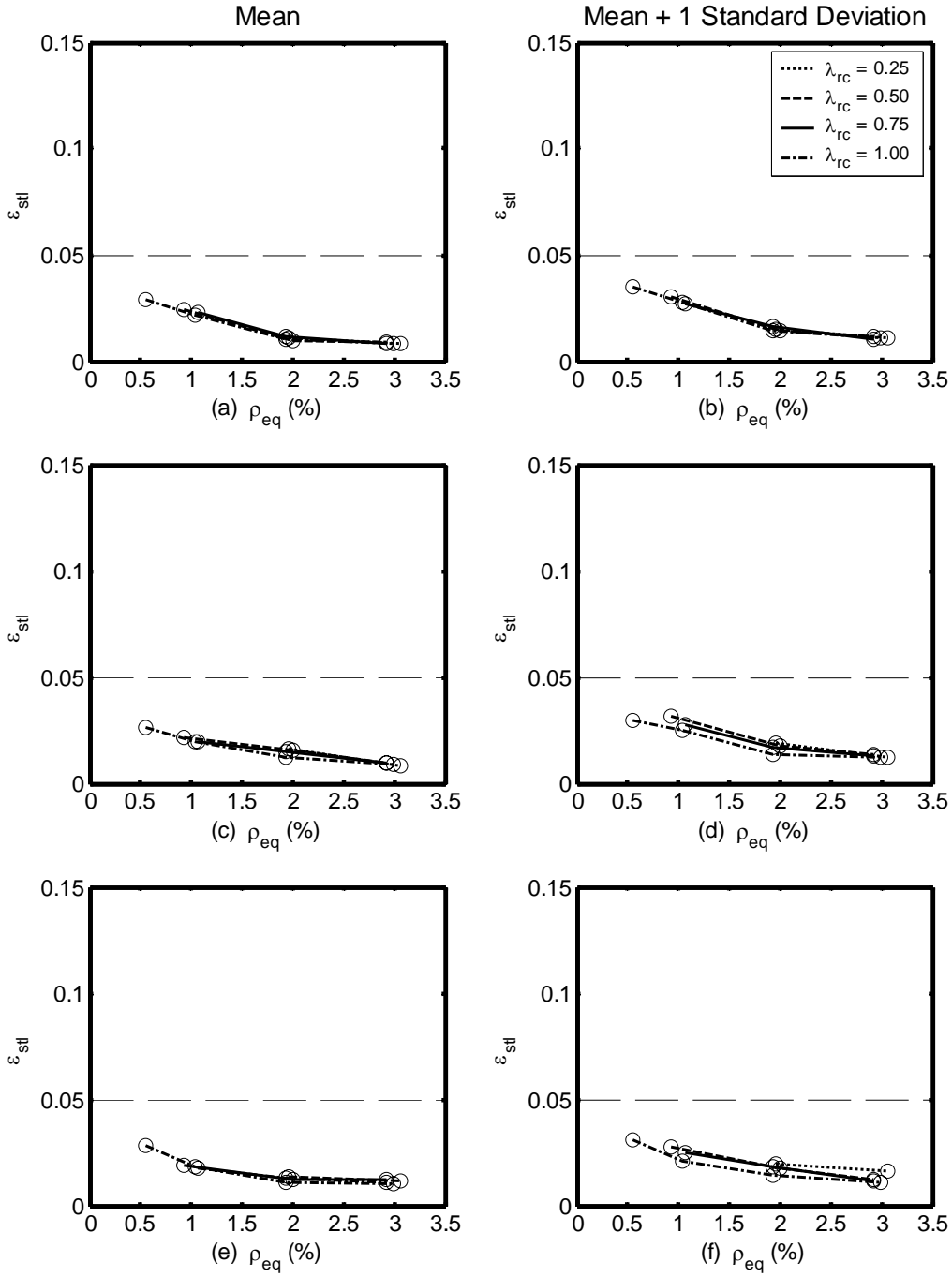
Figure 10.11: Maximum Steel Strain, 2 Percent in 50, Hybrid Frames, $P_{col}/(f_c' A_g) = 0.05$

(a) and (b) $L_{col}/D_{col} = 5$, **(c) and (d)** $L_{col}/D_{col} = 6$, **and (e) and (f)** $L_{col}/D_{col} = 7$
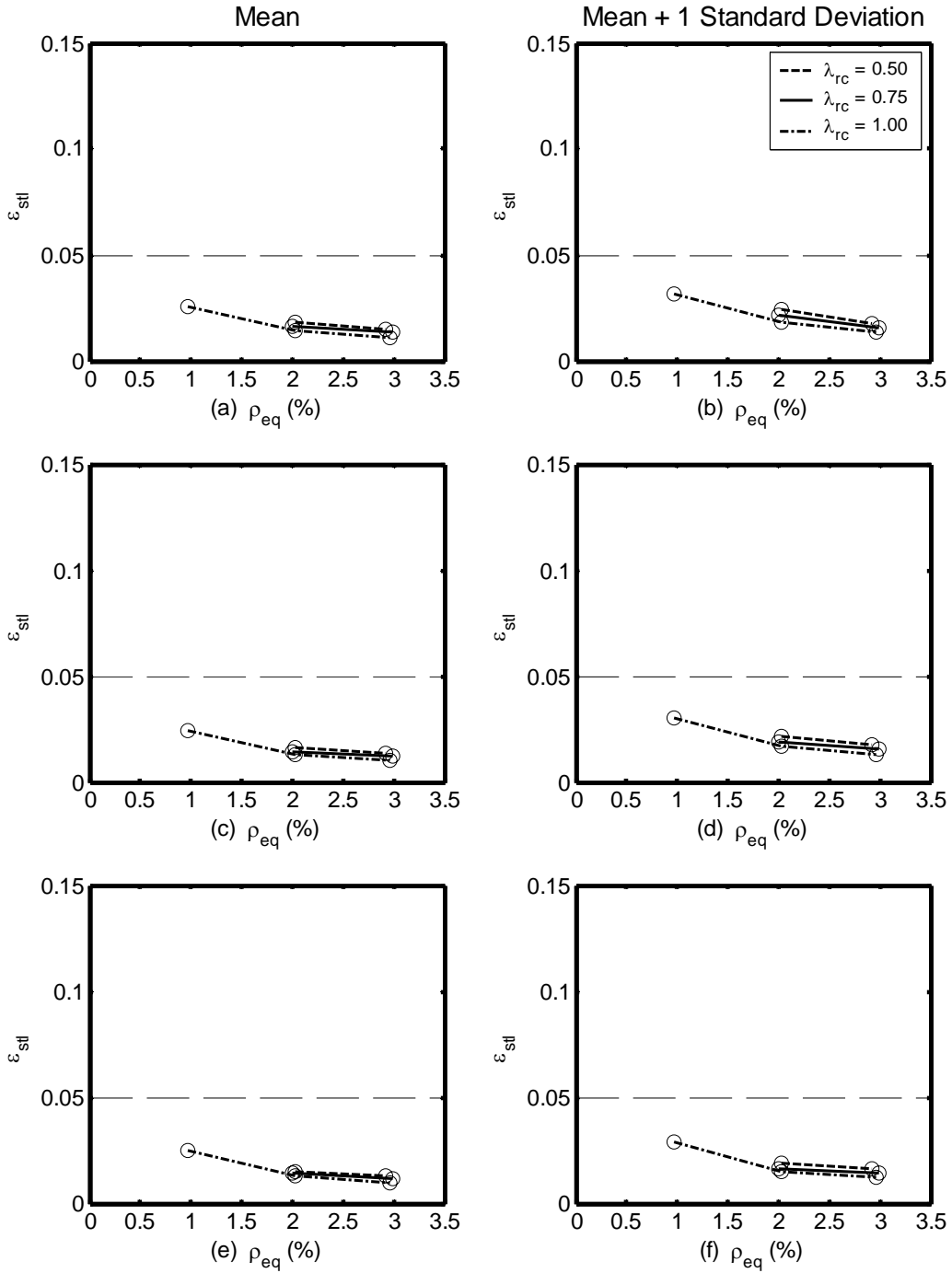
Figure 10.12: Maximum Steel Strain, 2 Percent in 50, Hybrid Frames, $P_{col}\big/(f_c^{'}A_g)=0.10$

(a) and (b) $L_{col}\big/D_{col}=$ **5, (c) and (d)** $L_{col}\big/D_{col}=$ **6, and (e) and (f)** $L_{col}\big/D_{col}=$**7**

195

The data presented in figures 10.10 through 10.12 show the following trends:

- As the steel ratio, ρ or ρ_{eq}, increased, ε_{stl} decreased. A larger decrease was observed between smaller steel ratios, as is evident in Figure 10.10 (a). This trend was anticipated because the earthquake analyses revealed that the maximum displacement decreased as the steel ratio increased.

- As the axial-load ratio, $P_{col}/(f_c^{'}A_g)$, increased, ε_{stl} also increased. Figure 10.10 (a) illustrates this observation. Although a few of the lines cross one another for the reinforced concrete frames, such as in Figure 10.10 (b), this is solely a result of the frames that had convergence problems. This observation was also expected because the earthquake analyses showed that as the axial-load ratio increased, and in turn the mass on the frame increased, the maximum displacement increased. With an increased maximum displacement during earthquake analysis, it was expected that the maximum strain would increase.

- For the hybrid frames, the ε_{stl} was not significantly influenced by L_{col}/D_{col} . This is evident by comparing between figures 10.12 (a) and (e). For the reinforced concrete frames, Figure 10.10 shows that as L_{col}/D_{col} increased, the maximum strain decreased.

- For the hybrid frames, the maximum steel strain was essentially independent of the re-centering ratio, λ_{rc} . This is reflected in figures 10.11 and 10.12.

- A comparison of the mean displacement ductility of the hybrid frame with an axial-load ratio equal to 0.05 (Figure 10.11) and that of the reinforced concrete frame with the same axial-load ratio (Figure 10.10)shows that the two types of frames had similar mean maximum steel strains, although the reinforced concrete

196

frames had a slightly larger ε_{stl} than the hybrid frames. These figures also show

that the mean plus one standard deviation was significantly larger for the

reinforced concrete frames than for the hybrid frames. The figures indicate that

bar rupture could be a serious concern for the reinforced concrete frames when

exposed to a 2 percent in 50 event, especially for higher axial-load ratios. The

partial debonding of the mild reinforcing steel in the hybrid frames explains the

relatively lower ε_{stl} found in the hybrid frames.

- The mean plus one standard deviation was approximately 25 percent larger than
  the mean values for the reinforced concrete frames, as is evident in Figure 10.10.
  The mean plus one standard deviation was essentially the same as the mean
  values for the hybrid frames.

- The ε_{stl} values were approximately 30 to 40 percent smaller for the 10 percent in
  50 ground motions for the reinforced concrete frames. For the hybrid frames, the
  ε_{stl} values were approximately 50 to 60 percent smaller for the 10 percent in 50
  ground motions. Figures D.10 through D.12 in Appendix D illustrate the ε_{stl}
  values for the 10 percent in 50 ground motions .

10.5 PROXIMITY TO ULTIMATE DISPLACEMENT

No unique definition exists for the ultimate limit state because typically some

amount of residual strength remains in a well-confined frame, even after a significant loss

of strength occurs during a pushover analysis (Preistley et al. 1996). For this study, the

displacement at the ultimate limit state, Δ_{ult} , was defined as the state that existed when

the first of the following two events occurred:

1. The frame's lateral resistance decreased to zero. Even though $P-\Delta$ effects were included in the analyses, this complete loss of lateral resistance only occurred in a few frames because of the presence of strain hardening and lack of fracture in the reinforcing steel.

2. The frame's horizontal displacement equaled 24.0 in. The maximum displacement imposed on the frames during the pushover analyses was 24.0 in. It was assumed that beyond this displacement, geometric issues, such as unseating of the girders, would control.

The ratio of the maximum displacement and the ultimate displacement provides a means of understanding how closely the frame came to reaching its ultimate limit state, which in turn indicates significant structural damage and potential safety concerns. Complete results for $\Delta_{max}/\Delta_{ult}$ are provided in the tables of Appendix D (tables D.13 through D.15). For the 10 percent in 50 ground motions, the ratio $\Delta_{max}/\Delta_{ult}$ ranged as follows:

- o Reinforced concrete frames
  - Minimum: 0.04 (frame 6.030.05, ground motion 10-3)
  - Maximum: 0.45 (frame 7.005.15, ground motion 10-3)
- o Hybrid frames with axial-load ratio equal to 0.05
  - Minimum: 0.04 (numerous frames and ground motions)
  - Maximum: 0.19 (numerous frames and ground motions)
- o Hybrid frames with axial-load ratio equal to 0.10
  - Minimum: 0.04 (numerous frames and ground motions)
  - Maximum: 0.27 (frame 7.010.100, ground motion 10-3)

  $\Delta_{max}/\Delta_{ult}$ ranged as follows for the 2 percent in 50 ground motions:

- o Reinforced concrete frames
  - Minimum: 0.08 (frame 5.030.05, ground motion 2-3)

- Maximum: 1.19 (frame 7.005.10, ground motion 2-3), this was the only value above 1.00 and indicates that this frame exceeded its ultimate limit state as defined in this section.
  - Hybrid frames with axial-load ratio equal to 0.05
    - Minimum: 0.07 (numerous frames and ground motions)
    - Maximum: 0.72 (frame 7.005.100, ground motion 2-3)
  - Hybrid frames with axial-load ratio equal to 0.10
    - Minimum: 0.15 (numerous frames and ground motions)
    - Maximum: 0.84 (frame 7.010.100, ground motion 2-5)

For the reinforced concrete frames, the mean values for $\Delta_{max}/\Delta_{ult}$ and the mean plus one standard deviation are presented in Figure 10.13 for the 2 percent in 50 ground motions. The same information is presented in figures 10.14 and 10.15 for the hybrid frames with axial-load ratio equal to 0.05 and 0.10, respectively. Similar data are presented in figures D.13 through D.15 in Appendix D for the 10 percent in 50 ground motions.
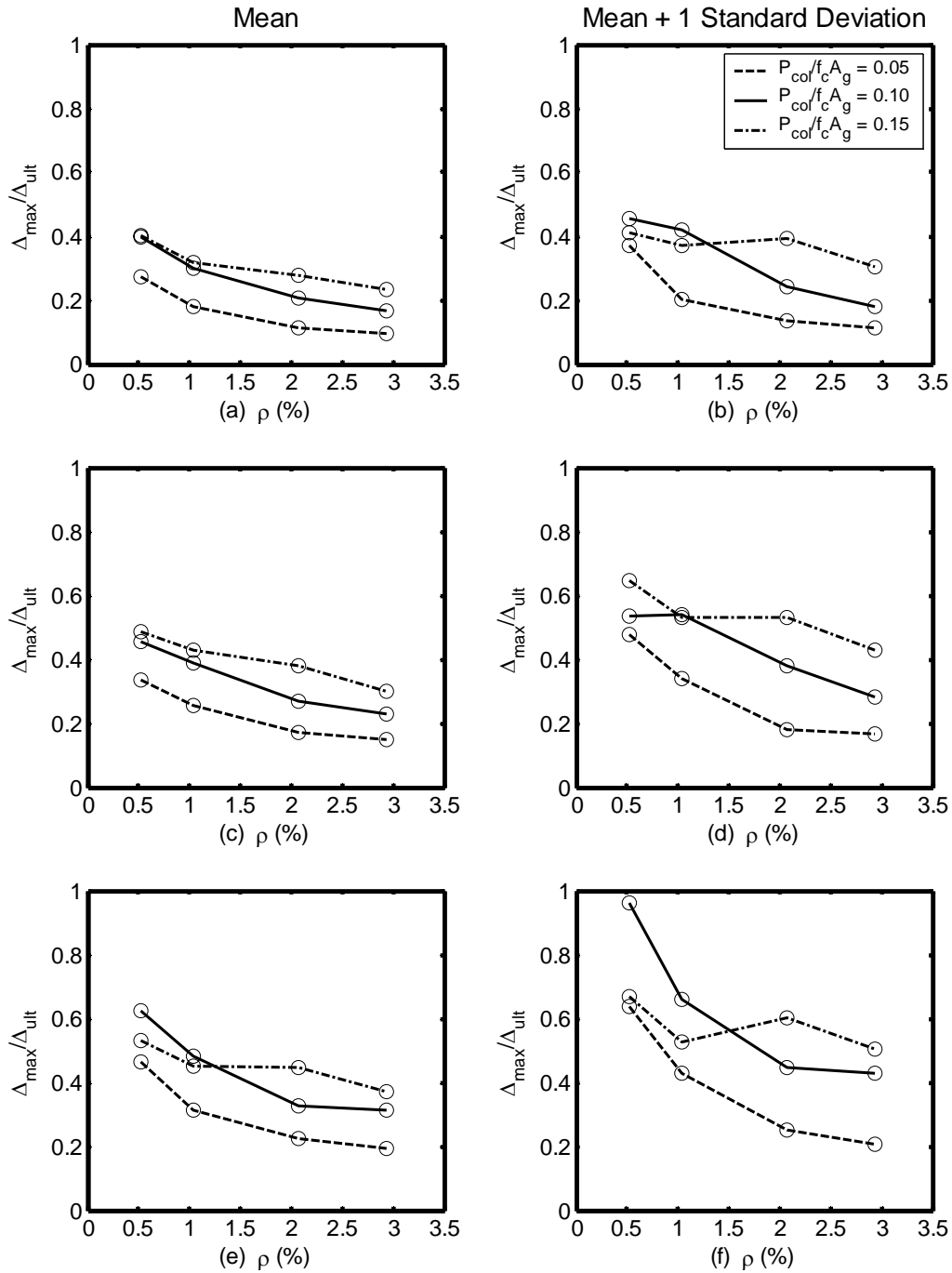
Figure 10.13: $\Delta_{max}/\Delta_{ult}$, **2 Percent in 50, Reinforced Concrete Frames**
(a) and (b) L_{col}/D_{col} **= 5, (c) and (d)** L_{col}/D_{col} **= 6, and (e) and (f)** L_{col}/D_{col} **=7**
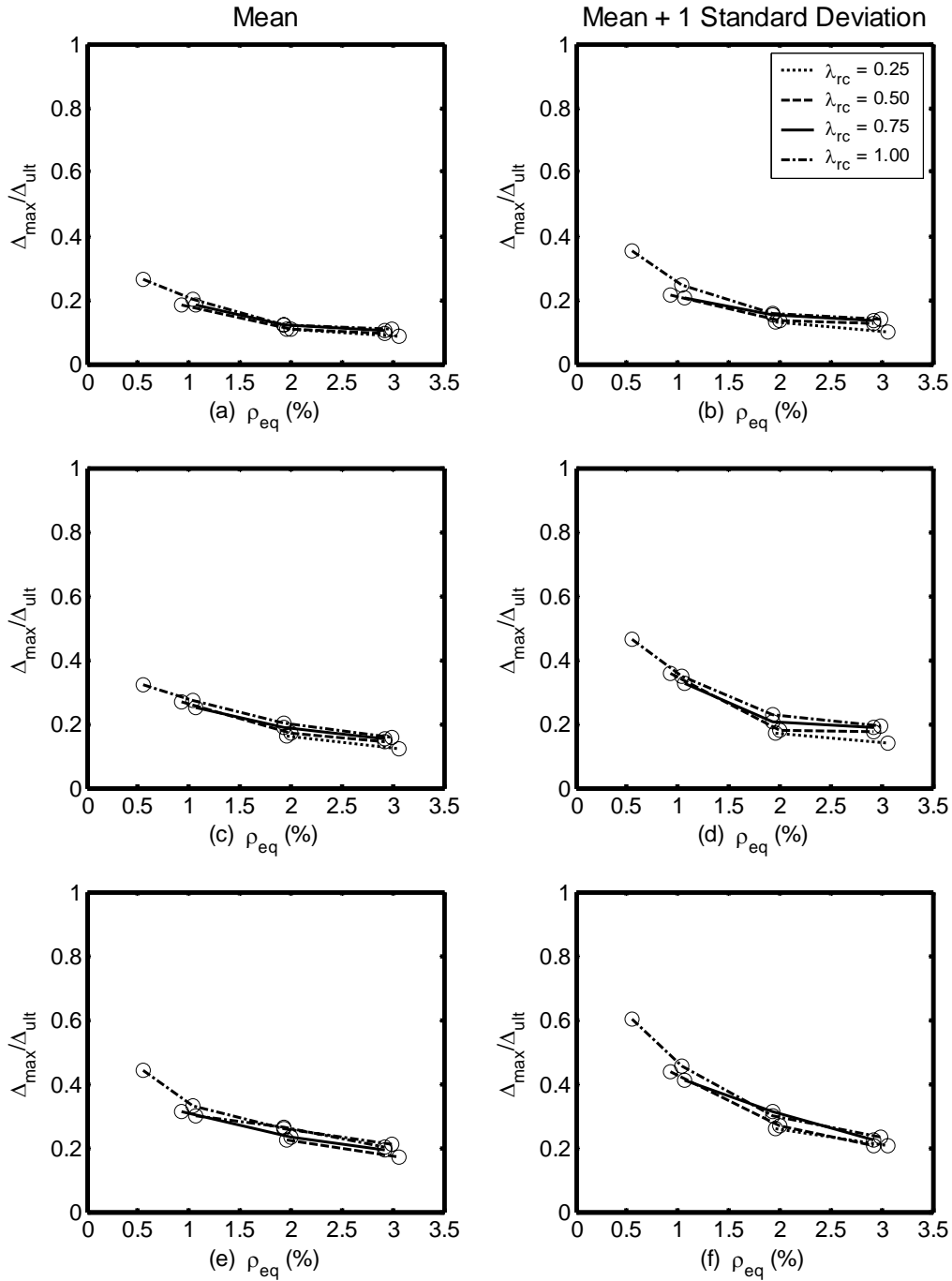
Figure 10.14: $\Delta_{\max}/\Delta_{ult}$, **2 Percent in 50, Hybrid Frames,** $P_{col}/(f_c' A_g) = 0.05$ **(a) and (b)** $L_{col}/D_{col} = 5$, **(c) and (d)** $L_{col}/D_{col} = 6$, **and (e) and (f)** $L_{col}/D_{col} = 7$
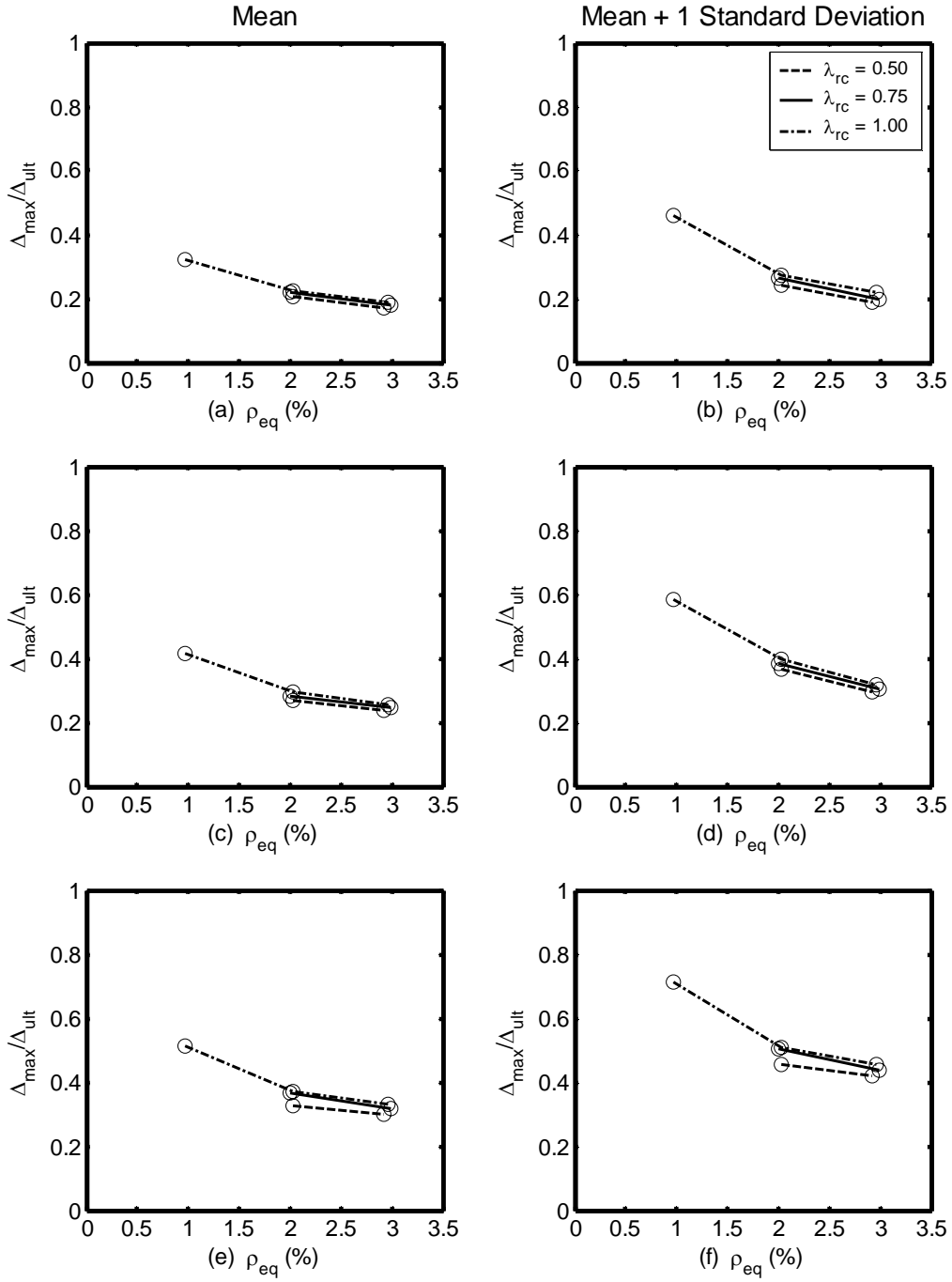
Figure 10.15: $\Delta_{max}/\Delta_{ult}$, **2 Percent in 50, Hybrid Frames,** $P_{col}/(f_c^{'}A_g) = 0.10$ **(a) and (b)** $L_{col}/D_{col} = 5$, **(c) and (d)** $L_{col}/D_{col} = 6$, **and (e) and (f)** $L_{col}/D_{col} = 7$

From figures 10.13 through 10.15 the following observations were made. Because the ultimate displacement equaled 24 in. for all the frames except for three reinforced concrete frames, these observations essentially reflect the trends and observations for the maximum displacements presented in chapters 7 and 9.

- As the steel ratio, ρ or ρ_{eq}, increased, $\Delta_{max}/\Delta_{ult}$ decreased. The results also suggest that a larger decrease occurred between smaller steel ratios, as is evident in Figure 10.14 (e). This trend is consistent with the decreased maximum displacement encountered during the earthquake analyses as the steel ratio increased.

- As the axial-load ratio, $P_{col}/(f_c'A_g)$, increased, $\Delta_{max}/\Delta_{ult}$ also increased. This observation is illustrated in Figure 10.13 (a). Although a few of the lines cross one another for the reinforced concrete frames, such as in Figure 10.13 (e), this is a result of the mean values calculated without the contribution from frames that had convergence problems. This trend was anticipated because the earthquake analyses found that as the axial-load ratio increased, and in turn the mass on the frame increased, the maximum displacement increased.

- As L_{col}/D_{col} increased, $\Delta_{max}/\Delta_{ult}$ also increased. This is evident in each of the figures. The earthquake analyses showed that as L_{col}/D_{col} increased the maximum displacement also increased, which corresponds to the trend observed for $\Delta_{max}/\Delta_{ult}$.

- For the hybrid frames, $\Delta_{max}/\Delta_{ult}$ was nearly independent of the re-centering ratio, λ_{rc}, which is the same trend observed in maximum displacement, as described in

chapters 7 and 9. This is reflected in figures 10.14 and 10.15.

- A comparison of the mean displacement ductility of the hybrid frame with an axial-load ratio equal to 0.05 (Figure 10.14) and that of the reinforced concrete frame with the same axial-load ratio and longitudinal reinforcement ratio (Figure 10.13) shows that the two types of frames had almost identical $\Delta_{max}/\Delta_{ult}$ values.

- The mean plus one standard deviation was approximately 40 percent larger than the mean values, as reflected in the figures.

- The $\Delta_{max}/\Delta_{ult}$ values for the 10 percent in 50 ground motions were approximately half those for the 2 percent in 50 ground motions. Figures illustrating the $\Delta_{max}/\Delta_{ult}$ values for the 10 percent in 50 ground motions can be found in Appendix D (figures D.13 through D.15).

10.6 SENSITIVITY OF PERFORMANCE TO FRAME PARAMETERS

This section summarizes the sensitivity of the response and performance evaluation quantities, discussed in chapters 6 through 10, to variation of the frame parameters. The responses of the reinforced concrete and hybrid frames were computed for the following baseline values:

- column aspect ratio, $L_{col}/D_{col} = 6$
- longitudinal reinforcement ratio, $\rho = 0.01$ (ρ_{eq} for hybrid frames)
- axial-load ratio, $P_{col}/(f_c' A_g) = 0.05$
- re-centering ratio, $\lambda_{rc} = 1.00$ (for hybrid frames).

Table 10.1 summarizes the results of the response and performance evaluation quantities for the reinforced concrete and hybrid frames with these baseline values. This table also summarizes the percentage of change between the two types of frames. The

response quantities calculated during earthquake analyses are shown in the table for the 2 percent in 50 ground motions. As shown in Table 10.1, the change from a reinforced concrete frame to a hybrid frame most significantly affected the displacement ductility demand, Δ_{max}/Δ_y. The stiffness ratio, Δ_y/L_{col}, probability of the onset of spalling, probability of the onset of bar buckling, and the maximum strain in the longitudinal reinforcing steel were affected moderately by the change between frame type. The maximum force, Δ_{max}/L_{col}, and $\Delta_{max}/\Delta_{ult}$ remained essentially unchanged as the frame type was changed.

Table 10.1: Comparison of Performance of Reinforced Concrete and Hybrid Frames

	Reinforced Concrete Frame	Hybrid Frame	Percent Difference
$\dfrac{k_{cracked}}{k_{uncracked}}$	0.276	0.369	34%
$\dfrac{\Delta_y}{L_{col}}$	0.58%	0.41%	29%
F_{max}	429 kips	382 kips	11%
$\dfrac{\Delta_{max}}{L_{col}}$	2.14%	2.26%	6%
$\dfrac{\Delta_{max}}{\Delta_y}$	3.69	5.51	49%
P_{spall}	0.33	0.40	21%
P_{bb}	0.0030	0.0037	23%
ε_{stl}	0.026	0.020	23%
$\dfrac{\Delta_{max}}{\Delta_{ult}}$	0.26	0.27	4%

To investigate the sensitivity of the calculated responses to the frame parameters, individual parameters of the baseline frame were varied while the remaining parameters were held fixed at the values selected for the baseline frame. The parameters were varied as follows:

- column aspect ratio, L_{col}/D_{col}, from 5 to 7
- longitudinal reinforcement ratio, ρ or ρ_{eq}, from 0.005 to 0.020
- axial-load ratio, $P_{col}/(f_c'A_g)$, from 0.05 to 0.10
- re-centering ratio, λ_{rc}, from 0.50 to 1.00.

Table 10.2 presents the percentage of increase or decrease in the response quantities as each individual parameter was varied for the reinforced concrete frames. Table 10.3 contains the same information for the hybrid frames. The response quantities calculated during earthquake analyses are shown in tables 10.2 and 10.3 for the 2 percent in 50 ground motions. The values contained in these tables were calculated from the tables included in chapters 6 through 10 and their associated appendices.

As shown in tables 10.2 and 10.3, varying L_{col}/D_{col} from 5 to 7 had a significant effect on P_{bb} and $\Delta_{max}/\Delta_{ult}$. The percentage of change in P_{bb} was large because the values of P_{bb} were small, below 0.01. As L_{col}/D_{col} varied from 5 to 7, a moderate change occurred in Δ_y/L_{col}, F_{max}, Δ_{max}/L_{col}, P_{spall}, and ε_{stl}. Both the stiffness ratio and the displacement ductility demand were essentially independent of L_{col}/D_{col}.

Table 10.2: Sensitivity of Performance, Reinforced Concrete Frames

Parameter	$\dfrac{L_{col}}{D_{col}}$	ρ	$\dfrac{P_{col}}{f'_c A_g}$
Range	5 to 7	0.005 to 0.020	0.05 to 0.10
$\dfrac{k_{cracked}}{k_{uncracked}}$	-2%	+56%	+24%
$\dfrac{\Delta_y}{L_{col}}$	+22%	+40%	-5%
F_{max}	-33%	+168%	+13%
$\dfrac{\Delta_{max}}{L_{col}}$	+25%	-50%	+51%
$\dfrac{\Delta_{max}}{\Delta_y}$	+2%	-63%	+59%
P_{spall}	+40%	-81%	+106%
P_{bb}	+170%	-95%	+1120%
ε_{stl}	-27%	-52%	+46%
$\dfrac{\Delta_{max}}{\Delta_{ult}}$	+72%	-48%	+50%

Table 10.3: Sensitivity of Performance, Hybrid Frames

Parameter	$\dfrac{L_{col}}{D_{col}}$	ρ_{eq}	$\dfrac{P_{col}}{f'_c A_g}$	I_{rc}
Range	5 to 7	0.005 to 0.020	0.05 to 0.10	0.50 to 1.00
$\dfrac{k_{cracked}}{k_{uncracked}}$	-2%	+61%	+13%	+16%
$\dfrac{\Delta_y}{L_{col}}$	+22%	+18%	+5%	-11%
F_{max}	-32%	+106%	+20%	+2%
$\dfrac{\Delta_{max}}{L_{col}}$	+16%	-37%	+53%	+2%
$\dfrac{\Delta_{max}}{\Delta_y}$	-6%	-48%	+46%	+14%
P_{spall}	+11%	-58%	+85%	+8%
P_{bb}	+70%	-90%	+1454%	-5%
ε_{stl}	-18%	-55%	+20%	-9%
$\dfrac{\Delta_{max}}{\Delta_{ult}}$	+65%	-38%	+56%	+1%

As the reinforcing ratio, ρ or ρ_{eq}, varied from 0.005 to 0.020, eight of the nine response or performance evaluation quantities were significantly affected. The only quantity that experienced a moderate change was Δ_y/L_{col} . The results presented in tables 10.2 and 10.3 show that the reinforcing ratio had an important effect on the response of the systems.

As the axial load ratio, $P_{col}/\left(f'_c A_g\right)$, varied from 0.05 to 0.10, Δ_{max}/L_{col} ,

Δ_{max}/Δ_y , P_{spall} , P_{bb} , ε_{stl} , and $\Delta_{max}/\Delta_{ult}$ were all significantly affected. The stiffness

ratio was moderately affected as the axial-load ratio varied, whereas Δ_y/L_{col} and F_{max}

were effectively independent of the change in axial-load ratio.

As shown in Table 10.3, as the re-centering ratio, λ_{rc}, varied from 0.50 to 1.00,

little change occurred in the response or performance evaluation quantities.

CHAPTER 11
SUMMARY, CONCLUSIONS, AND RECOMMENDATIONS

11.1 SUMMARY

The country's aging transportation infrastructure is subjected to ever-increasing traffic volumes, and it must be continuously renewed and improved. Today, construction operations that follow traditional practices lead to unacceptable traffic congestion, pollution, and economic loss (Shahawy 2003).

The Federal Highway Administration (FHWA), the American Association of State Highway and Transportation Officials (AASHTO), and many state departments of transportation have been working to accelerate the construction process and reduce the negative impacts of transportation construction on the traveling public.

The focus of this study was on the feasibility of using precast concrete pier systems for the rapid construction of bridges in seismic regions. Potential benefits include reduced traffic impacts caused by transportation construction, improved work zone safety, reduced environmental impacts, improved constructability, increased quality, and lowered life-cycle costs, providing benefits for bridge owners, designers, contractors, and the traveling public. A review of previous systems and applications of precast concrete components used for rapid bridge construction is summarized in Chapter 2 and in Hieber et al. (2004). The study described in this report focused on the development and evaluation of precast concrete bridge pier systems for use in the seismically active region of Western Washington State.

This study evaluated the potential of two precast concrete bridge pier systems; the first was a precast concrete emulation of a cast-in-place, reinforced concrete frame, and

the second was a precast hybrid frame (Chapter 3). Both systems consisted of a precast concrete cap-beam and precast concrete columns supported on cast-in-place concrete foundations. Components in the reinforced concrete system were connected with mild steel deformed bars grouted or cast into ducts or openings. In the hybrid system, the components were connected with deformed bars grouted or cast into ducts or openings, as well as with unbonded prestressing strand. The prestressing strand was anchored in the foundation, threaded through a duct located in the center of the column's cross section, and attached in the column-to-cap-beam connection. The hybrid system offered the additional benefit of reducing the residual displacement by re-centering the system after a seismic event.

The object-oriented analysis framework OpenSees (2000) was used to create nonlinear finite element models representing individual precast concrete bridge piers (Chapter 4). A parametric study, involving pushover analyses (chapters 6 and 8) and earthquake analyses (chapters 7 and 9) of 36 reinforced concrete frames and 57 hybrid frames, was conducted to quantify response characteristics and investigate the global seismic response of various configurations of the proposed systems. The following parameters were varied during the study:

- column aspect ratio, L_{col}/D_{col}
- longitudinal reinforcement ratio, $\rho = A_s/A_g$ (reinforced concrete frames)
- equivalent reinforcement ratio, $\rho_{eq} = \left(\rho_s f_y + \rho_p f_{py}\right)/f_y$ (hybrid frames)
- axial-load ratio, $P_{col}/(f_c' A_g)$
- re-centering ratio, $\lambda_{rc} = \left(P_{col} + A_p f_{p0}\right)/A_s f_y$ (hybrid frames).

During the earthquake analyses, each of the 36 reinforced concrete frames and 57 hybrid frames was subjected to five ground motions representing events with a 10 percent

211

probability of exceedance in 50 years (10 percent in 50) and five ground motions

representing events with a 2 percent probability of exceedance in 50 years (2 percent in

50), resulting in a total of 930 earthquake analyses performed during the parametric

study. The development of the ground motions is described in Chapter 5.

The results of the parametric study were used to develop a method for estimating

the response of the precast systems on the basis of an elastic design displacement

response spectrum (sections 7.5 and 9.5). In addition, the following performance

measures were used to evaluate the systems (Chapter 10):

- o displacement ductility demand, μ_Δ
- o probability of cover concrete spalling, P_{spall}
- o probability of bar buckling, P_{bb}
- o maximum strain in longitudinal mild steel, ε_{stl} (related to bar fracture)
- o proximity to ultimate limit state, $\Delta_{max}/\Delta_{ult}$.

11.2 CONCLUSIONS FROM SYSTEM DEVELOPMENT

To be considered for use, any alternative to the current cast-in-place concrete pier

system would need to possess numerous characteristics. Through an intensive literature

review and numerous discussions with WSDOT engineers, local precast concrete

producers, and local contractors, important attributes were identified. The following is a

list of the essential qualities of a feasible precast concrete bridge pier system for use in

Western Washington State.

- • Connections are central to the seismic performance and constructability of precast

    systems. Connections should be carefully designed, detailed, and constructed to

    ensure adequate performance of the system. Limiting the required number of

212

connections is key to reducing the on-site construction effort. Connections between components should provide acceptable construction tolerances.

- Fabrication, transportation, and erection weight limits, as well as length limits, should be considered. The WSDOT Bridge Design Manual (WSDOT 2002) suggests 180,000 lbs.

- Reducing the required quantity of cast-in-place concrete and formwork significantly increases the benefit provided by a potential system.

- The system should be versatile to allow its use on a variety of bridge geometries and configurations.

- The precast concrete system should be economically competitive with its cast-in-place counterpart, but the comparison should include the value of time.

- The system should be durable to ensure quality construction and reduce life-cycle costs.

11.3 CONCLUSIONS FROM THE PUSHOVER ANALYSES

The pushover analyses summarized in chapters 6 and 8, as well as in the tables of Section 10.6, revealed the following:

- As described in Section 10.6, the difference between the reinforced concrete frames and hybrid frames was around 30 percent for the stiffness ratio and Δ_y/L_{col}. The maximum force, F_{max}, was essentially independent of frame type.

- As L_{col}/D_{col} varied, a moderate change occurred in Δ_y/L_{col} and F_{max}. The stiffness ratio was essentially independent of L_{col}/D_{col}.

- As the reinforcing ratio, ρ or ρ_{eq}, varied, both the stiffness ratio and F_{max} were significantly affected. The only quantity that experienced a moderate change was Δ_y/L_{col}.

- The stiffness ratio was moderately affected as the axial-load ratio, $P_{col}/(f_c'A_g)$, varied whereas Δ_y/L_{col} and F_{max} were effectively independent of the change in axial-load ratio.

- For the hybrid frames, as the re-centering ratio, λ_{rc}, varied, little change occurred in the pushover response quantities.

11.4 CONCLUSIONS FROM THE EARTHQUAKE ANALYSES

The earthquake analyses indicated the following:

- Maximum drift ratio, Δ_{max}/L_{col}, significantly increased as the axial-load ratio, $P_{col}/(f_c'A_g)$, increased. The maximum drift ratio increased moderately with the column aspect ratio, L_{col}/D_{col}. An increase in longitudinal reinforcement ratio, ρ or ρ_{eq}, resulted in a significant decrease in Δ_{max}/L_{col}. These three behaviors are consistent with results from an elastic single-degree-of-freedom system. The first implies a larger seismic mass and the second a lower stiffness, both of which lead to a longer period and larger displacement. An increased ρ causes an increase in the cracked stiffness and a consequent reduction in peak displacement. The maximum drift ratio was nearly independent of the re-centering ratio, λ_{rc}.

- As a consequence of residual displacements encountered during the study, it was concluded that the viscous damping ratio and the strain hardening ratio

incorporated in the nonlinear finite element model significantly affected the residual displacements. Although detailed results were not presented in the study, in general it was found that as λ_{rc} increased, the residual displacement decreased. This reinforces conclusions drawn by other studies related to hybrid frames (Sakai and Mahin 2004 and Kwan and Billington 2003(b)).

A practical method was developed for estimating maximum seismic displacements on the basis of the cracked section properties of the columns, the elastic design displacement response spectrum, S_d, and base-shear strength ratio. The maximum displacement of the proposed systems, with no viscous damping included, was predicted well with the following relationship:

$$\Delta_{predicted} = \begin{cases} \left[\alpha(\eta - X) + \beta\right]S_d & \text{for } F_{con004}/S_a m \le \eta \\ \beta S_d & \text{for } F_{con004}/S_a m > \eta \end{cases} \qquad (11.1)$$

where α = absolute value slope of the linear portion, taken as 2.0.

η = value of $F_{con004}/S_a m$ corresponding to the transition from a linear relationship to a constant value. This value was taken as 0.04.

X = value of $F_{con004}/S_a m$

β = value for the constant portion, taken as 1.3.

S_d = spectral displacement

For the reinforced concrete frames, use of Equation 11.1 with $\alpha = 2.0$, $\beta = 1.3$, and $\eta = 0.4$ for each earthquake analysis produced a ratio of the maximum displacement computed with OpenSees to the predicted displacement computed with Equation 11.1, $\Delta_{max}/\Delta_{predicted}$, with a mean of 0.98 and standard deviation of 0.25. For the hybrid

frames, use of Equation 11.1 for each earthquake analysis resulted in a mean of 1.05 and standard deviation of 0.26.

11.5 CONCLUSIONS FROM THE SEISMIC PERFORMANCE EVALUATION

With the results obtained from the earthquake analyses, a performance evaluation was carried out to estimate the level of expected damage.

For the 10 percent in 50 ground motions, this study found moderate probabilities of the onset of cover concrete spalling, minimal probabilities of the onset of bar buckling, and very low values of maximum strain in the longitudinal reinforcement. For example, at an axial-load ratio of 0.10 and longitudinal reinforcement ratio of 0.01, the mean probability of cover concrete spalling occurring was 0.12 for the reinforced concrete frames and 0.10 for the hybrid frames. The mean probability of bar buckling occurring was 0.0005 for the reinforced concrete and hybrid frames. For the same conditions, the mean maximum strain in the longitudinal mild steel was 0.015 for the reinforced concrete frames and 0.012 for the hybrid frames.

For the 2 percent in 50 ground motions, this study found significant probabilities of cover concrete spalling occurring, minimal probabilities of bar buckling occurring, and moderate maximum strains in the longitudinal reinforcement. For example, at an axial-load ratio of 0.10 and longitudinal reinforcement ratio of 0.01, the mean probability of cover concrete spalling occurring was 0.68 for the reinforced concrete frames and 0.73 for the hybrid frames. The mean probability of bar buckling occurring was 0.04 for the reinforced concrete and hybrid frames. For this same axial-load ratio and reinforcement ratio, the mean maximum strain in the longitudinal mild steel was 0.042 for the reinforced concrete frames and 0.025 for the hybrid frames.

The performance evaluation described in Chapter 10 indicated the following:

- The displacement ductility demand was influenced by the steel ratio, ρ or ρ_{eq}, and decreased as the steel ratio increased. The displacement ductility demand significantly increased with the axial-load ratio, $P_{col}/(f_c'A_g)$ and was effectively independent of the column aspect ratio, L_{col}/D_{col}. For the hybrid frames, as the re-centering ratio, λ_{rc}, increased, the displacement ductility was essentially unchanged. The reinforced concrete frames had slightly larger displacement ductility demands than the hybrid frames.

- The probability of cover concrete spalling decreased significantly as the steel ratio, ρ or ρ_{eq}, increased and increased significantly as the axial-load ratio, $P_{col}/(f_c'A_g)$, increased. The column aspect ratio, L_{col}/D_{col}, had a moderate influence on the probability of the onset of spalling, whereas the re-centering ratio, λ_{rc}, had little influence. For the same axial-load ratio and reinforcement ratio, the reinforced concrete frames and hybrid frames had similar probabilities of the onset of cover concrete spalling.

- For the 10 percent in 50 and the 2 percent in 50 ground motions, the likelihood of bar buckling occurring was essentially nonexistent for all frames studied, except for the reinforced concrete frames with low longitudinal reinforcement ratios.

- The average maximum strain in the longitudinal steel only exceeded 0.05 in some of the reinforced concrete frames subjected to the 2 percent in 50 ground motions. The average maximum strain significantly decreased as the steel ratio, ρ or ρ_{eq}, increased and significantly increased as the axial-load ratio, $P_{col}/(f_c'A_g)$,

217

increased. The column aspect ratio, L_{col}/D_{col} , had a moderate effect on the

maximum strain, whereas the re-centering ratio, λ_{rc} , had little influence on the

maximum strain in the longitudinal steel. The maximum strain was generally

smaller for the hybrid frame in comparison to a reinforced concrete frame with

the same axial-load ratio and reinforcing ratio.

- The ratio of maximum displacement to the ultimate displacement, $\Delta_{max}/\Delta_{ult}$,

  significantly increased as the axial-load ratio, $P_{col}/(f_c' A_g)$, increased. The ratio

  also significantly increased with the column aspect ratio, L_{col}/D_{col} . An increase

  in longitudinal reinforcement ratio, ρ or ρ_{eq} , resulted in a moderate decrease in

  $\Delta_{max}/\Delta_{ult}$. The ratio was nearly independent of the re-centering ratio, λ_{rc} . The

  ratio of maximum displacement to the ultimate displacement remained effectively

  unchanged between the two types of frames with the same axial-load ratio and

  reinforcing ratio.

11.6 RECOMMENDATIONS FOR FURTHER STUDY

To further investigate the viability of the proposed precast concrete bridge pier

systems as alternatives to their cast-in-place counterparts, the following topics are

suggested for additional research:

- An experimental study should be conducted to verify the nonlinear finite element

  models developed during this study. Verification of the results obtained during

  this study was difficult because of the lack of experimental data relating to the

  systems. Data gained from experimental tests would provide additional

  confidence in the results obtained during nonlinear finite element modeling.

218

- Further consideration should be given to estimating more accurate residual displacements resulting from the earthquake analyses. This would further illuminate the significant benefit expected from the re-centering ability of the hybrid system.

- The behavior of the connection regions should be further examined. Local force transfer in these connection regions should be explored to ensure adequate performance. Strut and tie models are suitable candidates for the analysis. Insight acquired during such studies should be included in an improved nonlinear finite element model.

- The constructability of the systems should be scrutinized further, including development of detailed construction procedures and methods. A means of leveling, supporting, and bracing the columns before curing of the footing-to-column connection concrete should be addressed. A method of supporting the precast cap-beam before the curing of the column-to-cap-beam connection concrete should be taken into account.

- A detailed investigation of the constructability of the connection regions is needed. As part of an experimental study, constructability could be determined during construction of a specimen. The development of standard connections could result from such a study.

- Consideration should be given to the repair of the systems, should they be damaged in a seismic event. This is especially true for the hybrid frame because damage to, or corrosion of, the prestressing strand could result in the need for difficult and most likely destructive rehabilitation methods.

To broaden the applicability of the proposed bridge pier systems, the following areas could be considered:

- Near-fault earthquakes should be considered. The ground motion suite developed for this study did not include near-fault motions. This would provide additional understanding about the response of the proposed systems to seismic hazards.

- During this study only two-column bridge piers were considered. Studies could be conducted to verify the concepts presented in this document for other typical pier geometries, such as single-column and three-column piers.

- This study considered the isolated response of a single bridge pier. Future studies could determine the effect of these piers on global bridge behavior.

- Larger scale, hollow pier structures could also be taken into account.

ACKNOWLEDGMENTS

REFERENCES

AASHTO LRFD Bridge Design Specifications: Customary U.S. Units, American
Association of State Highway and Transportation Officials, Washington D.C., 1998.

American Heritage Dictionary of the English Language: Fourth Edition, Houghton
Mifflin Company, Massachusetts, 2000. <http://www.bartleby.com/61/>

Berry, M.P., "Estimating Flexural Damage in Reinforced Concrete Columns,"
Master's Thesis, Department of Civil and Environmental Engineering, University of
Washington, 2003.

Berry, M.P. and M.O. Eberhard, *Performance Models for Flexural Damage in
Reinforced Concrete Columns (PEER Report 2003/18)*, Pacific Earthquake
Engineering Research Center, University of California, Berkeley, 2004.

Billington, S.L, R.W. Barnes, and J.E. Breen, *Project Summary Report 1410-2F: A
Precast Substructure Design for Standard Bridge Systems*, Center for Transportation
Research, The University of Texas at Austin, 1998.

Billington, S.L., R.W. Barnes, and J.E. Breen, "A Precast Segmental Substructure System
for Standard Bridges," *PCI Journal*, Vol. 44, No. 4, August 1999, pp. 56-73.

Billington, S.L., R.W. Barnes, and J.E. Breen, "Alternate Substructure Systems for
Standard Highway Bridges," *ASCE Journal of Bridge Engineering*, Vol. 6, No. 2,
March/April 2001, pp. 87-94.

Billington, S.L. and J.K. Yoon, "Cyclic Response of Unbonded Post-Tensioned Precast
Columns with Ductile Fiber-Reinforced Concrete," *ASCE Journal of Bridge
Engineering*, Vol. 9, No. 4, July 2004, pp. 353-363.

Blakeley, R.W.G. and R. Park, "Seismic Resistance of Prestressed Concrete Beam-
Column Assemblies," *ACI Journal*, Vol. 68, No. 9, September 1971, pp. 677-692.

Camarillo, H.R., "Evaluation of Shear Strength Methodologies for Reinforced Concrete
Columns," Master's Thesis, Department of Civil and Environmental Engineering,
University of Washington, 2003.

Chopra, A.K., *Dynamics of Structures: Theory and Applications to Earthquake
Engineering*, Prentice Hall, New Jersey, 2001.

Cheok, G.S., W.C. Stone, and S.K. Kunnath, "Seismic Response of Precast Concrete
Frames with Hybrid Connections," *ACI Structural Journal*, Vol. 95, No. 5,
September/October 1998, pp. 527-539.

Coleman, J. and E. Spacone, "Localization Issues in Force-Based Frame Elements," *ASCE Journal of Structural Engineering,* Vol. 127, No. 11, November 2001, pp. 1257-1265.

El-Sheikh, M.T., R. Sause, S. Pessiki, and L. Lu, "Seismic Behavior and Design of Unbonded Post-Tensioned Precast Concrete Frames," *PCI Journal*, Vol. 44, No. 3, May/June 1999, pp. 54-71.

Fenves, G.L., F. McKenna, M.H. Scott, and Y. Takahashi, "An Object-Oriented Software Environment for Collaborative Network Simulation," *Proceedings, 13th World Conference on Earthquake Engineering*, Vancouver, B.C., 2004.

FHWA Accelerated Bridge Construction Technologies, Federal Highway Administration, U.S. Department of Transportation, Washington DC, 2004. <http://www.fhwa.dot.gov/bridge/accelerated/>

Freeby, G., R. Medlock, and S. Slage, "Prefabricated Bridge Innovations," *Proceedings, Second New York City Bridge Conference*, New York City, New York, 2003.

French, C.W., O. Amu, and C. Tarzikhan, "Connection Between Precast Elements – Failure Outside Connection Region," *ASCE Journal of Structural Engineering*, Vol. 115, No. 2, February 1989(a), pp. 316-340.

French, C.W., M. Hafner, and V. Jayshankar, "Connections Between Precast Elements – Failure Within Connection Region," *ASCE Journal of Structural Engineering*, Vol. 115, No. 12, December 1989(b), pp. 3171-3192.

Haldar, A. and S. Mahadevan, *Probability, Reliability and Statistical Methods in Engineering Design*, John Wiley & Sons, Inc., New York, 2000.

Hewes J.T. and M.J.N. Priestly, *Proceedings, Sixth CALTRANS Seismic Research Workshop*, Division of Engineering Services, California Department of Transportation, Sacramento, CA, 2001.

Hieber, D.G., "Precast Concrete Pier Systems for Rapid Construction of Bridges in Seismic Regions," Master's Thesis, Department of Civil and Environmental Engineering, University of Washington, 2005.

Hieber, D.G., J.M. Wacker, M.O. Eberhard, and J.F. Stanton, *State-of-the-Art Report on Precast Concrete Systems for Rapid Construction of Bridges*, Washington State Transportation Center, University of Washington, 2004.

Hognestad, E., *A Study of Combined Bending and Axial Load in Reinforced Concrete Members*, *Bulletin 399*, University of Illinois, Urbana, Illinois, 1951.

Jonsson, R., "Direct Displacement Based Design of Seismic Moment Resisting Concrete Frames," Master's Thesis, Department of Civil and Environmental Engineering, University of Washington, 2002.

Karsan, I.D. and J.O. Jirsa, "Behavior of Concrete Under Compressive Loading," *ASCE Journal of the Structural Division*, Vol. 95, No. ST12, December 1969, pp. 2543-2563.

Kawashima, K., G.A. MacRae, J. Hoshikuma, and K. Nagaya, "Residual Displacement Response Spectrum," *ASCE Journal of Structural Engineering*, Vol. 124, No. 5, May 1998, pp. 523-530.

Kent, D.C. and R. Park, "Flexural Members with Confined Concrete," *ASCE Journal of the Structural Division*, Vol. 97, No. ST7, July 1971, pp. 1969-1990.

Kwan, W. and S.L. Billington, "Unbonded Posttensioned Concrete Bridge Piers. I: Monotonic and Cyclic Analyses," *ASCE Journal of Bridge Engineering*, Vol. 8, No. 2, March/April 2003(a), pp. 92-101.

Kwan, W. and S.L. Billington, "Unbonded Posttensioned Concrete Bridge Piers. II: Seismic Analyses," *ASCE Journal of Bridge Engineering*, Vol. 8, No. 2, March/April 2003(b), pp. 102-111.

Kramer, S.L., *Geotechnical Earthquake Engineering*, Prentice Hall, New Jersey, 1996.

Lehman, D.E. and J.P. Moehle, *Seismic Performance of Well-Confined Concrete Bridge Columns (PEER Report 1998/01)*, Pacific Earthquake Engineering Research Center, University of California, Berkeley, 2000.

LoBuono, Armstrong, & Associates, *Development of Precast Bridge Substructures*, Florida Department of Transportation, Tallahassee, FL, 1996.

MacGregor, J.G., *Reinforced Concrete: Mechanics and Design*, Prentice Hall, New Jersey, 1997.

Mander, J.B., M.J.N. Preistley, and R. Park, "Theoretical Stress-Strain Model for Confined Concrete," *ASCE Journal of Structural Engineering*, Vol. 114, No. 8, August 1988, pp. 1804-1826.

Mandawe, J., S. Mislinski, and E.E. Matsumoto, "Reinforcement Anchorage in Grouted Duct Connections for a Precast Bent Cap System in Seismic Regions," *Proceedings, Concrete Bridge Conference*, Nashville, TN, 2002.

Matsumoto, E.E., M.E. Kreger, M.C. Waggoner, and G. Sumen, "Grouted Connection Tests in Development of Precast Bent Cap Systems," *Transportation Research Record 1814*, Transportation Research Board, Washington DC, 2002, pp. 55-64.

Menegotto, M. and P. Pinto, "Method of Analysis for Cyclically Loaded Reinforced Concrete Plane Frames Including Changes in Geometry and Nonelastic Behavior of Elements Under Combined Normal Force and Bending," *IABSE Symposium on the Resistance and Ultimate Deformability of Structures Acted on by Well-Defined Repeated Loads*, Lisbon, 1973.

Nawy, E.G., *Reinforced Concrete: A Fundamental Approach*, Prentice Hall, New Jersey, 2000.

NCHRP 12-49: Comprehensive Specifications for the Seismic Design of Bridges (Third Draft), National Cooperative Highway Research Program, Transportation Research Board, Washington DC, 2001.

NISEE Strong Motion Data Over the Internet, National Information Services for Earthquake Engineering (NISEE), University of California, Berkeley, CA, 2005. <http://nisee.berkeley.edu/data/strong_motion/>

Open System for Earthquake Engineering Simulation (OpenSees), Pacific Earthquake Engineering Research Center (PEER), University of California, Berkeley, CA, 2000. <http://opensees.berkeley.edu/>

Park, R., M.J.N. Priestley, and W.D. Gill, "Ductility of Square-Confined Concrete Columns," *ASCE Journal of the Structural Division*, Vol. 108, No. ST4, April 1982, pp. 929-951.

Paulay, T. and M.J.N. Priestley, *Seismic Design of Reinforced Concrete and Masonry Buildings*, John Wiley & Sons, Inc., New York, 1992.

Popovics, S., "Numerical Approach to the Complete Stress-Strain Curve of Concrete," *Cement and Concrete Research*, Vol. 3, No. 5, September 1973, pp. 583-599.

Priestley, M.J.N, "Overview of PRESSS Research Program," *PCI Journal*, Vol. 36, No. 4, July/August 1991, pp. 50-57.

Priestley, M.J.N. and G.A. MacRae, "Seismic Tests of Precast Beam-to-Column Joint Subassemblages with Unbonded Tendons," *PCI Journal*, Vol. 41, No. 1, January/February 1996, pp. 64-81.

Priestley, M.J.N. and T. Paulay, "What is the Stiffness of Reinforced Concrete Walls?," *Journal of the Structural Engineering Society New Zealand*, Vol. 15, No. 1, April 2002.

Priestley, M.J.N., F. Seible and G.M. Calvi, *Seismic Design and Retrofit of Bridges*, John Wiley & Sons, Inc., New York, 1996.

Priestley, M.J.N. and J.R. Tao, "Seismic Response of Precast Prestressed Concrete Frames with Partially Debonded Tendons," *PCI Journal*, Vol. 38, No. 1, January/February 1993, pp. 64-81.

Ralls, M.L. and B. Tang, "Prefabricated Bridges for Rapid Construction," *Bridge Views Newsletter*, No. 33, May/June 2004. <http://www.cement.org/bridges/>

Ross Bryan Associates, Inc., "Recommended Practice for Precast Concrete Composite Bridge Deck Panels," *PCI Journal*, Vol. 33, No. 2, March/April 1988, pp. 67-109.

Sakai, J. and S.A. Mahin, "Mitigation of Residual Displacements of Circular Reinforced Concrete Bridge Columns," *Proceedings, 13th World Conference on Earthquake Engineering*, Vancouver, B.C., 2004.

Shahawy, M.A., *NCHRP Synthesis 324: Prefabricated Bridge Elements and Systems to Limit Traffic Disruption During Construction*, National Cooperative Highway Research Program, Transportation Research Board, Washington, DC, 2003.

Sprinkel, M.M., *NCHRP Synthesis 119: Prefabricated Bridge Elements and Systems*, National Cooperative Highway Research Program, Transportation Research Board, Washington, DC, 1985.

Stanton, J.F., R.G. Anderson, C.W. Dolan, and D.E. McCleary, *Moment Resistant Connections and Simple Connections*, Prestressed Concrete Institute, Chicago, IL, 1986.

Stanton, J.F. and S.D. Nakaki, *Design Guidelines for Precast Concrete Seismic Structural Systems (PRESSS Report No. 01/03-09)*, University of Washington, 2002.

Stone, W.C., G.S. Cheok, and J.F. Stanton, "Performance of Hybrid Moment-Resisting Precast Beam-Column Concrete Connections Subjected to Cyclic Loading," *ACI Structural Journal*, Vol. 91, No. 2, March/April 1995, pp. 229-249.

USGS National Seismic Hazard Mapping Project, US Geological Survey (USGS), Washington D.C., 2005. <http://eqhazmaps.usgs.gov/>

Wacker, J.M., D.G. Hieber, J.F. Stanton, and M.O. Eberhard, *Design of Precast Concrete Piers for Rapid Bridge Construction in Seismic Regions*, Washington State Transportation Center, University of Washington, 2005.

Wolf, L.M. and M.D. Hyzak, "Design of Precast Bent Cap to Column Connections," *Proceedings, Second Concrete Bridge Conference*, Charlotte, NC, 2004.

Woodward-Clyde Federal Services, *Draft Report: Develop Suites of Time Histories*, SAC Joint Venture Steel Project Phase 2, Pasadena, CA, 1997. <http://nisee.berkeley.edu/data/strong_motion/sacsteel/>

WSDOT Bridge and Structures Plans: State Route 18 over State Route 516, Washington State Department of Transportation, Olympia, WA, 1996.

WSDOT Bridge Design Manual (M23-50), Washington State Department of Transportation, Olympia, WA, 2002(a). <http://www.wsdot.wa.gov/eesc/bridge/bdm/>

WSDOT Design Manual (M22-01), Washington State Department of Transportation, Olympia, WA, 2002(b). <http://www.wsdot.wa.gov/fasc/EngineeringPublications/>

WSDOT Bridge Standard Drawings, Washington State Department of Transportation, Olympia, WA, 2002(c). <http://www.wsdot.wa.gov/eesc/bridge/drawings/>

Washington State Department of Transportation (WSDOT), Personal Communication, Olympia, WA, January 29, 2004.

Zatar, W.A. and H. Mutsuyoshi, "Residual Displacements of Concrete Bridge Piers Subjected to Near Field Earthquakes," *ACI Structural Journal*, Vol. 99, No. 6, November-December 2002, pp. 740-749.

APPENDIX A
GROUND MOTION CHARACTERISTICS

Five ground motions were selected from the SAC Suite, found in the NISEE

Strong Ground Motion Database (NISEE 2005), and scaled to create a suite of ground

motions for the dynamic analyses described in chapters 7 and 9.

As described in Chapter 5, five ground motions (10-1, 10-2, 10-3, 10-4, and 10-5)

were selected and scaled to represent seismic events that could likely occur in Western

Washington State with a 10 percent probability of exceedance in 50 years (10 percent in

50). Time histories for these motions are shown in figures A.1 through A.5 of this

appendix. Figures A.1 through A.5 also show an *Acceleration Response Spectrum, ARS*,

superimposed on the 10 percent in 50 *Design Acceleration Response Spectrum, DARS*,

for each of these motions. Included on these figures is the region used for matching

between the ARS and DARS, as described in Chapter 5.

The same five ground motions (2-1, 2-2, 2-3, 2-4, and 2-5) were also scaled by a

factor of two to represent seismic events that could likely occur in Western Washington

State with a 2 percent probability of exceedance in 50 years (2 percent in 50). Time

histories for these motions are shown in figures A.6 through A.10 of this appendix.

Figures A.6 through A.10 also show an ARS superimposed on the 2 percent in 50 DARS

for each of these motions. Included on these figures is the region used for matching

between the ARS and DARS, as described in Chapter 5.

The average ARS for these two groups of five ground motions are shown in the

figures of Chapter 5. The ARS and DARS found in this appendix are based on a

damping ratio of 0.05.
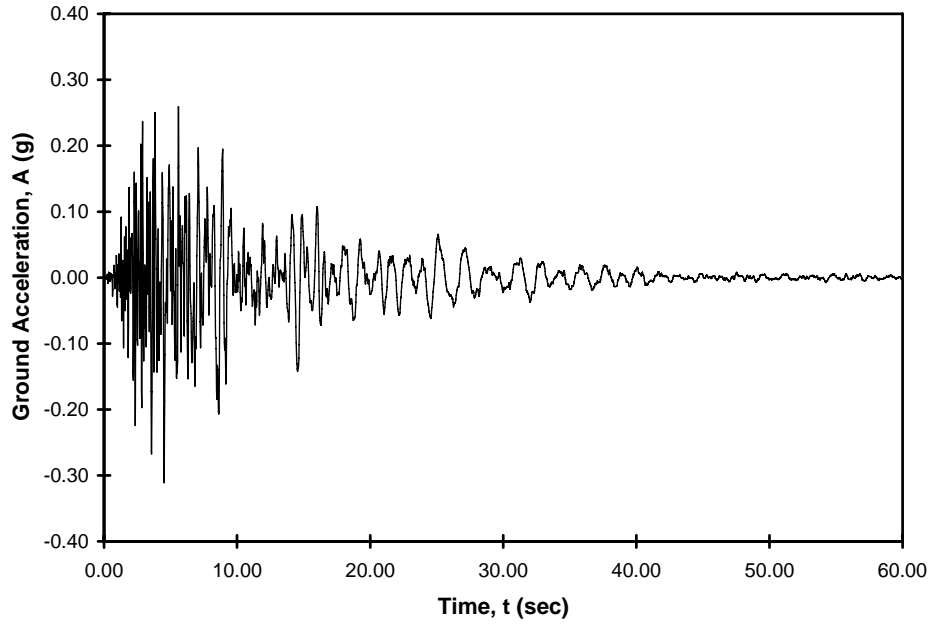
(a) Acceleration Time History
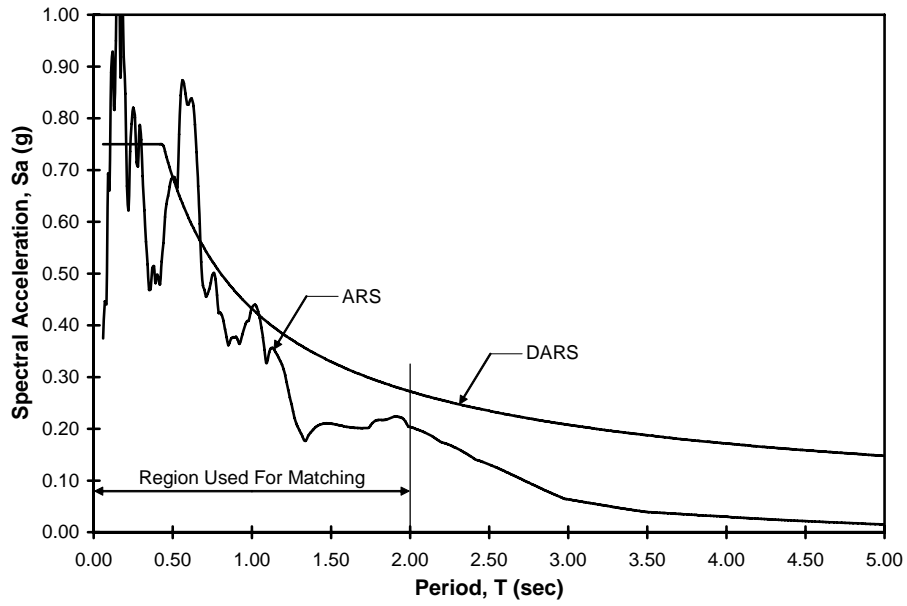
(b) ARS and 10 Percent in 50 DARS

Figure A.1:   Characteristics of Ground Motion 10-1
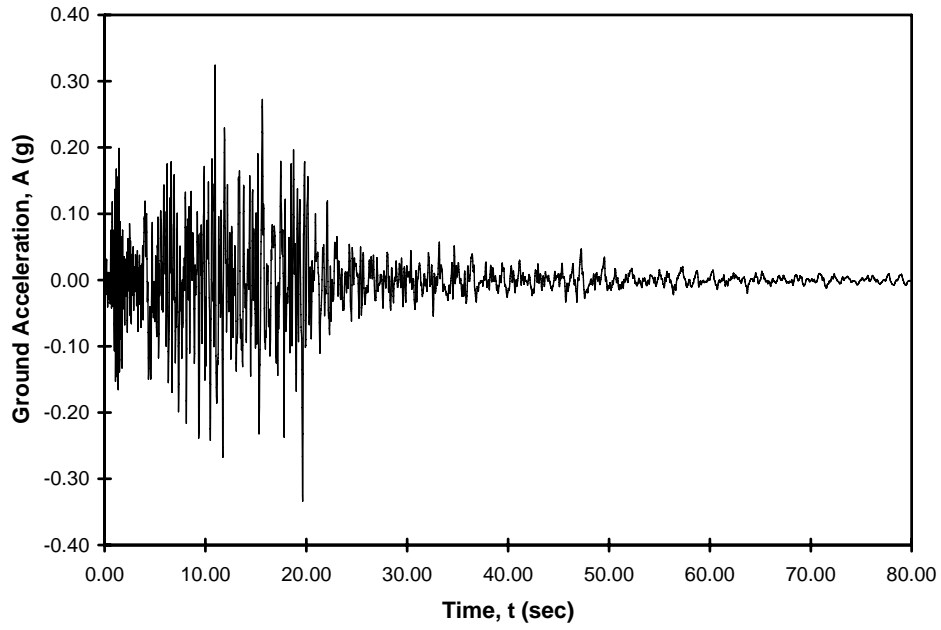
(a) Acceleration Time History
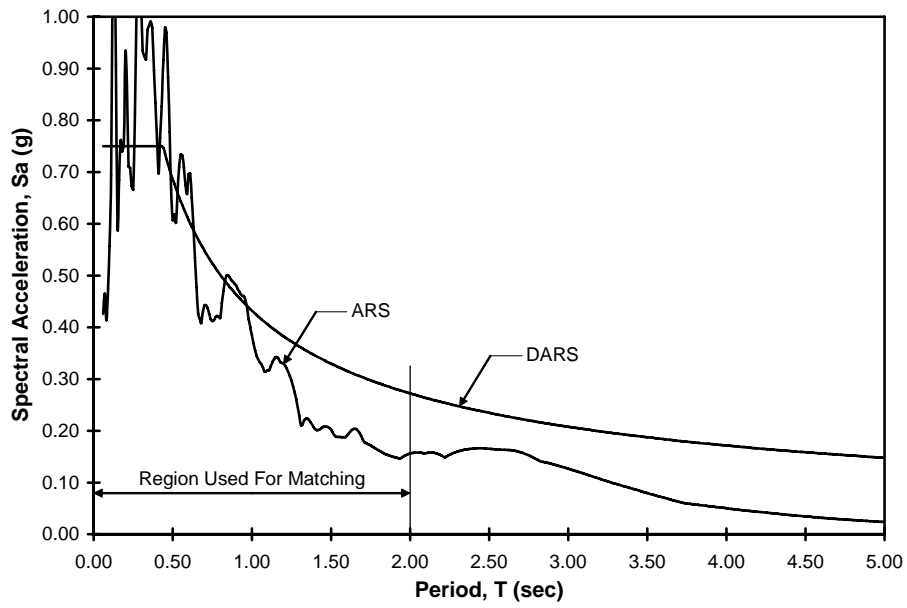
(b) ARS and 10 Percent in 50 DARS

Figure A.2: Characteristics of Ground Motion 10-2

A-3
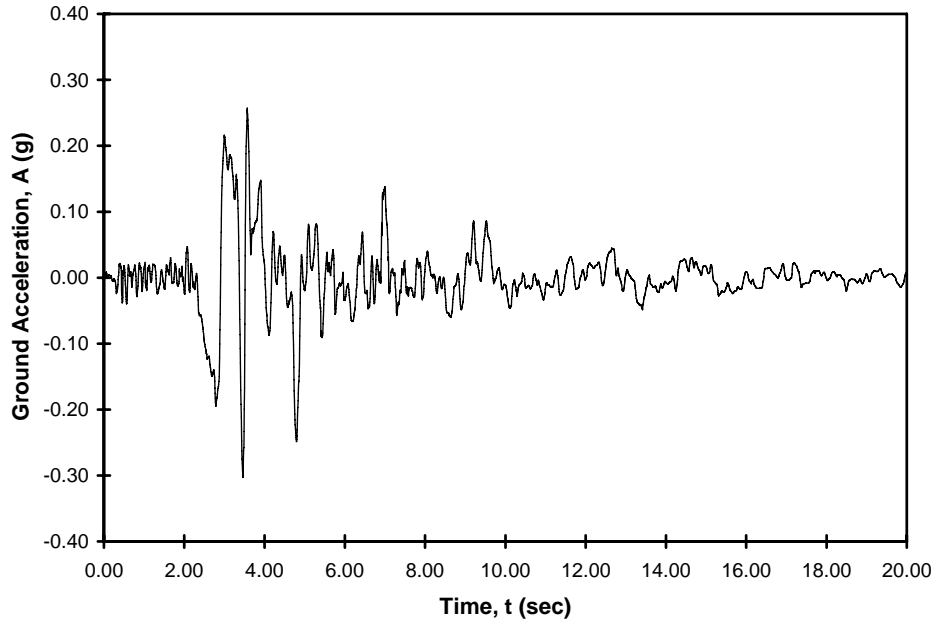
(a) Acceleration Time History
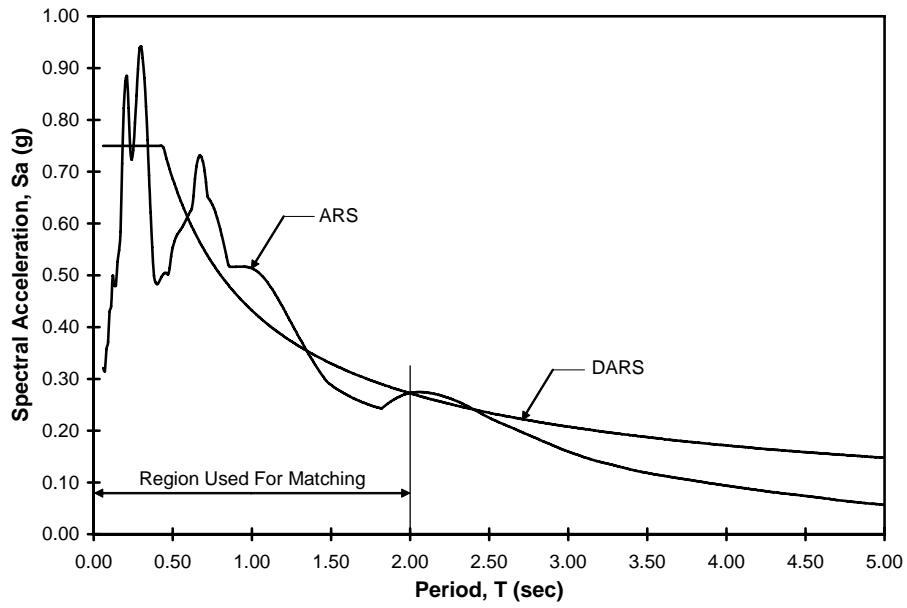
(b) ARS and 10 Percent in 50 DARS

Figure A.3: Characteristics of Ground Motion 10-3
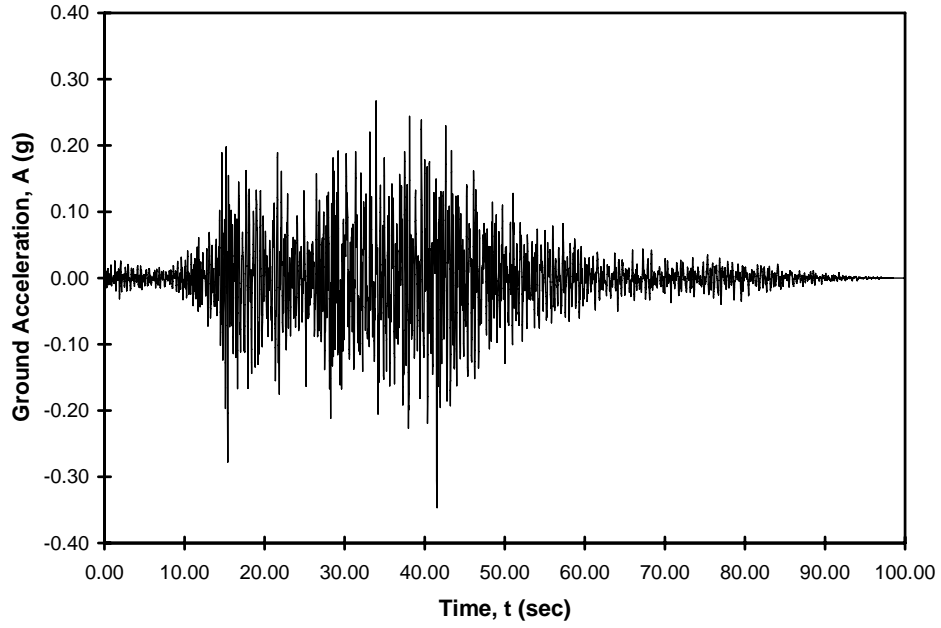
(a) Acceleration Time History
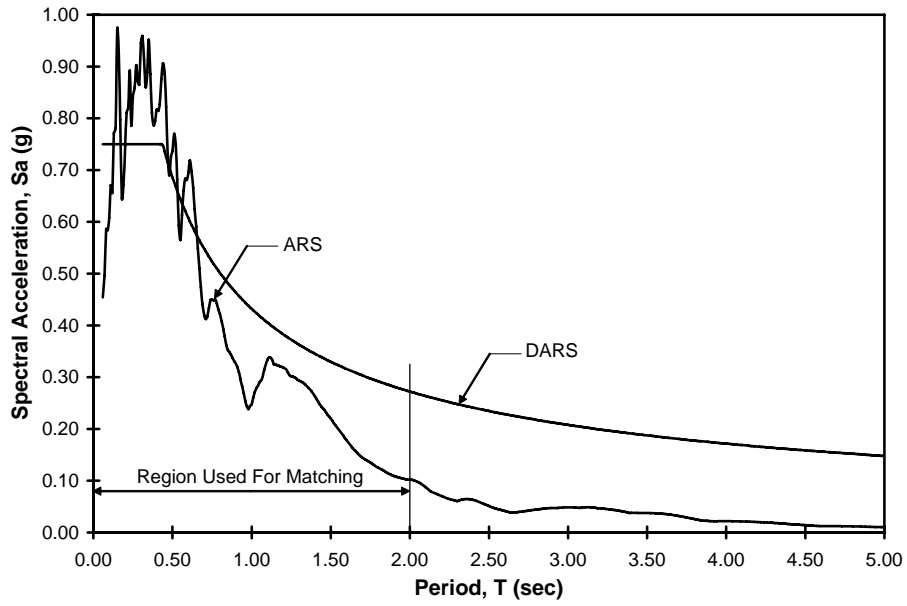
(b) ARS and 10 Percent in 50 DARS

Figure A.4: Characteristics of Ground Motion10-4

A-5
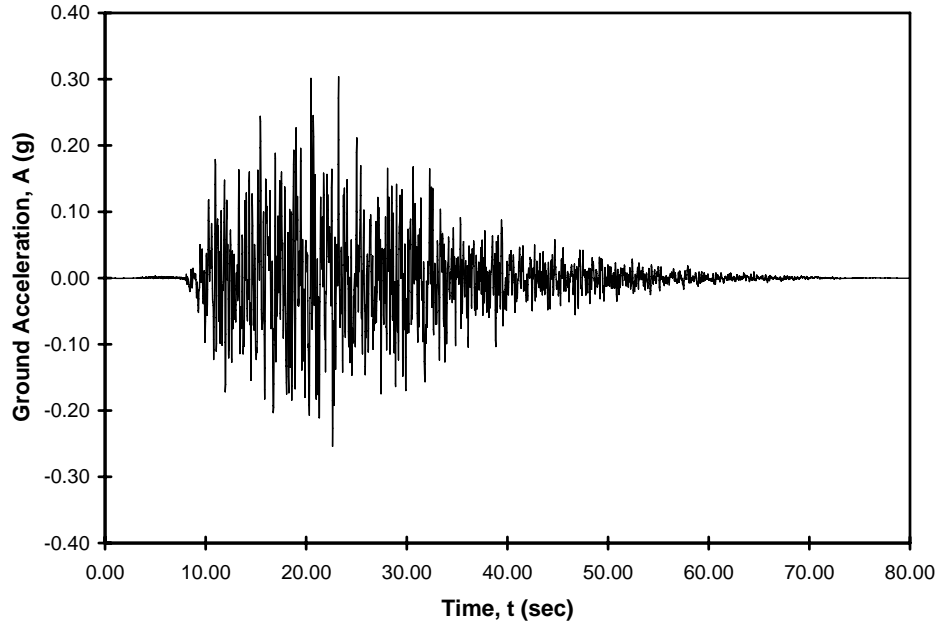
(a) Acceleration Time History
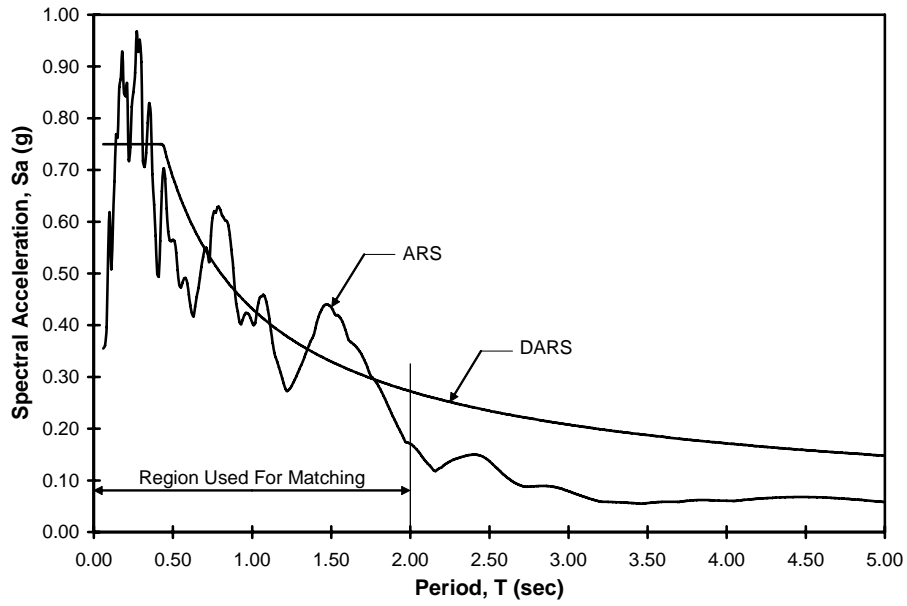
(b) ARS and 10 Percent in 50 DARS

Figure A.5: Characteristics of Ground Motion 10-5
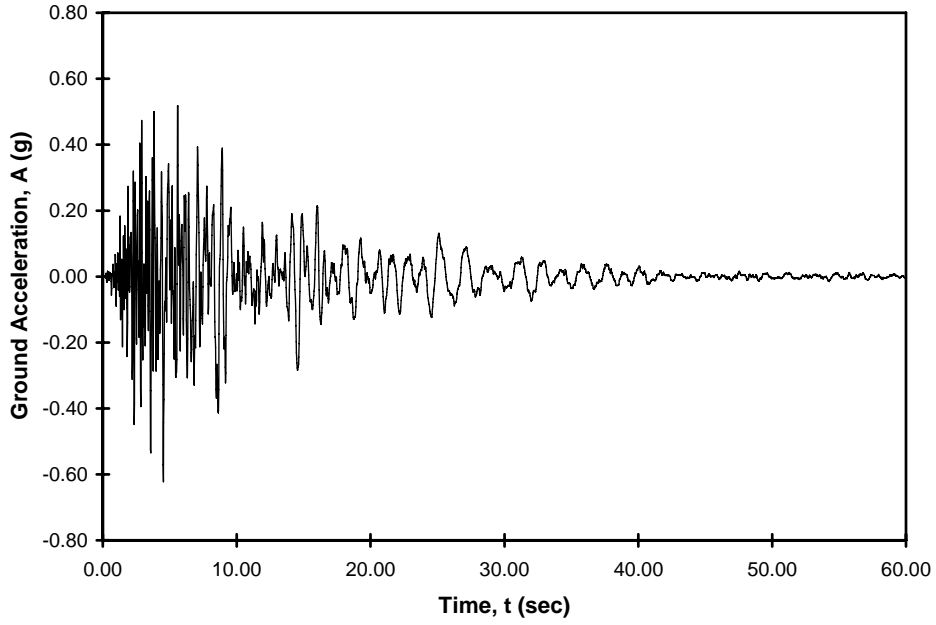
(a) Acceleration Time History
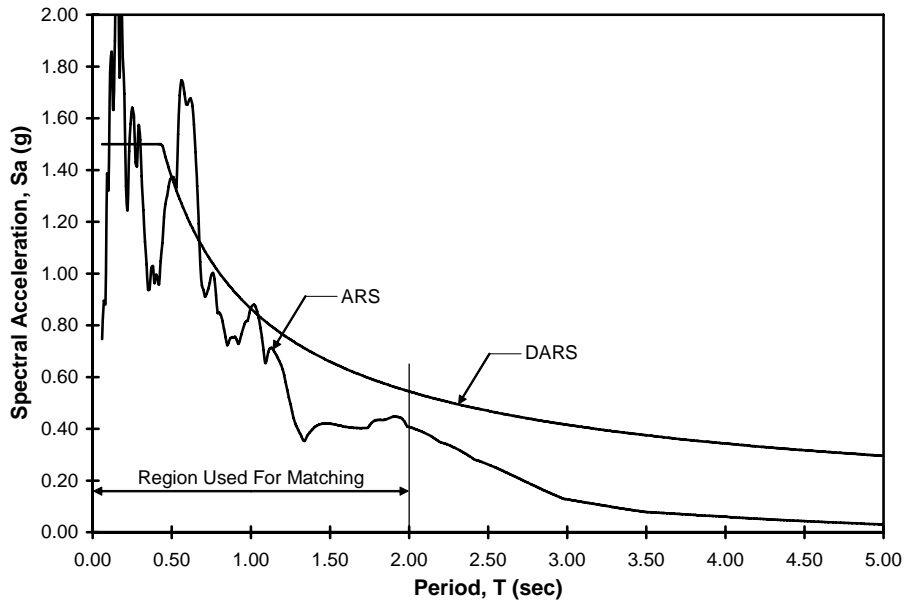
(b) ARS and 2 Percent in 50 DARS

Figure A.6: Characteristics of Ground Motion 2-1
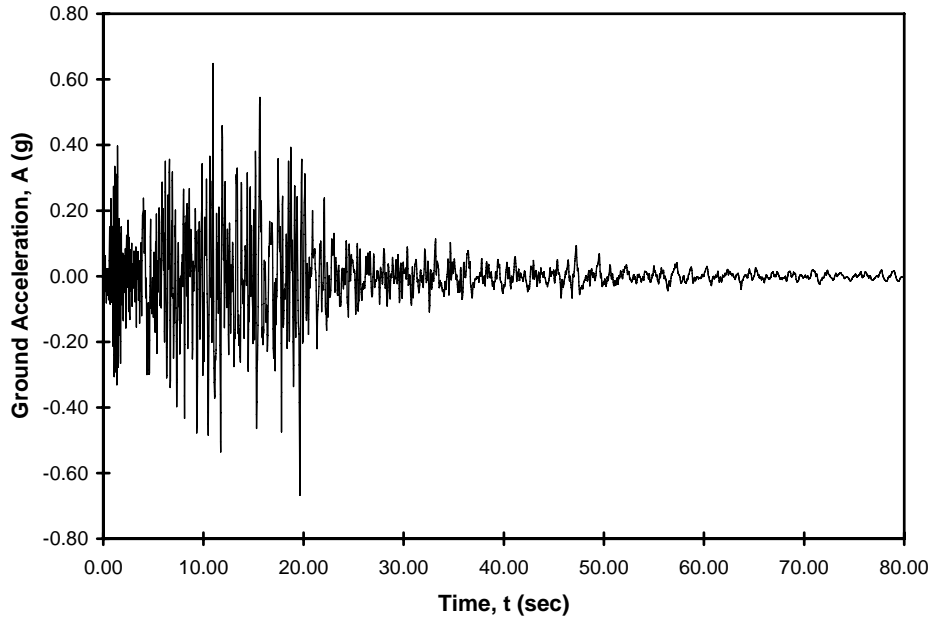
(a) Acceleration Time History
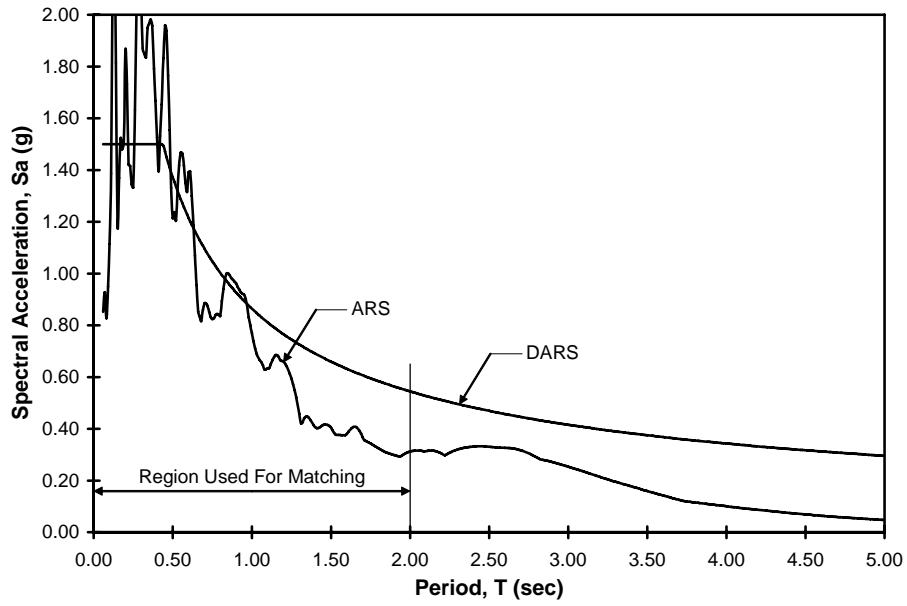
(b) ARS and 2 Percent in 50 DARS

Figure A.7: Characteristics of Ground Motion 2-2
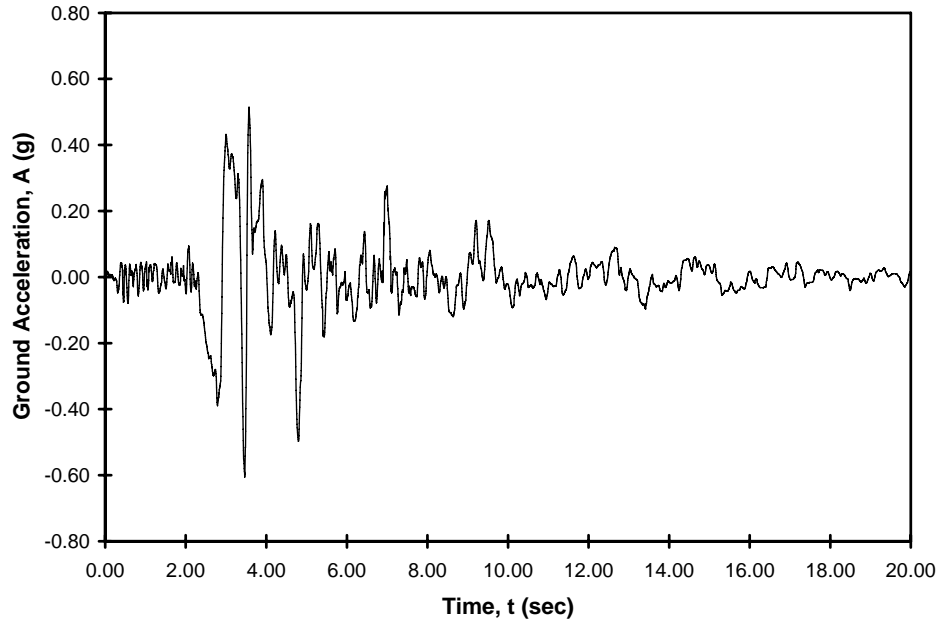
(a) Acceleration Time History
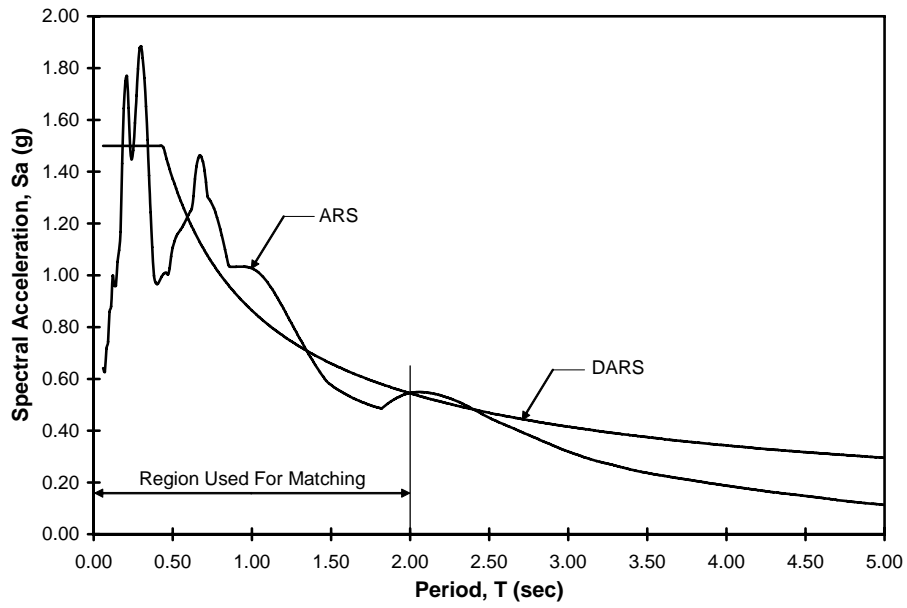
(b) ARS and 2 Percent in 50 DARS

Figure A.8: Characteristics of Ground Motion 2-3
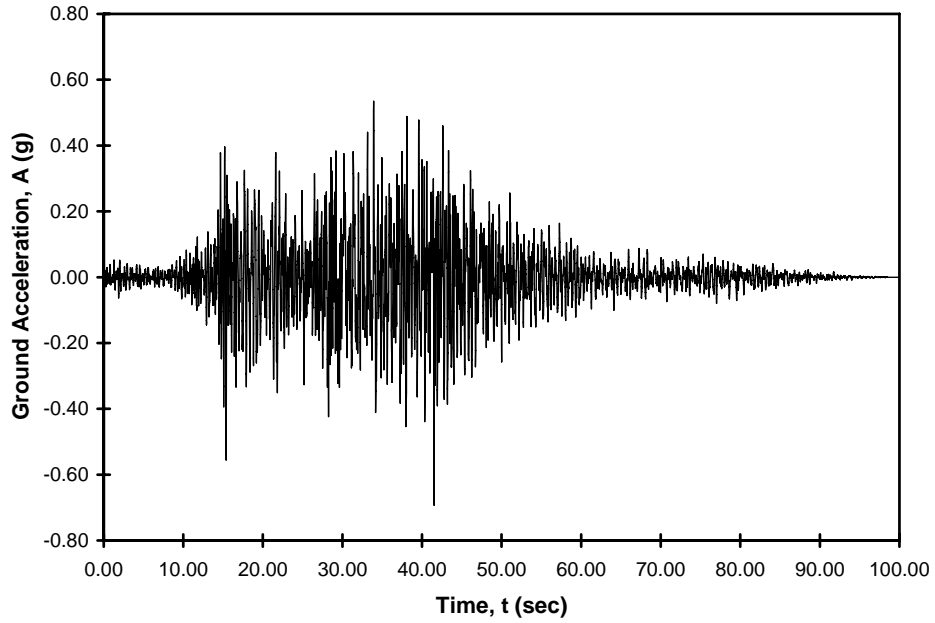
(a) Acceleration Time History
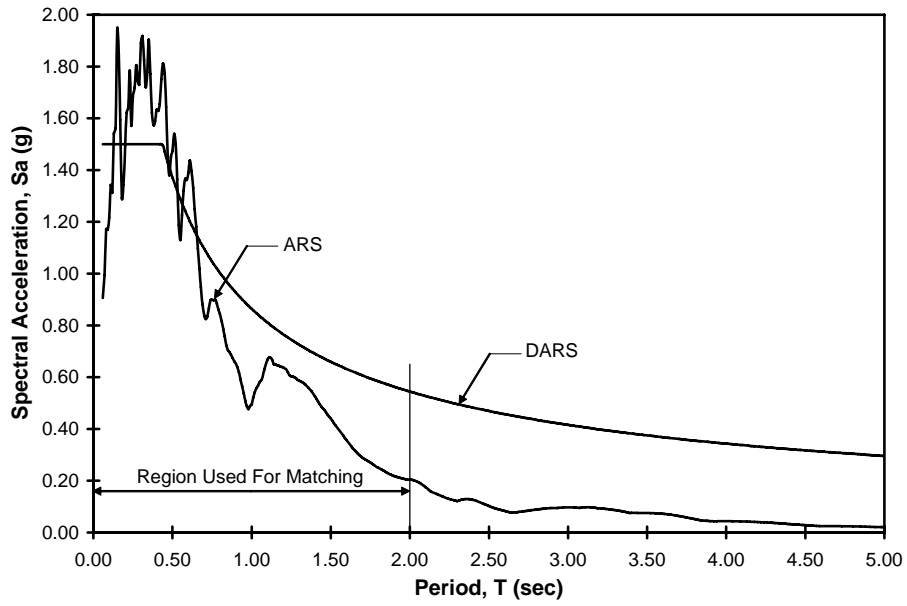
(b) ARS and 2 Percent in 50 DARS

Figure A.9: Characteristics of Ground Motion 2-4
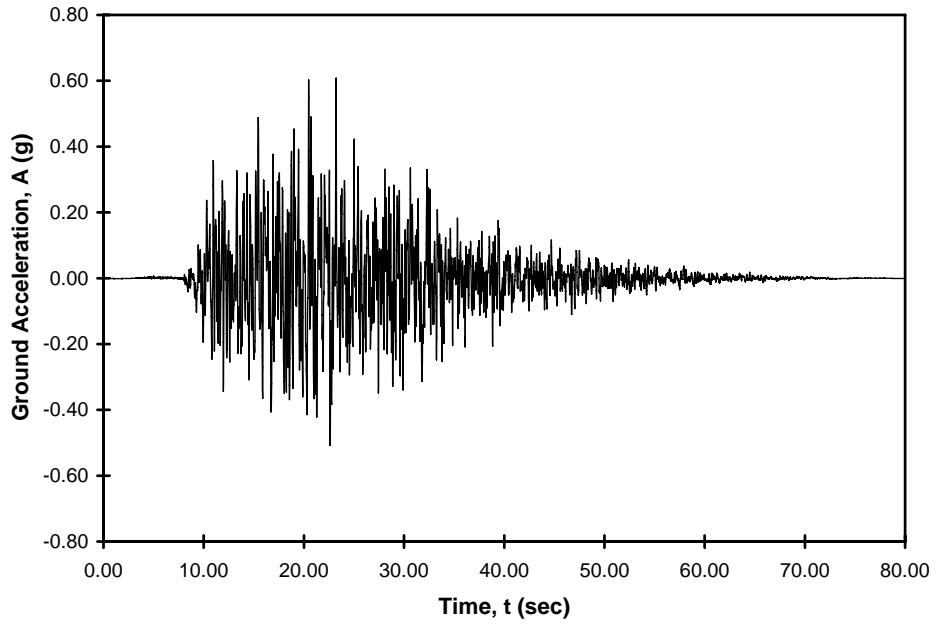
(a) Acceleration Time History
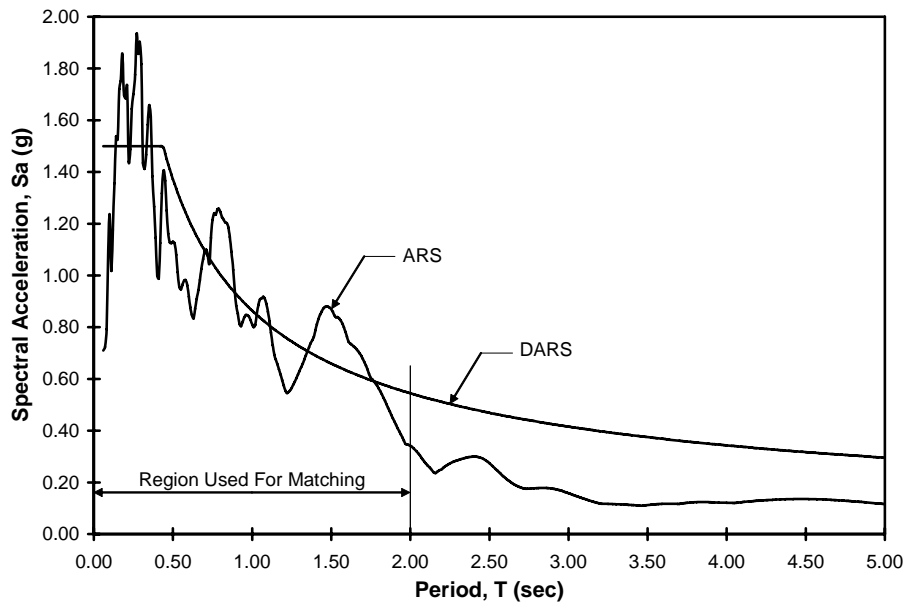
(b) ARS and 2 Percent in 50 DARS

Figure A.10: Characteristics of Ground Motion 2-5

APPENDIX B
RESULTS FROM EARTHQUAKE ANALYSES
OF REINFORCED CONCRETE FRAMES

Chapter 7 describes earthquake analyses of the reinforced concrete frames and discusses the results from those analyses. The reinforced concrete frames were subjected to the 10 ground motions described in Chapter 5 to establish maximum displacements and residual displacements. The 10 ground motions contained five motions with a 10 percent probability of exceedance in 50 years (10 percent in 50) and five motions with a 2 percent probability of exceedance in 50 years (2 percent in 50). Chapter 7 contains only the plots for response quantities resulting from the 2% in 50 ground motions. This appendix contains the tables and plots that summarize the responses of the reinforced concrete frames to the 10 percent in 50 ground motions. This appendix also includes the tables that summarize the responses of the hybrid frames to the 2 percent in 50 ground motions. Chapter 7 may be consulted for further information regarding the plots and quantities presented in this appendix.

Throughout this appendix, the mean values shown in the tables and figures are the average calculated from the five 10 percent in 50 ground motions. For the 2 percent in 50 ground motions, ten frame/ground motion combinations had a displacement of over 100 in., with OpenSees encountering convergence problems with each occurrence. For this study, these values were omitted when the mean values were calculated for the 2 percent in 50 ground motions. The combinations that encountered convergence problems are shown in Table B.2 as DNC (Did Not Converge).

Table B.1: Maximum Displacements, 10 Percent in 50, Reinforced Concrete Frames

Frame	Ground Motion 10 - 1 Δ_{max} (in.)	$\frac{\Delta_{max}}{L_{col}}$ (%)	Ground Motion 10 - 2 Δ_{max} (in.)	$\frac{\Delta_{max}}{L_{col}}$ (%)	Ground Motion 10 - 3 Δ_{max} (in.)	$\frac{\Delta_{max}}{L_{col}}$ (%)	Ground Motion 10 - 4 Δ_{max} (in.)	$\frac{\Delta_{max}}{L_{col}}$ (%)	Ground Motion 10 - 5 Δ_{max} (in.)	$\frac{\Delta_{max}}{L_{col}}$ (%)	Mean Δ_{max} (in.)	$\frac{\Delta_{max}}{L_{col}}$ (%)
5.005.05	2.491	1.04	2.625	1.09	2.577	1.07	2.370	0.99	3.070	1.28	2.626	1.09
5.005.10	3.063	1.28	3.469	1.45	4.153	1.73	2.784	1.16	4.861	2.03	3.666	1.53
5.005.15	4.282	1.78	3.488	1.45	5.417	2.26	2.763	1.15	7.431	3.10	4.676	1.95
5.010.05	2.662	1.11	2.366	0.99	1.214	0.51	2.300	0.96	1.799	0.75	2.068	0.86
5.010.10	2.783	1.16	2.808	1.17	3.261	1.36	2.570	1.07	3.382	1.41	2.961	1.23
5.010.15	3.613	1.51	3.181	1.33	3.870	1.61	2.966	1.24	3.650	1.52	3.456	1.44
5.020.05	1.484	0.62	2.345	0.98	1.177	0.49	1.786	0.74	2.186	0.91	1.795	0.75
5.020.10	2.630	1.10	3.037	1.27	2.159	0.90	2.451	1.02	2.511	1.05	2.558	1.07
5.020.15	2.656	1.11	2.632	1.10	3.219	1.34	2.358	0.98	3.074	1.28	2.788	1.16
5.030.05	1.081	0.45	2.039	0.85	1.242	0.52	1.585	0.66	1.841	0.77	1.558	0.65
5.030.10	2.651	1.10	2.152	0.90	1.473	0.61	2.071	0.86	1.337	0.56	1.937	0.81
5.030.15	2.605	1.09	2.668	1.11	2.805	1.17	2.509	1.05	2.477	1.03	2.613	1.09
6.005.05	3.668	1.27	3.392	1.18	3.131	1.09	2.491	0.87	3.467	1.20	3.230	1.12
6.005.10	4.212	1.46	4.437	1.54	6.035	2.10	3.349	1.16	6.687	2.32	4.944	1.72
6.005.15	7.711	2.68	3.831	1.33	8.069	2.80	6.413	2.23	6.389	2.22	6.483	2.25
6.010.05	2.646	0.92	2.551	0.89	3.019	1.05	2.392	0.83	3.433	1.19	2.808	0.98
6.010.10	4.273	1.48	3.874	1.35	4.133	1.44	3.123	1.08	4.280	1.49	3.937	1.37
6.010.15	4.872	1.69	4.481	1.56	6.744	2.34	4.273	1.48	6.885	2.39	5.451	1.89
6.020.05	2.743	0.95	2.657	0.92	1.638	0.57	2.524	0.88	1.976	0.69	2.308	0.80
6.020.10	3.330	1.16	3.326	1.15	3.587	1.25	2.984	1.04	3.421	1.19	3.329	1.16
6.020.15	3.244	1.13	3.492	1.21	4.828	1.68	3.227	1.12	4.710	1.64	3.900	1.35
6.030.05	2.273	0.79	2.384	0.83	0.947	0.33	2.525	0.88	2.480	0.86	2.122	0.74
6.030.10	3.170	1.10	2.967	1.03	3.131	1.09	2.696	0.94	2.897	1.01	2.972	1.03
6.030.15	3.694	1.28	3.675	1.28	3.550	1.23	2.640	0.92	3.959	1.37	3.504	1.22
7.005.05	5.132	1.53	3.564	1.06	4.783	1.42	3.030	0.90	4.696	1.40	4.241	1.26
7.005.10	7.678	2.29	3.879	1.15	7.877	2.34	6.538	1.95	6.606	1.97	6.516	1.94
7.005.15	7.932	2.36	5.437	1.62	10.723	3.19	6.355	1.89	8.134	2.42	7.716	2.30
7.010.05	3.843	1.14	3.880	1.15	3.632	1.08	2.867	0.85	3.670	1.09	3.578	1.07
7.010.10	5.003	1.49	5.003	1.49	6.671	1.99	4.995	1.49	5.856	1.74	5.505	1.64
7.010.15	6.996	2.08	4.635	1.38	7.705	2.29	4.639	1.38	6.275	1.87	6.050	1.80
7.020.05	3.379	1.01	3.210	0.96	3.872	1.15	3.242	0.96	3.449	1.03	3.430	1.02
7.020.10	3.616	1.08	3.953	1.18	4.573	1.36	3.314	0.99	4.224	1.26	3.936	1.17
7.020.15	4.175	1.24	5.151	1.53	6.571	1.96	3.525	1.05	4.783	1.42	4.841	1.44
7.030.05	3.364	1.00	3.743	1.11	2.082	0.62	3.375	1.00	2.587	0.77	3.030	0.90
7.030.10	3.384	1.01	4.207	1.25	4.055	1.21	3.737	1.11	4.602	1.37	3.997	1.19
7.030.15	5.739	1.71	3.811	1.13	5.581	1.66	3.458	1.03	5.112	1.52	4.740	1.41

Table B.2: Maximum Displacements, 2 Percent in 50, Reinforced Concrete Frames

Frame	Ground Motion 2 - 1 Δ_{max} (in.)	$\frac{\Delta_{max}}{L_{col}}$ (%)	Ground Motion 2 - 2 Δ_{max} (in.)	$\frac{\Delta_{max}}{L_{col}}$ (%)	Ground Motion 2 - 3 Δ_{max} (in.)	$\frac{\Delta_{max}}{L_{col}}$ (%)	Ground Motion 2 - 4 Δ_{max} (in.)	$\frac{\Delta_{max}}{L_{col}}$ (%)	Ground Motion 2 - 5 Δ_{max} (in.)	$\frac{\Delta_{max}}{L_{col}}$ (%)	Mean Δ_{max} (in.)	$\frac{\Delta_{max}}{L_{col}}$ (%)
5.005.05	5.668	2.36	5.965	2.49	10.205	4.25	3.702	1.54	7.185	2.99	6.545	2.73
5.005.10	10.281	4.28	7.693	3.21	DNC	DNC	9.336	3.89	10.920	4.55	9.558	3.98
5.005.15	DNC	DNC	9.393	3.91	DNC	DNC	9.811	4.09	DNC	DNC	9.602	4.00
5.010.05	4.123	1.72	4.237	1.77	5.108	2.13	3.679	1.53	4.310	1.80	4.291	1.79
5.010.10	6.723	2.80	5.991	2.50	11.777	4.91	3.935	1.64	7.372	3.07	7.159	2.98
5.010.15	6.496	2.71	6.626	2.76	DNC	DNC	8.489	3.54	8.997	3.75	7.652	3.19
5.020.05	2.819	1.17	3.236	1.35	1.996	0.83	2.727	1.14	3.004	1.25	2.756	1.15
5.020.10	4.556	1.90	4.422	1.84	6.212	2.59	4.007	1.67	5.438	2.27	4.927	2.05
5.020.15	5.697	2.37	5.596	2.33	11.305	4.71	3.815	1.59	6.848	2.85	6.652	2.77
5.030.05	1.899	0.79	3.151	1.31	2.019	0.84	2.186	0.91	2.039	0.85	2.259	0.94
5.030.10	4.345	1.81	4.215	1.76	3.985	1.66	3.635	1.51	3.739	1.56	3.984	1.66
5.030.15	5.090	2.12	5.090	2.12	8.313	3.46	3.601	1.50	5.892	2.46	5.597	2.33
6.005.05	6.435	2.23	5.647	1.96	12.829	4.45	4.646	1.61	10.541	3.66	8.020	2.78
6.005.10	11.342	3.94	9.987	3.47	DNC	DNC	8.907	3.09	13.426	4.66	10.916	3.79
6.005.15	11.500	3.99	16.021	5.56	DNC	DNC	6.696	2.33	12.333	4.28	11.637	4.04
6.010.05	5.581	1.94	5.407	1.88	9.365	3.25	4.019	1.40	6.412	2.23	6.157	2.14
6.010.10	6.638	2.31	7.568	2.63	15.605	5.42	8.290	2.88	8.564	2.97	9.333	3.24
6.010.15	13.208	4.59	9.754	3.39	DNC	DNC	7.382	2.56	10.972	3.81	10.329	3.59
6.020.05	4.118	1.43	4.384	1.52	4.189	1.45	3.705	1.29	3.993	1.39	4.078	1.42
6.020.10	5.204	1.81	5.364	1.86	10.686	3.71	4.092	1.42	7.122	2.47	6.494	2.25
6.020.15	6.274	2.18	6.842	2.38	14.457	5.02	6.573	2.28	11.269	3.91	9.083	3.15
6.030.05	4.217	1.46	3.725	1.29	2.921	1.01	3.474	1.21	3.563	1.24	3.580	1.24
6.030.10	5.143	1.79	5.368	1.86	7.186	2.50	3.892	1.35	6.064	2.11	5.531	1.92
6.030.15	6.755	2.35	5.254	1.82	12.425	4.31	4.445	1.54	7.051	2.45	7.186	2.50
7.005.05	11.207	3.34	7.738	2.30	18.212	5.42	8.682	2.58	9.756	2.90	11.119	3.31
7.005.10	11.657	3.47	16.067	4.78	28.443	8.47	7.041	2.10	11.551	3.44	14.952	4.45
7.005.15	12.741	3.79	16.979	5.05	DNC	DNC	8.908	2.65	12.517	3.73	12.786	3.81
7.010.05	7.337	2.18	5.493	1.63	12.155	3.62	4.947	1.47	7.551	2.25	7.497	2.23
7.010.10	12.158	3.62	9.380	2.79	18.736	5.58	7.994	2.38	9.781	2.91	11.610	3.46
7.010.15	11.041	3.29	11.642	3.46	DNC	DNC	8.188	2.44	12.367	3.68	10.810	3.22
7.020.05	5.188	1.54	5.264	1.57	6.210	1.85	4.719	1.40	5.808	1.73	5.438	1.62
7.020.10	6.777	2.02	6.828	2.03	12.662	3.77	5.012	1.49	7.814	2.33	7.819	2.33
7.020.15	11.351	3.38	8.327	2.48	16.922	5.04	8.190	2.44	8.942	2.66	10.746	3.20
7.030.05	4.413	1.31	4.813	1.43	5.100	1.52	4.266	1.27	4.511	1.34	4.621	1.38
7.030.10	7.330	2.18	5.449	1.62	12.100	3.60	4.954	1.47	7.516	2.24	7.470	2.22
7.030.15	7.268	2.16	7.778	2.31	13.063	3.89	5.119	1.52	11.248	3.35	8.895	2.65

Note: DNC indicates earthquake analysis did not converge
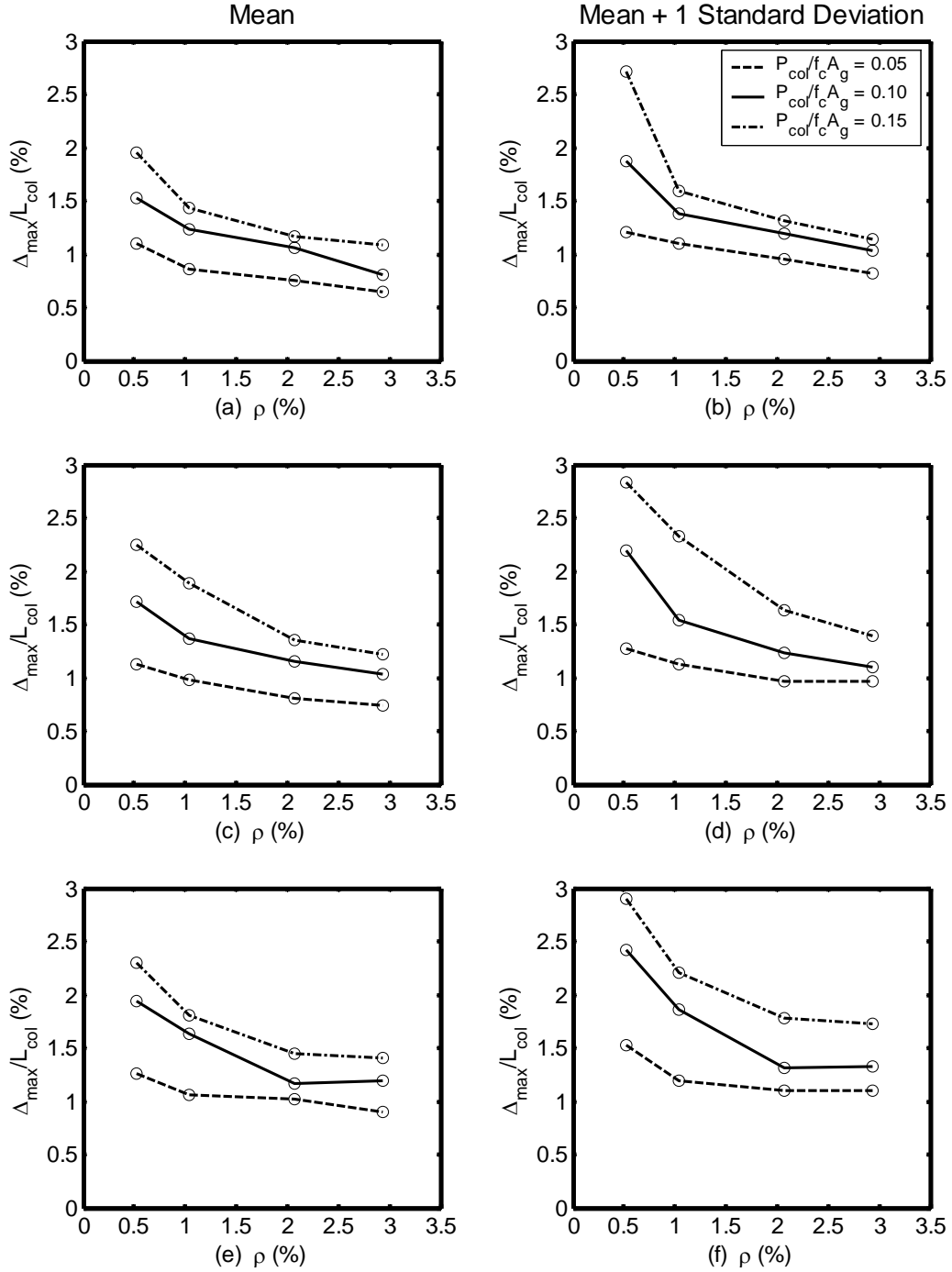
Figure B.1: Trends in Drift Ratio, 10 Percent in 50, Reinforced Concrete Frames
(a) and (b) $L_{col}/D_{col} = 5$, (c) and (d) $L_{col}/D_{col} = 6$, and (e) and (f) $L_{col}/D_{col} = 7$
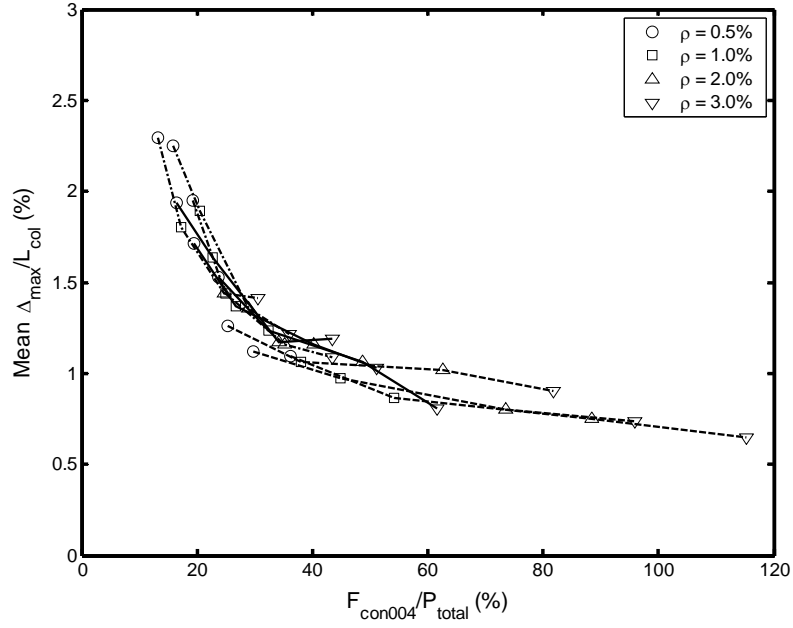
Figure B.2: Effect of Strength on Mean Drift Ratio, 10 Percent in 50, Reinforced Concrete Frames
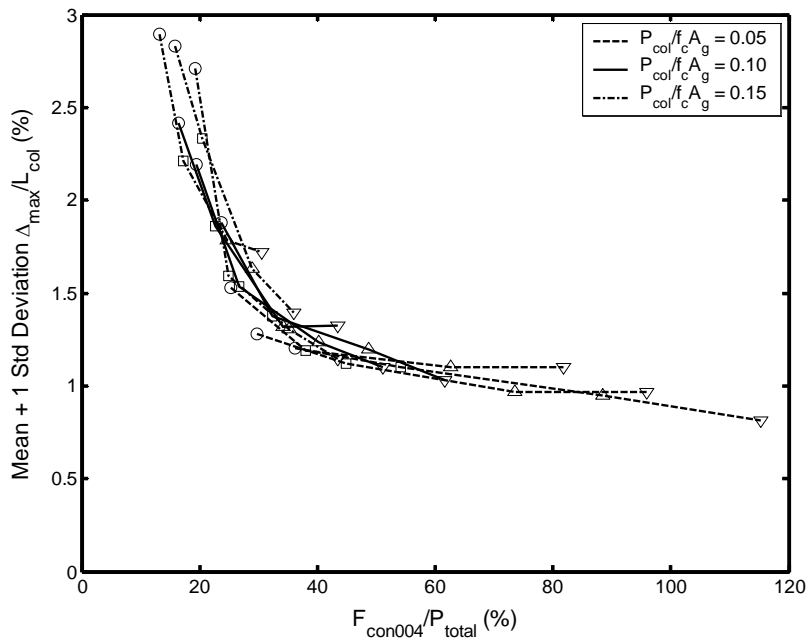
Figure B.3: Effect of Strength on Mean Plus One Standard Deviation Drift Ratio, 10 Percent in 50, Reinforced Concrete Frames
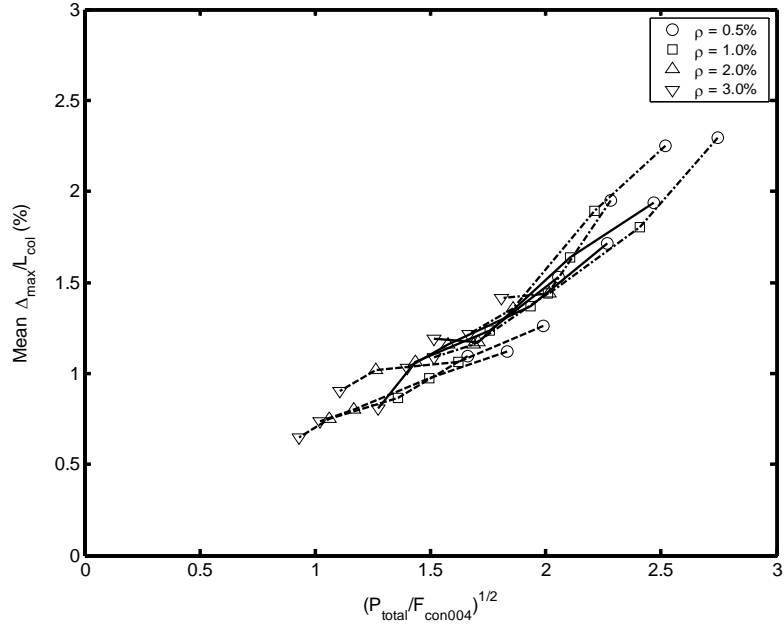
Figure B.4: Effect of Stiffness on Mean Drift Ratio, 10 Percent in 50, Reinforced Concrete Frames
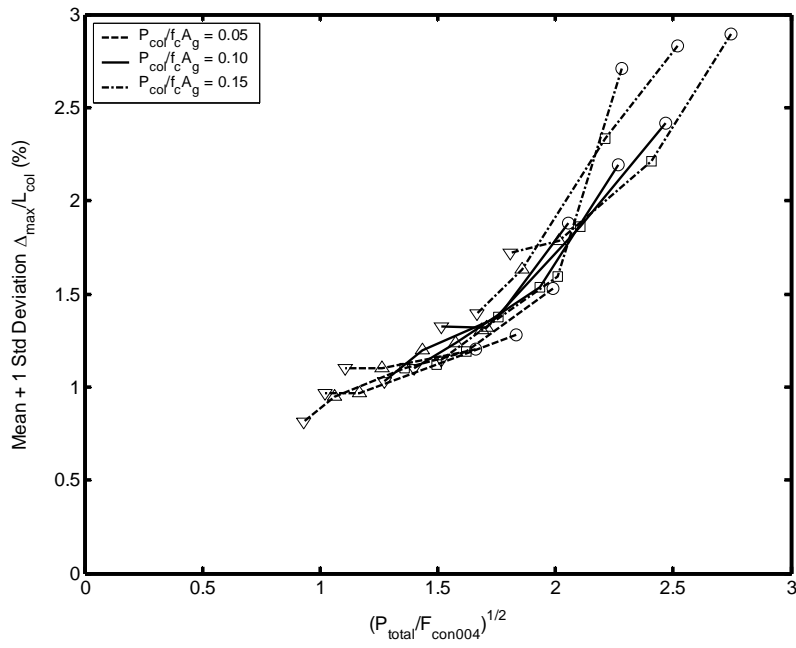
Figure B.5: Effect of Stiffness on Mean Plus One Standard Deviation Drift Ratio, 10 Percent in 50, Reinforced Concrete Frames
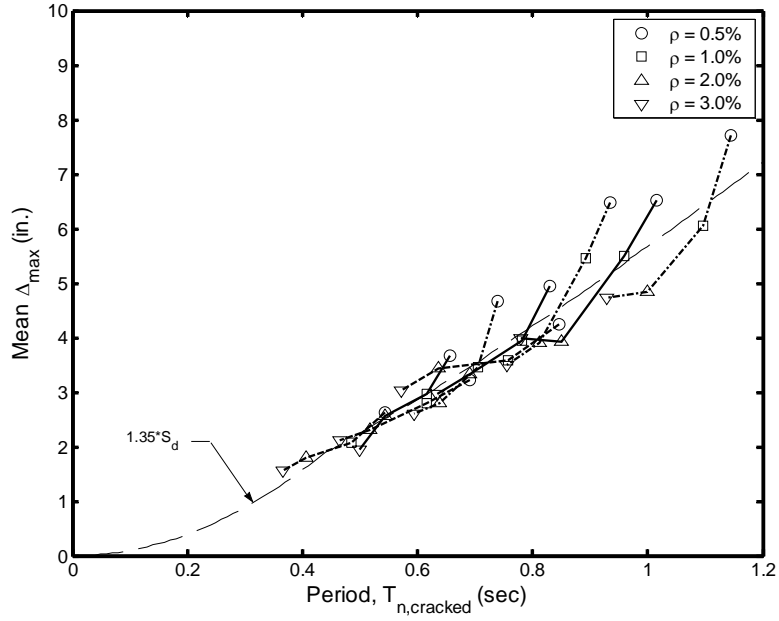
Figure B.6: Predicted and Mean Response, 10 Percent in 50, Reinforced Concrete Frames
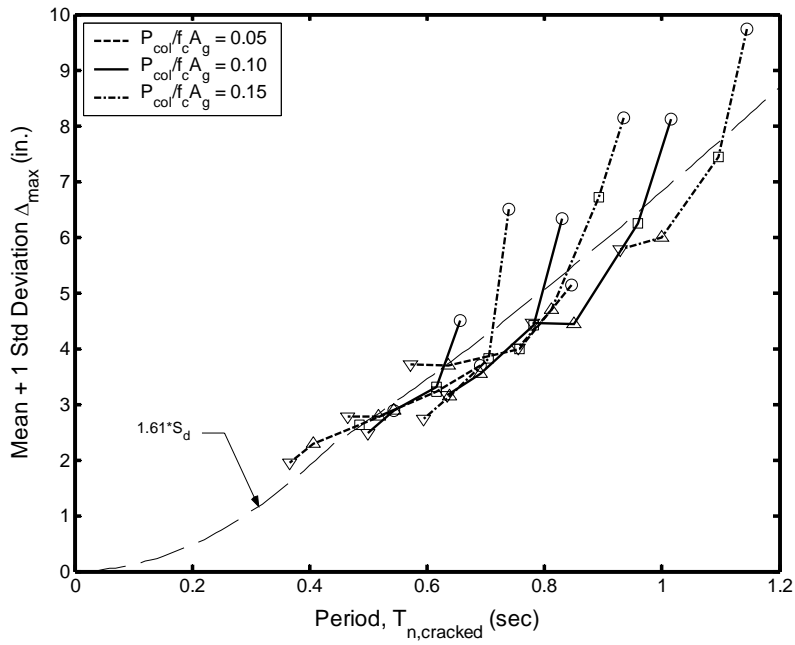
Figure B.7: Predicted and Mean Plus One Standard Deviation Response, 10 Percent in 50, Reinforced Concrete Frames

APPENDIX C
RESULTS FROM EARTHQUAKE ANALYSES
OF HYBRID FRAMES

Chapter 9 describes the earthquake analyses of the hybrid frames and discusses the results from those analyses. The hybrid frames were subjected to the 10 ground motions described in Chapter 5 to establish maximum displacements and residual displacements. The 10 ground motions contained five motions with a 10 percent probability of exceedance in 50 years (10 percent in 50) and five motions with a 2 percent probability of exceedance in 50 years (2 percent in 50). Chapter 9 contains only the plots for response quantities resulting from the 2 percent in 50 ground motions. This appendix contains the tables and plots that summarize the responses of the hybrid frames to the 10 percent in 50 ground motions. This appendix also includes the tables that summarize the responses of the hybrid frames to the 2 percent in 50 ground motions. Chapter 9 may be consulted for further information regarding the plots and quantities presented in this appendix.

Table C.1: Maximum Displacements, 10 Percent in 50, Hybrid Frames, $P_{col}/(f_c' A_g) = 0.05$

Frame	Ground Motion 10-1 Δ_{max} (in.)	$\frac{\Delta_{max}}{L_{col}}$ (%)	Ground Motion 10-2 Δ_{max} (in.)	$\frac{\Delta_{max}}{L_{col}}$ (%)	Ground Motion 10-3 Δ_{max} (in.)	$\frac{\Delta_{max}}{L_{col}}$ (%)	Ground Motion 10-4 Δ_{max} (in.)	$\frac{\Delta_{max}}{L_{col}}$ (%)	Ground Motion 10-5 Δ_{max} (in.)	$\frac{\Delta_{max}}{L_{col}}$ (%)	Mean Δ_{max} (in.)	$\frac{\Delta_{max}}{L_{col}}$ (%)
5.020.025	1.147	0.48	1.927	0.80	1.176	0.49	1.412	0.59	1.278	0.53	1.388	0.58
5.030.025	0.994	0.41	1.359	0.57	1.402	0.58	1.502	0.63	1.558	0.65	1.363	0.57
5.010.050	2.107	0.88	1.772	0.74	0.956	0.40	1.737	0.72	1.932	0.81	1.701	0.71
5.020.050	1.306	0.54	1.808	0.75	1.279	0.53	1.616	0.67	1.243	0.52	1.451	0.60
5.030.050	1.349	0.56	1.476	0.61	1.351	0.56	1.442	0.60	1.714	0.71	1.467	0.61
5.010.075	2.017	0.84	1.823	0.76	0.915	0.38	1.914	0.80	1.992	0.83	1.732	0.72
5.020.075	1.515	0.63	1.812	0.76	1.281	0.53	1.666	0.69	1.389	0.58	1.533	0.64
5.030.075	1.300	0.54	1.397	0.58	1.349	0.56	1.503	0.63	1.513	0.63	1.412	0.59
5.005.100	3.037	1.27	2.566	1.07	2.496	1.04	2.332	0.97	2.875	1.20	2.661	1.11
5.010.100	2.343	0.98	2.069	0.86	1.025	0.43	1.967	0.82	1.467	0.61	1.774	0.74
5.020.100	1.573	0.66	1.760	0.73	1.266	0.53	1.729	0.72	1.396	0.58	1.545	0.64
5.030.100	1.325	0.55	1.506	0.63	1.315	0.55	1.481	0.62	1.732	0.72	1.472	0.61
6.020.025	2.798	0.97	2.019	0.70	1.097	0.38	2.081	0.72	1.622	0.56	1.923	0.67
6.030.025	1.856	0.64	2.423	0.84	0.926	0.32	2.241	0.78	2.332	0.81	1.956	0.68
6.010.050	2.719	0.94	2.337	0.81	2.762	0.96	2.405	0.83	3.192	1.11	2.683	0.93
6.020.050	2.960	1.03	2.116	0.73	0.923	0.32	2.248	0.78	1.764	0.61	2.002	0.70
6.030.050	1.881	0.65	2.523	0.88	1.051	0.37	1.928	0.67	1.919	0.67	1.860	0.65
6.010.075	2.494	0.87	2.875	1.00	3.104	1.08	2.674	0.93	3.076	1.07	2.844	0.99
6.020.075	3.240	1.12	2.179	0.76	0.876	0.30	2.201	0.76	1.475	0.51	1.994	0.69
6.030.075	1.769	0.61	2.903	1.01	1.103	0.38	2.125	0.74	1.935	0.67	1.967	0.68
6.005.100	3.034	1.05	3.161	1.10	3.058	1.06	2.448	0.85	4.313	1.50	3.203	1.11
6.010.100	2.562	0.89	2.823	0.98	3.342	1.16	2.907	1.01	3.557	1.24	3.038	1.05
6.020.100	3.389	1.18	2.514	0.87	0.967	0.34	2.250	0.78	1.529	0.53	2.130	0.74
6.030.100	1.580	0.55	2.855	0.99	1.105	0.38	2.392	0.83	2.161	0.75	2.019	0.70
7.020.025	3.075	0.92	2.885	0.86	3.340	0.99	2.723	0.81	2.996	0.89	3.004	0.89
7.030.025	3.390	1.01	2.574	0.77	1.631	0.49	2.850	0.85	2.219	0.66	2.533	0.75
7.010.050	3.466	1.03	3.396	1.01	3.305	0.98	2.802	0.83	4.501	1.34	3.494	1.04
7.020.050	2.956	0.88	3.291	0.98	3.033	0.90	2.958	0.88	2.973	0.88	3.042	0.91
7.030.050	3.588	1.07	3.284	0.98	1.720	0.51	2.706	0.81	2.008	0.60	2.661	0.79
7.010.075	3.688	1.10	2.338	0.70	3.574	1.06	2.576	0.77	4.481	1.33	3.331	0.99
7.020.075	3.061	0.91	3.516	1.05	3.065	0.91	2.967	0.88	2.773	0.83	3.076	0.92
7.030.075	2.544	0.76	3.388	1.01	1.128	0.34	3.014	0.90	2.430	0.72	2.501	0.74
7.005.100	4.114	1.22	3.457	1.03	4.571	1.36	2.992	0.89	4.603	1.37	3.948	1.17
7.010.100	3.859	1.15	3.366	1.00	3.644	1.08	2.986	0.89	3.834	1.14	3.538	1.05
7.020.100	3.184	0.95	3.677	1.09	2.869	0.85	3.679	1.09	3.922	1.17	3.466	1.03
7.030.100	3.387	1.01	3.418	1.02	1.017	0.30	3.181	0.95	2.578	0.77	2.716	0.81

Table C.2: Maximum Displacements, 10 Percent in 50, Hybrid Frames, $P_{col}/(f_c' A_g) = 0.10$

Frame	Ground Motion 10-1 Δ_{max} (in.)	$\frac{\Delta_{max}}{L_{col}}$ (%)	Ground Motion 10-2 Δ_{max} (in.)	$\frac{\Delta_{max}}{L_{col}}$ (%)	Ground Motion 10-3 Δ_{max} (in.)	$\frac{\Delta_{max}}{L_{col}}$ (%)	Ground Motion 10-4 Δ_{max} (in.)	$\frac{\Delta_{max}}{L_{col}}$ (%)	Ground Motion 10-5 Δ_{max} (in.)	$\frac{\Delta_{max}}{L_{col}}$ (%)	Mean Δ_{max} (in.)	$\frac{\Delta_{max}}{L_{col}}$ (%)
5.020.050	2.883	1.20	2.793	1.16	1.821	0.76	2.234	0.93	2.116	0.88	2.369	0.99
5.030.050	2.321	0.97	1.792	0.75	1.042	0.43	1.960	0.82	2.034	0.85	1.830	0.76
5.020.075	3.073	1.28	2.874	1.20	1.873	0.78	2.382	0.99	1.965	0.82	2.433	1.01
5.030.075	2.556	1.06	1.999	0.83	0.915	0.38	1.921	0.80	2.085	0.87	1.895	0.79
5.010.100	2.499	1.04	1.999	0.83	3.032	1.26	2.542	1.06	3.196	1.33	2.654	1.11
5.020.100	2.872	1.20	2.974	1.24	1.855	0.77	2.493	1.04	1.287	0.54	2.296	0.96
5.030.100	2.887	1.20	2.031	0.85	0.953	0.40	1.957	0.82	2.123	0.88	1.990	0.83
6.020.050	2.786	0.97	2.823	0.98	3.249	1.13	2.420	0.84	3.277	1.14	2.911	1.01
6.030.050	2.529	0.88	2.816	0.98	2.965	1.03	2.628	0.91	2.522	0.88	2.692	0.93
6.020.075	2.877	1.00	2.882	1.00	3.335	1.16	2.541	0.88	3.407	1.18	3.008	1.04
6.030.075	2.628	0.91	2.817	0.98	3.038	1.05	2.676	0.93	2.742	0.95	2.780	0.97
6.010.100	3.718	1.29	3.588	1.25	3.980	1.38	2.772	0.96	4.697	1.63	3.751	1.30
6.020.100	3.030	1.05	2.884	1.00	3.371	1.17	2.918	1.01	3.396	1.18	3.120	1.08
6.030.100	2.835	0.98	2.725	0.95	2.913	1.01	2.419	0.84	3.029	1.05	2.784	0.97
7.020.050	3.865	1.15	3.621	1.08	4.182	1.24	3.369	1.00	4.241	1.26	3.856	1.15
7.030.050	3.653	1.09	4.153	1.24	3.735	1.11	2.997	0.89	3.808	1.13	3.669	1.09
7.020.075	4.065	1.21	3.625	1.08	4.254	1.27	3.375	1.00	4.091	1.22	3.882	1.16
7.030.075	3.775	1.12	2.601	0.77	3.754	1.12	3.013	0.90	3.683	1.10	3.365	1.00
7.010.100	4.719	1.40	4.725	1.41	6.574	1.96	3.756	1.12	5.504	1.64	5.056	1.50
7.020.100	3.961	1.18	3.786	1.13	4.197	1.25	2.519	0.75	4.292	1.28	3.751	1.12
7.030.100	3.913	1.16	2.090	0.62	3.747	1.12	2.914	0.87	4.033	1.20	3.339	0.99

Table C.3: Maximum Displacements, 2 Percent in 50, Hybrid Frames, $P_{col}/(f_c' A_g) = 0.05$

Frame	Ground Motion 2 - 1		Ground Motion 2 - 2		Ground Motion 2 - 3		Ground Motion 2 - 4		Ground Motion 2 - 5		Mean	
	Δ_{max}	$\dfrac{\Delta_{max}}{L_{col}}$	Δ_{max}	$\dfrac{\Delta_{max}}{L_{col}}$	Δ_{max}	$\dfrac{\Delta_{max}}{L_{col}}$	Δ_{max}	$\dfrac{\Delta_{max}}{L_{col}}$	Δ_{max}	$\dfrac{\Delta_{max}}{L_{col}}$	Δ_{max}	$\dfrac{\Delta_{max}}{L_{col}}$
	(in.)	(%)	(in.)	(%)	(in.)	(%)	(in.)	(%)	(in.)	(%)	(in.)	(%)
5.020.025	2.356	0.98	3.318	1.38	1.960	0.82	2.472	1.03	2.818	1.17	2.585	1.08
5.030.025	1.726	0.72	2.602	1.08	2.065	0.86	2.250	0.94	1.874	0.78	2.104	0.88
5.010.050	4.259	1.77	4.100	1.71	5.052	2.10	3.546	1.48	5.272	2.20	4.446	1.85
5.020.050	2.200	0.92	3.599	1.50	1.844	0.77	2.444	1.02	2.982	1.24	2.614	1.09
5.030.050	1.757	0.73	3.482	1.45	2.144	0.89	2.345	0.98	1.976	0.82	2.341	0.98
5.010.075	4.283	1.78	4.750	1.98	4.339	1.81	3.617	1.51	5.145	2.14	4.427	1.84
5.020.075	2.681	1.12	3.812	1.59	1.810	0.75	3.169	1.32	3.194	1.33	2.933	1.22
5.030.075	1.901	0.79	3.785	1.58	2.205	0.92	2.384	0.99	2.059	0.86	2.467	1.03
5.005.100	5.954	2.48	5.805	2.42	9.567	3.99	3.579	1.49	6.844	2.85	6.350	2.65
5.010.100	4.853	2.02	4.805	2.00	4.709	1.96	3.694	1.54	6.418	2.67	4.896	2.04
5.020.100	2.235	0.93	3.684	1.54	1.790	0.75	3.641	1.52	3.327	1.39	2.936	1.22
5.030.100	1.957	0.82	3.893	1.62	2.256	0.94	2.596	1.08	2.107	0.88	2.562	1.07
6.020.025	4.360	1.51	3.706	1.29	3.863	1.34	3.675	1.28	3.773	1.31	3.875	1.35
6.030.025	3.301	1.15	3.000	1.04	2.140	0.74	2.917	1.01	3.234	1.12	2.919	1.01
6.010.050	5.748	2.00	5.782	2.01	9.843	3.42	3.761	1.31	6.888	2.39	6.404	2.22
6.020.050	4.143	1.44	4.421	1.54	4.218	1.46	3.797	1.32	4.080	1.42	4.132	1.43
6.030.050	4.606	1.60	3.349	1.16	2.528	0.88	3.390	1.18	3.369	1.17	3.448	1.20
6.010.075	5.426	1.88	5.539	1.92	8.609	2.99	3.799	1.32	6.832	2.37	6.041	2.10
6.020.075	4.354	1.51	4.516	1.57	4.767	1.66	3.907	1.36	5.164	1.79	4.542	1.58
6.030.075	4.985	1.73	3.630	1.26	2.651	0.92	3.534	1.23	3.739	1.30	3.708	1.29
6.005.100	6.513	2.26	5.321	1.85	12.143	4.22	4.394	1.53	10.508	3.65	7.776	2.70
6.010.100	6.075	2.11	6.079	2.11	9.030	3.14	4.105	1.43	7.291	2.53	6.516	2.26
6.020.100	4.715	1.64	4.925	1.71	5.071	1.76	3.981	1.38	5.711	1.98	4.881	1.69
6.030.100	5.115	1.78	3.971	1.38	2.557	0.89	3.346	1.16	3.784	1.31	3.755	1.30
7.020.025	5.194	1.55	5.282	1.57	6.798	2.02	4.361	1.30	5.204	1.55	5.368	1.60
7.030.025	4.836	1.44	4.673	1.39	4.355	1.30	3.963	1.18	2.869	0.85	4.139	1.23
7.010.050	7.001	2.08	5.665	1.69	12.086	3.60	4.350	1.29	8.370	2.49	7.494	2.23
7.020.050	4.796	1.43	5.330	1.59	6.766	2.01	4.908	1.46	6.307	1.88	5.622	1.67
7.030.050	4.593	1.37	4.539	1.35	4.788	1.43	4.174	1.24	5.034	1.50	4.626	1.38
7.010.075	6.898	2.05	5.925	1.76	11.283	3.36	4.138	1.23	7.895	2.35	7.228	2.15
7.020.075	5.425	1.61	6.225	1.85	7.214	2.15	4.844	1.44	7.762	2.31	6.294	1.87
7.030.075	4.742	1.41	4.451	1.32	5.125	1.53	4.503	1.34	5.655	1.68	4.895	1.46
7.005.100	9.575	2.85	7.516	2.24	17.283	5.14	8.931	2.66	9.557	2.84	10.573	3.15
7.010.100	6.480	1.93	6.532	1.94	11.527	3.43	4.475	1.33	10.650	3.17	7.933	2.36
7.020.100	5.787	1.72	5.890	1.75	7.296	2.17	4.853	1.44	7.201	2.14	6.206	1.85
7.030.100	4.786	1.42	4.524	1.35	5.228	1.56	4.602	1.37	6.024	1.79	5.033	1.50

Table C.4: Maximum Displacements, 2 Percent in 50, Hybrid Frames, $P_{col}/(f_c' A_g) = 0.10$

Frame	Ground Motion 2 - 1		Ground Motion 2 - 2		Ground Motion 2 - 3		Ground Motion 2 - 4		Ground Motion 2 - 5		Mean	
	Δ_{max}	$\dfrac{\Delta_{max}}{L_{col}}$	Δ_{max}	$\dfrac{\Delta_{max}}{L_{col}}$	Δ_{max}	$\dfrac{\Delta_{max}}{L_{col}}$	Δ_{max}	$\dfrac{\Delta_{max}}{L_{col}}$	Δ_{max}	$\dfrac{\Delta_{max}}{L_{col}}$	Δ_{max}	$\dfrac{\Delta_{max}}{L_{col}}$
	(in.)	(%)	(in.)	(%)	(in.)	(%)	(in.)	(%)	(in.)	(%)	(in.)	(%)
5.020.050	4.538	1.89	4.511	1.88	6.164	2.57	3.840	1.60	5.505	2.29	4.911	2.05
5.030.050	4.235	1.76	4.694	1.96	4.035	1.68	3.607	1.50	3.873	1.61	4.089	1.70
5.020.075	4.750	1.98	4.760	1.98	6.634	2.76	4.096	1.71	6.141	2.56	5.276	2.20
5.030.075	4.221	1.76	4.897	2.04	4.384	1.83	3.774	1.57	4.530	1.89	4.361	1.82
5.010.100	6.959	2.90	5.682	2.37	12.015	5.01	4.105	1.71	10.124	4.22	7.777	3.24
5.020.100	5.037	2.10	4.730	1.97	6.691	2.79	4.150	1.73	6.529	2.72	5.427	2.26
5.030.100	4.276	1.78	4.599	1.92	4.711	1.96	3.686	1.54	5.564	2.32	4.567	1.90
6.020.050	5.418	1.88	5.463	1.90	10.319	3.58	4.006	1.39	6.822	2.37	6.406	2.22
6.030.050	5.066	1.76	5.266	1.83	7.586	2.63	3.873	1.34	6.501	2.26	5.659	1.96
6.020.075	5.762	2.00	5.942	2.06	10.828	3.76	4.186	1.45	7.162	2.49	6.776	2.35
6.030.075	5.063	1.76	5.394	1.87	7.760	2.69	4.286	1.49	6.997	2.43	5.900	2.05
6.010.100	7.461	2.59	7.318	2.54	17.075	5.93	8.901	3.09	9.226	3.20	9.996	3.47
6.020.100	5.983	2.08	6.232	2.16	10.943	3.80	4.330	1.50	7.876	2.73	7.073	2.46
6.030.100	5.542	1.92	5.489	1.91	8.139	2.83	4.357	1.51	6.990	2.43	6.104	2.12
7.020.050	6.598	1.96	6.048	1.80	12.572	3.74	4.720	1.40	9.210	2.74	7.830	2.33
7.030.050	6.403	1.91	5.658	1.68	11.893	3.54	4.582	1.36	7.605	2.26	7.228	2.15
7.020.075	6.708	2.00	8.012	2.38	13.230	3.94	4.974	1.48	11.125	3.31	8.810	2.62
7.030.075	7.620	2.27	5.918	1.76	12.176	3.62	4.840	1.44	7.765	2.31	7.664	2.28
7.010.100	12.983	3.86	9.569	2.85	20.180	6.01	7.953	2.37	11.113	3.31	12.360	3.68
7.020.100	7.192	2.14	8.245	2.45	13.616	4.05	5.075	1.51	10.419	3.10	8.910	2.65
7.030.100	7.324	2.18	6.078	1.81	12.624	3.76	4.873	1.45	8.785	2.61	7.937	2.36
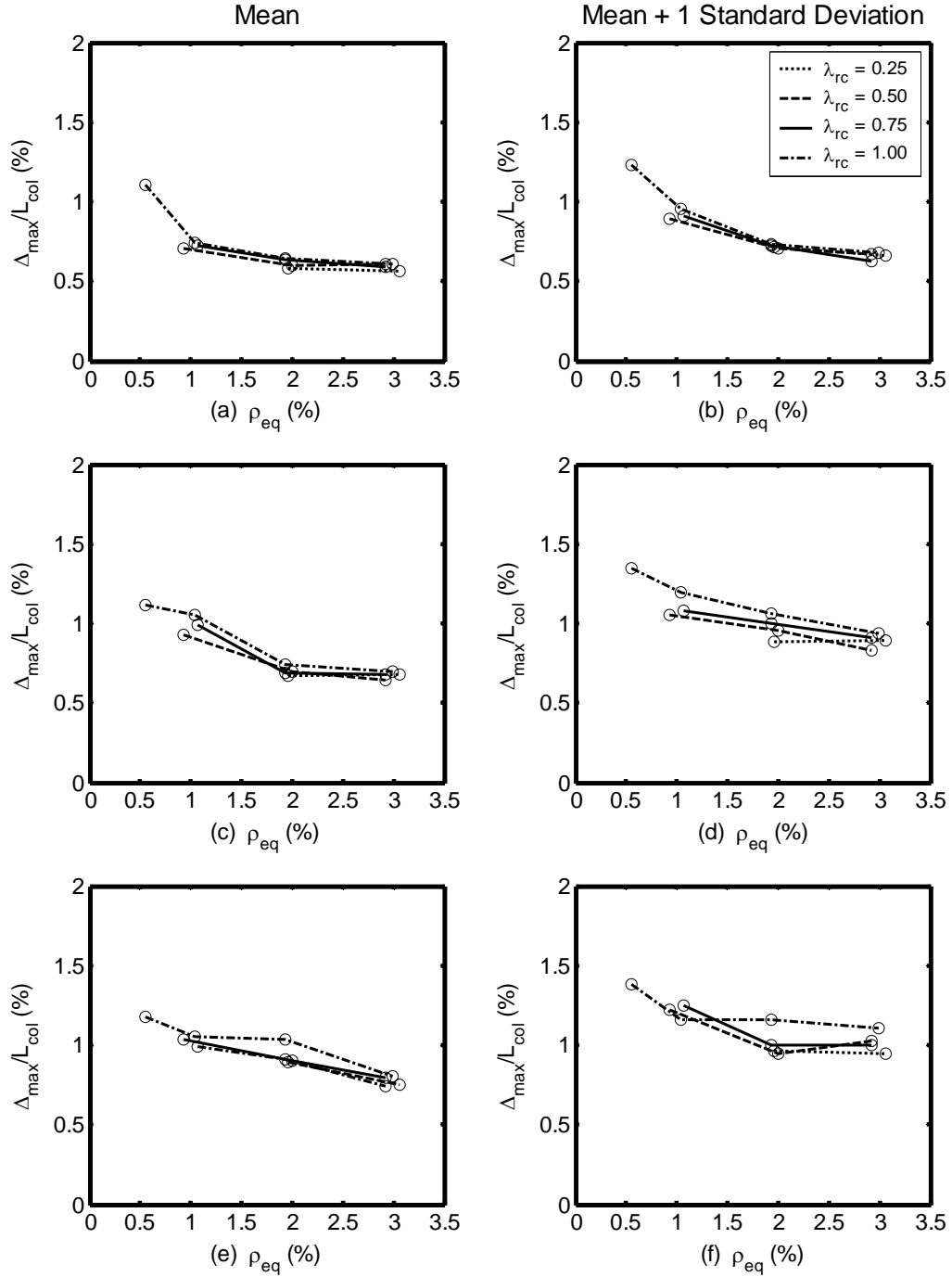
Figure C.1: Trends in Drift Ratio, 10 Percent in 50, Hybrid Frames, $P_{col}/(f_c^{'}A_g) = 0.05$

(a) and (b) $L_{col}/D_{col} = 5$, **(c) and (d)** $L_{col}/D_{col} = 6$, **and (e) and (f)** $L_{col}/D_{col} = 7$
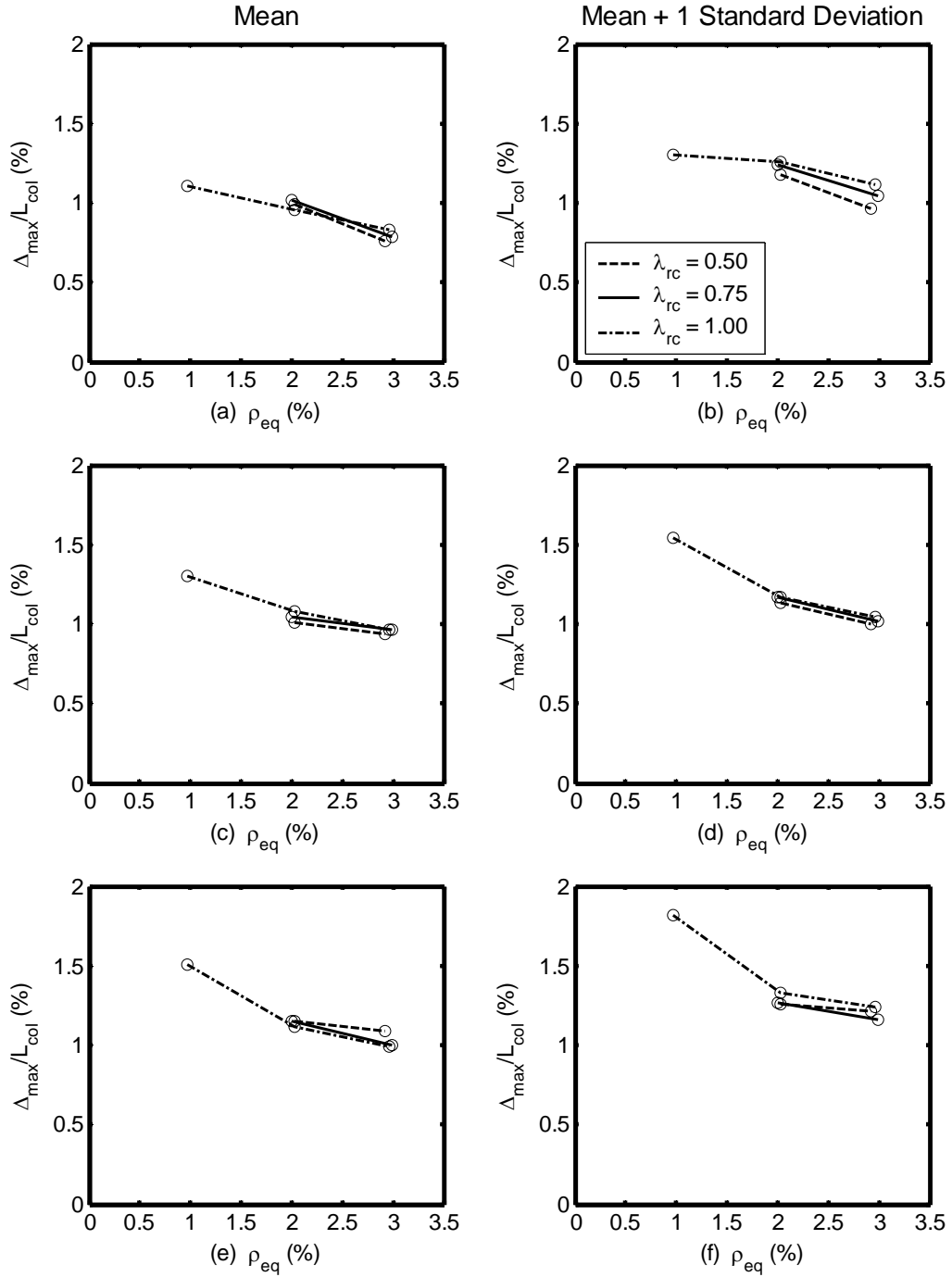
Figure C.2: Trends in Drift Ratio, 10 Percent in 50, Hybrid Frames, $P_{col}/(f_c^{'} A_g) = 0.10$
(a) and (b) $L_{col}/D_{col} = 5$**, (c) and (d)** $L_{col}/D_{col} = 6$**, and (e) and (f)** $L_{col}/D_{col} = 7$
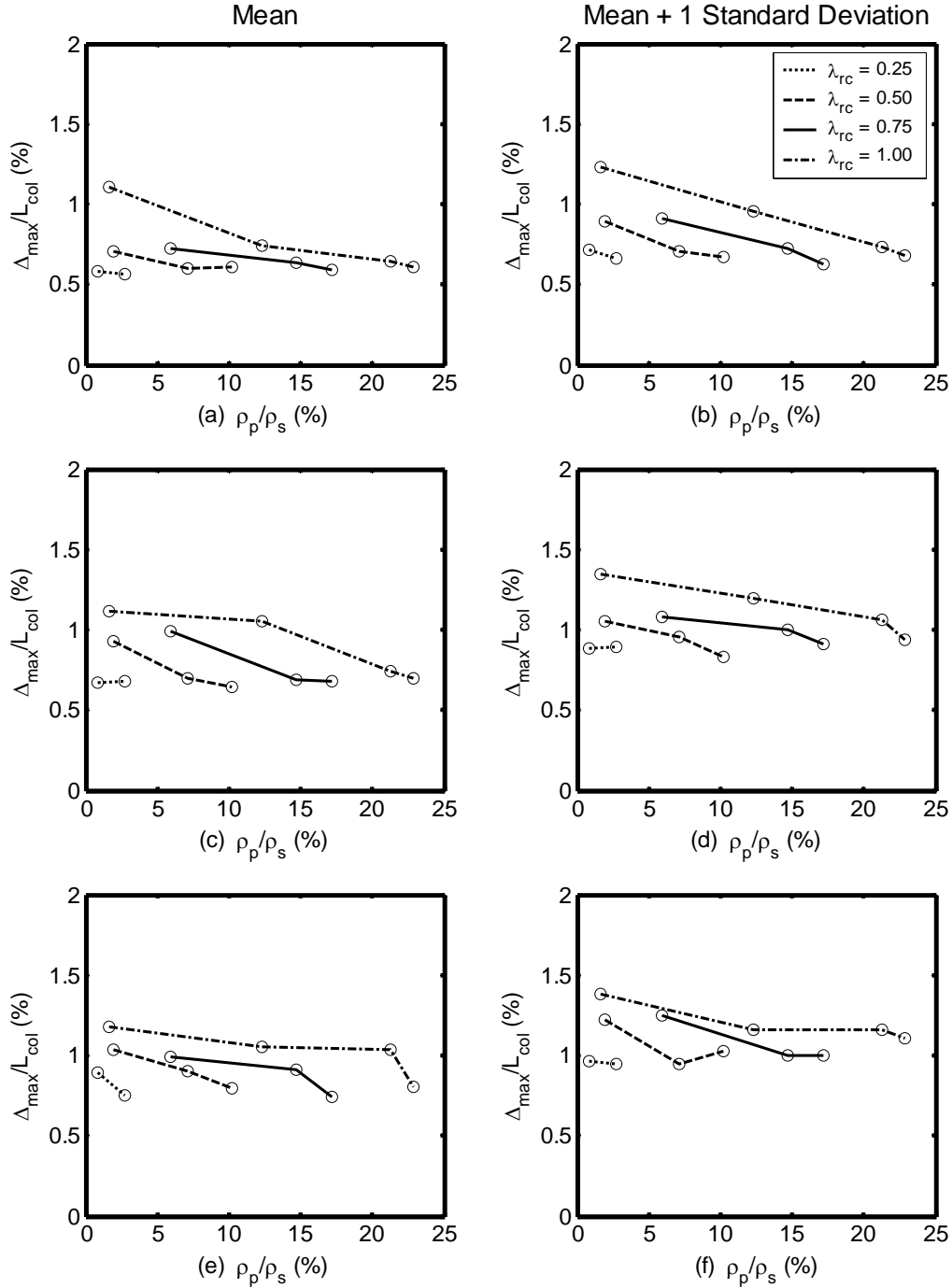
Figure C.3: Effect of Steel Ratio, 10 Percent in 50, Hybrid Frames, $P_{col}/(f_c' A_g) = 0.05$
(a) and (b) $L_{col}/D_{col} = 5$, (c) and (d) $L_{col}/D_{col} = 6$, and (e) and (f) $L_{col}/D_{col} = 7$
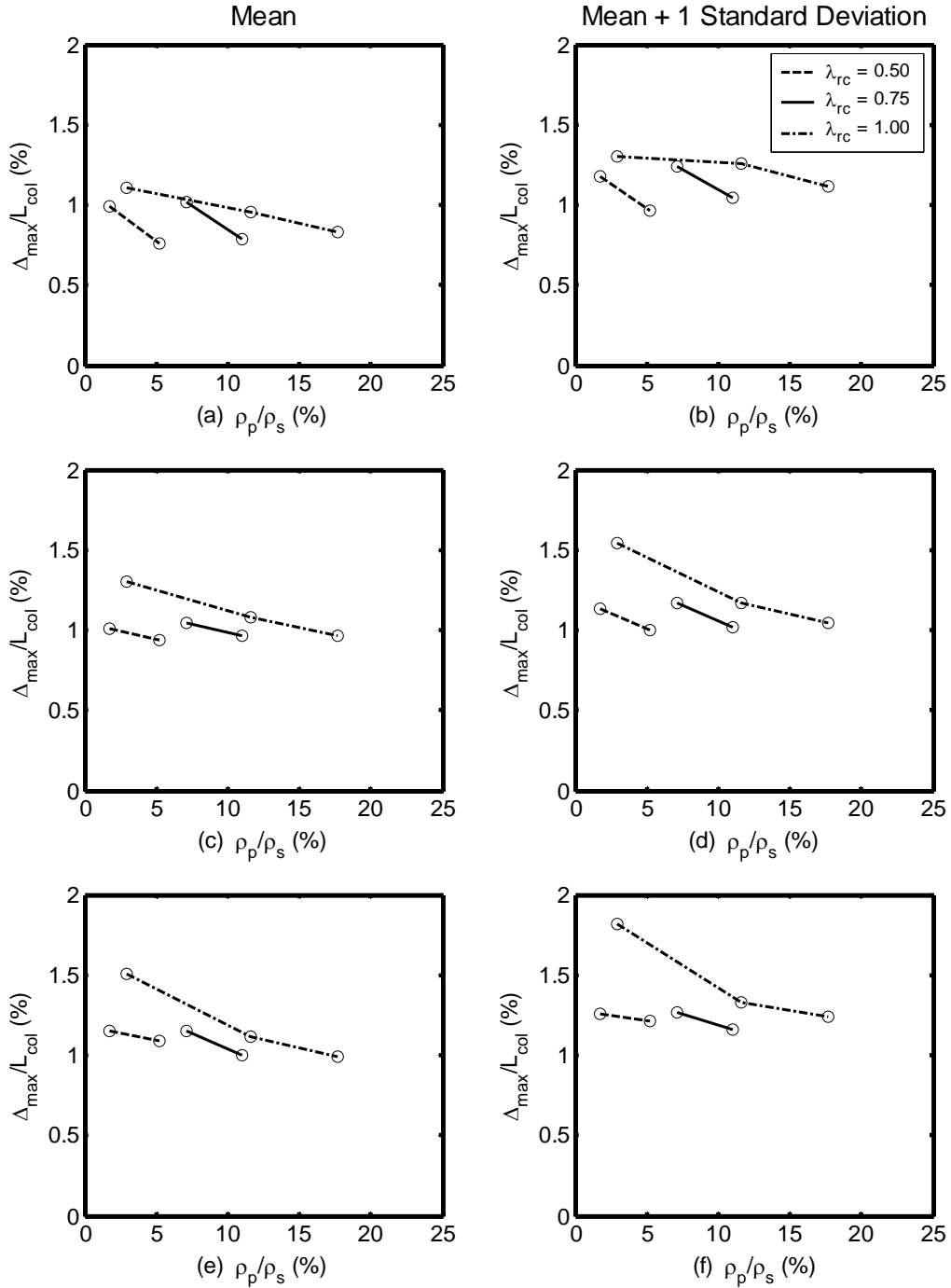
Figure C.4: Effect of Steel Ratio, 10 Percent in 50, Hybrid Frames, $P_{col}/(f_c' A_g) = 0.10$

(a) and (b) $L_{col}/D_{col} = 5$, (c) and (d) $L_{col}/D_{col} = 6$, and (e) and (f) $L_{col}/D_{col} = 7$
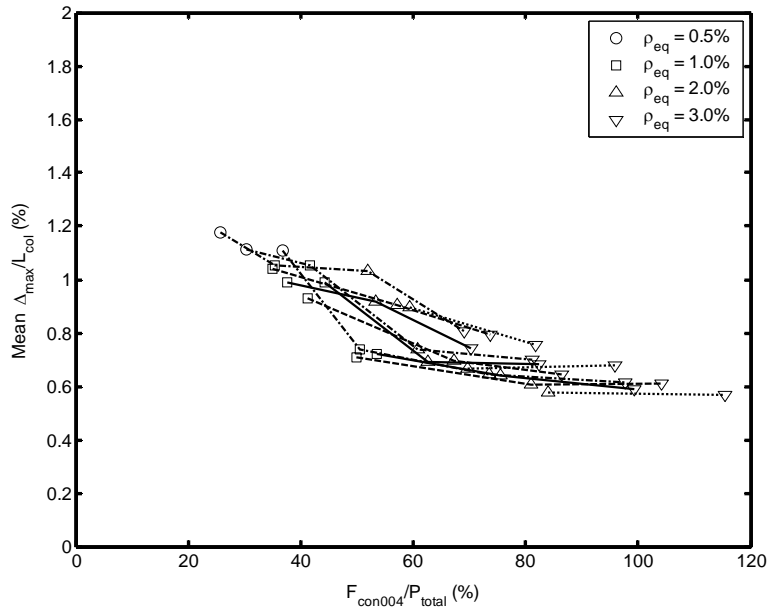
Figure C.5: Effect of Strength on Mean Drift Ratio, 10 Percent
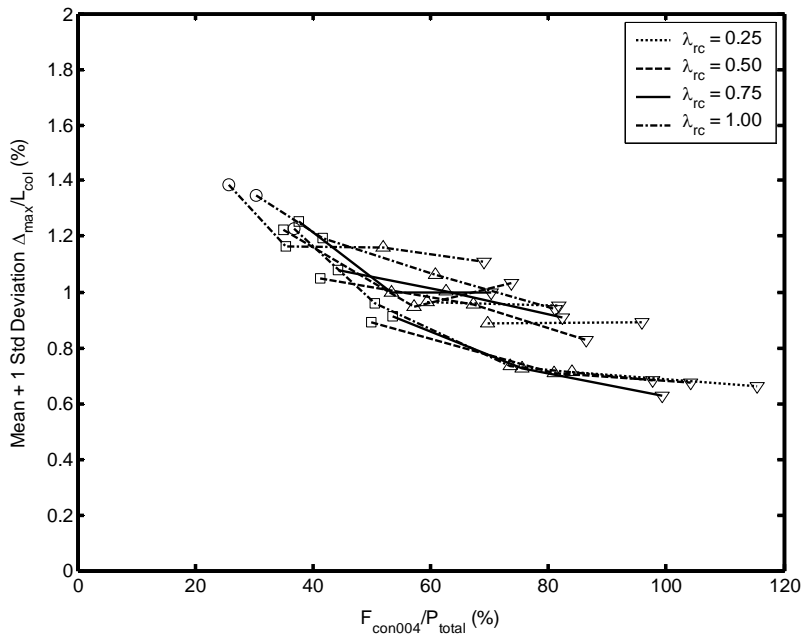
Figure C.6: Effect of Strength on Mean Plus One Standard Deviation Drift Ratio, 10 Percent in 50, Hybrid Frames, $P_{col}/(f_c^{'} A_g) = 0.05$
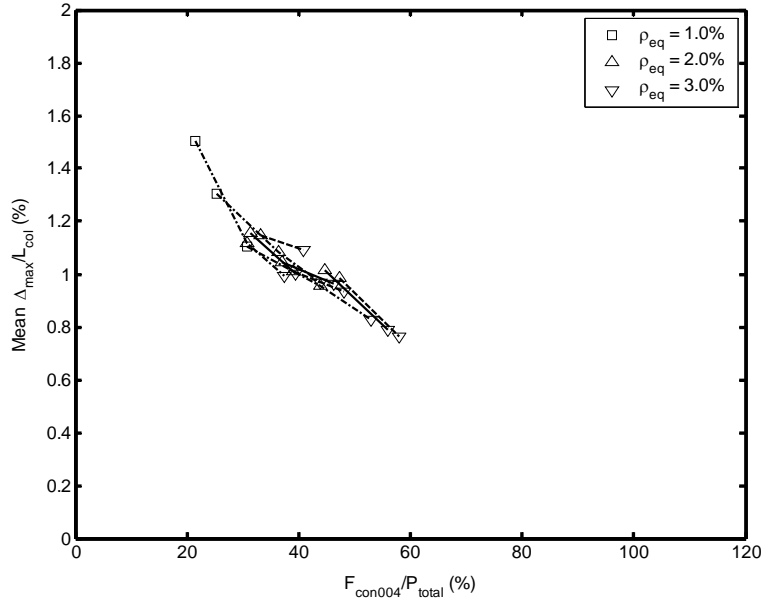
Figure C.7: Effect of Strength on Mean Drift Ratio, 10 Percent in 50, Hybrid Frames,
$$P_{col}\big/(f_c^{'}A_g) = 0.10$$
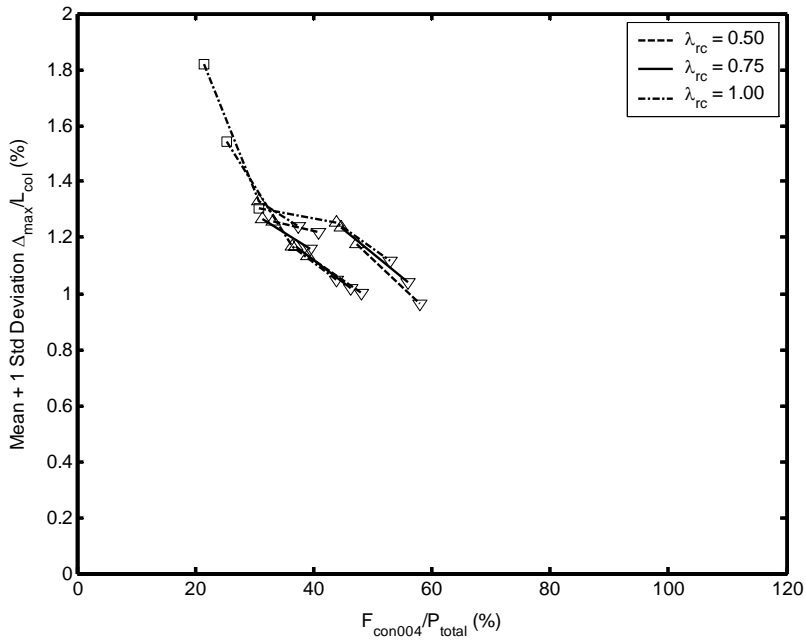
Figure C.8: Effect of Strength on Mean Plus One Standard Deviation Drift Ratio, 10 Percent in 50, Hybrid Frames, $P_{col}\big/(f_c^{'}A_g) = 0.10$

C-9
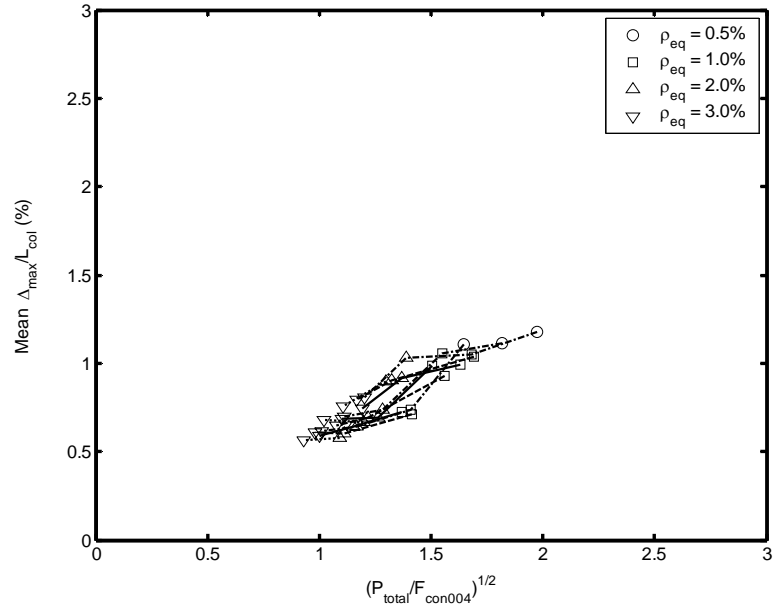
Figure C.9: **Effect of Stiffness on Mean Drift Ratio, 10 Percent in 50, Hybrid Frames,**
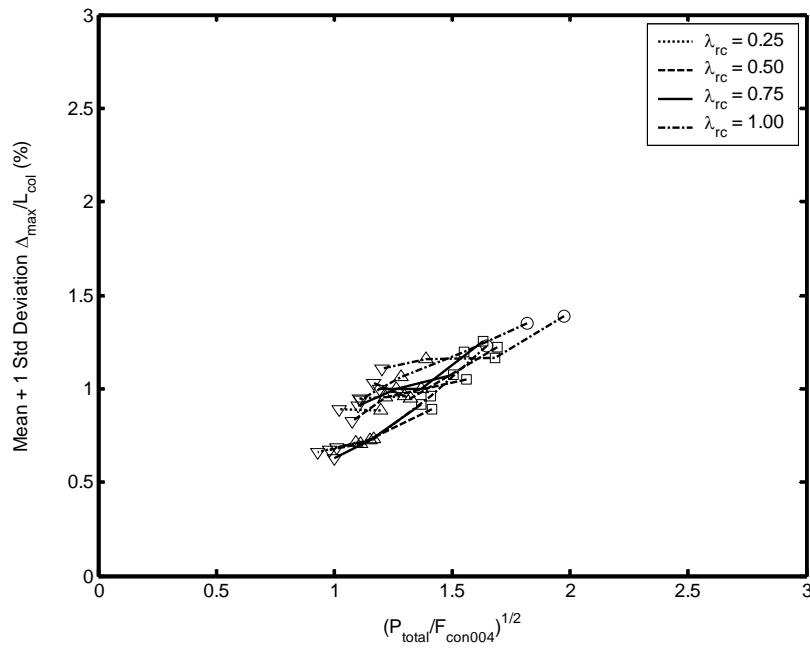
$$P_{col}/(f_c'A_g) = 0.05$$

Figure C.10: **Effect of Stiffness on Mean Plus One Standard Deviation Drift Ratio, 10 Percent in 50,**
Hybrid Frames, $P_{col}/(f_c'A_g) = 0.05$
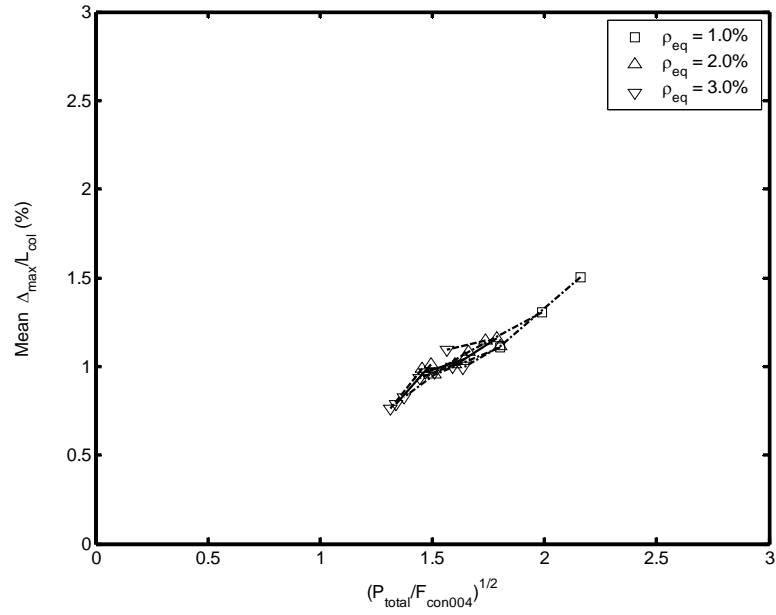
Figure C.11: Effect of Stiffness on Mean Drift Ratio, 10 Percent in 50, Hybrid Frames,
$$P_{col}\big/(f_c^{'}A_g) = 0.10$$
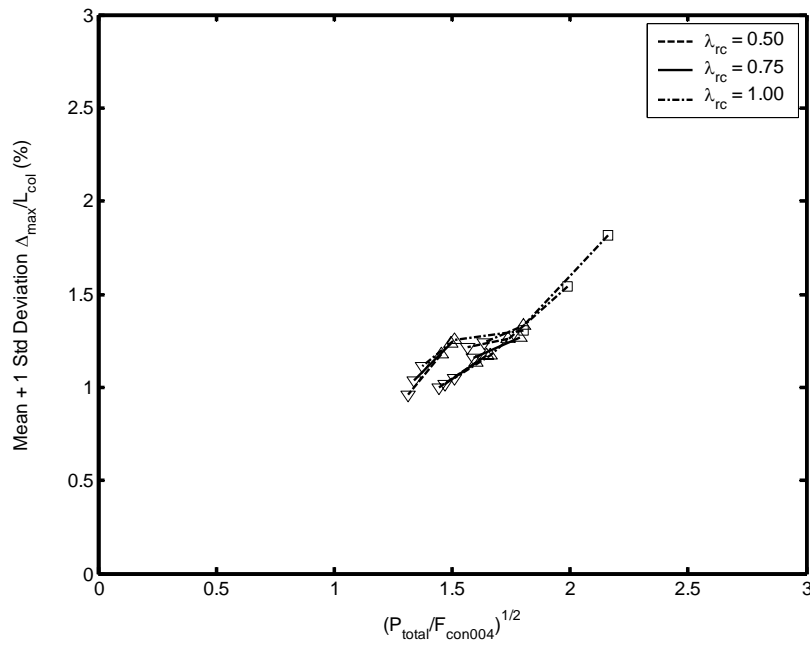
Figure C.12: Effect of Stiffness on Mean Plus One Standard Deviation Drift Ratio, 10 Percent in 50, Hybrid Frames, $P_{col}\big/(f_c^{'}A_g) = 0.10$

C-11
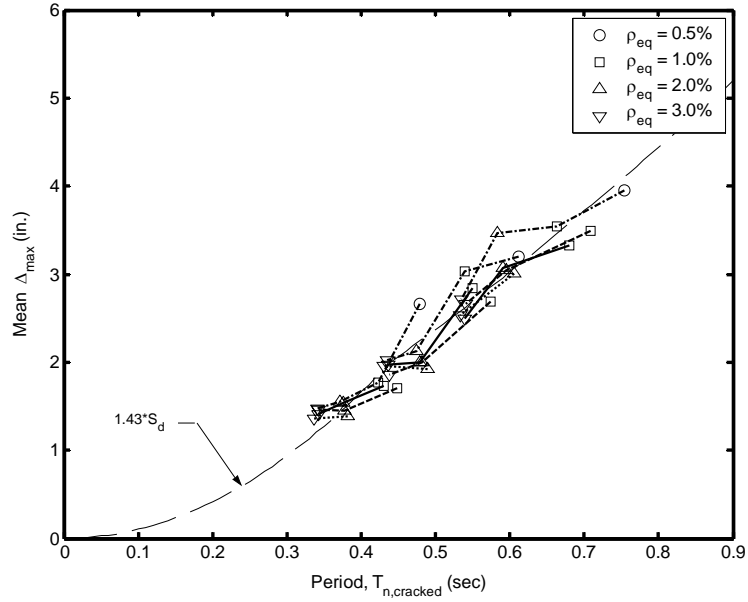
Figure C.13: Predicted and Mean Response, 10 Percent in 50, Hybrid Frames, $P_{col}/(f_c^{'}A_g) = 0.05$
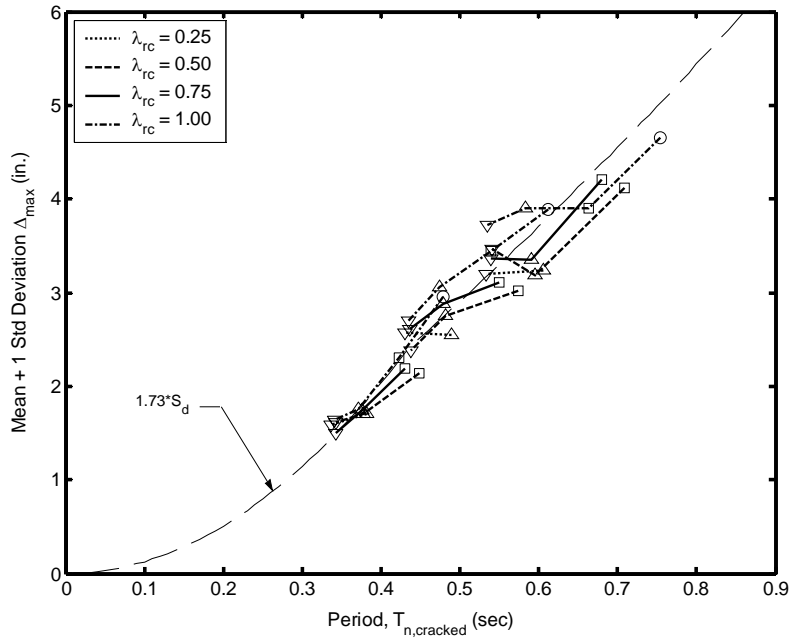
Figure C.14: Predicted and Mean Plus One Standard Deviation Response, 10 Percent in 50, Hybrid Frames, $P_{col}/(f_c^{'}A_g) = 0.05$
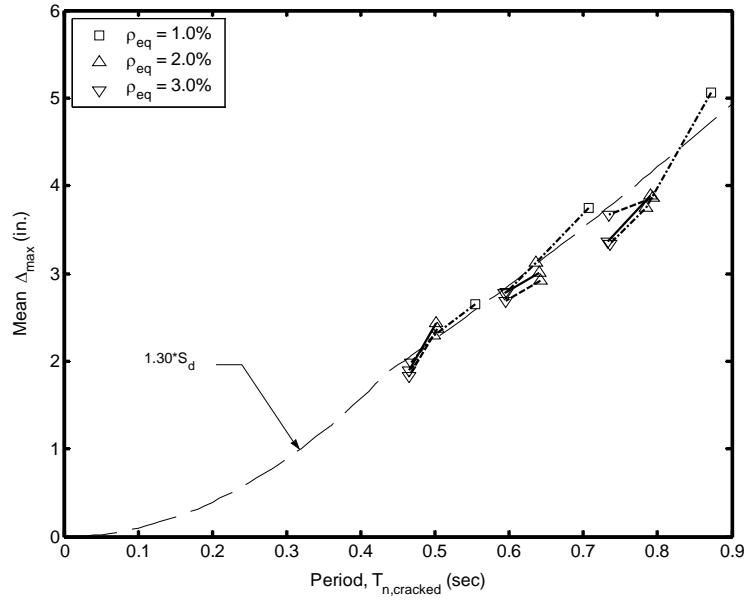
Figure C.15: **Predicted and Mean Response, 10 Percent in 50, Hybrid Frames,** $P_{col}/(f_c'A_g) = 0.10$
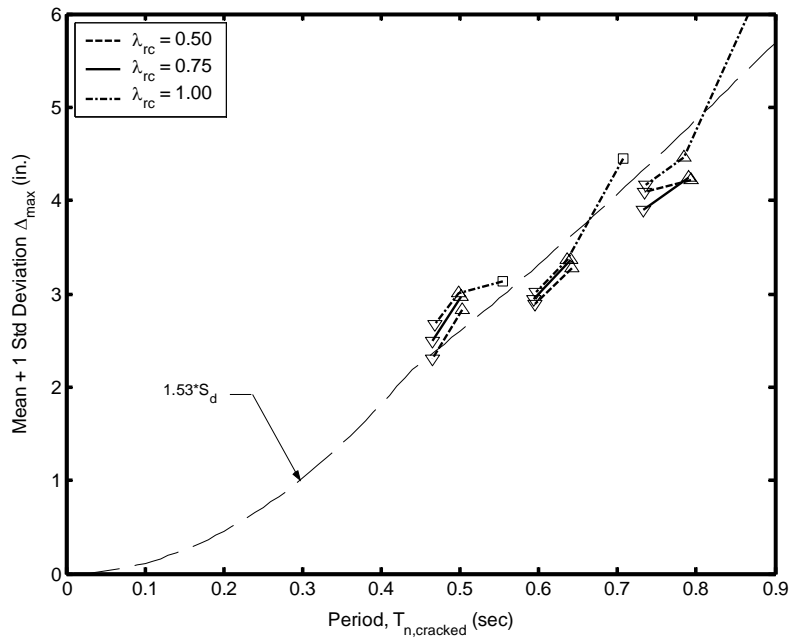
Figure C.16: **Predicted and Mean Plus One Standard Deviation Response, 10 Percent in 50, Hybrid Frames,** $P_{col}/(f_c'A_g) = 0.10$

C-13

APPENDIX D
DETAILS OF SEISMIC PERFORMANCE EVALUATION

Chapter 10 evaluated and compared the reinforced concrete frame and the hybrid frames. Displacement ductility, the onset of cover concrete spalling, the onset of bar buckling, the maximum strain in the longitudinal reinforcing bars, and an ultimate limit state were discussed. Chapter 10 contains figures of these quantities for the 2 percent in 50 ground motions. Except for the absolute values, the trends observed in the 2 percent in 50 ground motion plots were the same as those observed in the 10 percent in 50 ground motion plots. This appendix presents plots of these quantities for the 10 percent in 50 ground motions because these plots were not provided in Chapter 10. This appendix also contains tables summarizing these quantities for both 10 percent in 50 ground motions and the 2 percent in 50 ground motions. For further details relating to the quantities presented in the figures of this appendix, refer to Chapter 10.

Table D.1: Displacement Ductility Demand, Reinforced Concrete Frames

Frame	10% in 50 Ground Motions						2% in 50 Ground Motions					
	10 - 1	10 - 2	10 - 3	10 - 4	10 - 5	Mean	2 - 1	2 - 2	2 - 3	2 - 4	2 - 5	Mean
5.005.05	2.38	2.50	2.46	2.26	2.93	2.51	5.41	5.69	9.74	3.53	6.86	6.25
5.005.10	3.08	3.49	4.17	2.80	4.89	3.68	10.33	7.73	DNC	9.38	10.98	9.61
5.005.15	4.17	3.39	5.27	2.69	7.23	4.55	DNC	9.14	DNC	9.54	DNC	9.34
5.010.05	2.14	1.90	0.97	1.85	1.44	1.66	3.31	3.40	4.10	2.95	3.46	3.44
5.010.10	2.32	2.34	2.71	2.14	2.81	2.46	5.59	4.99	9.80	3.27	6.13	5.96
5.010.15	3.00	2.64	3.21	2.46	3.03	2.87	5.39	5.50	DNC	7.05	7.47	6.35
5.020.05	1.04	1.64	0.82	1.25	1.53	1.25	1.97	2.26	1.39	1.90	2.10	1.92
5.020.10	1.87	2.16	1.53	1.74	1.78	1.82	3.23	3.14	4.41	2.85	3.86	3.50
5.020.15	1.89	1.87	2.29	1.68	2.19	1.98	4.06	3.98	8.05	2.72	4.88	4.74
5.030.05	0.71	1.35	0.82	1.05	1.22	1.03	1.26	2.08	1.33	1.44	1.35	1.49
5.030.10	1.76	1.43	0.98	1.38	0.89	1.29	2.89	2.80	2.65	2.42	2.49	2.65
5.030.15	1.74	1.78	1.87	1.67	1.65	1.74	3.39	3.39	5.54	2.40	3.92	3.73
6.005.05	2.64	2.44	2.26	1.79	2.50	2.33	4.64	4.07	9.24	3.35	7.59	5.78
6.005.10	3.22	3.39	4.62	2.56	5.12	3.78	8.68	7.64	DNC	6.81	10.27	8.35
6.005.15	5.72	2.84	5.99	4.76	4.74	4.81	8.53	11.89	DNC	4.97	9.15	8.63
6.010.05	1.59	1.53	1.81	1.44	2.06	1.68	3.35	3.24	5.62	2.41	3.85	3.69
6.010.10	2.68	2.43	2.59	1.96	2.68	2.47	4.16	4.74	9.78	5.20	5.37	5.85
6.010.15	3.06	2.81	4.23	2.68	4.32	3.42	8.29	6.12	DNC	4.63	6.89	6.48
6.020.05	1.43	1.38	0.85	1.31	1.03	1.20	2.14	2.28	2.18	1.93	2.08	2.12
6.020.10	1.77	1.77	1.91	1.58	1.82	1.77	2.76	2.85	5.68	2.17	3.78	3.45
6.020.15	1.73	1.87	2.58	1.72	2.52	2.08	3.35	3.66	7.72	3.51	6.02	4.85
6.030.05	1.12	1.17	0.47	1.24	1.22	1.04	2.08	1.83	1.44	1.71	1.75	1.76
6.030.10	1.57	1.47	1.55	1.34	1.44	1.48	2.55	2.67	3.57	1.93	3.01	2.75
6.030.15	1.84	1.83	1.77	1.32	1.97	1.75	3.37	2.62	6.20	2.22	3.52	3.58
7.005.05	2.90	2.02	2.70	1.71	2.66	2.40	6.34	4.38	10.30	4.91	5.52	6.29
7.005.10	4.64	2.35	4.76	3.95	3.99	3.94	7.05	9.72	17.20	4.26	6.99	9.04
7.005.15	4.66	3.19	6.30	3.73	4.78	4.53	7.48	9.97	DNC	5.23	7.35	7.51
7.010.05	1.79	1.81	1.69	1.34	1.71	1.67	3.42	2.56	5.67	2.31	3.52	3.50
7.010.10	2.45	2.45	3.27	2.45	2.87	2.70	5.96	4.60	9.19	3.92	4.80	5.70
7.010.15	3.45	2.28	3.80	2.29	3.09	2.98	5.44	5.74	DNC	4.04	6.10	5.33
7.020.05	1.36	1.29	1.56	1.31	1.39	1.38	2.09	2.12	2.50	1.90	2.34	2.19
7.020.10	1.49	1.63	1.89	1.37	1.75	1.63	2.80	2.82	5.23	2.07	3.23	3.23
7.020.15	1.74	2.15	2.74	1.47	1.99	2.02	4.73	3.47	7.05	3.41	3.72	4.48
7.030.05	1.28	1.43	0.79	1.29	0.99	1.16	1.68	1.83	1.94	1.63	1.72	1.76
7.030.10	1.31	1.62	1.56	1.44	1.78	1.54	2.83	2.10	4.67	1.91	2.90	2.88
7.030.15	2.23	1.48	2.17	1.34	1.98	1.84	2.82	3.02	5.07	1.99	4.36	3.45

Note: DNC indicates earthquake analysis did not converge

Table D.2: Displacement Ductility Demand, Hybrid Frames, $P_{col}/(f_c' A_g) = 0.05$

Frame	10% in 50 Ground Motions						2% in 50 Ground Motions					
	10 - 1	10 - 2	10 - 3	10 - 4	10 - 5	Mean	2 - 1	2 - 2	2 - 3	2 - 4	2 - 5	Mean
5.020.025	0.96	1.61	0.98	1.18	1.06	1.16	1.96	2.76	1.63	2.06	2.35	2.15
5.030.025	0.78	1.06	1.09	1.17	1.22	1.06	1.35	2.03	1.61	1.76	1.46	1.64
5.010.050	2.14	1.80	0.97	1.77	1.96	1.73	4.33	4.17	5.13	3.60	5.36	4.52
5.020.050	1.16	1.60	1.13	1.43	1.10	1.28	1.95	3.19	1.63	2.16	2.64	2.31
5.030.050	1.13	1.23	1.13	1.21	1.43	1.23	1.47	2.91	1.79	1.96	1.65	1.96
5.010.075	2.07	1.87	0.94	1.97	2.05	1.78	4.40	4.88	4.46	3.72	5.29	4.55
5.020.075	1.45	1.74	1.23	1.60	1.33	1.47	2.57	3.65	1.73	3.04	3.06	2.81
5.030.075	1.14	1.22	1.18	1.32	1.33	1.24	1.66	3.32	1.93	2.09	1.80	2.16
5.005.100	3.66	3.10	3.01	2.81	3.47	3.21	7.18	7.00	11.54	4.32	8.26	7.66
5.010.100	2.65	2.34	1.16	2.23	1.66	2.01	5.50	5.44	5.33	4.18	7.27	5.55
5.020.100	1.58	1.77	1.27	1.74	1.40	1.55	2.25	3.70	1.80	3.66	3.34	2.95
5.030.100	1.19	1.36	1.18	1.33	1.56	1.32	1.76	3.50	2.03	2.34	1.90	2.31
6.020.025	1.71	1.24	0.67	1.27	0.99	1.18	2.67	2.27	2.37	2.25	2.31	2.37
6.030.025	1.06	1.39	0.53	1.29	1.34	1.12	1.89	1.72	1.23	1.67	1.85	1.67
6.010.050	2.05	1.76	2.08	1.81	2.40	2.02	4.33	4.35	7.41	2.83	5.19	4.82
6.020.050	1.93	1.38	0.60	1.47	1.15	1.31	2.71	2.89	2.76	2.48	2.67	2.70
6.030.050	1.16	1.56	0.65	1.19	1.18	1.15	2.84	2.07	1.56	2.09	2.08	2.13
6.010.075	1.90	2.19	2.37	2.04	2.35	2.17	4.14	4.23	6.57	2.90	5.21	4.61
6.020.075	2.30	1.55	0.62	1.57	1.05	1.42	3.10	3.21	3.39	2.78	3.67	3.23
6.030.075	1.15	1.88	0.72	1.38	1.26	1.28	3.23	2.35	1.72	2.29	2.43	2.41
6.005.100	2.73	2.85	2.76	2.21	3.89	2.89	5.87	4.80	10.95	3.96	9.47	7.01
6.010.100	2.17	2.39	2.83	2.46	3.01	2.57	5.14	5.14	7.63	3.47	6.16	5.51
6.020.100	2.53	1.88	0.72	1.68	1.14	1.59	3.53	3.68	3.79	2.98	4.27	3.65
6.030.100	1.06	1.91	0.74	1.60	1.44	1.35	3.42	2.65	1.71	2.24	2.53	2.51
7.020.025	1.44	1.35	1.57	1.28	1.41	1.41	2.44	2.48	3.19	2.05	2.44	2.52
7.030.025	1.49	1.13	0.72	1.25	0.97	1.11	2.12	2.05	1.91	1.74	1.26	1.82
7.010.050	2.02	1.98	1.92	1.63	2.62	2.03	4.07	3.30	7.03	2.53	4.87	4.36
7.020.050	1.49	1.65	1.53	1.49	1.50	1.53	2.41	2.68	3.40	2.47	3.17	2.83
7.030.050	1.70	1.56	0.82	1.28	0.95	1.26	2.18	2.15	2.27	1.98	2.39	2.20
7.010.075	2.18	1.38	2.11	1.52	2.64	1.97	4.07	3.50	6.66	2.44	4.66	4.26
7.020.075	1.68	1.93	1.68	1.63	1.52	1.69	2.98	3.42	3.96	2.66	4.26	3.46
7.030.075	1.27	1.69	0.56	1.51	1.22	1.25	2.37	2.23	2.56	2.25	2.83	2.45
7.005.100	2.89	2.43	3.21	2.10	3.23	2.77	6.72	5.28	12.13	6.27	6.71	7.42
7.010.100	2.54	2.21	2.39	1.96	2.52	2.32	4.26	4.29	7.57	2.94	7.00	5.21
7.020.100	1.84	2.13	1.66	2.13	2.27	2.01	3.35	3.41	4.23	2.81	4.17	3.60
7.030.100	1.75	1.76	0.52	1.64	1.33	1.40	2.47	2.34	2.70	2.38	3.11	2.60

Table D.3: Displacement Ductility Demand, Hybrid Frames, $P_{col}/(f_c' A_g) = 0.10$

Frame	10% in 50 Ground Motions						2% in 50 Ground Motions					
	10 - 1	10 - 2	10 - 3	10 - 4	10 - 5	Mean	2 - 1	2 - 2	2 - 3	2 - 4	2 - 5	Mean
5.020.050	2.47	2.40	1.56	1.92	1.81	2.03	3.89	3.87	5.29	3.29	4.72	4.21
5.030.050	1.89	1.46	0.85	1.59	1.65	1.49	3.45	3.82	3.28	2.93	3.15	3.33
5.020.075	2.79	2.61	1.70	2.16	1.79	2.21	4.31	4.32	6.03	3.72	5.58	4.79
5.030.075	2.16	1.69	0.77	1.62	1.76	1.60	3.56	4.13	3.70	3.19	3.82	3.68
5.010.100	2.70	2.16	3.27	2.74	3.45	2.86	7.51	6.13	12.97	4.43	10.92	8.39
5.020.100	2.69	2.78	1.74	2.33	1.20	2.15	4.71	4.43	6.26	3.88	6.11	5.08
5.030.100	2.54	1.79	0.84	1.72	1.87	1.75	3.76	4.04	4.14	3.24	4.89	4.02
6.020.050	1.77	1.79	2.06	1.53	2.08	1.85	3.43	3.46	6.54	2.54	4.32	4.06
6.030.050	1.52	1.69	1.78	1.58	1.52	1.62	3.04	3.16	4.56	2.33	3.91	3.40
6.020.075	1.94	1.94	2.25	1.71	2.30	2.03	3.88	4.00	7.30	2.82	4.83	4.57
6.030.075	1.64	1.76	1.90	1.67	1.71	1.74	3.17	3.37	4.85	2.68	4.38	3.69
6.010.100	3.00	2.89	3.21	2.24	3.79	3.03	6.02	5.90	13.77	7.18	7.44	8.06
6.020.100	2.11	2.01	2.35	2.03	2.36	2.17	4.16	4.34	7.62	3.01	5.48	4.92
6.030.100	1.85	1.78	1.90	1.58	1.98	1.82	3.62	3.59	5.32	2.85	4.57	3.99
7.020.050	1.89	1.77	2.04	1.65	2.07	1.88	3.22	2.95	6.14	2.31	4.50	3.82
7.030.050	1.69	1.92	1.73	1.39	1.76	1.70	2.96	2.62	5.50	2.12	3.52	3.34
7.020.075	2.12	1.89	2.22	1.76	2.13	2.02	3.49	4.17	6.89	2.59	5.79	4.59
7.030.075	1.82	1.25	1.81	1.45	1.78	1.62	3.68	2.85	5.87	2.33	3.75	3.70
7.010.100	2.96	2.97	4.13	2.36	3.46	3.17	8.15	6.01	12.67	4.99	6.98	7.76
7.020.100	2.13	2.04	2.26	1.36	2.31	2.02	3.88	4.44	7.34	2.74	5.62	4.80
7.030.100	1.98	1.06	1.89	1.47	2.04	1.69	3.70	3.07	6.38	2.46	4.44	4.01

Table D.4: Probability of the Occurrence of Cover Spalling, Reinforced Concrete Frames

Frame	10% in 50 Ground Motions						2% in 50 Ground Motions					
	10 - 1	10 - 2	10 - 3	10 - 4	10 - 5	Mean	2 - 1	2 - 2	2 - 3	2 - 4	2 - 5	Mean
5.005.05	0.05	0.06	0.06	0.05	0.09	0.06	0.46	0.52	0.98	0.15	0.74	0.57
5.005.10	0.10	0.14	0.24	0.08	0.36	0.18	0.99	0.86	DNC	0.97	1.00	0.96
5.005.15	0.30	0.17	0.54	0.09	0.88	0.40	DNC	0.99	DNC	0.99	DNC	0.99
5.010.05	0.06	0.05	0.01	0.04	0.02	0.04	0.20	0.22	0.36	0.15	0.23	0.23
5.010.10	0.08	0.08	0.12	0.06	0.13	0.10	0.73	0.59	1.00	0.20	0.83	0.67
5.010.15	0.19	0.13	0.23	0.11	0.19	0.17	0.75	0.77	DNC	0.96	0.98	0.87
5.020.05	0.02	0.04	0.01	0.02	0.04	0.03	0.07	0.10	0.03	0.06	0.08	0.07
5.020.10	0.07	0.10	0.04	0.06	0.06	0.06	0.31	0.28	0.63	0.22	0.48	0.38
5.020.15	0.08	0.08	0.14	0.06	0.12	0.10	0.60	0.58	1.00	0.22	0.81	0.64
5.030.05	0.01	0.03	0.01	0.02	0.03	0.02	0.03	0.09	0.03	0.04	0.03	0.04
5.030.10	0.07	0.04	0.02	0.04	0.02	0.04	0.27	0.25	0.21	0.16	0.18	0.21
5.030.15	0.08	0.08	0.09	0.07	0.07	0.08	0.47	0.47	0.95	0.19	0.64	0.54
6.005.05	0.07	0.06	0.05	0.03	0.06	0.05	0.34	0.24	0.98	0.14	0.88	0.52
6.005.10	0.12	0.14	0.33	0.07	0.43	0.22	0.96	0.88	DNC	0.77	0.99	0.90
6.005.15	0.66	0.11	0.72	0.45	0.45	0.48	0.98	1.00	DNC	0.50	0.99	0.87
6.010.05	0.03	0.03	0.04	0.03	0.06	0.04	0.23	0.21	0.76	0.09	0.34	0.33
6.010.10	0.13	0.10	0.12	0.06	0.13	0.11	0.43	0.57	1.00	0.68	0.72	0.68
6.010.15	0.22	0.17	0.51	0.15	0.53	0.32	1.00	0.90	DNC	0.61	0.96	0.87
6.020.05	0.04	0.03	0.01	0.03	0.02	0.03	0.10	0.12	0.11	0.08	0.09	0.10
6.020.10	0.07	0.07	0.08	0.05	0.07	0.07	0.22	0.24	0.92	0.11	0.50	0.40
6.020.15	0.07	0.09	0.21	0.07	0.20	0.13	0.43	0.52	1.00	0.48	0.97	0.68
6.030.05	0.02	0.03	0.01	0.03	0.03	0.02	0.11	0.08	0.04	0.06	0.07	0.07
6.030.10	0.06	0.05	0.06	0.04	0.05	0.05	0.22	0.24	0.51	0.10	0.34	0.28
6.030.15	0.10	0.10	0.09	0.04	0.12	0.09	0.51	0.27	0.99	0.17	0.56	0.50
7.005.05	0.10	0.04	0.08	0.03	0.08	0.07	0.72	0.32	1.00	0.43	0.56	0.60
7.005.10	0.36	0.06	0.38	0.23	0.24	0.25	0.82	0.99	1.00	0.29	0.81	0.78
7.005.15	0.45	0.16	0.80	0.25	0.48	0.43	0.93	1.00	DNC	0.58	0.92	0.86
7.010.05	0.05	0.05	0.04	0.02	0.04	0.04	0.28	0.12	0.81	0.09	0.30	0.32
7.010.10	0.11	0.11	0.25	0.11	0.17	0.15	0.86	0.57	1.00	0.40	0.62	0.69
7.010.15	0.33	0.10	0.42	0.10	0.24	0.24	0.82	0.87	DNC	0.48	0.92	0.77
7.020.05	0.04	0.03	0.05	0.03	0.04	0.04	0.10	0.11	0.17	0.08	0.14	0.12
7.020.10	0.05	0.06	0.09	0.04	0.07	0.06	0.26	0.26	0.89	0.11	0.37	0.38
7.020.15	0.08	0.14	0.28	0.05	0.11	0.13	0.85	0.50	1.00	0.48	0.59	0.68
7.030.05	0.03	0.04	0.01	0.04	0.02	0.03	0.07	0.09	0.10	0.06	0.07	0.08
7.030.10	0.04	0.07	0.06	0.05	0.09	0.06	0.32	0.14	0.86	0.11	0.34	0.35
7.030.15	0.19	0.06	0.18	0.05	0.14	0.12	0.36	0.43	0.95	0.14	0.84	0.54

Note: DNC indicates earthquake analysis did not converge

Table D.5: Probability of the Occurrence of Cover Spalling, Hybrid Frames, $P_{col}/(f_c' A_g) = 0.05$

Frame	10% in 50 Ground Motions						2% in 50 Ground Motions					
	10 - 1	10 - 2	10 - 3	10 - 4	10 - 5	Mean	2 - 1	2 - 2	2 - 3	2 - 4	2 - 5	Mean
5.020.025	0.01	0.03	0.01	0.02	0.01	0.02	0.05	0.11	0.03	0.05	0.07	0.06
5.030.025	0.01	0.02	0.02	0.02	0.02	0.02	0.02	0.06	0.04	0.04	0.03	0.04
5.010.050	0.04	0.02	0.01	0.02	0.03	0.02	0.22	0.20	0.35	0.13	0.40	0.26
5.020.050	0.01	0.03	0.01	0.02	0.01	0.02	0.04	0.16	0.03	0.05	0.09	0.07
5.030.050	0.02	0.02	0.02	0.02	0.03	0.02	0.03	0.16	0.04	0.05	0.04	0.06
5.010.075	0.03	0.03	0.01	0.03	0.03	0.03	0.24	0.31	0.24	0.15	0.38	0.26
5.020.075	0.02	0.03	0.01	0.02	0.02	0.02	0.07	0.20	0.03	0.12	0.12	0.11
5.030.075	0.02	0.02	0.02	0.02	0.02	0.02	0.04	0.22	0.05	0.06	0.04	0.08
5.005.100	0.09	0.06	0.05	0.04	0.07	0.06	0.52	0.49	0.97	0.14	0.69	0.56
5.010.100	0.05	0.04	0.01	0.03	0.02	0.03	0.34	0.33	0.32	0.16	0.65	0.36
5.020.100	0.02	0.03	0.02	0.03	0.02	0.02	0.05	0.19	0.03	0.18	0.14	0.12
5.030.100	0.02	0.02	0.02	0.02	0.03	0.02	0.04	0.26	0.06	0.08	0.05	0.10
6.020.025	0.04	0.02	0.01	0.02	0.01	0.02	0.12	0.08	0.09	0.08	0.08	0.09
6.030.025	0.02	0.03	0.01	0.02	0.03	0.02	0.06	0.05	0.02	0.04	0.06	0.05
6.010.050	0.04	0.03	0.04	0.03	0.05	0.04	0.26	0.26	0.82	0.08	0.42	0.37
6.020.050	0.05	0.02	0.01	0.03	0.02	0.02	0.12	0.14	0.12	0.09	0.11	0.12
6.030.050	0.02	0.04	0.01	0.02	0.02	0.02	0.18	0.07	0.04	0.08	0.07	0.09
6.010.075	0.03	0.04	0.05	0.04	0.05	0.04	0.23	0.24	0.69	0.09	0.42	0.33
6.020.075	0.06	0.03	0.01	0.03	0.01	0.03	0.14	0.16	0.18	0.11	0.23	0.16
6.030.075	0.02	0.06	0.01	0.03	0.02	0.03	0.24	0.10	0.04	0.09	0.11	0.12
6.005.100	0.05	0.05	0.05	0.03	0.11	0.06	0.36	0.21	0.96	0.12	0.88	0.50
6.010.100	0.03	0.04	0.06	0.04	0.07	0.05	0.32	0.32	0.76	0.11	0.51	0.40
6.020.100	0.08	0.04	0.01	0.03	0.01	0.03	0.19	0.21	0.23	0.12	0.32	0.21
6.030.100	0.02	0.06	0.01	0.04	0.03	0.03	0.28	0.14	0.04	0.09	0.12	0.13
7.020.025	0.03	0.03	0.03	0.02	0.03	0.03	0.11	0.11	0.23	0.07	0.11	0.12
7.030.025	0.04	0.02	0.01	0.03	0.02	0.02	0.09	0.09	0.07	0.06	0.03	0.07
7.010.050	0.04	0.04	0.03	0.02	0.07	0.04	0.25	0.14	0.81	0.07	0.40	0.33
7.020.050	0.03	0.04	0.03	0.03	0.03	0.03	0.10	0.13	0.25	0.10	0.20	0.16
7.030.050	0.05	0.04	0.01	0.03	0.01	0.03	0.10	0.09	0.11	0.07	0.12	0.10
7.010.075	0.05	0.02	0.04	0.02	0.07	0.04	0.25	0.16	0.75	0.06	0.35	0.31
7.020.075	0.03	0.05	0.03	0.03	0.03	0.03	0.15	0.21	0.32	0.11	0.39	0.23
7.030.075	0.03	0.05	0.01	0.04	0.02	0.03	0.12	0.10	0.14	0.10	0.19	0.13
7.005.100	0.06	0.04	0.08	0.03	0.08	0.05	0.54	0.30	0.99	0.46	0.54	0.56
7.010.100	0.05	0.04	0.05	0.03	0.05	0.04	0.21	0.22	0.79	0.08	0.70	0.40
7.020.100	0.04	0.05	0.03	0.05	0.06	0.05	0.18	0.19	0.35	0.11	0.33	0.23
7.030.100	0.05	0.05	0.01	0.04	0.03	0.04	0.13	0.11	0.16	0.11	0.24	0.15

Table D.6: Probability of the Occurrence of Cover Spalling, Hybrid Frames, $P_{col}/(f_c' A_g) = 0.10$

Frame	10% in 50 Ground Motions						2% in 50 Ground Motions					
	10 - 1	10 - 2	10 - 3	10 - 4	10 - 5	Mean	2 - 1	2 - 2	2 - 3	2 - 4	2 - 5	Mean
5.020.050	0.09	0.08	0.03	0.05	0.04	0.06	0.31	0.31	0.64	0.20	0.51	0.39
5.030.050	0.06	0.03	0.01	0.04	0.04	0.04	0.29	0.38	0.26	0.19	0.23	0.27
5.020.075	0.12	0.10	0.03	0.06	0.04	0.07	0.39	0.39	0.76	0.26	0.68	0.49
5.030.075	0.08	0.04	0.01	0.04	0.05	0.04	0.33	0.47	0.36	0.24	0.39	0.36
5.010.100	0.06	0.04	0.10	0.06	0.12	0.08	0.78	0.54	1.00	0.24	0.99	0.71
5.020.100	0.10	0.11	0.03	0.07	0.02	0.07	0.47	0.40	0.80	0.29	0.77	0.55
5.030.100	0.13	0.05	0.01	0.05	0.06	0.06	0.37	0.44	0.47	0.25	0.67	0.44
6.020.050	0.04	0.05	0.06	0.03	0.07	0.05	0.26	0.27	0.91	0.11	0.47	0.40
6.030.050	0.04	0.05	0.06	0.04	0.04	0.04	0.24	0.27	0.64	0.11	0.46	0.35
6.020.075	0.05	0.05	0.07	0.04	0.08	0.06	0.34	0.36	0.96	0.14	0.57	0.47
6.030.075	0.05	0.06	0.07	0.05	0.05	0.05	0.27	0.33	0.72	0.17	0.60	0.42
6.010.100	0.09	0.08	0.11	0.04	0.17	0.10	0.57	0.55	1.00	0.78	0.81	0.74
6.020.100	0.06	0.05	0.08	0.06	0.08	0.07	0.39	0.43	0.97	0.16	0.70	0.53
6.030.100	0.06	0.06	0.07	0.04	0.07	0.06	0.38	0.37	0.81	0.20	0.64	0.48
7.020.050	0.06	0.05	0.07	0.04	0.07	0.06	0.25	0.19	0.90	0.10	0.57	0.40
7.030.050	0.06	0.08	0.06	0.03	0.06	0.06	0.26	0.18	0.89	0.10	0.40	0.37
7.020.075	0.07	0.05	0.08	0.04	0.07	0.06	0.28	0.45	0.95	0.12	0.82	0.53
7.030.075	0.07	0.03	0.07	0.04	0.06	0.05	0.45	0.23	0.93	0.13	0.47	0.45
7.010.100	0.10	0.10	0.24	0.05	0.15	0.13	0.92	0.61	1.00	0.40	0.78	0.74
7.020.100	0.07	0.06	0.08	0.02	0.09	0.07	0.36	0.51	0.97	0.14	0.78	0.55
7.030.100	0.08	0.02	0.07	0.04	0.09	0.06	0.45	0.28	0.97	0.15	0.66	0.50

Table D.7: Probability of the Occurrence of Bar Buckling, Reinforced Concrete Frames

Frame	10% in 50 Ground Motions						2% in 50 Ground Motions					
	10 - 1	10 - 2	10 - 3	10 - 4	10 - 5	Mean	2 - 1	2 - 2	2 - 3	2 - 4	2 - 5	Mean
5.005.05	0.0003	0.0003	0.0003	0.0002	0.0004	0.0003	0.0033	0.0041	0.0514	0.0007	0.0093	0.0138
5.005.10	0.0005	0.0007	0.0013	0.0004	0.0022	0.0010	0.0698	0.0167	DNC	0.0432	0.0941	0.0559
5.005.15	0.0017	0.0009	0.0044	0.0004	0.0186	0.0052	DNC	0.0592	DNC	0.0735	DNC	0.0664
5.010.05	0.0003	0.0002	0.0001	0.0002	0.0001	0.0002	0.0010	0.0011	0.0022	0.0007	0.0012	0.0013
5.010.10	0.0004	0.0004	0.0006	0.0003	0.0007	0.0005	0.0088	0.0053	0.1356	0.0011	0.0136	0.0329
5.010.15	0.0010	0.0006	0.0012	0.0005	0.0010	0.0009	0.0098	0.0108	DNC	0.0358	0.0478	0.0260
5.020.05	0.0001	0.0002	0.0001	0.0001	0.0002	0.0001	0.0003	0.0005	0.0002	0.0003	0.0004	0.0003
5.020.10	0.0003	0.0005	0.0002	0.0003	0.0003	0.0003	0.0018	0.0016	0.0062	0.0011	0.0035	0.0028
5.020.15	0.0004	0.0004	0.0007	0.0003	0.0006	0.0005	0.0054	0.0050	0.1465	0.0012	0.0126	0.0341
5.030.05	0.0001	0.0002	0.0001	0.0001	0.0001	0.0001	0.0002	0.0005	0.0002	0.0002	0.0002	0.0002
5.030.10	0.0003	0.0002	0.0001	0.0002	0.0001	0.0002	0.0015	0.0013	0.0011	0.0008	0.0009	0.0011
5.030.15	0.0004	0.0004	0.0005	0.0003	0.0003	0.0004	0.0034	0.0034	0.0322	0.0010	0.0063	0.0092
6.005.05	0.0004	0.0003	0.0002	0.0002	0.0003	0.0003	0.0021	0.0013	0.0470	0.0007	0.0178	0.0138
6.005.10	0.0006	0.0007	0.0020	0.0003	0.0030	0.0013	0.0333	0.0178	DNC	0.0104	0.0771	0.0347
6.005.15	0.0070	0.0005	0.0085	0.0032	0.0031	0.0045	0.0474	0.2330	DNC	0.0038	0.0672	0.0879
6.010.05	0.0002	0.0002	0.0002	0.0001	0.0003	0.0002	0.0012	0.0011	0.0102	0.0005	0.0020	0.0030
6.010.10	0.0006	0.0005	0.0006	0.0003	0.0006	0.0005	0.0029	0.0050	0.1596	0.0075	0.0086	0.0367
6.010.15	0.0011	0.0009	0.0039	0.0007	0.0043	0.0022	0.0943	0.0210	DNC	0.0057	0.0375	0.0396
6.020.05	0.0002	0.0002	0.0001	0.0002	0.0001	0.0001	0.0005	0.0006	0.0005	0.0004	0.0004	0.0005
6.020.10	0.0003	0.0003	0.0004	0.0003	0.0003	0.0003	0.0012	0.0013	0.0248	0.0006	0.0039	0.0063
6.020.15	0.0004	0.0004	0.0011	0.0003	0.0010	0.0006	0.0029	0.0041	0.1458	0.0035	0.0429	0.0398
6.030.05	0.0001	0.0001	0.0001	0.0002	0.0002	0.0001	0.0005	0.0004	0.0002	0.0003	0.0003	0.0004
6.030.10	0.0003	0.0002	0.0003	0.0002	0.0002	0.0003	0.0011	0.0013	0.0040	0.0005	0.0020	0.0018
6.030.15	0.0005	0.0005	0.0004	0.0002	0.0006	0.0004	0.0039	0.0015	0.0698	0.0008	0.0047	0.0161
7.005.05	0.0005	0.0002	0.0004	0.0002	0.0004	0.0003	0.0086	0.0019	0.0921	0.0029	0.0047	0.0220
7.005.10	0.0022	0.0003	0.0024	0.0012	0.0013	0.0015	0.0134	0.0648	0.6728	0.0016	0.0128	0.1531
7.005.15	0.0031	0.0008	0.0118	0.0014	0.0035	0.0041	0.0271	0.1126	DNC	0.0051	0.0249	0.0424
7.010.05	0.0002	0.0002	0.0002	0.0001	0.0002	0.0002	0.0015	0.0006	0.0126	0.0004	0.0017	0.0034
7.010.10	0.0005	0.0005	0.0013	0.0005	0.0009	0.0008	0.0163	0.0050	0.1373	0.0026	0.0060	0.0334
7.010.15	0.0019	0.0005	0.0028	0.0005	0.0013	0.0014	0.0135	0.0175	DNC	0.0036	0.0234	0.0145
7.020.05	0.0002	0.0002	0.0002	0.0002	0.0002	0.0002	0.0005	0.0005	0.0009	0.0004	0.0007	0.0006
7.020.10	0.0002	0.0003	0.0004	0.0002	0.0003	0.0003	0.0014	0.0014	0.0199	0.0005	0.0024	0.0051
7.020.15	0.0004	0.0007	0.0015	0.0003	0.0006	0.0007	0.0155	0.0038	0.1108	0.0036	0.0052	0.0278
7.030.05	0.0002	0.0002	0.0001	0.0002	0.0001	0.0002	0.0003	0.0004	0.0005	0.0003	0.0004	0.0004
7.030.10	0.0002	0.0003	0.0003	0.0003	0.0004	0.0003	0.0019	0.0007	0.0160	0.0005	0.0020	0.0042
7.030.15	0.0010	0.0003	0.0009	0.0002	0.0007	0.0006	0.0022	0.0029	0.0307	0.0007	0.0148	0.0103

Note: DNC indicates earthquake analysis did not converge

Table D.8: Probability of the Occurrence of Bar Buckling, Hybrid Frames, $P_{col}/\left(f_c^{'}A_g\right)=0.05$

Frame	10% in 50 Ground Motions						2% in 50 Ground Motions					
	10 - 1	10 - 2	10 - 3	10 - 4	10 - 5	Mean	2 - 1	2 - 2	2 - 3	2 - 4	2 - 5	Mean
5.020.025	0.0001	0.0002	0.0001	0.0001	0.0001	0.0001	0.0002	0.0005	0.0002	0.0003	0.0004	0.0003
5.030.025	0.0001	0.0001	0.0001	0.0001	0.0001	0.0001	0.0001	0.0003	0.0002	0.0002	0.0002	0.0002
5.010.050	0.0002	0.0001	0.0001	0.0001	0.0002	0.0001	0.0012	0.0010	0.0022	0.0007	0.0026	0.0015
5.020.050	0.0001	0.0002	0.0001	0.0001	0.0001	0.0001	0.0002	0.0008	0.0002	0.0003	0.0004	0.0004
5.030.050	0.0001	0.0001	0.0001	0.0001	0.0001	0.0001	0.0002	0.0008	0.0002	0.0003	0.0002	0.0003
5.010.075	0.0002	0.0001	0.0001	0.0002	0.0002	0.0001	0.0013	0.0018	0.0013	0.0007	0.0025	0.0015
5.020.075	0.0001	0.0002	0.0001	0.0001	0.0001	0.0001	0.0004	0.0010	0.0002	0.0006	0.0006	0.0005
5.030.075	0.0001	0.0001	0.0001	0.0001	0.0001	0.0001	0.0002	0.0012	0.0003	0.0003	0.0002	0.0004
5.005.100	0.0004	0.0003	0.0003	0.0002	0.0004	0.0003	0.0041	0.0037	0.0379	0.0007	0.0076	0.0108
5.010.100	0.0002	0.0002	0.0001	0.0002	0.0001	0.0002	0.0021	0.0020	0.0018	0.0008	0.0065	0.0027
5.020.100	0.0001	0.0002	0.0001	0.0002	0.0001	0.0001	0.0002	0.0010	0.0002	0.0009	0.0007	0.0006
5.030.100	0.0001	0.0001	0.0001	0.0001	0.0002	0.0001	0.0002	0.0014	0.0003	0.0004	0.0003	0.0005
6.020.025	0.0002	0.0001	0.0001	0.0001	0.0001	0.0001	0.0006	0.0004	0.0004	0.0004	0.0004	0.0004
6.030.025	0.0001	0.0002	0.0001	0.0001	0.0001	0.0001	0.0003	0.0002	0.0001	0.0002	0.0003	0.0002
6.010.050	0.0002	0.0001	0.0002	0.0002	0.0003	0.0002	0.0014	0.0014	0.0132	0.0004	0.0028	0.0039
6.020.050	0.0002	0.0001	0.0001	0.0001	0.0001	0.0001	0.0006	0.0007	0.0006	0.0004	0.0005	0.0006
6.030.050	0.0001	0.0002	0.0001	0.0001	0.0001	0.0001	0.0009	0.0004	0.0002	0.0004	0.0004	0.0004
6.010.075	0.0002	0.0002	0.0003	0.0002	0.0003	0.0002	0.0012	0.0013	0.0076	0.0004	0.0028	0.0027
6.020.075	0.0003	0.0001	0.0001	0.0001	0.0001	0.0001	0.0007	0.0008	0.0009	0.0005	0.0012	0.0008
6.030.075	0.0001	0.0003	0.0001	0.0001	0.0001	0.0001	0.0013	0.0005	0.0002	0.0005	0.0005	0.0006
6.005.100	0.0002	0.0003	0.0002	0.0002	0.0006	0.0003	0.0022	0.0011	0.0363	0.0006	0.0178	0.0116
6.010.100	0.0002	0.0002	0.0003	0.0002	0.0004	0.0003	0.0019	0.0019	0.0101	0.0005	0.0039	0.0037
6.020.100	0.0004	0.0002	0.0001	0.0002	0.0001	0.0002	0.0010	0.0011	0.0012	0.0006	0.0019	0.0011
6.030.100	0.0001	0.0003	0.0001	0.0002	0.0002	0.0002	0.0016	0.0007	0.0002	0.0004	0.0006	0.0007
7.020.025	0.0002	0.0001	0.0002	0.0001	0.0002	0.0002	0.0005	0.0005	0.0012	0.0003	0.0005	0.0006
7.030.025	0.0002	0.0001	0.0001	0.0001	0.0001	0.0001	0.0005	0.0004	0.0003	0.0003	0.0001	0.0003
7.010.050	0.0002	0.0002	0.0002	0.0001	0.0004	0.0002	0.0013	0.0007	0.0127	0.0003	0.0026	0.0035
7.020.050	0.0002	0.0002	0.0002	0.0002	0.0002	0.0002	0.0005	0.0006	0.0013	0.0005	0.0011	0.0008
7.030.050	0.0003	0.0002	0.0001	0.0001	0.0001	0.0002	0.0005	0.0004	0.0005	0.0004	0.0006	0.0005
7.010.075	0.0002	0.0001	0.0002	0.0001	0.0004	0.0002	0.0013	0.0008	0.0098	0.0003	0.0022	0.0029
7.020.075	0.0002	0.0002	0.0002	0.0002	0.0001	0.0002	0.0007	0.0011	0.0019	0.0005	0.0025	0.0013
7.030.075	0.0001	0.0002	0.0001	0.0002	0.0001	0.0002	0.0006	0.0005	0.0007	0.0005	0.0010	0.0006
7.005.100	0.0003	0.0002	0.0004	0.0002	0.0004	0.0003	0.0044	0.0017	0.0723	0.0033	0.0043	0.0172
7.010.100	0.0003	0.0002	0.0002	0.0002	0.0003	0.0002	0.0011	0.0011	0.0115	0.0004	0.0080	0.0044
7.020.100	0.0002	0.0003	0.0002	0.0003	0.0003	0.0002	0.0009	0.0010	0.0021	0.0005	0.0020	0.0013
7.030.100	0.0003	0.0003	0.0001	0.0002	0.0002	0.0002	0.0006	0.0005	0.0008	0.0006	0.0013	0.0008

Table D.9: Probability of the Occurrence of Bar Buckling, Hybrid Frames, $P_{col}/\left(f_c^{'}A_g\right)=0.10$

Frame	10% in 50 Ground Motions						2% in 50 Ground Motions					
	10 - 1	10 - 2	10 - 3	10 - 4	10 - 5	Mean	2 - 1	2 - 2	2 - 3	2 - 4	2 - 5	Mean
5.020.050	0.0004	0.0004	0.0002	0.0002	0.0002	0.0003	0.0018	0.0018	0.0064	0.0010	0.0039	0.0030
5.030.050	0.0003	0.0002	0.0001	0.0002	0.0002	0.0002	0.0016	0.0024	0.0014	0.0009	0.0012	0.0015
5.020.075	0.0006	0.0005	0.0002	0.0003	0.0002	0.0003	0.0025	0.0025	0.0103	0.0014	0.0073	0.0048
5.030.075	0.0004	0.0002	0.0001	0.0002	0.0002	0.0002	0.0019	0.0035	0.0022	0.0013	0.0025	0.0023
5.010.100	0.0003	0.0002	0.0005	0.0003	0.0006	0.0004	0.0109	0.0044	0.1568	0.0013	0.0682	0.0483
5.020.100	0.0005	0.0006	0.0002	0.0003	0.0001	0.0003	0.0034	0.0026	0.0119	0.0016	0.0107	0.0061
5.030.100	0.0006	0.0003	0.0001	0.0002	0.0003	0.0003	0.0023	0.0031	0.0034	0.0013	0.0070	0.0034
6.020.050	0.0002	0.0002	0.0003	0.0002	0.0003	0.0003	0.0014	0.0015	0.0224	0.0005	0.0034	0.0059
6.030.050	0.0002	0.0003	0.0003	0.0002	0.0002	0.0002	0.0013	0.0015	0.0064	0.0006	0.0033	0.0026
6.020.075	0.0003	0.0003	0.0004	0.0002	0.0004	0.0003	0.0020	0.0023	0.0334	0.0007	0.0048	0.0086
6.030.075	0.0002	0.0003	0.0003	0.0002	0.0003	0.0003	0.0015	0.0019	0.0087	0.0009	0.0055	0.0037
6.010.100	0.0004	0.0004	0.0005	0.0002	0.0009	0.0005	0.0049	0.0045	0.2512	0.0109	0.0128	0.0569
6.020.100	0.0003	0.0003	0.0004	0.0003	0.0004	0.0003	0.0025	0.0030	0.0394	0.0008	0.0081	0.0108
6.030.100	0.0003	0.0003	0.0003	0.0002	0.0004	0.0003	0.0024	0.0023	0.0129	0.0010	0.0064	0.0050
7.020.050	0.0003	0.0002	0.0003	0.0002	0.0004	0.0003	0.0013	0.0010	0.0206	0.0005	0.0049	0.0057
7.030.050	0.0003	0.0004	0.0003	0.0002	0.0003	0.0003	0.0014	0.0009	0.0191	0.0005	0.0026	0.0049
7.020.075	0.0004	0.0003	0.0004	0.0002	0.0004	0.0003	0.0016	0.0031	0.0311	0.0006	0.0134	0.0100
7.030.075	0.0003	0.0002	0.0003	0.0002	0.0003	0.0003	0.0032	0.0012	0.0269	0.0007	0.0034	0.0071
7.010.100	0.0005	0.0005	0.0013	0.0003	0.0007	0.0006	0.0237	0.0057	0.2036	0.0026	0.0112	0.0494
7.020.100	0.0003	0.0003	0.0004	0.0001	0.0004	0.0003	0.0022	0.0039	0.0402	0.0007	0.0109	0.0116
7.030.100	0.0004	0.0001	0.0004	0.0002	0.0004	0.0003	0.0031	0.0015	0.0385	0.0007	0.0068	0.0101

Table D.10: Maximum Steel Strain, Reinforced Concrete Frames

Frame	10% in 50 Ground Motions						2% in 50 Ground Motions					
	10 - 1	10 - 2	10 - 3	10 - 4	10 - 5	Mean	2 - 1	2 - 2	2 - 3	2 - 4	2 - 5	Mean
5.005.05	0.013	0.020	0.018	0.018	0.025	0.019	0.053	0.044	0.034	0.028	0.065	0.045
5.005.10	0.025	0.024	0.008	0.022	0.045	0.025	0.099	0.059	DNC	0.052	0.106	0.079
5.005.15	0.034	0.028	0.014	0.020	0.057	0.031	DNC	0.078	DNC	0.074	DNC	0.076
5.010.05	0.018	0.015	0.002	0.014	0.005	0.011	0.035	0.035	0.021	0.025	0.036	0.030
5.010.10	0.010	0.018	0.011	0.016	0.024	0.016	0.060	0.041	0.035	0.031	0.067	0.047
5.010.15	0.026	0.021	0.009	0.013	0.027	0.019	0.056	0.057	DNC	0.044	0.080	0.059
5.020.05	0.004	0.009	0.003	0.007	0.007	0.006	0.019	0.016	0.002	0.014	0.013	0.013
5.020.10	0.011	0.019	0.008	0.013	0.011	0.013	0.035	0.030	0.016	0.022	0.044	0.029
5.020.15	0.008	0.013	0.009	0.011	0.018	0.012	0.044	0.035	0.054	0.018	0.056	0.041
5.030.05	0.002	0.008	0.002	0.005	0.005	0.004	0.006	0.016	0.003	0.011	0.008	0.009
5.030.10	0.013	0.006	0.003	0.008	0.003	0.007	0.030	0.029	0.024	0.020	0.020	0.025
5.030.15	0.009	0.013	0.012	0.012	0.012	0.011	0.037	0.034	0.032	0.023	0.045	0.034
6.005.05	0.020	0.015	0.005	0.010	0.018	0.014	0.042	0.035	0.048	0.029	0.048	0.040
6.005.10	0.022	0.024	0.008	0.017	0.040	0.023	0.077	0.068	DNC	0.060	0.092	0.074
6.005.15	0.050	0.020	0.049	0.026	0.040	0.037	0.064	0.073	DNC	0.042	0.085	0.066
6.010.05	0.009	0.009	0.010	0.008	0.016	0.010	0.033	0.026	0.011	0.021	0.039	0.026
6.010.10	0.021	0.019	0.005	0.009	0.021	0.015	0.038	0.027	0.038	0.034	0.052	0.038
6.010.15	0.025	0.018	0.012	0.014	0.028	0.019	0.084	0.060	DNC	0.043	0.069	0.064
6.020.05	0.009	0.009	0.003	0.007	0.004	0.006	0.020	0.021	0.019	0.017	0.016	0.019
6.020.10	0.009	0.011	0.006	0.007	0.011	0.009	0.027	0.025	0.020	0.017	0.040	0.026
6.020.15	0.010	0.013	0.008	0.009	0.021	0.012	0.033	0.032	0.043	0.024	0.036	0.034
6.030.05	0.004	0.005	0.001	0.006	0.003	0.004	0.019	0.015	0.003	0.014	0.005	0.011
6.030.10	0.005	0.008	0.009	0.007	0.009	0.007	0.025	0.022	0.013	0.016	0.031	0.021
6.030.15	0.006	0.013	0.005	0.006	0.015	0.009	0.034	0.021	0.035	0.010	0.037	0.027
7.005.05	0.020	0.012	0.005	0.008	0.020	0.013	0.055	0.037	0.055	0.037	0.048	0.046
7.005.10	0.037	0.014	0.028	0.019	0.031	0.026	0.058	0.082	0.047	0.033	0.058	0.056
7.005.15	0.036	0.022	0.050	0.016	0.037	0.032	0.048	0.068	DNC	0.042	0.062	0.055
7.010.05	0.009	0.012	0.005	0.006	0.009	0.008	0.032	0.021	0.011	0.010	0.034	0.022
7.010.10	0.018	0.014	0.007	0.013	0.023	0.015	0.057	0.042	0.034	0.034	0.045	0.042
7.010.15	0.028	0.013	0.017	0.011	0.024	0.019	0.049	0.053	DNC	0.034	0.057	0.048
7.020.05	0.006	0.006	0.010	0.007	0.008	0.007	0.018	0.017	0.006	0.012	0.022	0.015
7.020.10	0.009	0.008	0.004	0.006	0.008	0.007	0.026	0.018	0.017	0.016	0.032	0.022
7.020.15	0.010	0.011	0.008	0.008	0.009	0.009	0.048	0.032	0.034	0.030	0.036	0.036
7.030.05	0.005	0.008	0.002	0.007	0.003	0.005	0.013	0.015	0.012	0.012	0.013	0.013
7.030.10	0.005	0.010	0.004	0.008	0.013	0.008	0.027	0.014	0.018	0.010	0.028	0.019
7.030.15	0.017	0.008	0.007	0.005	0.014	0.010	0.025	0.027	0.021	0.014	0.025	0.023

Note: DNC indicates earthquake analysis did not converge

Table D.11: Maximum Steel Strain, Hybrid Frames, $P_{col}/\left(f_c' A_g\right) = 0.05$

Frame	10% in 50 Ground Motions						2% in 50 Ground Motions					
	10 - 1	10 - 2	10 - 3	10 - 4	10 - 5	Mean	2 - 1	2 - 2	2 - 3	2 - 4	2 - 5	Mean
5.020.025	0.003	0.007	0.002	0.005	0.004	0.004	0.013	0.015	0.003	0.012	0.011	0.011
5.030.025	0.002	0.004	0.004	0.005	0.004	0.004	0.007	0.012	0.006	0.011	0.006	0.008
5.010.050	0.013	0.009	0.003	0.011	0.007	0.009	0.026	0.026	0.016	0.020	0.032	0.024
5.020.050	0.005	0.008	0.002	0.007	0.004	0.005	0.009	0.013	0.003	0.013	0.011	0.010
5.030.050	0.004	0.004	0.004	0.005	0.005	0.004	0.007	0.013	0.006	0.011	0.007	0.009
5.010.075	0.012	0.010	0.003	0.012	0.007	0.009	0.023	0.027	0.018	0.020	0.027	0.023
5.020.075	0.005	0.008	0.002	0.008	0.006	0.006	0.014	0.014	0.003	0.015	0.012	0.012
5.030.075	0.004	0.005	0.004	0.005	0.004	0.005	0.008	0.011	0.006	0.010	0.007	0.008
5.005.100	0.021	0.017	0.017	0.016	0.019	0.018	0.033	0.027	0.024	0.023	0.037	0.029
5.010.100	0.014	0.012	0.002	0.011	0.007	0.009	0.022	0.021	0.014	0.021	0.031	0.022
5.020.100	0.006	0.007	0.003	0.008	0.006	0.006	0.011	0.013	0.003	0.013	0.011	0.010
5.030.100	0.004	0.005	0.004	0.005	0.004	0.004	0.008	0.011	0.006	0.010	0.007	0.009
6.020.025	0.011	0.006	0.001	0.006	0.004	0.005	0.020	0.016	0.017	0.014	0.013	0.016
6.030.025	0.004	0.006	0.001	0.006	0.005	0.004	0.013	0.011	0.003	0.010	0.007	0.009
6.010.050	0.012	0.010	0.011	0.011	0.016	0.012	0.028	0.023	0.007	0.019	0.032	0.022
6.020.050	0.011	0.006	0.001	0.006	0.003	0.006	0.013	0.019	0.016	0.014	0.015	0.015
6.030.050	0.004	0.007	0.002	0.005	0.004	0.004	0.015	0.011	0.004	0.012	0.006	0.009
6.010.075	0.008	0.013	0.014	0.012	0.015	0.012	0.024	0.023	0.007	0.018	0.028	0.020
6.020.075	0.012	0.007	0.001	0.008	0.004	0.006	0.013	0.016	0.013	0.015	0.017	0.015
6.030.075	0.004	0.008	0.002	0.006	0.004	0.005	0.014	0.011	0.004	0.011	0.009	0.010
6.005.100	0.015	0.016	0.008	0.012	0.022	0.015	0.027	0.024	0.028	0.023	0.030	0.027
6.010.100	0.009	0.013	0.016	0.013	0.017	0.014	0.023	0.019	0.010	0.020	0.025	0.020
6.020.100	0.012	0.008	0.002	0.008	0.004	0.007	0.012	0.014	0.011	0.012	0.014	0.012
6.030.100	0.003	0.008	0.002	0.007	0.004	0.005	0.013	0.010	0.004	0.009	0.008	0.009
7.020.025	0.007	0.007	0.009	0.006	0.008	0.007	0.019	0.013	0.005	0.013	0.018	0.014
7.030.025	0.008	0.005	0.002	0.006	0.003	0.005	0.015	0.014	0.013	0.013	0.004	0.012
7.010.050	0.010	0.012	0.005	0.006	0.016	0.010	0.026	0.020	0.007	0.013	0.028	0.019
7.020.050	0.006	0.009	0.008	0.008	0.008	0.008	0.014	0.013	0.005	0.011	0.020	0.013
7.030.050	0.008	0.008	0.002	0.006	0.003	0.005	0.012	0.012	0.012	0.012	0.013	0.012
7.010.075	0.009	0.006	0.007	0.008	0.016	0.009	0.023	0.018	0.006	0.015	0.025	0.017
7.020.075	0.007	0.010	0.008	0.009	0.007	0.008	0.014	0.014	0.005	0.015	0.018	0.013
7.030.075	0.005	0.008	0.002	0.007	0.004	0.005	0.010	0.011	0.010	0.011	0.012	0.011
7.005.100	0.017	0.014	0.003	0.011	0.019	0.013	0.030	0.024	0.030	0.028	0.030	0.028
7.010.100	0.010	0.011	0.006	0.007	0.014	0.010	0.019	0.018	0.015	0.016	0.023	0.018
7.020.100	0.007	0.011	0.007	0.008	0.012	0.009	0.012	0.013	0.005	0.012	0.013	0.011
7.030.100	0.008	0.008	0.002	0.007	0.004	0.006	0.009	0.010	0.009	0.010	0.011	0.010

Table D.12: Maximum Steel Strain, Hybrid Frames, $P_{col}/\left(f_c' A_g\right) = 0.10$

Frame	10% in 50 Ground Motions						2% in 50 Ground Motions					
	10 - 1	10 - 2	10 - 3	10 - 4	10 - 5	Mean	2 - 1	2 - 2	2 - 3	2 - 4	2 - 5	Mean
5.020.050	0.013	0.014	0.003	0.011	0.007	0.010	0.021	0.019	0.011	0.015	0.026	0.019
5.030.050	0.010	0.006	0.002	0.007	0.007	0.006	0.017	0.018	0.013	0.013	0.015	0.015
5.020.075	0.012	0.013	0.004	0.011	0.004	0.009	0.018	0.017	0.010	0.014	0.023	0.016
5.030.075	0.010	0.008	0.002	0.008	0.006	0.007	0.014	0.016	0.011	0.012	0.015	0.013
5.010.100	0.010	0.012	0.010	0.013	0.015	0.012	0.029	0.023	0.027	0.019	0.033	0.026
5.020.100	0.011	0.012	0.004	0.011	0.003	0.008	0.016	0.015	0.009	0.011	0.020	0.014
5.030.100	0.009	0.008	0.002	0.007	0.006	0.006	0.012	0.013	0.008	0.010	0.014	0.011
6.020.050	0.007	0.009	0.007	0.007	0.012	0.009	0.019	0.017	0.010	0.014	0.023	0.016
6.030.050	0.006	0.008	0.009	0.008	0.007	0.008	0.016	0.013	0.007	0.012	0.019	0.014
6.020.075	0.008	0.009	0.007	0.008	0.011	0.009	0.017	0.015	0.008	0.013	0.020	0.015
6.030.075	0.006	0.008	0.009	0.008	0.008	0.008	0.013	0.012	0.007	0.012	0.017	0.012
6.010.100	0.014	0.014	0.004	0.012	0.016	0.012	0.023	0.018	0.031	0.020	0.030	0.024
6.020.100	0.008	0.009	0.007	0.009	0.010	0.009	0.015	0.014	0.009	0.011	0.018	0.013
6.030.100	0.006	0.007	0.008	0.007	0.009	0.007	0.012	0.011	0.006	0.010	0.013	0.010
7.020.050	0.010	0.010	0.004	0.007	0.012	0.009	0.016	0.014	0.011	0.014	0.021	0.015
7.030.050	0.005	0.007	0.005	0.005	0.009	0.006	0.015	0.012	0.009	0.012	0.017	0.013
7.020.075	0.010	0.010	0.004	0.008	0.011	0.009	0.014	0.012	0.014	0.013	0.018	0.014
7.030.075	0.005	0.005	0.005	0.005	0.009	0.006	0.014	0.011	0.008	0.011	0.015	0.012
7.010.100	0.016	0.014	0.004	0.012	0.015	0.012	0.030	0.021	0.025	0.021	0.027	0.025
7.020.100	0.010	0.010	0.004	0.006	0.011	0.008	0.013	0.012	0.014	0.012	0.016	0.013
7.030.100	0.005	0.003	0.005	0.005	0.009	0.005	0.011	0.010	0.007	0.008	0.013	0.010

Table D.13: $\Delta_{max}/\Delta_{ult}$ **, Reinforced Concrete Frames**

Frame	10% in 50 Ground Motions						2% in 50 Ground Motions					
	10 - 1	10 - 2	10 - 3	10 - 4	10 - 5	Mean	2 - 1	2 - 2	2 - 3	2 - 4	2 - 5	Mean
5.005.05	0.10	0.11	0.11	0.10	0.13	0.11	0.24	0.25	0.43	0.15	0.30	0.27
5.005.10	0.13	0.14	0.17	0.12	0.20	0.15	0.43	0.32	DNC	0.39	0.46	0.40
5.005.15	0.18	0.15	0.23	0.12	0.31	0.19	DNC	0.39	DNC	0.41	DNC	0.40
5.010.05	0.11	0.10	0.05	0.10	0.07	0.09	0.17	0.18	0.21	0.15	0.18	0.18
5.010.10	0.12	0.12	0.14	0.11	0.14	0.12	0.28	0.25	0.49	0.16	0.31	0.30
5.010.15	0.15	0.13	0.16	0.12	0.15	0.14	0.27	0.28	DNC	0.35	0.37	0.32
5.020.05	0.06	0.10	0.05	0.07	0.09	0.07	0.12	0.13	0.08	0.11	0.13	0.11
5.020.10	0.11	0.13	0.09	0.10	0.10	0.11	0.19	0.18	0.26	0.17	0.23	0.21
5.020.15	0.11	0.11	0.13	0.10	0.13	0.12	0.24	0.23	0.47	0.16	0.29	0.28
5.030.05	0.05	0.08	0.05	0.07	0.08	0.06	0.08	0.13	0.08	0.09	0.08	0.09
5.030.10	0.11	0.09	0.06	0.09	0.06	0.08	0.18	0.18	0.17	0.15	0.16	0.17
5.030.15	0.11	0.11	0.12	0.10	0.10	0.11	0.21	0.21	0.35	0.15	0.25	0.23
6.005.05	0.15	0.14	0.13	0.10	0.14	0.13	0.27	0.24	0.53	0.19	0.44	0.33
6.005.10	0.18	0.18	0.25	0.14	0.28	0.21	0.47	0.42	DNC	0.37	0.56	0.45
6.005.15	0.32	0.16	0.34	0.27	0.27	0.27	0.48	0.67	DNC	0.28	0.51	0.48
6.010.05	0.11	0.11	0.13	0.10	0.14	0.12	0.23	0.23	0.39	0.17	0.27	0.26
6.010.10	0.18	0.16	0.17	0.13	0.18	0.16	0.28	0.32	0.65	0.35	0.36	0.39
6.010.15	0.20	0.19	0.28	0.18	0.29	0.23	0.55	0.41	DNC	0.31	0.46	0.43
6.020.05	0.11	0.11	0.07	0.11	0.08	0.10	0.17	0.18	0.17	0.15	0.17	0.17
6.020.10	0.14	0.14	0.15	0.12	0.14	0.14	0.22	0.22	0.45	0.17	0.30	0.27
6.020.15	0.14	0.15	0.20	0.13	0.20	0.16	0.26	0.29	0.60	0.27	0.47	0.38
6.030.05	0.09	0.10	0.04	0.11	0.10	0.09	0.18	0.16	0.12	0.14	0.15	0.15
6.030.10	0.13	0.12	0.13	0.11	0.12	0.12	0.21	0.22	0.30	0.16	0.25	0.23
6.030.15	0.15	0.15	0.15	0.11	0.16	0.15	0.28	0.22	0.52	0.19	0.29	0.30
7.005.05	0.21	0.15	0.20	0.13	0.20	0.18	0.47	0.32	0.76	0.36	0.41	0.46
7.005.10	0.32	0.16	0.33	0.27	0.28	0.27	0.49	0.67	1.19	0.29	0.48	0.62
7.005.15	0.33	0.23	0.45	0.26	0.34	0.32	0.53	0.71	DNC	0.37	0.52	0.53
7.010.05	0.16	0.16	0.15	0.12	0.15	0.15	0.31	0.23	0.51	0.21	0.31	0.31
7.010.10	0.21	0.21	0.28	0.21	0.24	0.23	0.51	0.39	0.78	0.33	0.41	0.48
7.010.15	0.29	0.19	0.32	0.19	0.26	0.25	0.46	0.49	DNC	0.34	0.52	0.45
7.020.05	0.14	0.13	0.16	0.14	0.14	0.14	0.22	0.22	0.26	0.20	0.24	0.23
7.020.10	0.15	0.16	0.19	0.14	0.18	0.16	0.28	0.28	0.53	0.21	0.33	0.33
7.020.15	0.17	0.21	0.27	0.15	0.20	0.20	0.47	0.35	0.71	0.34	0.37	0.45
7.030.05	0.14	0.16	0.09	0.14	0.11	0.13	0.18	0.20	0.21	0.18	0.19	0.19
7.030.10	0.14	0.18	0.17	0.16	0.19	0.17	0.31	0.23	0.50	0.21	0.31	0.31
7.030.15	0.24	0.16	0.23	0.14	0.21	0.20	0.30	0.32	0.54	0.21	0.47	0.37

Note: DNC indicates earthquake analysis did not converge

Table D.14: $\Delta_{\max}/\Delta_{ult}$ **, Hybrid Frames,** $P_{col}/\left(f_c'A_g\right)=0.05$

Frame	10% in 50 Ground Motions						2% in 50 Ground Motions					
	10 - 1	10 - 2	10 - 3	10 - 4	10 - 5	Mean	2 - 1	2 - 2	2 - 3	2 - 4	2 - 5	Mean
5.020.025	0.05	0.08	0.05	0.06	0.05	0.06	0.10	0.14	0.08	0.10	0.12	0.11
5.030.025	0.04	0.06	0.06	0.06	0.06	0.06	0.07	0.11	0.09	0.09	0.08	0.09
5.010.050	0.09	0.07	0.04	0.07	0.08	0.07	0.18	0.17	0.21	0.15	0.22	0.19
5.020.050	0.05	0.08	0.05	0.07	0.05	0.06	0.09	0.15	0.08	0.10	0.12	0.11
5.030.050	0.06	0.06	0.06	0.06	0.07	0.06	0.07	0.15	0.09	0.10	0.08	0.10
5.010.075	0.08	0.08	0.04	0.08	0.08	0.07	0.18	0.20	0.18	0.15	0.21	0.18
5.020.075	0.06	0.08	0.05	0.07	0.06	0.06	0.11	0.16	0.08	0.13	0.13	0.12
5.030.075	0.05	0.06	0.06	0.06	0.06	0.06	0.08	0.16	0.09	0.10	0.09	0.10
5.005.100	0.13	0.11	0.10	0.10	0.12	0.11	0.25	0.24	0.40	0.15	0.29	0.26
5.010.100	0.10	0.09	0.04	0.08	0.06	0.07	0.20	0.20	0.20	0.15	0.27	0.20
5.020.100	0.07	0.07	0.05	0.07	0.06	0.06	0.09	0.15	0.07	0.15	0.14	0.12
5.030.100	0.06	0.06	0.05	0.06	0.07	0.06	0.08	0.16	0.09	0.11	0.09	0.11
6.020.025	0.12	0.08	0.05	0.09	0.07	0.08	0.18	0.15	0.16	0.15	0.16	0.16
6.030.025	0.08	0.10	0.04	0.09	0.10	0.08	0.14	0.13	0.09	0.12	0.13	0.12
6.010.050	0.11	0.10	0.12	0.10	0.13	0.11	0.24	0.24	0.41	0.16	0.29	0.27
6.020.050	0.12	0.09	0.04	0.09	0.07	0.08	0.17	0.18	0.18	0.16	0.17	0.17
6.030.050	0.08	0.11	0.04	0.08	0.08	0.08	0.19	0.14	0.11	0.14	0.14	0.14
6.010.075	0.10	0.12	0.13	0.11	0.13	0.12	0.23	0.23	0.36	0.16	0.28	0.25
6.020.075	0.13	0.09	0.04	0.09	0.06	0.08	0.18	0.19	0.20	0.16	0.22	0.19
6.030.075	0.07	0.12	0.05	0.09	0.08	0.08	0.21	0.15	0.11	0.15	0.16	0.15
6.005.100	0.13	0.13	0.13	0.10	0.18	0.13	0.27	0.22	0.51	0.18	0.44	0.32
6.010.100	0.11	0.12	0.14	0.12	0.15	0.13	0.25	0.25	0.38	0.17	0.30	0.27
6.020.100	0.14	0.10	0.04	0.09	0.06	0.09	0.20	0.21	0.21	0.17	0.24	0.20
6.030.100	0.07	0.12	0.05	0.10	0.09	0.08	0.21	0.17	0.11	0.14	0.16	0.16
7.020.025	0.13	0.12	0.14	0.11	0.12	0.13	0.22	0.22	0.28	0.18	0.22	0.22
7.030.025	0.14	0.11	0.07	0.12	0.09	0.11	0.20	0.19	0.18	0.17	0.12	0.17
7.010.050	0.14	0.14	0.14	0.12	0.19	0.15	0.29	0.24	0.50	0.18	0.35	0.31
7.020.050	0.12	0.14	0.13	0.12	0.12	0.13	0.20	0.22	0.28	0.20	0.26	0.23
7.030.050	0.15	0.14	0.07	0.11	0.08	0.11	0.19	0.19	0.20	0.17	0.21	0.19
7.010.075	0.15	0.10	0.15	0.11	0.19	0.14	0.29	0.25	0.47	0.17	0.33	0.30
7.020.075	0.13	0.15	0.13	0.12	0.12	0.13	0.23	0.26	0.30	0.20	0.32	0.26
7.030.075	0.11	0.14	0.05	0.13	0.10	0.10	0.20	0.19	0.21	0.19	0.24	0.20
7.005.100	0.17	0.14	0.19	0.12	0.19	0.16	0.40	0.31	0.72	0.37	0.40	0.44
7.010.100	0.16	0.14	0.15	0.12	0.16	0.15	0.27	0.27	0.48	0.19	0.44	0.33
7.020.100	0.13	0.15	0.12	0.15	0.16	0.14	0.24	0.25	0.30	0.20	0.30	0.26
7.030.100	0.14	0.14	0.04	0.13	0.11	0.11	0.20	0.19	0.22	0.19	0.25	0.21

Table D.15: $\Delta_{\max}/\Delta_{ult}$ **, Hybrid Frames,** $P_{col}/\left(f_c'A_g\right)=0.10$

| Frame	10% in 50 Ground Motions						2% in 50 Ground Motions					
	10 - 1	10 - 2	10 - 3	10 - 4	10 - 5	Mean	2 - 1	2 - 2	2 - 3	2 - 4	2 - 5	Mean
5.020.050	0.12	0.12	0.08	0.09	0.09	0.10	0.19	0.19	0.26	0.16	0.23	0.20
5.030.050	0.10	0.07	0.04	0.08	0.08	0.08	0.18	0.20	0.17	0.15	0.16	0.17
5.020.075	0.13	0.12	0.08	0.10	0.08	0.10	0.20	0.20	0.28	0.17	0.26	0.22
5.030.075	0.11	0.08	0.04	0.08	0.09	0.08	0.18	0.20	0.18	0.16	0.19	0.18
5.010.100	0.10	0.08	0.13	0.11	0.13	0.11	0.29	0.24	0.50	0.17	0.42	0.32
5.020.100	0.12	0.12	0.08	0.10	0.05	0.10	0.21	0.20	0.28	0.17	0.27	0.23
5.030.100	0.12	0.08	0.04	0.08	0.09	0.08	0.18	0.19	0.20	0.15	0.23	0.19
6.020.050	0.12	0.12	0.14	0.10	0.14	0.12	0.23	0.23	0.43	0.17	0.28	0.27
6.030.050	0.11	0.12	0.12	0.11	0.11	0.11	0.21	0.22	0.32	0.16	0.27	0.24
6.020.075	0.12	0.12	0.14	0.11	0.14	0.13	0.24	0.25	0.45	0.17	0.30	0.28
6.030.075	0.11	0.12	0.13	0.11	0.11	0.12	0.21	0.22	0.32	0.18	0.29	0.25
6.010.100	0.15	0.15	0.17	0.12	0.20	0.16	0.31	0.30	0.71	0.37	0.38	0.42
6.020.100	0.13	0.12	0.14	0.12	0.14	0.13	0.25	0.26	0.46	0.18	0.33	0.29
6.030.100	0.12	0.11	0.12	0.10	0.13	0.12	0.23	0.23	0.34	0.18	0.29	0.25
7.020.050	0.16	0.15	0.17	0.14	0.18	0.16	0.27	0.25	0.52	0.20	0.38	0.33
7.030.050	0.15	0.17	0.16	0.12	0.16	0.15	0.27	0.24	0.50	0.19	0.32	0.30
7.020.075	0.17	0.15	0.18	0.14	0.17	0.16	0.28	0.33	0.55	0.21	0.46	0.37
7.030.075	0.16	0.11	0.16	0.13	0.15	0.14	0.32	0.25	0.51	0.20	0.32	0.32
7.010.100	0.20	0.20	0.27	0.16	0.23	0.21	0.54	0.40	0.84	0.33	0.46	0.51
7.020.100	0.17	0.16	0.17	0.10	0.18	0.16	0.30	0.34	0.57	0.21	0.43	0.37
7.030.100	0.16	0.09	0.16	0.12	0.17	0.14	0.31	0.25	0.53	0.20	0.37	0.33
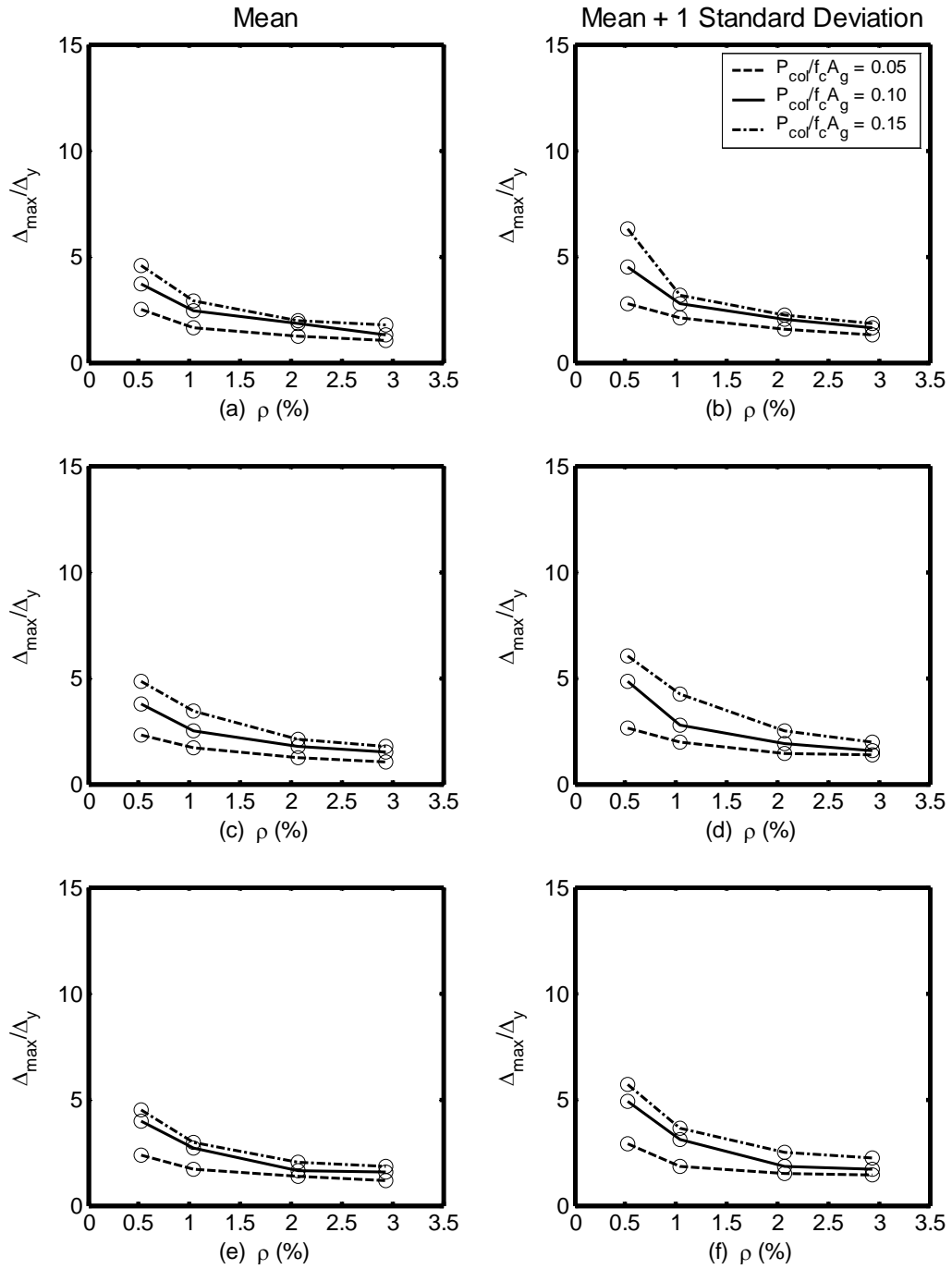
Figure D.1: Displacement Ductility, 10 Percent in 50, Reinforced Concrete Frames
(a) and (b) $L_{col}/D_{col} = $ **5,** (c) and (d) $L_{col}/D_{col} = $ **6, and (e) and (f)** $L_{col}/D_{col} = $ **7**
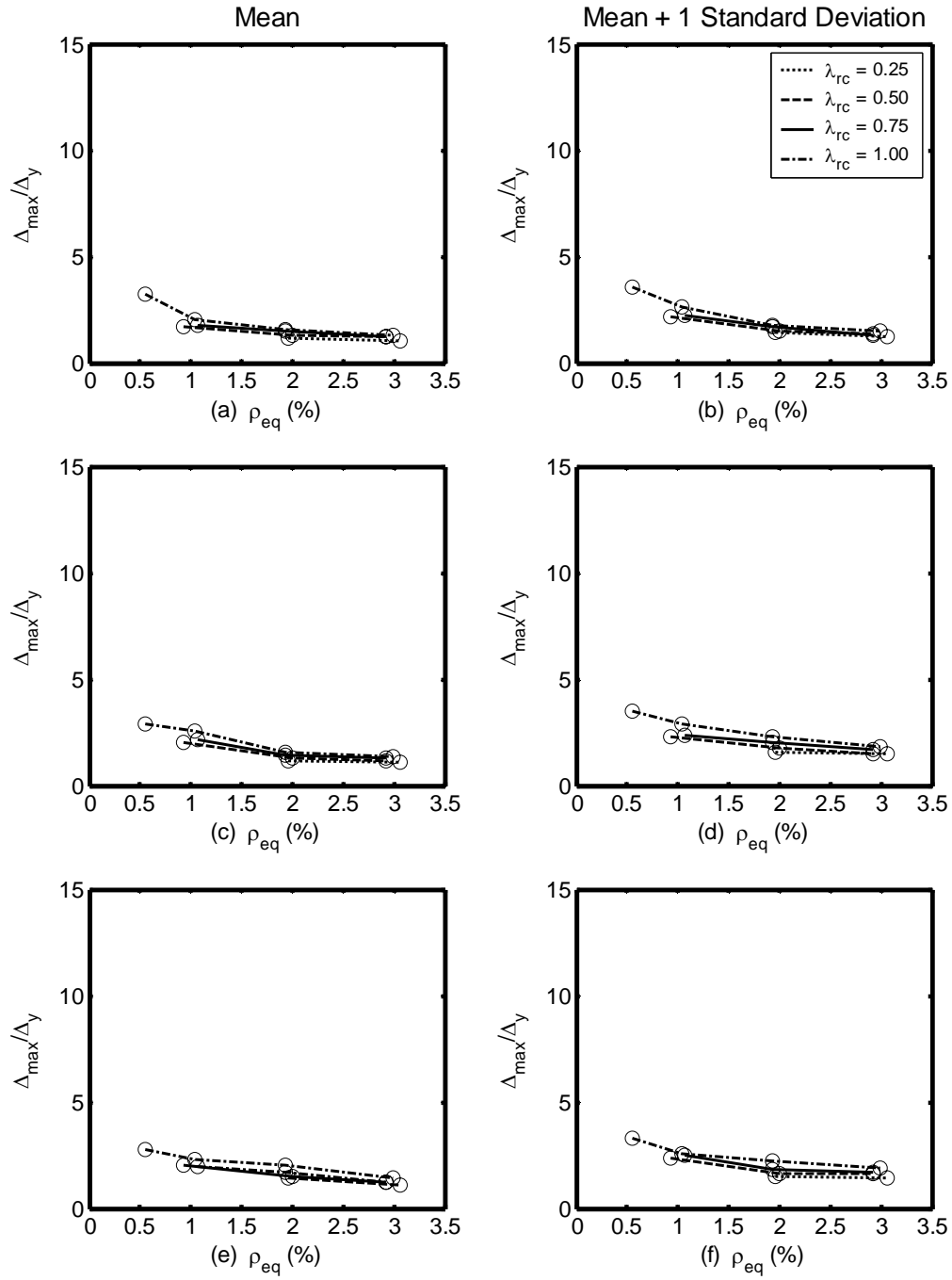
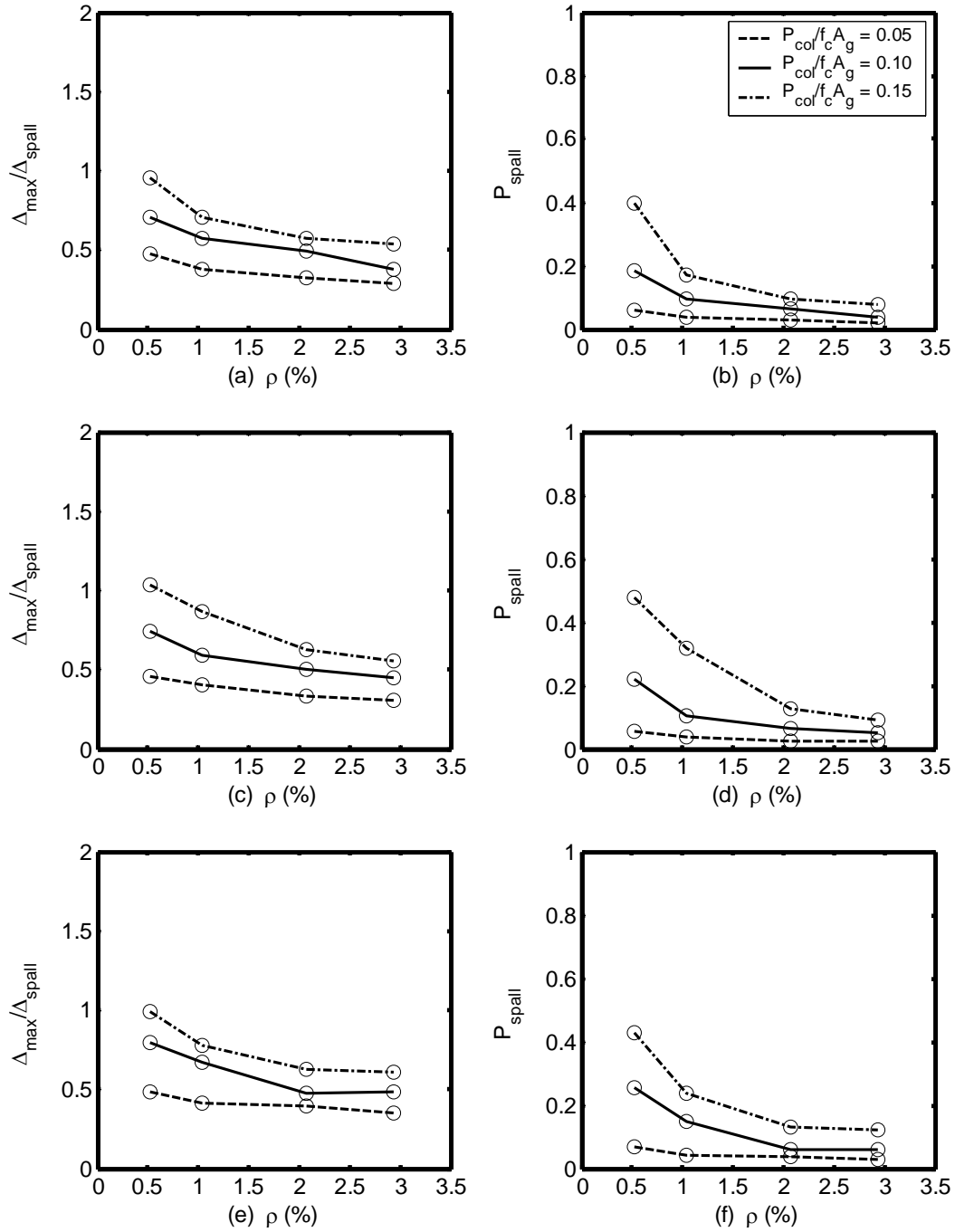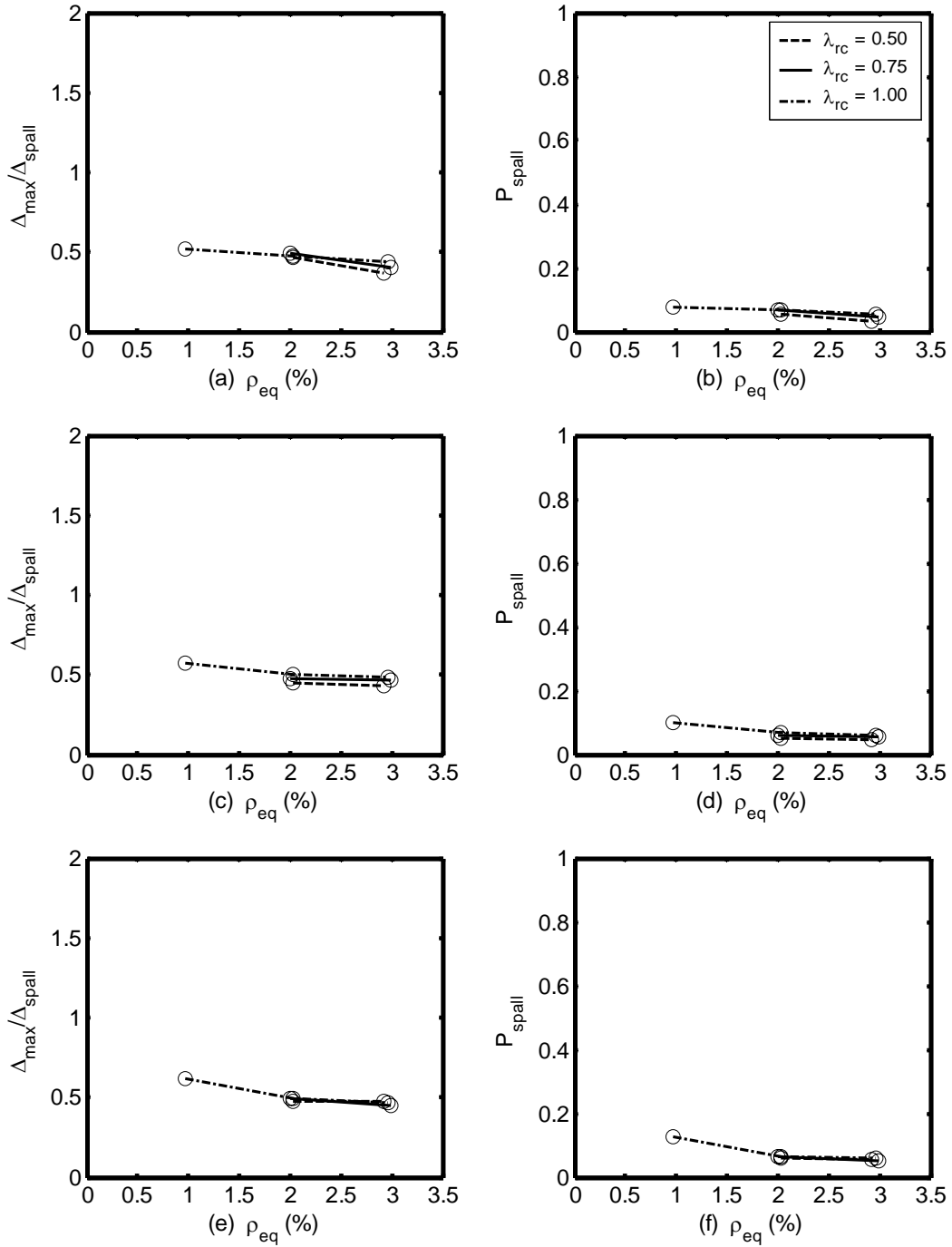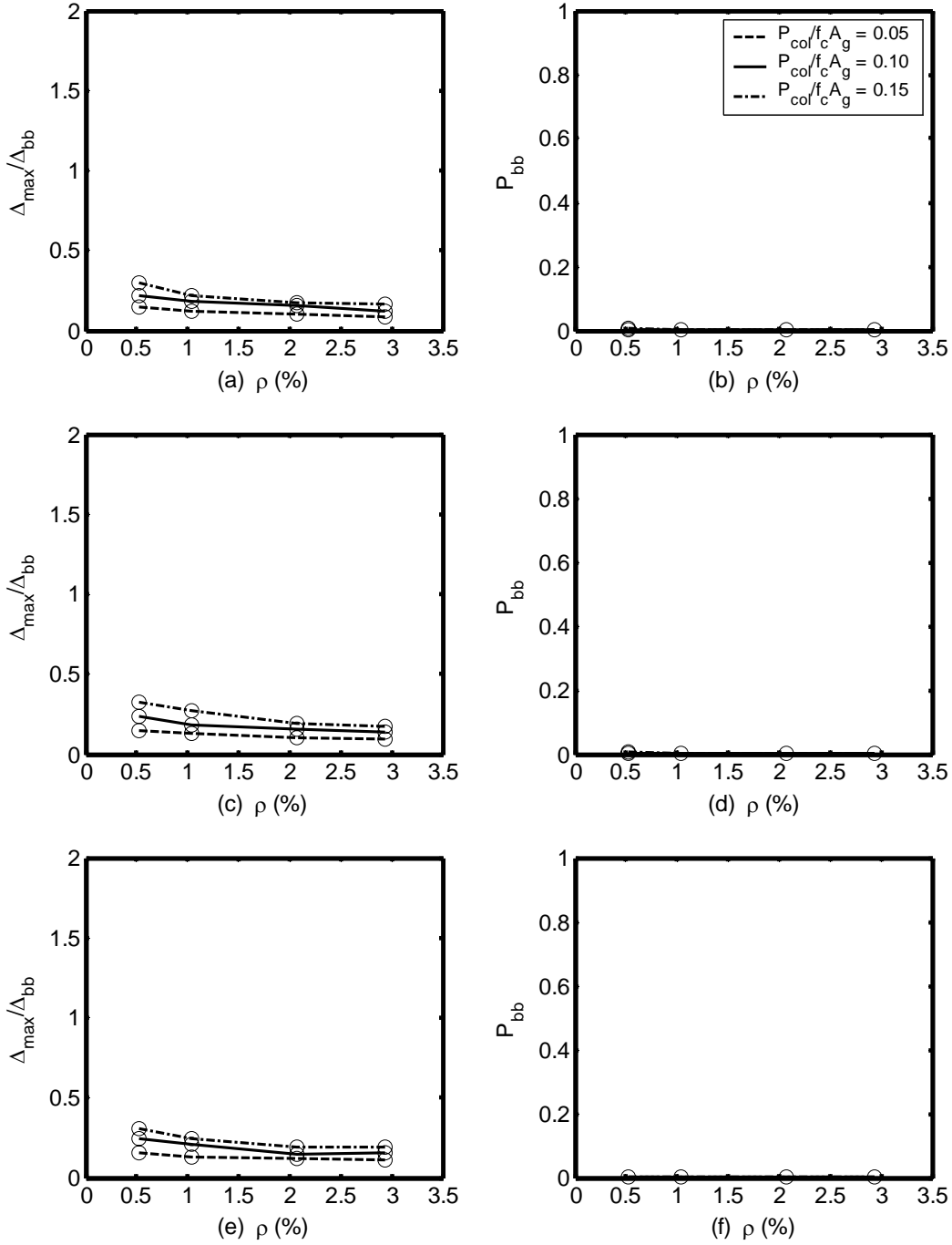**Figure D.2: Displacement Ductility, 10 Percent in 50, Hybrid Frames,** $P_{col}\big/\big(f_c^{'} A_g\big) = 0.05$

(a) and (b) $L_{col}\big/D_{col} = 5$, **(c) and (d)** $L_{col}\big/D_{col} = 6$, **and (e) and (f)** $L_{col}\big/D_{col} = 7$
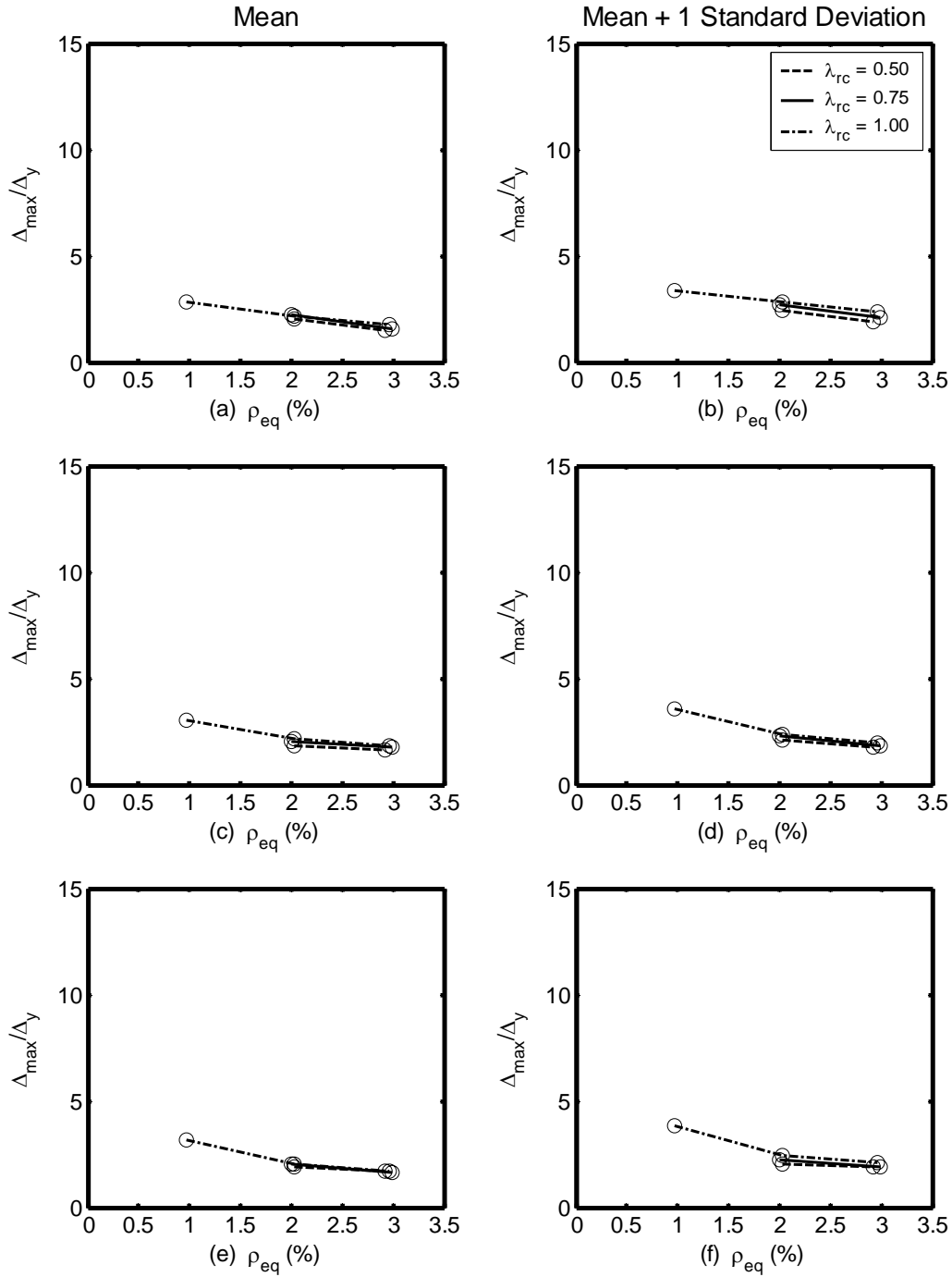
Figure D.3: Displacement Ductility, 10 Percent in 50, Hybrid Frames, $P_{col}\big/\left(f_c^{'}A_g\right)=0.10$
(a) and (b) $L_{col}\big/D_{col}=$ **5, (c) and (d)** $L_{col}\big/D_{col}=$ **6, and (e) and (f)** $L_{col}\big/D_{col}=$ **7**

Figure D.4: Cover Spalling, 10 Percent in 50, Reinforced Concrete Frames
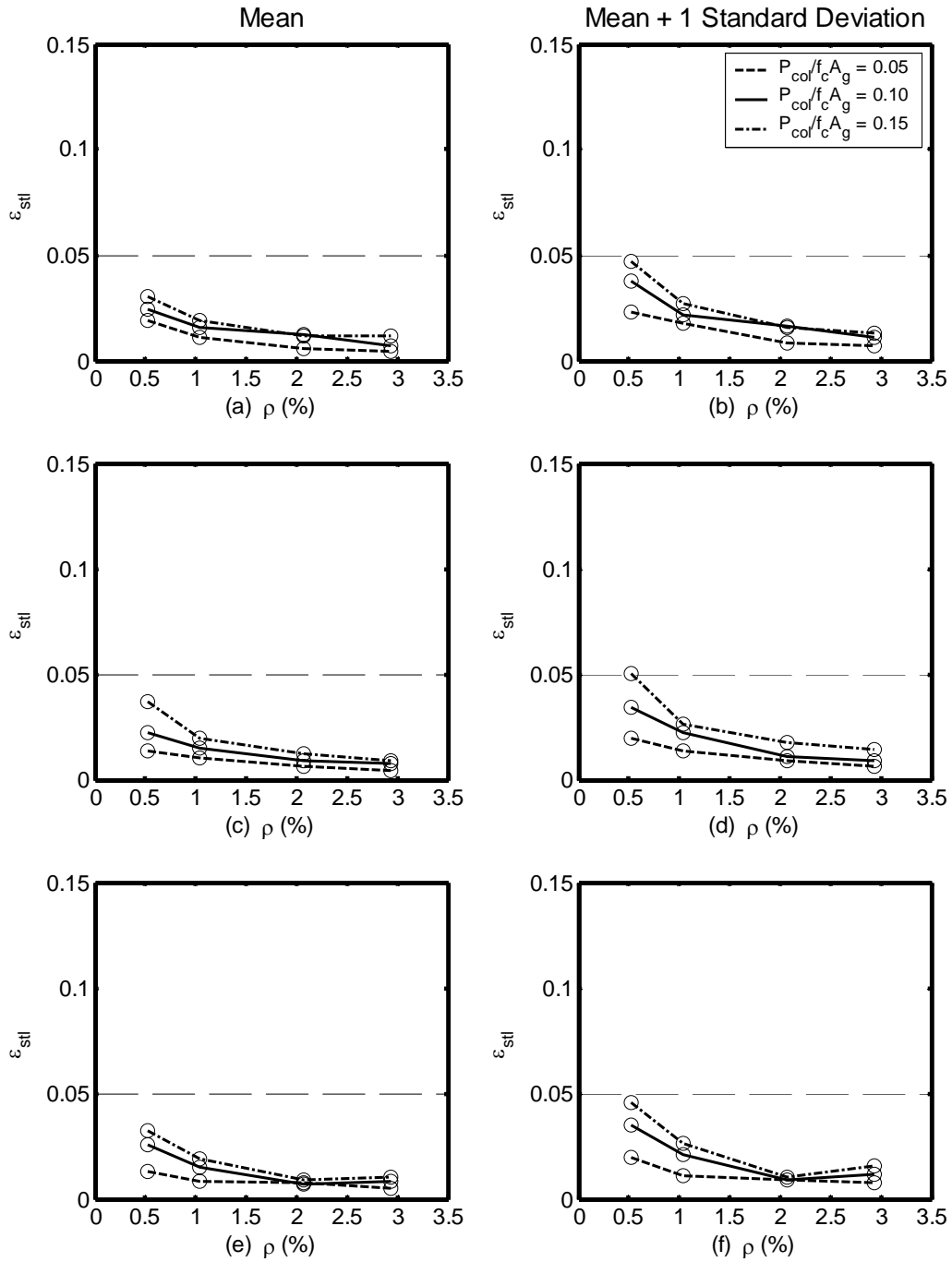(a) and (b) $L_{col}/D_{col} = 5$, (c) and (d) $L_{col}/D_{col} = 6$, and (e) and (f) $L_{col}/D_{col} = 7$
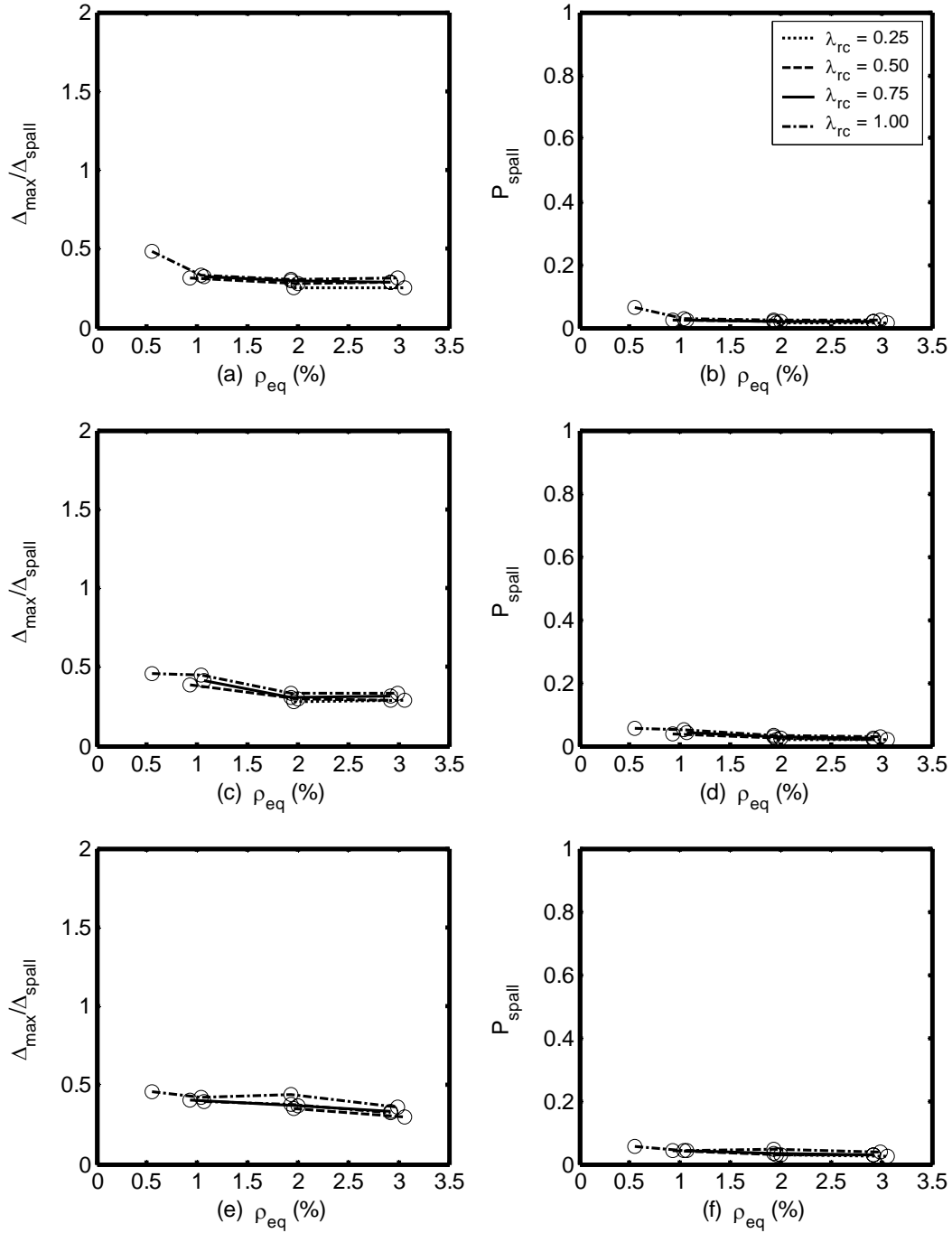
Figure D.5: Cover Spalling, 10 Percent in 50, Hybrid Frames, $P_{col}/\left(f_c^{'} A_g \right) = 0.05$

(a) and (b) $L_{col}/D_{col} = 5$, **(c) and (d)** $L_{col}/D_{col} = 6$, **and (e) and (f)** $L_{col}/D_{col} = 7$
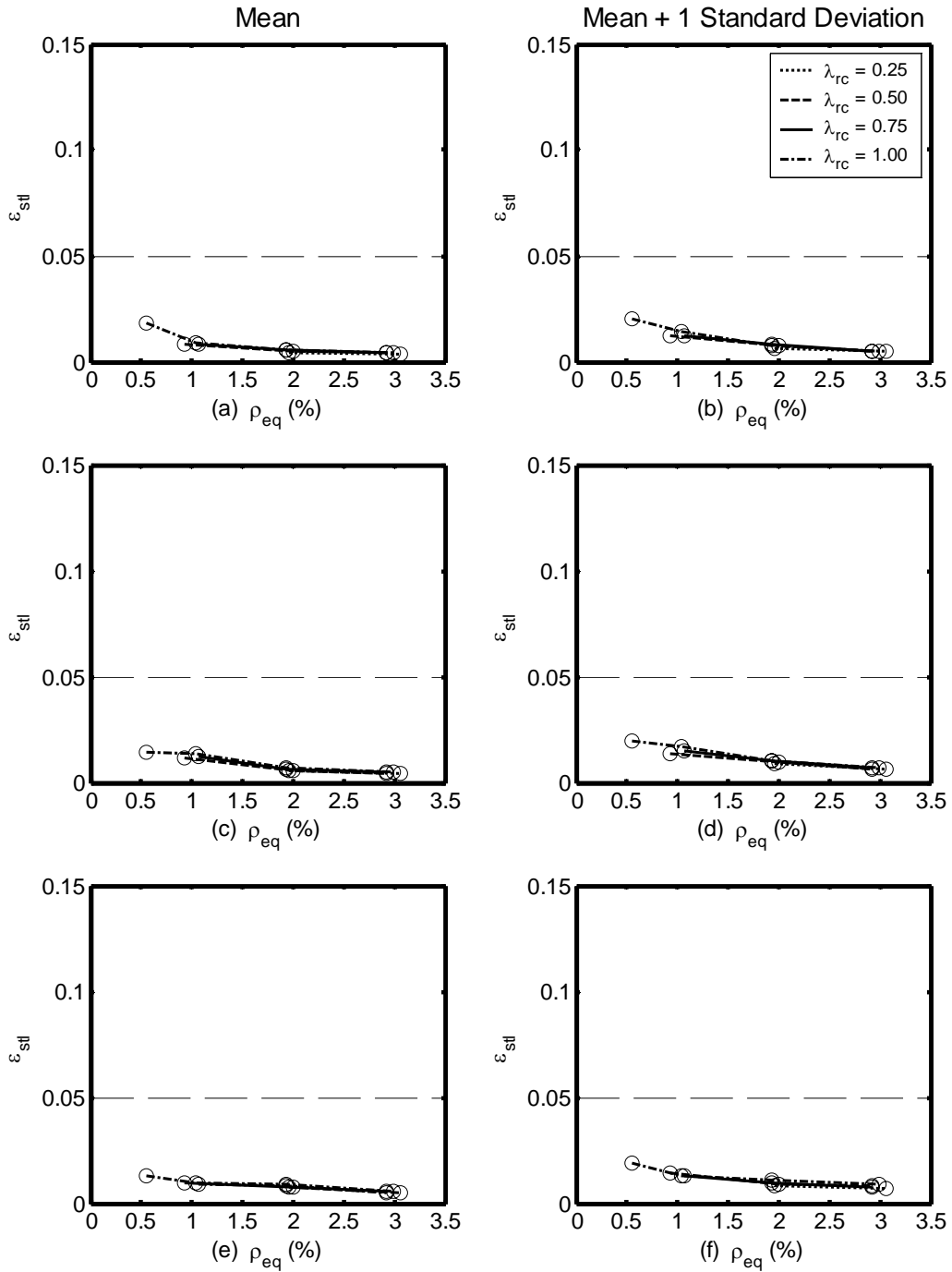
Figure D.6: Cover Spalling, 10 Percent in 50, Hybrid Frames, $P_{col}\big/\left(f_c^{'}A_g\right)=0.10$

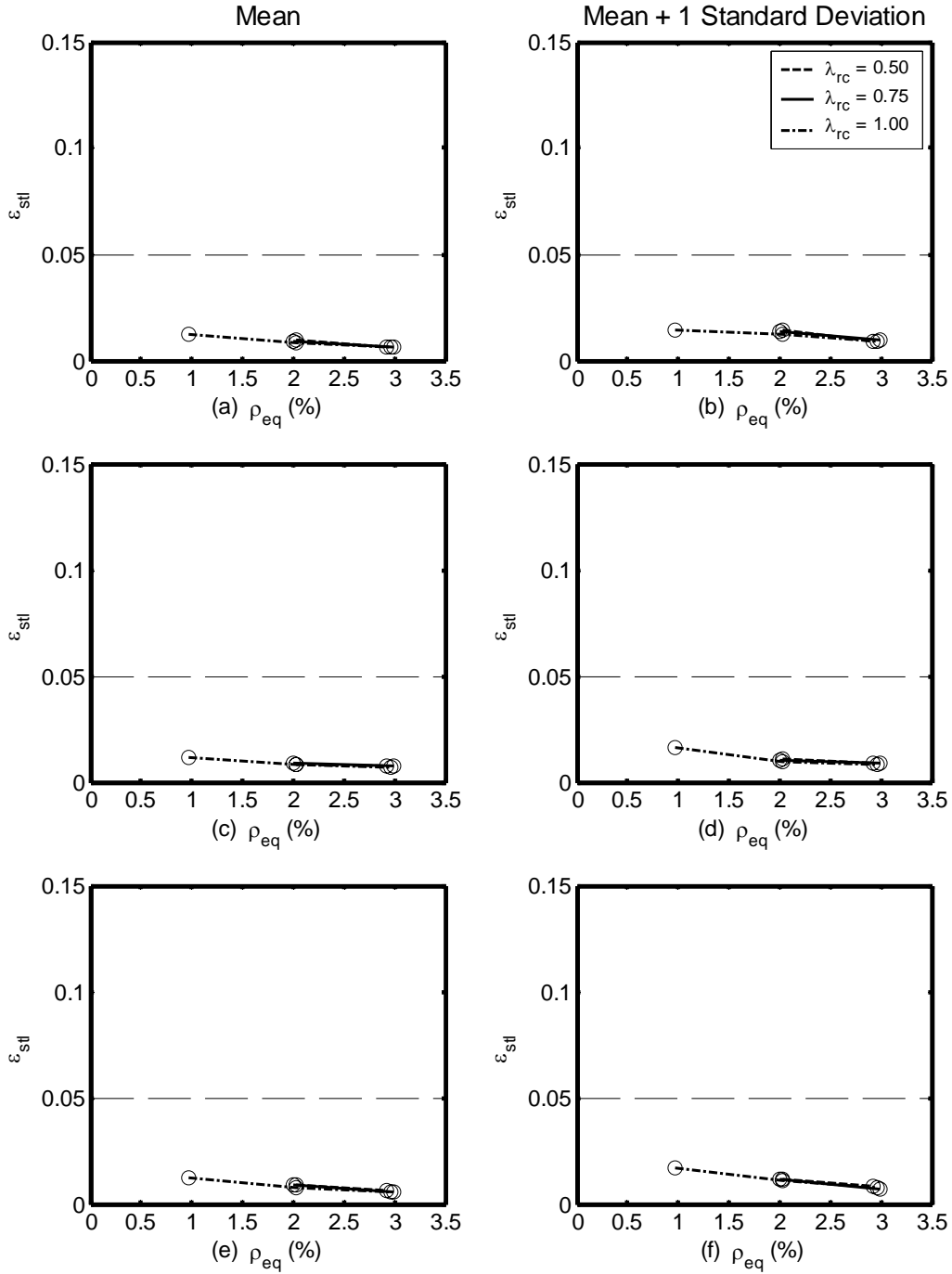**(a) and (b) $L_{col}/D_{col}=5$, (c) and (d) $L_{col}/D_{col}=6$, and (e) and (f) $L_{col}/D_{col}=7$**

Figure D.7: Bar Buckling, 10 Percent in 50, Reinforced Concrete Frames
(a) and (b) $L_{col}/D_{col} = 5$, (c) and (d) $L_{col}/D_{col} = 6$, and (e) and (f) $L_{col}/D_{col} = 7$
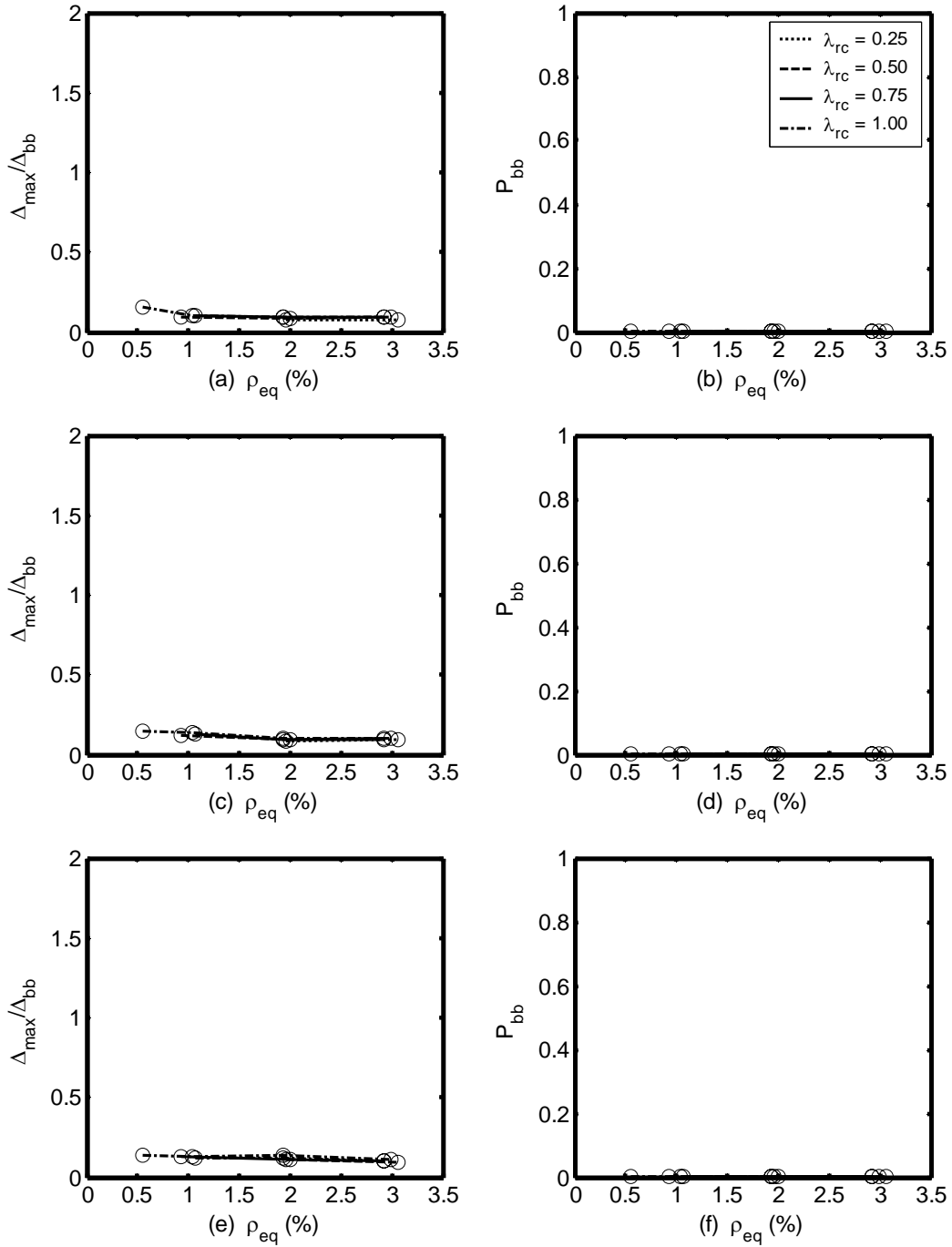
Figure D.8: **Bar Buckling, 10 Percent in 50, Hybrid Frames,** $P_{col}\big/\big(f_c^{'}A_g\big)=0.05$
(a) and (b) $L_{col}\big/D_{col}=5$**, (c) and (d)** $L_{col}\big/D_{col}=6$**, and (e) and (f)** $L_{col}\big/D_{col}=7$
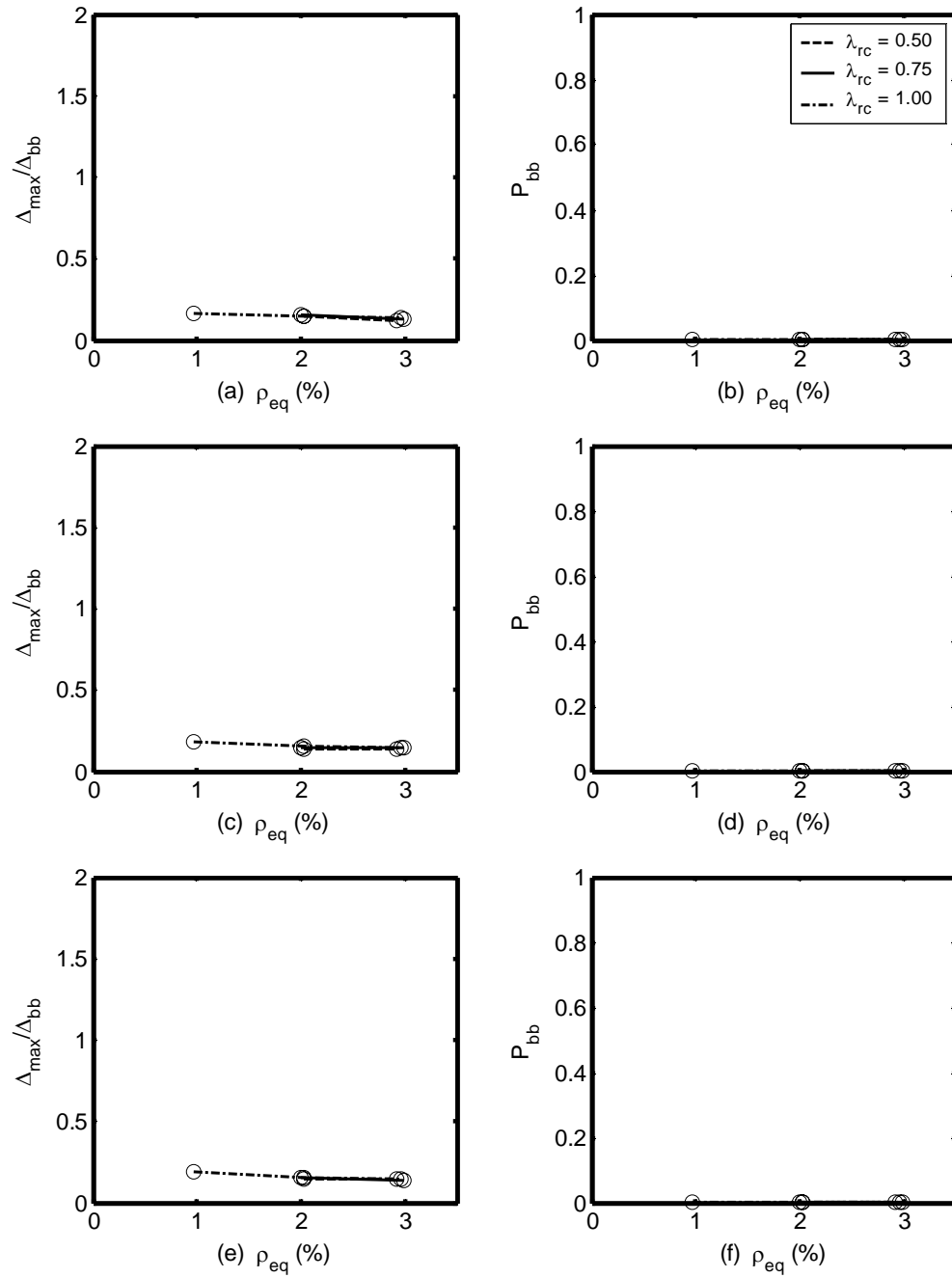
Figure D.9: Bar Buckling, 10 Percent in 50, Hybrid Frames, $P_{col}/\left(f_c^{'}A_g\right)=0.10$
(a) and (b) $L_{col}/D_{col}=$ **5, (c) and (d)** $L_{col}/D_{col}=$ **6, and (e) and (f)** $L_{col}/D_{col}=$**7**

Figure D.10: Maximum Steel Strain, 10 Percent in 50, Reinforced Concrete Frames
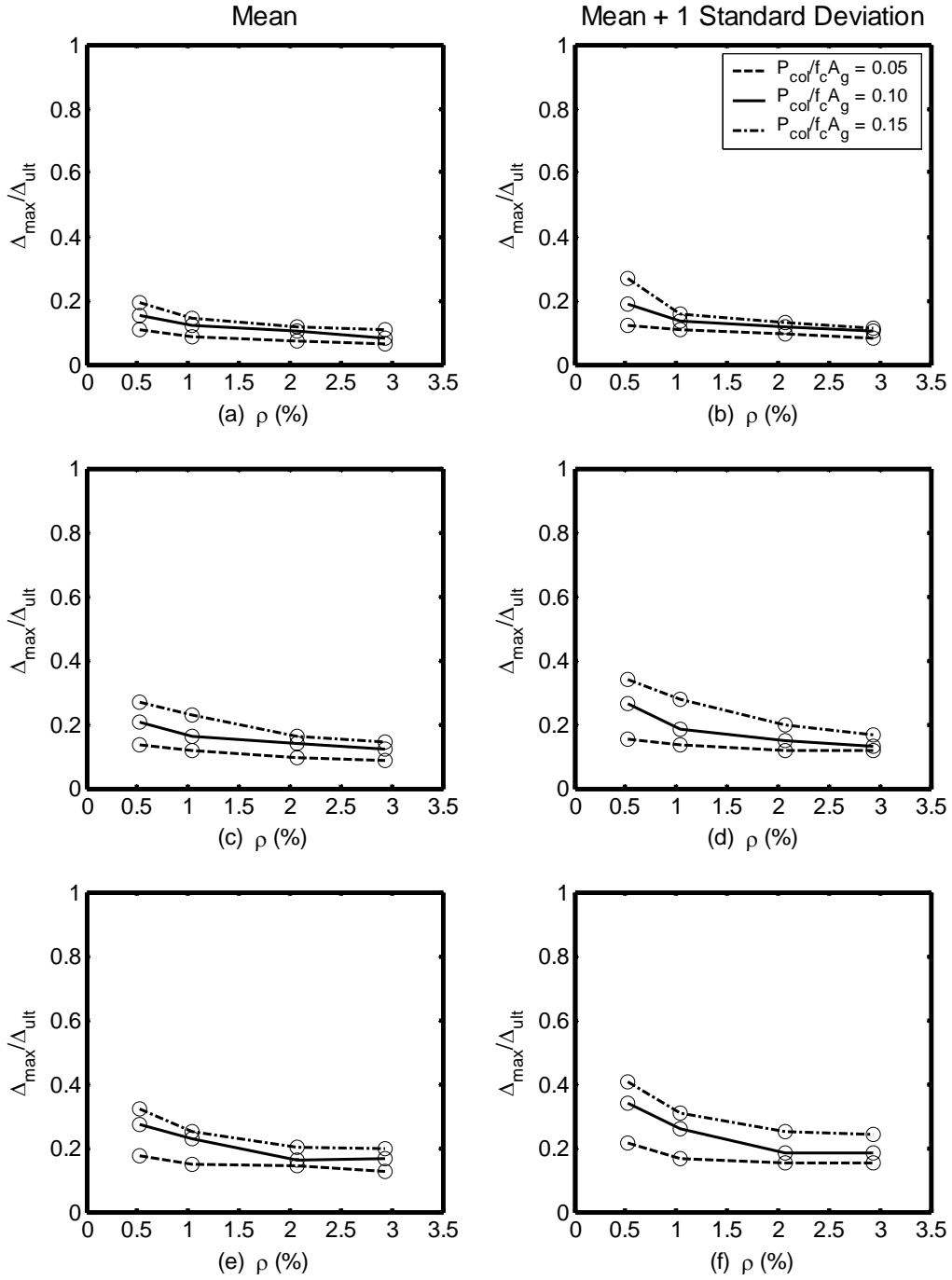(a) and (b) $L_{col}/D_{col} = 5$, (c) and (d) $L_{col}/D_{col} = 6$, and (e) and (f) $L_{col}/D_{col} = 7$
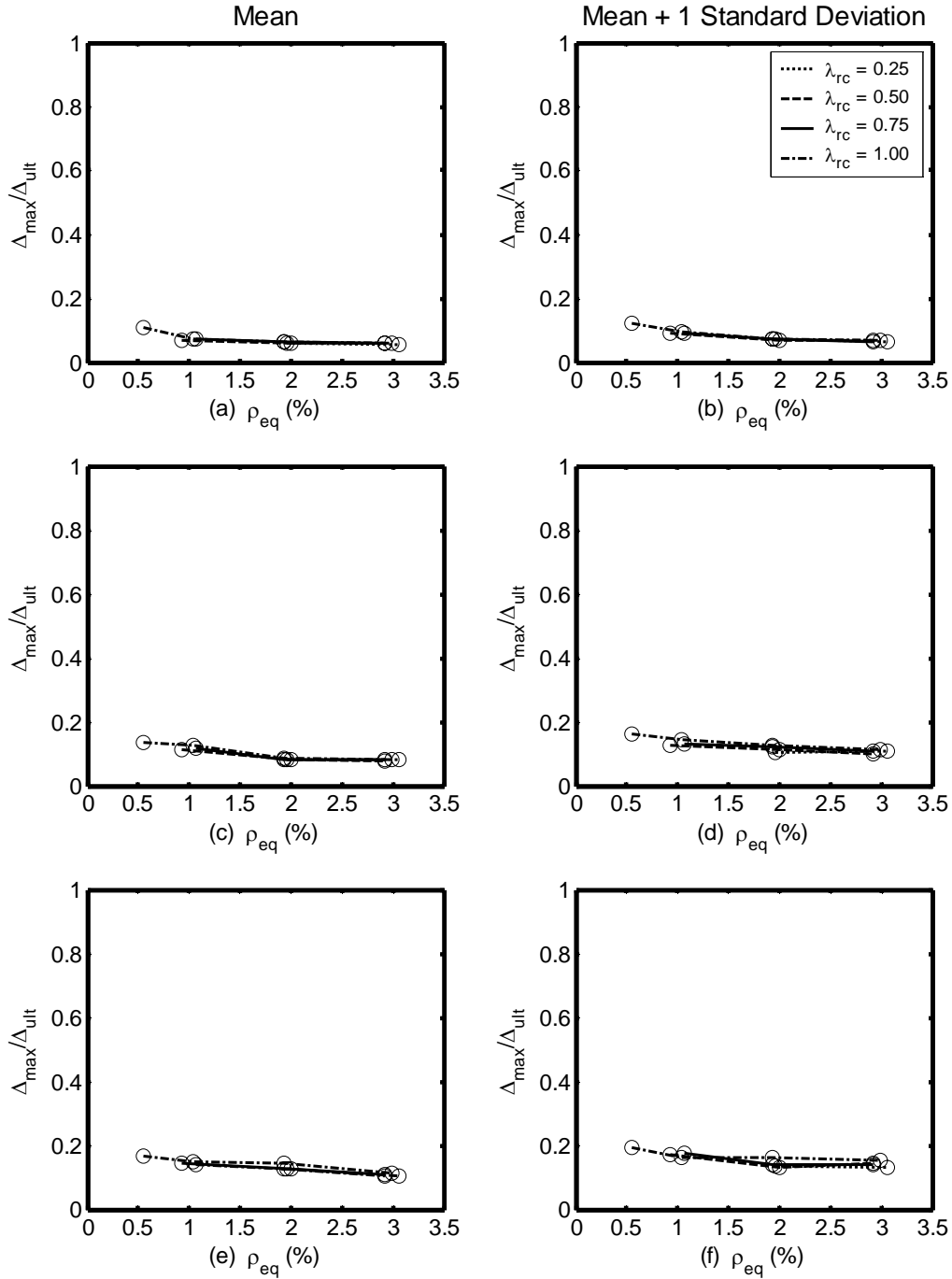
Figure D.11: Maximum Steel Strain, 10 Percent in 50, Hybrid Frames, $P_{col}/\left(f_c'A_g\right)=0.05$
(a) and (b) $L_{col}/D_{col}=5$, **(c) and (d)** $L_{col}/D_{col}=6$, **and (e) and (f)** $L_{col}/D_{col}=7$
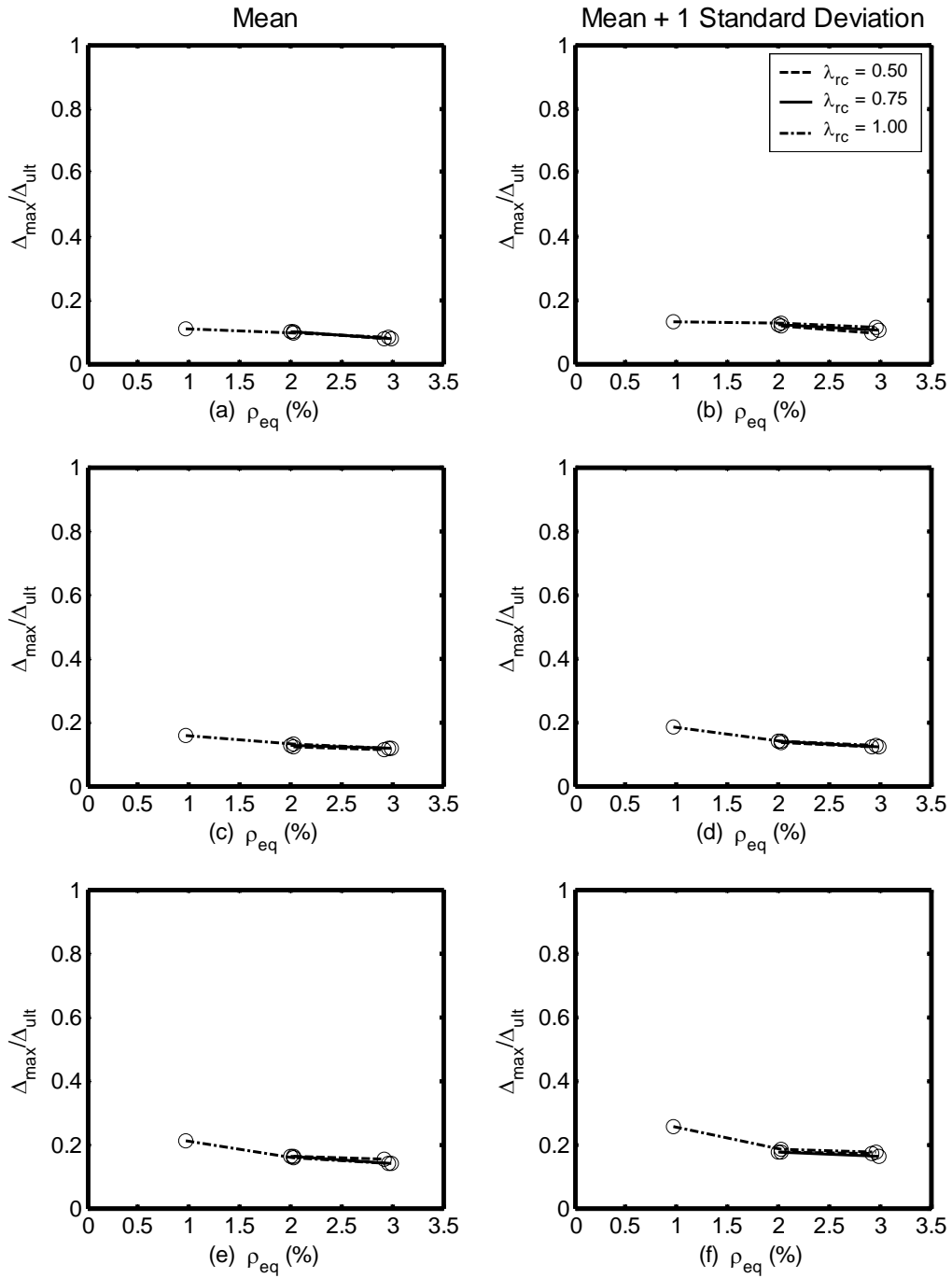
Figure D.12: Maximum Steel Strain, 10 Percent in 50, Hybrid Frames, $P_{col}/\left(f_c^{'}A_g\right) = 0.10$

(a) and (b) $L_{col}/D_{col} = 5$**, (c) and (d)** $L_{col}/D_{col} = 6$**, and (e) and (f)** $L_{col}/D_{col} = 7$

Figure D.13: $\Delta_{\max}\big/\Delta_{ult}$, **10 Percent in 50, Reinforced Concrete Frames**
(a) and (b) $L_{col}\big/D_{col}$ **= 5, (c) and (d)** $L_{col}\big/D_{col}$ **= 6, and (e) and (f)** $L_{col}\big/D_{col}$ **=7**

Figure D.14: $\Delta_{\max}/\Delta_{ult}$ **, 10 Percent in 50, Hybrid Frames,** $P_{col}/\left(f_c^{'}A_g\right)=0.05$
(a) and (b) L_{col}/D_{col} **= 5, (c) and (d)** L_{col}/D_{col} **= 6, and (e) and (f)** L_{col}/D_{col} **=7**

Figure D.15: $\Delta_{\max}\big/\Delta_{ult}$ **, 10 Percent in 50, Hybrid Frames,** $P_{col}\big/\left(f_c^{'}A_g\right)=0.10$

(a) and (b) $L_{col}\big/D_{col}$ **= 5, (c) and (d)** $L_{col}\big/D_{col}$ **= 6, and (e) and (f)** $L_{col}\big/D_{col}$ **=7**